Regulation of inflammation and autophagy: Role of CD14 in biglycan-mediated sterile inflammation and impact of ABIN-1 on selective autophagy

Dissertation
zur Erlangung des Doktorgrades der Naturwissenschaften

vorgelegt beim Fachbereich 14 Biochemie, Chemie und Pharmazie
der Johann Wolfgang Goethe-Universität
in Frankfurt am Main

von
Heiko Rödig
aus Rüsselsheim

Frankfurt am Main, 2020
(D30)

Vom Fachbereich 14 der Johann Wolfgang Goethe-Universität als Dissertation angenommen.

Dekan: Prof. Dr. Clemens Glaubitz

Gutachter 1: Prof. Dr. Rolf Marschalek
Gutachter 2: Prof. Dr. Josef Pfeilschifter

Datum der Disputation:

Table of contents

List of abbreviations

ABIN-1	A20 binding inhibitor of NF-κB1
ACN	Acetonitrile
ADAMTS	A disintergrin and metalloproteinase with thrombospondin motifs
AHD	ABIN Homology Domains
ATG	Autophagy-related proteins
BafA1	Bafilomycin A1
CCL	chemokine (C–C motif) ligand
CD	Cluster of differentiation
cDNA	Complementary DNA
Co-IP	Co-immunoprecipitation
CS	Chondroitin sulfate
CXCL	chemokine (C-X-C motif) ligand
CXCR	chemokine (C-X-C) motif receptor
DAMP	Damage-associated molecular pattern
DEAE	Diethylaminoethanol
DEPC	Diethylpyrocarbonate
DMSO	Dimethylsulfoxide
dNTP	Desoxyribonucleosidephosphates
DOX	Doxycycline
DS	Dermatan sulfate
DTT	Dithiothreitol
ECL	Enhanced chemiluminescence
ECM	Extracellular matrix
ELISA	Enzyme-linked immunosorbent assay
Erk	Extracellular signal-regulated kinase
FA	Formic acid
FACS	Fluorescence-activated cell sorting
FBS	Fetal bovine serum
FUNDC1	FUN14 domain-containing protein 1
GABARAP	γ- aminobutyric acid receptor- associated protein
GAG	Glycosaminoglycan
h	Hours
HA	Hemagglutinin
HEK	Human embryonic kidney
HMGB1	High-mobility group box 1 protein

HSP	Heat shock protein
IFN	Interferon
IgG	Immunoglobulin G
IL	Interleukin
IRAK1	Interleukin-1 receptor-associated kinase 1
IRF	Interferon regulatory factor
IRI	Ischemia/reperfusion injury
K_D	Dissociation constant
KO	Knockout
LBP	LPS-binding protein
LIR	LC3-interacting region
LIVE	Liver in vivo expression
LPS	Lipopolysaccharide
LRR	Leucine-rich repeat
M	Molar
MAP1LC3	Microtubule- associated protein light chain 3
MAPK	Mitogen-activated protein kinase
MD2	Myeloid differentiation 2
mEGFP	Monomeric enhanced green fluorescent protein
MFN	Mitofusin
min	Minutes
MMP	Matrix metalloproteinase
mRNA	Messenger RNA
MS	Mass spectrometry
MST	Microscale thermophoresis
mTORC1	MTOR complex 1
MyD88	Adaptor molecule myeloid differentiation primary response gene 88
n.s.	Not significant
NBR1	Neighbor of BRCA1
NDP52	Nuclear dot protein 52
NEMO	NF-κB essential modulator
NF-κB	Nuclear factor kappa-light-chain enhancer of activated B cells
NLRP3	NOD-like receptor pyrin domain-containing-3
NOX	NADPH oxidase
OA	Oligomycin/antimycin A
OMM	Outer mitochondrial membrane
PAMP	Pathogen-associated molecular pattern

PBS	Phosphate buffered saline
PE	Phosphatidylethanolamine
PG	Proteoglycan
PGN	Peptidoglycan
PINK1	Phosphatase and tensin homologue (PTEN)-induced putative kinase 1
PIP3	Phosphatidylinositol-3-phosphate
PRR	Pattern recognition receptor
PVDF	Polyvinyl difluoride
qRT-PCR	Quantitative real-time PCR
RIPK1	Receptor-interacting serine/threonine kinase 1
ROS	Reactive oxygen species
rpm	Revolution per minute
RPMI	Roswell Park Memorial Institute 1640
SB	Sleeping beauty
SDS	Sodium Dodecyl Sulfate
SDS-Page	Polyacrylamide gel electrophoresis
SEAP	Secreted embryonic alkaline phosphatase
sgRNA	Single guide RNA
SLE	Systemic lupus erythematosus
SLRP	Small leucine-rich proteoglycans
Sphk	Sphingosine kinase
TAX1BP	Tax1-binding protein 1
TBK1	TANK-binding kinase 1
TIR	Toll/IL-1R homology
TMT	Tandem mass tags
TNF-α	Tumor necrosis factor-α
TNIP1	TNFα-induced protein 3-(TNFAIP3-) interacting protein 1
TOM20	Translocase of outer mitochondrial membrane 20
TRIF	TIR domain-containing adaptor-inducing interferon-β
Ub	Ubiquitin
UBAN	Ubiquitin-binding domain of ABIN and NEMO
ULK1	Unc-51-like kinase 1
VDAC	Voltage-dependent anion channel
WIPI	WD repeat domain phosphoinositide- interacting
WT	Wild-type

List of tables

List of figures

1 Summary

The innate immune system is the first line of host defense that senses invading pathogens by various surveillance mechanisms, involving pattern recognition receptors (PRRs) such as Toll-like receptors (TLRs). Furthermore, in response to stress, tissue injury or ischemia, cells release endogenous danger-associated molecular patterns (DAMPs) which activate PRRs in order to prompt an effective immune response. Activation of PRRs by DAMPs initiates signaling transduction pathways which drive sterile inflammation by the production of pro-inflammatory effector molecules. Biglycan, a class I small leucine-rich proteoglycan (SLRP), is proteolytically released from the extracellular matrix (ECM) in response to tissue stress and injury or *de novo* synthesized by activated macrophages. In its soluble form, biglycan operates as an ECM-derived DAMP and triggers a potent inflammatory response by engaging TLR2 and TLR4 on immune cells. By selective utilization of TLR2/4 and the TLR adaptor molecules adaptor molecule myeloid differentiation primary response gene 88 (MyD88) or TIR domain-containing adaptor-inducing interferon-β (TRIF) biglycan differentially regulates the production of TLR downstream mediators or inflammatory molecules. In this way, biglycan triggers the activation of mitogen-activated protein kinase (MAPK) p38, extracellular signal-regulated kinase (Erk) and nuclear factor kappa-light-chain enhancer of activated B cells (NF-κB) in a primarily MyD88-dependent manner. In contrast, biglycan induces the expression of (C–C motif) ligand (CCL)5 and chemokine (C-X-C motif) ligand (CXCL)10 over TLR4/TRIF, heat shock protein 70 (HSP70) production over TLR2 and the synthesis of tumor necrosis factor (TNF)-α, CCL2 and CCL20 by utilizing TLR2/4/MyD88. As a consequence, biglycan promotes the recruitment of immune cells such as neutrophils, T cells, B cells and macrophages into the inflamed tissue. Research over the past years showed that biglycan-induced inflammation is involved in the pathogenesis of various inflammatory diseases such as lupus nephritis (LN), sepsis and renal ischemia/reperfusion injury (IRI), whereby genetic deletion of biglycan or TLR2/4 alleviated disease outcome. Unfortunately, the selective interaction of biglycan to TLRs and TLR adaptors complicates the identification of an efficient pharmacological target in biglycan-mediated inflammation. Yet, the necessity of possible co-receptors in biglycan signaling such as cluster of differentiation 14 (CD14) which was found in a high molecular complex with biglycan was not addressed so far.

In the first part of the present study, by utilizing primary peritoneal murine macrophages we demonstrated that the biglycan-induced expression and synthesis of TNF-α and CCL2 via TLR2/4/MyD88, CCL5 through TLR4/TRIF and HSP70 over TLR2 is blunted in CD14 deficient mice, proving that CD14 is essential in TLR2- and TLR4-mediated biglycan signaling. Pre-incubation of macrophages with an anti-CD14 antibody significantly reduced the protein levels

of TNF-α, CCL2, CCL5 and HSP70. In line with these data, pharmacological inhibition of CD14 alleviated the transcriptional activation of NF-κB by biglycan in HEK-Blue cells expressing hTLR2/CD14 as well as hTLR4/CD14/MD2 supporting CD14-dependency for biglycan/TLR2/4 signaling. Western blot analysis of phosphorylated p38, p44/42 and NF-κB in WT and CD14 deficient mice revealed that activation of biglycan-mediated TLR downstream signaling is CD14-dependent. Accordingly, biglycan-induced activation and nuclear translocation of p38, p44/42 and NF-κB was blocked in *Cd14*$^{-/-}$ mice as analyzed by confocal microscopy. Co-immunoprecipitation studies combined with microscale thermophoresis analysis showed that biglycan is in complex with CD14 in macrophages and *in vitro* binds directly with high affinity to CD14, thereby sustaining the concept that CD14 is a novel co-receptor in biglycan-mediated inflammation. Additionally, we provided proof-of-principle of our concept in an *in vivo* mouse model of renal IRI. Transient overexpression of biglycan in WT mice exacerbated the expression and production of TNF-α, CCL2, CCL5 and HSP70 in a CD14-dependent manner. Interestingly, pLIVE or pLIVE-h*BGN*-injected *Cd14*$^{-/-}$ mice displayed lower chemo- and cytokine levels in reperfused kidneys as compared to respective WT controls during renal IRI (30 h), indicating a renoprotective effect by CD14 deficiency. Flow cytometry analysis of kidney homogenates underlined the pivotal effect of CD14 in biglycan signaling as biglycan-mediated infiltration of CD11b- and F4/80-positive renal macrophages was abolished in *Cd14*$^{-/-}$ mice. Additionally, pLIVE or pLIVE-h*BGN*-injected CD14 deficient mice displayed lower numbers of renal CD11b- and F4/80-positive cells during renal IRI compared to WT mice. Analysis of F4/80- and CD38-positive cells isolated from mononuclear cell extracts from kidney homogenates of pLIVE or pLIVE-h*BGN*-injected WT and *Cd14*$^{-/-}$ mice revealed that biglycan triggers the polarization of pro-inflammatory M1 macrophages in a CD14-dependent manner. In line with this, *Cd14*$^{-/-}$ mice, either injected with pLIVE or pLIVE-h*BGN*, showed less F4/80- and CD38-positive cells during renal IRI than the respective WT control. As a corroboration of our data PAS-stained renal sections of pLIVE- or pLIVE-h*BGN*-injected WT or *Cd14*$^{-/-}$ mice uncovered that biglycan worsens tubular damage in IRI-subjected mice via CD14. At the same time, tubular damage was significantly reduced in IRI-subjected *Cd14*$^{-/-}$ mice as compared to WT mice. In correlation with these data, serum creatine levels were increased in pLIVE-h*BGN*-injected WT mice during renal IRI. In contrast, serum creatine levels were significantly less increased in pLIVE- or pLIVE-h*BGN*-injected *Cd14*$^{-/-}$ mice than in WT littermate controls. In conclusion we demonstrated that CD14 is a new high affinity ligand for biglycan-mediated pro-inflammatory signaling over TLR2 and TLR4 in macrophages. *In vivo*, soluble biglycan triggers the expression of various inflammatory mediators by utilizing the co-receptor CD14. Ablation of CD14 abolishes biglycan-induced renal macrophage infiltration and M1 macrophage polarization as well as overall kidney function by reduced tubular damage and serum creatinine

levels. Therefore, this study identifies CD14 as a promising therapeutic target to ameliorate biglycan-induced inflammation.

Whether sterile or pathogen-induced inflammation during innate immunity persists is based on the balance of inflammatory and resolution pathways. Uncontrolled inflammation results in various inflammatory diseases leading to chronicity and autoimmunity. Therefore, several mechanisms and proteins ensure a tight regulation of the inflammatory response. As such, A20 binding inhibitor of NF-κB1 (ABIN-1) is a potent inhibitor of inflammation by suppressing TLR-induced NF-κB signaling. ABIN-1 inhibits inflammation and apoptosis by binding to polyubiquitinated target proteins via its ubiquitin-binding domain of ABIN and NEMO (UBAN), thereby mediating their inactivation or proteasomal degradation. The UBAN domain of ABIN-1 shares sequence homology to the one present in optineurin, which exhibits similar functions in NF-κB suppression but as well functions as a selective autophagy receptor. As selective autophagy is implicated in regulating inflammation in a broad range of inflammatory diseases we decided to analyze if ABIN-1 is involved in autophagy.

In the second part of this study we analyzed the interactome of ABIN-1 during pathogen-induced inflammation in spleen samples and compared the whole proteome of macrophages derived from WT and ABIN1[D485N] mice under basal conditions. ABIN1[D485N] mice carry a mutation in ABIN-1 which alters its ability to bind polyubiquitin. Surprisingly, interactome analysis revealed that ABIN-1 binds to various proteins connected to autophagy such as ATG8 proteins and to proteins involved in the selective degradation of damaged mitochondria by autophagy. Additionally, proteome analysis demonstrated that several autophagy related proteins were upregulated in macrophages from ABIN1[D485N] mice. Thus, we postulated that ABIN-1 by simultaneously binding polyubiquitinated cargo proteins and ATG8 proteins would serve as an autophagy receptor mediating the target-orientated and selective degradation of cargo proteins by autophagy. Sequence analysis of ABIN-1 identified two undescribed and conserved LC3-interacting region (LIR) motifs in ABIN-1. By utilizing Co-immunoprecipitation (Co-IP) studies in HeLa cells overexpressing HA-tagged ABIN-1 we could show that ABIN-1 is in complex with LC3B in a LIR-dependent manner. In line with this, reciprocal Co-IP validated complex formation of ABIN-1 and LC3B. By employing bacterial expressed ABIN-1 and GST-tagged LC3A and LC3B, we showed direct binding of ABIN-1 to LC3 proteins. Mutation of both LIR domains abrogated the binding of ABIN-1 to LC3A or LC3B and did not affect the binding of ABIN-1 to polyubiquitin. Moreover, mutation of the UBAN domain of ABIN-1 did not influence the binding properties of ABIN-1 to LC3A or LC3B. Co-localization of mEGFP-ABIN-1/mCherry-LC3B or mEGFP-ABIN-1/LAMP-1 was visualized by confocal microscopy in HeLa cells stimulated either with BafilomycinA1 (BafA1) with or without Torin-1, confirming that ABIN-1 is localized to LC3B-positive autophagosomes and LAMP-1-positive

autophagolysosomes. Moreover, Western blot analysis of ABIN-1 and p62 showed that ABIN-1 protein levels are increased upon blocking the fusion of autophagosomes with lysosomes by BafA1 at various time points. Autophagic flux of ABIN-1 and p62 protein levels was confirmed at 4 h by treatment with either rapamycin and/or BafA1. In line with our mass spectrometry data, ABIN-1 involvement in mitophagy was shown by translocation of ABIN-1 to damaged mitochondria upon oligomycin/antimycin A (OA) treatment in HeLa cells stably expressing mCherry-Parkin. CRISPR/Cas9-mediated deletion of ABIN-1 in mCherry-Parkin expressing HeLa cells treated with OA demonstrated that a loss of ABIN-1 slows the selective degradation of mitochondrial outer membrane (OMM) proteins by mitophagy. Importantly, by using HeLa cells stably expressing Parkin and the fluorescence reporter mt-mKEIMA we could show by FACS analysis that a siRNA-mediated knockdown of ABIN-1 significantly decreased the overall percentage of lysosomal-positive mitochondria. In contrast, FACS analysis of HeLa cells, expressing the fluorescence reporter mKEIMA-LC3B, revealed no effect of a siRNA-mediated knockdown of ABIN-1 on overall autophagy levels. In summary, we show for the first time that ABIN-1 binds directly to ATG8 proteins via two undescribed LIR motifs and specifically localizes to autophagosomes and autophagolysosomes upon autophagy induction. Furthermore, ABIN-1 protein levels are processed via the autophagic pathway. Importantly, ABIN-1 is involved in the selective elimination of mitochondria by mitophagy. ABIN-1 translocates to damaged mitochondria, regulates the degradation of OMM proteins during mitophagy and influences overall mitophagic activity. This study determines ABIN-1 as a new selective autophagy receptor for damaged mitochondria and provides the basis for future studies elucidating the involvement of ABIN-1 in inhibiting inflammation by selective autophagy.

Zusammenfassung

Das angeborene Immunsystem ist die erste Verteidigungslinie des Körpers die eindringende Pathogene durch Mustererkennungsrezeptoren wie Toll-like Rezeptoren (TLRs) erkennt. In Folge von Stress, Gewebeschäden oder Ischämie setzen Zellen endogene *danger-associated molecular patterns* (DAMPs) frei, die zur Aktivierung von Mustererkennungsrezeptoren führen und eine effektive Immunantwort auslösen. Die Aktivierung der Mustererkennungsrezeptoren durch DAMPs initiiert eine Signaltransduktion, die durch die Produktion von inflammatorischen Molekülen eine sterile Entzündungsreaktion hervorruft. Biglykan ist ein Klasse I leucinreiches Proteoglykan welches zum einen durch Gewebsverletzungen mit Hilfe von proteolytischer Spaltung aus der extrazellulären Matrix (ECM) freigesetzt wird oder *de novo* von aktivierten Makrophagen synthetisiert wird. In seiner löslichen Form fungiert Biglykan als DAMP und ruft durch die Bindung an TLR2 und TLR4 auf Immunzellen eine starke inflammatorische Reaktion hervor. Durch die selektive Nutzung von TLR2/4 und den TLR Adaptermolekülen *adaptor molecule myeloid differentiation primary response gene 88* (MyD88) oder *TIR domain-containing adaptor-inducing interferon-β* (TRIF) reguliert Biglykan die Produktion von TLR nachgeschalteten Mediatoren oder inflammatorischen Molekülen. Auf diese Weise löst Biglykan die Aktivierung von *mitogen-activated protein kinase* (MAPK) p38, *extracellular signal-regulated kinase* (Erk) und *nuclear factor kappa-light-chain enhancer of activated B cells* (NF-κB) in einer hauptsächlich MyD88-abhängigen Weise aus. Dagegen ruft Biglykan die Expression von *(C–C motif) ligand* (CCL)5 und *chemokine (C-X-C motif) ligand* (CXCL)10 durch die Verwendung von TLR4/TRIF hervor, wobei die Expression von *heat shock protein 70* (HSP70) über TLR2 und die Synthese von *tumor necrosis factor* (TNF)-α, CCL2 und CCL20 über TLR2/4/MyD88 gesteuert wird. Dadurch fördert Biglykan die Rekrutierung von Immunzellen wie Neutrophile, T-Zellen und Makrophagen zu dem entzündeten Gewebe. Die Forschung der vergangenen Jahre konnte nicht nur zeigen, dass eine Biglykan-induzierte Inflammation in der Pathogenese von verschiedenen inflammatorischen Krankheiten wie etwa Lupus Nephritis (LN), Sepsis und renalem ischämischen Reperfusionsschaden (IRI) involviert ist, sondern auch, dass eine genetische Deletion von Biglykan oder TLR2/4 das Krankheitsbild abschwächt. Unglücklicherweise kompliziert die selektive Interaktion von Biglykan mit TLRs und TLR Adaptermolekülen die Identifikation eines leistungsstarken pharmakologischen Angriffspunktes für eine Biglykan-induzierte Inflammation. Nichtsdestotrotz wurde die Notwendigkeit von Ko-Rezeptoren für die Biglykan Signalgebung wie etwa *cluster of differentiation* 14 (CD14), welches bereits zuvor in einem Komplex mit Biglykan gefunden wurde, bisher nicht untersucht.

Im ersten Teil dieser Arbeit wurde anhand von primären peritonealen Mausmakrophagen gezeigt, dass die Biglykan-induzierte Expression von TNF-α und CCL2 über TLR2/4/MyD88, die Expression von CCL5 über TLR4/TRIF und die Synthese von HSP70 über TLR2 in CD14

defizienten Mäusen komplett inhibiert ist. Dies zeigt, dass CD14 ein essenzieller Bestandteil in der TLR2- und TLR4-induzierten Signalgebung von Biglykan ist. Eine Prä-Inkubation von Makrophagen mit einem anti-CD14 Antikörper zeigte eine signifikante Reduktion der Proteinlevel von TNF-α, CCL2, CCL5 und HSP70. Im Einklang mit diesen Daten schwächte eine pharmakologische Inhibition von CD14 die transkriptionelle Aktivierung von NF-κB in HEK-Blue Zellen die hTLR2/CD14 oder hTLR4/CD14/MD2 exprimieren und stärkte damit die beobachtete Abhängigkeit von Biglykan/TLR2/4 von CD14. Durch Western Blot Analysen von phosphoryliertem p38, p44/42 und NF-κB in WT und CD14 defizienten Mäusen konnte gezeigt werden, dass eine Biglykan-ausgelöste Aktivierung von TLR nachgeschalteten Mediatoren in Abhängigkeit zu CD14 steht. Im Einklang damit konnte mit Hilfe von konfokaler Mikroskopie bewiesen werden, dass eine Biglykan-induzierte Aktivierung und nukleäre Translokation von p38, p44/42 und NF-κB von CD14 abhängig ist. Ko-Immunopräzipitationsstudien in Makrophagen zeigten eine Komplexbildung von Biglykan mit CD14. Mit Hilfe von *Microscale* Thermophorese konnte *in vitro* gezeigt werden, dass Biglykan mit einer hohen Affinität direkt an CD14 bindet. Dies unterstützt das Konzept, dass CD14 ein neuartiger Ko-Rezeptor für Biglykan ist. Darüber hinaus erbrachten wir den Beweis unseres Konzeptes in einem *in vivo* Mausmodell der renalen IRI. Eine transiente Überexpression von Biglykan in WT Mäusen erhöhte die Genexpression und Proteinsynthese von TNF-α, CCL2, CCL5 und HSP70 in Abhängigkeit von CD14. Interessanterweise zeigten pLIVE oder pLIVE-h*BGN*-injizierte *Cd14$^{-/-}$* Mäuse eine renoprotektive Wirkung, ersichtlich durch verringerte Chemokin- und Zytokin-Levels in Nieren von IRI-operierten (30 h) Tieren im Vergleich zu WT Mäusen. Analysen mit Durchflusszytometrie (FACS) von Nierenhomogenaten zeigten, dass eine Biglykan-induzierte Infiltration von CD11b- und F4/80-positiven renalen Makrophagen in CD14 defizienten Mäusen verringert wurde und bestätigte damit den bedeutsamen Einfluss von CD14 für die Biglykan Signalgebung. Zusätzlich wiesen pLIVE oder pLIVE-h*BGN*-injizierte CD14 defiziente Mäuse nach renaler IRI eine reduzierte Anzahl von infiltrierenden CD11b- und F4/80-positiven Zellen auf im Vergleich zu WT Mäusen. Eine Analyse von F4/80- und CD38-positiven Zellen aus mononukleären Zellextrakten von Nierenhomogenaten von pLIVE oder pLIVE-h*BGN*-injizierten WT und *Cd14$^{-/-}$* Mäusen zeigte, dass Biglykan die Polarisierung von Makrophagen in einen pro-inflammatorischen M1 Phänotyp in Abhängigkeit vom Ko-Rezeptor CD14 steuert. Darüber hinaus wiesen IRI-operierte *Cd14$^{-/-}$* Mäuse die entweder mit pLIVE oder pLIVE-h*BGN*-injiziert wurden weniger F4/80- und CD38-positive Zellen auf als die entsprechenden WT Kontrollen. In Unterstützung zu unseren Daten zeigten PAS-gefärbte Nierenschnitte von pLIVE oder pLIVE-h*BGN*-injizierten WT und *Cd14$^{-/-}$* Mäusen, dass Biglykan tubuläre Schäden in IRI in Abhängigkeit von CD14 hervorruft. Weiterhin zeigten IRI-operierte *Cd14$^{-/-}$* Mäuse reduzierte tubuläre Schäden im Vergleich zu WT Mäusen. In Korrelation zu diesen Daten bewirkte eine pLIVE-h*BGN*-Injektion in WT Mäusen eine Erhöhung der Serumkreatinin Level während

6

renaler IRI. Im Gegensatz dazu wurden signifikant verringerte Serumkreatinin Level in pLIVE oder pLIVE-h*BGN*-injizierten *Cd14*$^{-/-}$ Mäusen im Vergleich zu entsprechenden WT Mäusen nachgewiesen.

Zusammenfassend konnten wir in dieser Studie demonstrieren, dass CD14 ein neuer Ligand mit hoher Affinität für Biglykan in Makrophagen ist, der für alle untersuchten Biglykan-abhängigen inflammatorischen Signalwege über TLR2 und TLR4 erforderlich ist. *In vivo* steuert Biglykan die Expression von verschiedenen inflammatorischen Mediatoren über die Nutzung des Ko-Rezeptors CD14. Eine Ablation von CD14 inhibiert vollständig die Biglykan-induzierte renale Makrophageninfiltration und die M1 Makrophagenpolarisation und verbessert die Nierenfunktion durch eine Reduzierung von tubulären Schäden und gesenkten Serumkreatininspiegeln. Daher identifiziert diese Studie CD14 als ein neues vielversprechendes therapeutisches Ziel um eine Biglykan-induzierte Inflammation aufzuheben.

Ob eine sterile oder Pathogen-induzierte Inflammation während der angeborenen Immunantwort andauert, ist von einem Gleichgewicht zwischen inflammatorischen und krankheitsrückbildenden Signalwegen abhängig. Eine unkontrollierte Inflammation führt zu verschiedenen inflammatorischen Krankheiten und zu Chronifizierung oder Autoimmunität. Daher existieren verschiedene Mechanismen und Proteine, die eine stringente Regulation der inflammatorischen Antwort bewerkstelligen. Ein solches Protein ist ABIN-1, ein leistungsstarker Inhibitor der Inflammation, der die TLR-induzierte NF-κB Signalgebung unterdrückt. ABIN-1 inhibiert Inflammation und Apoptose durch die Bindung von polyubiquitinierten Proteinen anhand seiner Ubiquitin Bindungsdomäne in ABIN und NEMO (UBAN). Dadurch bewirkt ABIN-1 eine Inaktivierung oder proteasomale Degradation der Zielproteine. Die UBAN Domäne von ABIN-1 zeigt Sequenzhomologien zu derer, die auch in Optineurin vorhanden ist, welches ebenfalls in der NF-κB Inhibierung beteiligt ist aber auch als selektiver Autophagie-Rezeptor fungiert. Da selektive Autophagie in der Regulation von Inflammation bei einer großen Zahl von inflammatorischen Krankheiten impliziert wird, haben wir uns entschlossen die Rolle von ABIN-1 in der selektiven Autophagie zu analysieren.

Im zweiten Teil dieser Arbeit analysierten wir das Interaktom von ABIN-1 während einer Pathogen-induzierten Inflammation in Milzproben und verglichen das komplette Proteom von Makrophagen aus WT und ABIN1[D485N] Mäusen unter basalen Konditionen. ABIN1[D485N] Mäuse tragen eine Mutation in ABIN-1, die das Protein unfähig macht Polyubiquitin zu binden. Erstaunlicherweise zeigte die Interaktomanalyse, dass ABIN-1 an zahlreiche Proteine bindet, die an Autophagie beteiligt sind, wie z.B. Proteine der ATG8 Familie, sowie Bindungen zu Proteinen, die in der selektiven Degradierung von schadhaften Mitochondrien beteiligt sind. Zusätzlich zeigte die Proteomanalyse, dass einige Autophagie-assoziierte Proteine in

Makrophagen von ABIN1[D485N] Mäusen hochreguliert waren. Daher postulierten wir, dass ABIN-1 durch eine simultane Bindung von polyubiquitinierten Cargo und ATG8 Proteinen als selektiver Autophagie-Rezeptor fungiert, der den zielgerichteten Transport und die selektive Degradation von Zielproteinen durch Autophagie bewirkt. Sequenz-Analysen von ABIN-1 deckten auf, dass ABIN-1 zwei bisher unbeschriebene *LC3-interacting region* (LIR) Motive besitzt. Durch Ko-Immunopräzipitationsstudien (Co-IP) in HeLa Zellen, die HA-getaggtes ABIN-1 exprimieren, konnten wir eine Komplexbildung zwischen ABIN-1 und LC3B in einer LIR-abhängigen Weise zeigen. Einhergehend damit konnten wir durch eine reziproke Co-IP diese Komplexbildung bestätigen. Durch die Verwendung von bakteriell exprimierten ABIN-1 und GST-getaggtem LC3A und LC3B zeigten wir, dass ABIN-1 direkt an LC3A und LC3B bindet. Eine Mutation beider LIR Domänen von ABIN-1 hob diese Bindung auf, währenddessen die Bindung zu Ubiquitin unbeeinträchtigt blieb. Zusätzlich beeinträchtigte eine Mutation der UBAN Domäne von ABIN-1 die Bindung zu LC3A oder LC3B in keiner Weise. Mit Hilfe von konfokaler Mikroskopie konnten wir in HeLa Zellen, die mit BafilomycinA1 oder Torin-1 stimuliert wurden, eine Kolokalisation von mEGFP-ABIN-1/mCherry-LC3B oder mEGFP-ABIN-1/LAMP 1 visualisieren und damit validieren, dass ABIN-1 in LC3B-positiven Autophagosomen und LAMP-1-positiven Autophagolysosomen lokalisiert ist. Darüber hinaus zeigten Western Blot Analysen von ABIN-1 und p62, dass die Proteinlevel von ABIN-1 durch Applikation des Autophagosom-Lysosom Inhibitors BafA1 zu verschiedenen Zeitpunkten erhöht vorliegt. Daneben wurde der autophagische Fluss von ABIN1- und p62 Proteinen nach Behandlung mit BafA1 mit oder ohne Rapamycin nach 4 h validiert. Als Bestätigung unserer Daten aus der Massenspektrometrie konnte eine Involvierung von ABIN-1 bei der Mitophagie anhand einer Translokation von ABIN-1 zu schadhaften Mitochondrien in Folge von Oligomycin/Antimycin A (OA) Behandlung in HeLa Zellen, die mCherry-Parkin stabil überexprimieren, gezeigt werden. Eine CRISPR/Cas9-vermittelte Deletion von ABIN-1 in mCherry-Parkin exprimierenden Zellen zeigte nach OA Applikation, dass ein Verlust von ABIN-1 die selektive Degradierung von *mitochondrial outer membrane* (OMM) Proteinen durch Mitophagie signifikant verlangsamt. Die FACS Analyse von HeLa Zellen, die Parkin und den Fluoreszenzreporter mt-mKEIMA exprimieren, zeigte, dass ein siRNA-vermittelter Knockdown von ABIN-1 den Anteil an lysosomal-positiven Mitochondrien während der Mitophagie verringert. Dagegen konnte eine FACS Analyse in HeLa Zellen mit dem Reporter mKEIMA-LC3B keine Effekte eines Knockdowns von ABIN-1 auf die gesamtheitliche Autophagie demonstrieren.

Zusammengefasst zeigen wir zum ersten Mal, dass ABIN-1 direkt an ATG8 Proteine über zwei bisher unbekannte LIR Domänen bindet und speziell in Autophagosomen und Autophagolysosomen lokalisiert, sobald Autophagie induziert wird. Darüber hinaus werden ABIN-1 Proteinlevel über den autophagischen Abbauweg reguliert. Abschließend zeigen wir,

dass eine Translokation von ABIN-1 zu beschädigten Mitochondrien, die Degradierung von OOM Proteinen während der Mitophagie reguliert, und dass ABIN-1 die mitophagische Aktivität direkt beeinflusst. Diese Arbeit identifiziert damit ABIN-1 als neuen selektiven Autophagie-Rezeptor für beschädigte Mitochondrien und stellt die Basis bereit für nachfolgende Studien, die die Involvierung von selektiver Autophagie in der ABIN-1-vermittelten Inhibition von Inflammation aufklären könnten.

2 Introduction

2.1 Proteoglycans

Proteoglycans (PG) are macromolecules mainly found in the extracellular matrix or on the cell surface consisting out of a core protein with one or more covalently linked glycosaminoglycan (GAG) chains. GAGs are built of linear negatively charged polysaccharide chains made of repeating disaccharide building blocks either highly sulfated or non-sulfated, resulting in the differentiation between heparan sulfate (HS), heparin (He), chondroitin sulfate (CS), dermatan sulfate (DS), keratan sulfate (KS) or hyaluronic acid (hyaluronan) [1, 2]. The multitude of combinations of protein cores with or without different GAG chain subtypes provides the structural basis for a plethora of biological processes in which PGs are involved. PGs are not only classified by their protein core, or GAG chain composition but also by their cellular and subcellular localization, dividing them into 4 different classes: Intracellular, cell surface, pericellular or extracellular PGs [1, 3]. Up to now, serglycin represents the only intracellular PG with functions in protease packaging and the regulation of inflammation [4, 5]. Cell surface PGs are associated with cell adhesion and migration and facilitate the binding of various growth and morphogenic factors to their respective receptors [6]. Similar, functions are reported for pericellular PGs which are closely connected to the cell surface either by being anchored through integrins and receptors or through their localization in the basement membrane zone [6, 7]. In contrast, extracellular PGs have a fundamental role as structural constituents of tendon or cartilage by binding to fibrous matrix proteins like collagen [8-10]. Extracellular PGs contain the subgroup of small leucine-rich PGs (SLRPs) which bind to cell surface receptors, growth factors, cytokines and various other components of the ECM, thereby affecting a multitude of biological processes such as cell proliferation, migration, adhesion, differentiation, cancer, innate immunity and inflammation [1, 11-16].

2.2 Biglycan

Biglycan is a ubiquitously expressed extracellular matrix-derived protein which belongs to the class I small leucine-rich proteoglycans (SLRPs) [1, 6, 17, 18]. It is built of 10 leucine-rich repeats (LRRs) with a core protein size of 42-kDa and harbors one or two tissue specific chondroitin sulfate and/or dermatan sulfate GAG side chains, covalently bound to its N-terminus [19-21]. The protein core of biglycan facilitates various interactions to collagen types such as I, II, III and VI or elastin to mediate collagen fibril assembly and its fragmentation [22-27]. Therefore, it is of no surprise that biglycan knockout mice display an abnormal phenotype

with structural anomalies in collagen fibrils of bone and tendon together with decreased bone length and mineral density [28, 29]. The interactions of biglycan to fibrous matrix proteins lead to its tight sequestration into the ECM of most organs, providing stability and organization [30]. Over the past years, it became increasingly clear that biglycan originally thought to be merely a structural element of the ECM, exerts potent signaling capabilities. Biglycan interacts with Toll-like receptors 2/4 [31], various cytokines like tumor necrosis factor (TNF)-α, growth factors such as transforming growth factor β (TGF-β) [32, 33] or vascular endothelial growth factor (VEGF) [34], bone morphogenetic protein (BMP)-2, -4, -6, chordin [35-38], Wnt-1-induced secreted protein 1 (WISP1) [39], Wnt3a/LRP6 [40], activin like kinase 6 (ALK6) [36] and class A scavenger receptor (SR-A) [41]. Through this magnitude of interactions biglycan modulates various biological processes, for example osteogenesis [34-36, 42], degeneration or loss of muscle tissue [43, 44], synapse stability [45], angiogenesis [34, 46, 47], cell growth [14, 48, 49], tumorigenesis [14, 50], autophagy [12, 14, 51] and inflammation [11, 16, 31, 52].

2.2.1 Soluble biglycan - an endogenous danger signal from the matrix

Under physiological conditions, biglycan is tightly bound to the ECM. In contrast, following tissue stress and injury biglycan is liberated from its ECM-bound form mainly by proteolytic cleavage by proteinases [52] or *de novo* synthesis of soluble biglycan in macrophages and resident cells [31]. So far, many proteinases are identified which mediate the proteolytic cleavage of biglycan into fragments such as BMP-1, matrix metalloproteinase (MMP)-2, MMP-3, MMP-8, MMP-9, MMP-12-14, a disintergrin and metalloproteinase with thrombospondin motifs (ADAMTS)-4, ADAMTS-5 and granzyme B [52]. Accordingly, soluble biglycan is released into the circulation during inflammatory conditions [31, 53]. The fact that soluble biglycan can be found in the bloodstream or synovial fluid in many acute or chronic inflammatory diseases gave rise to the evaluation of biglycan as a potent biomarker for inflammation [52-62]. Once freed from the ECM, soluble biglycan operates as a damage-associated molecular pattern (DAMP) and engages the innate immune pattern recognition receptors (PRRs) TLR2 and TLR4 on macrophages [31], dendritic cells [63] or chondrocytes [53], thereby mimicking the microbial gram-positive and gram-negative response [31]. Notably, only fully glycanated biglycan seems to be able to activate TLR2/4 [53, 64]. Downstream of the engagement with TLR2/4, soluble biglycan triggers the activation of mitogen-activated protein kinase (MAPK) p38, extracellular signal-regulated kinase (Erk) and nuclear factor kappa-light-chain enhancer of activated B cells (NF-κB) [31, 53, 64, 65]. In turn, this leads to the expression of various pro-inflammatory cyto- and chemokines like interleukin (IL)-1β, TNF-α, chemokine (C–C motif) ligand (CCL)2, CCL3, CCL5 as well as chemokine (C-X-C motif) ligand (CXCL)1, CXCL2 and CXCL13 [31, 53, 61, 66]. As a consequence, immune cells such as neutrophils, T cells, B cells and macrophages are recruited into the inflamed tissue [31, 53, 61, 66, 67].

Interestingly, biglycan-induced inflammation extends to various chronic and acute inflammatory pathologies such as lupus nephritis (LN) [53, 62], diabetes [54, 62, 68], autoimmune perimyocarditis [69], calcified aortic valve disease (CAVD) [70], atherosclerosis [71, 72], fibrosis [64, 73], sepsis [31] and renal ischemia/reperfusion injury (IRI) [61, 74].

2.2.2 TLR and TLR adaptor molecules orchestrate biglycan-mediated signaling

Mounting evidence over the past years brought to light that biglycan-induced downstream signaling is tightly regulated by selective interaction of biglycan with TLR2/4 and their adaptor proteins adaptor molecule myeloid differentiation primary response gene 88 (MyD88) or TIR domain-containing adaptor-inducing interferon-β (TRIF) (Fig. 2.1) [62, 66, 67, 74] .

Biglycan clusters the purinergic receptors $P2X_7/P2X_4$ with the innate immune receptors TLR2/4 to induce the NOD-like receptor pyrin domain-containing-3 (NLRP3) inflammasome, followed by caspase-1 activation, leading to the release of mature IL-1β [64]. Later studies could show that biglycan triggers the expression and maturation of IL-1β over TLR2/4 through NADPH oxidase (NOX)1/NOX4-derived reactive oxygen species (ROS) production in macrophages [74]. At the same time, biglycan induces an anti-inflammatory effect by restricting the expression and maturation of IL-1β by triggering *Nox2* expression in a TLR4/TRIF-dependent manner. In a second step, NOX2 is activated via TLR4/MyD88 and inhibits the biglycan-induced expression of IL-1β [74]. Surprisingly, biglycan counteracts its anti-inflammatory effect by inducing heat shock protein 70 (HSP70) expression in a TLR2-dependent manner. HSP70 binds to NOX2 and impairs its inhibitory function on biglycan-induced IL-1β expression. Accordingly, NOX2 deficient mice lacking endogenous biglycan display lower *Ccl2* and *Il1β* levels and are protected from the hyper-inflammatory phenotype as well as macrophage infiltration in a model of renal IRI [74].

Moreover, biglycan works in concert with sphingosine kinase (SphK)1-mediated lipid signaling to regulate the expression of CCL2 and CCL5 [67]. Biglycan triggers by selective utilization of TLR4/TRIF the expression of SphK1. In return, SphK1 impacts on biglycan-driven *Ccl2* and *Ccl5* expression by affecting biglycan-mediated downstream signaling of p38, Erk1/2 and NF-κB. Importantly, Sphk1 deficient mice exhibit reduced *Ccl2* and *Ccl5* levels as well as renal macrophage infiltration after biglycan-overexpression [67].

Overexpression studies with biglycan support the notion that biglycan regulates immune cell infiltration by selective interaction with TLRs and TLR adaptor proteins. Studies with MyD88, TRIF and double-deficient mice revealed that biglycan triggers renal neutrophil infiltration in a MyD88-dependent manner while T cell and macrophage recruitment is regulated exclusively
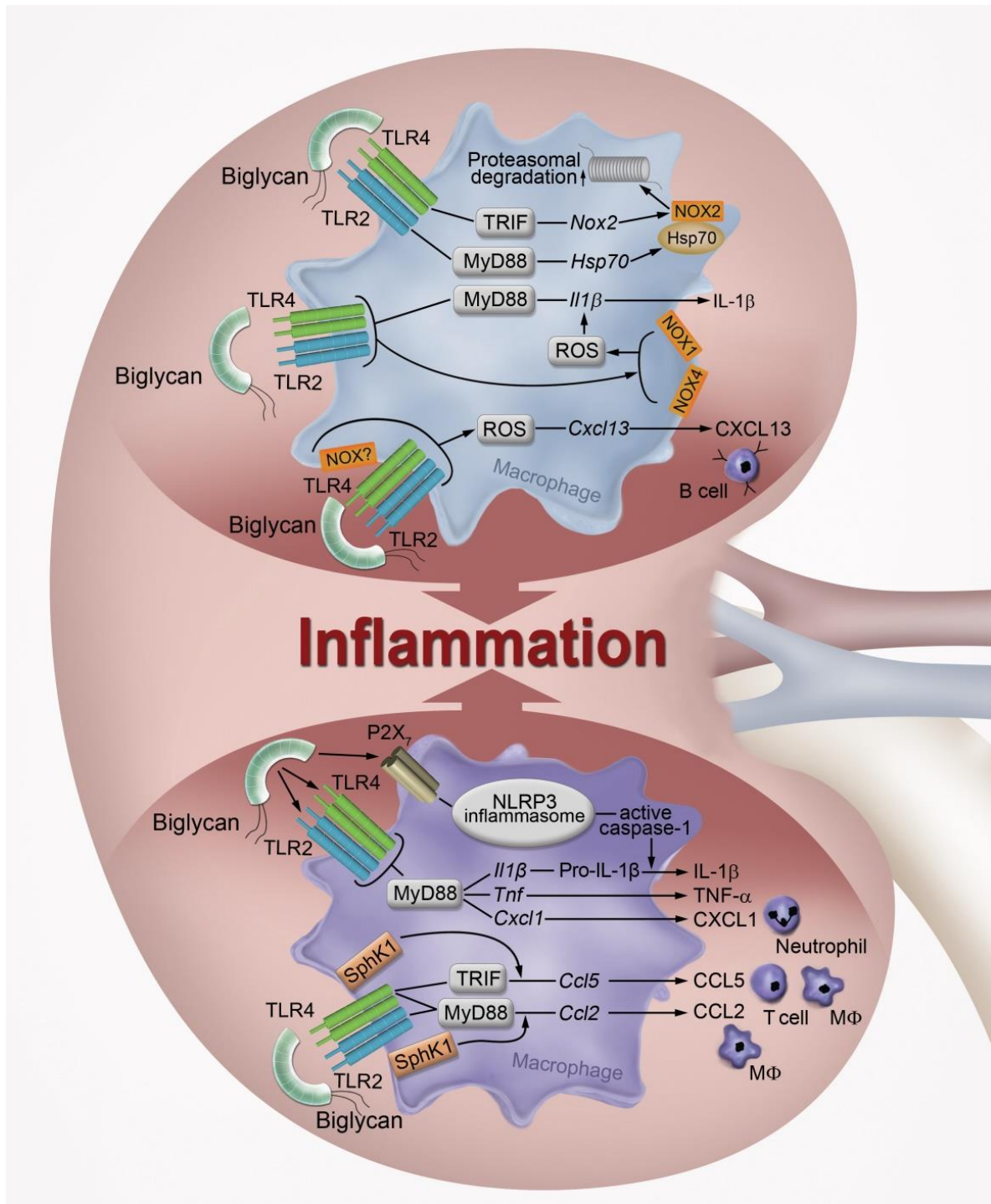
Figure 2.1. Biglycan-induced signaling in renal inflammation. (Upper panel) In macrophages, soluble biglycan induces the expression of NOX2 via TLR4/TRIF and Hsp70 expression by signaling exclusively over TLR2/MyD88. Interaction of Hsp70 and NOX2 leads to proteasomal degradation. Biglycan triggers IL-1β production over TLR2/4/MyD88 by involving TLR2/4-dependent NOX1-/NOX4-derived ROS. Additionally, biglycan leads to the synthesis of CXCL13 over TLR2/4/NOX, thereby promoting B cell recruitment. (Lower panel) Soluble biglycan induces pro-IL-1β, CXCL1 and TNF-α production in a TLR2/4/MyD88-dependent manner. At the same time, biglycan clusters the purinergic receptor P2X7 with TLR2/4 to induce the NLRP3 inflammasome, consequently leading to the activation of caspase-1 and to the maturation of IL-1β. Furthermore, by cross talk with SphK1, biglycan utilizes TLR2/4/MyD88 to trigger the production of CCL2, whereas CCL5 synthesis is mediated solely over TLR4/TRIF. In turn, the release of CCL5 and CCL2 promotes the recruitment of macrophages and T cells. Figure is reproduced from [11].

via MyD88 and TRIF [66]. A recent study utilizing a murine model of lupus nephritis in combination with biglycan overexpression or deficiency showed that biglycan is a portent trigger of renal Th1 and Th17 cell recruitment [62]. In macrophages, biglycan triggers the expression and secretion of CXCL9 and CXCL10 in a TLR4/TRIF-dependent manner, leading to the infiltration of chemokine (C-X-C) motif receptor 3 (CXCR3)-positive Th1 and Th17 cells into the kidney. Consequently, Th1 and Th17 cells release interferon (IFN)-γ and IL-17, respectively. IFN-γ creates with biglycan a positive feedback loop to induce the expression of CXCL9, subsequently leading to Th1 and Th17 recruitment. In contrast, biglycan triggers renal CCR6-positive Th17 cell infiltration by inducing the expression of CCL20 over TLR2/4/MyD88 [62].

Interestingly, a current study shows that biglycan induces autophagy by binding to the cell surface glycoprotein CD44 with high affinity [51]. In macrophages, biglycan triggers autophagy in a TLR4/CD44-dependent manner, thereby regulating cytokine levels [51]. Moreover, stable overexpression of biglycan was marked with increased infiltration of macrophages in various organs and elevated autophagy levels. Despite the role of biglycan as a classical TLR-dependent DAMP during inflammation, *in vivo* experiments using a mouse model of renal IRI showed that biglycan-induced macrophage autophagy triggers tissue repair by impacting on the polarization of infiltrating macrophages, consequently lowering renal damage [51].

Furthermore, engagement of biglycan with TLRs is also found in non-immune cells. By selective interaction with TLR2, biglycan triggers the synthesis of erythropoietin (Epo) in the kidney and liver [75]. This is caused by biglycan-mediated stabilization of hypoxia-inducible factor (HIF)-2α on protein level in a TLR2-dependent manner. Constitutive overexpression of biglycan in mice gives rise to secondary polycythemia, evident by an increased abundance of red blood cells, enhanced total iron binding capacity and elevated hemoglobin concentrations in the blood [75].

2.3   Toll-like receptors

Toll-like receptors (TLRs) are a family of PRRs receptors originated from the toll gene family identified in *Drosophila melanogaster* [76, 77]. PRRs such as TLRs, NOD like receptors (NLR) and RIG like receptors (RLR) play a crucial role in innate immunity by sensing distinct pathogen-associated molecular patterns (PAMPs) and DAMPs as well as discriminate between self- and non-self-antigens [78]. TLRs have a typical structure containing an extracellular leucine-rich repeat domain, responsible for ligand recognition and an intracellular Toll/IL-1R homology (TIR) domain which mediates TLR downstream signaling pathways [79, 80]. There are more than 10 TLRs described which have different cellular localization patterns and are expressed in immune cells like macrophages, T and B cells, natural killer (NK) cells

as well as in non-immune cells such as epithelial cells and endothelial cells [78]. TLRs can be grouped according to their localization into those that are expressed either at the cell surface (TLR1, TLR2, TLR4, TLR5 and TLR6) or cytosolic compartments like endosomes (i.e. TLR3, TLR7, TLR8 and TLR9). Engagement of PAMPs or DAMPs with TLRs at their ectodomain triggers receptor dimerization of the TIR domains. Subsequently, the association of the TIR-TIR domains provides scaffold for a variety of adaptor proteins such as MyD88, MyD88 adaptor-like molecule (MAL), TRIF, TIR domain–containing adaptor molecule (TIRAP) and TRIF-related adaptor molecule (TRAM), leading to either NF-κB or interferon regulatory factor (IRF) activation [80]. Ultimately, this leads to the induction and secretion of various pro-inflammatory cytokines, chemokines and co-stimulatory molecules as well as anti-inflammatory mediators to create an effective immune response [77, 81, 82].

Ligand recognition and signaling of TLR2 is mediated by heterodimerization with TLR1, TLR6 or TLR10 on the cell surface, followed by internalization of the receptor complex into endosomes [83, 84]. In general, TLR2 heterodimers with TLR1 are formed when recognizing triacylated lipopeptides from gram-negative bacteria, while TLR2-TLR6 complexes are formed in response to diacylated lipopeptides from gram-positive bacteria [85, 86]. This differentiation is mediated by different binding pockets of TLR1 and TLR6. Consequently, this enables TLR2 to bind to a broad range of microbial agonists but as well endogenous ligands including high-mobility group box 1 protein (HMGB1), HSP70, biglycan, versican and decorin [31, 86-89]. The variety of ligands that TLR2 recognizes is expanded by its ability to form heterodimers with co-receptors such as cluster of differentiation (CD) 36, CD14, integrins or Dectin-1 [90-93]. Notably, CD14 and CD36 are primarily not absolutely necessary for TLR2 ligand recognition, they rather lower the threshold of required ligand concentrations to activate TLR2 and amplify the signaling [83, 86, 94, 95]. For example the recognition of ligands like dUTPase from Epstein-Barr virus [96], FSL-1 lipopeptide [94] or *Toxoplasma gondii glycosylphosphatidylinositols* by TLR2 is independent on the presence of CD14 [97].

The ligand spectrum of TLR4 ranges from PAMPs such as bacterial components like the bacterial lipopolysaccharide (LPS) from gram-negative bacteria [98] to viruses und fungi. Furthermore, TLR4 binds a variety of endogenous ligands including hyaluronan, biglycan, fibronectin and HMGB1 [31, 99-101]. Signaling of TLR4 is initiated by receptor homodimerization which induces mutual interactions of the TIR domains. Importantly, TLR4 is the only TLR which involves both the MyD88/NF-κB- and TRIF/IRF3-dependent pathway with their respective adaptor proteins TIRAP and TRAM [85, 102]. Moreover, TLR4 forms a complex at the cell surface with several different co-receptors such as CD14 and myeloid differentiation 2 (MD2) to detect specific ligands. Notably, the availability of CD14 is not a requirement for ligand recognition via TLR4. For instance, ligands such as hyaluronan are independently recognized by TLR4 without the need of CD14 [103].

TLRs are essential PRRs of the immune system, counteracting infection with an early inflammatory response [104], while at later stages they initiate the adaptive immune response [105]. Therefore it is of no surprise that dysregulated TLR2 and TLR4 signaling is associated with various autoimmune diseases like rheumatoid arthritis (RA) [106], systemic lupus erythematosus (SLE) [107], diabetes [108] or multiple sclerosis (MS) [109, 110]. Moreover, TLR2 and TLR4 signaling is an important modulator of infectious diseases like sepsis and non-infectious diseases such as IRI, atherosclerosis, osteoarthritis or Alzheimer's disease [111]. Given the role of TLR2 and TLR4 in the regulation of inflammation they became very attractive pharmacological targets in order to control acute and chronic inflammatory diseases in which excessive chemo- and cytokine production plays a role [110, 112-114].

2.4   Cluster of differentiation 14 (CD14)

CD14 is a glycosylphosphatidylinositol-anchored glycoprotein containing 10 leucine-rich repeats in its structure [115]. It is primarily expressed in monocytes, macrophages and neutrophils [115] and exists either as a membrane bound or soluble form (sCD14) in a variety of body fluids [116]. CD14 belongs to the class of PRRs of the innate immune system and is best known for its prominent role as a co-receptor in mediating LPS delivery to the TLR4/MD2-complex, yet on itself cannot induce downstream signaling [117, 118]. Upon binding to the LPS-binding protein (LBP) LPS is disaggregated and transferred as LPS monomers to CD14. This greatly enhances the efficiency of CD14 binding to LPS [119, 120]. In turn, CD14-LPS complexes are delivered to the TLR4/MD2 complex [121], triggering its dimerization and activation of the MyD88-dependent pathway, thereby resulting in the production of pro-inflammatory cyto- and chemokines as well as adhesion molecules to mediate a local clearance of pathogens [95, 122]. Afterwards, the LPS/TLR4/MD2 complex is internalized by endocytosis in a CD14-dependent manner [123] and triggers the TRIF-dependent pathway, leading to type I interferons production [124]. Consequently, CD14 mediates both ligand delivery and internalization of the TLR4 complex. Besides the beneficial effects of LPS recognition by CD14, the activation of TLR4/CD14/MD2 during sepsis leads to an uncontrolled cytokine storm, ultimately inducing organ failure [112]. Accordingly, CD14 deficient mice are protected in response to otherwise lethal doses of LPS, showing a reduced pro-inflammatory cytokine production such as TNF-α and IL-6 and an overall mitigated systemic septic shock [125].

Apart from TLR4, CD14 functions as a co-receptor for TLR2, TLR3, TLR7 and TLR9 [117]. For instance, CD14 induces heterocomplex formation of CD14/TLR2/TLR1 in order to detect triacylated lipoproteins while the CD36/CD14/TLR2/TLR6 complex is triggered by lipoteichoic acid as well as diacylated lipoproteins [117]. Furthermore, the CD14/TLR2 complex is involved

in pro-inflammatory signaling of carcinoma-derived versican in myeloid cells [126] and Alzheimer´s disease [127]. Moreover, CD14 mediates pro-inflammatory cytokine production in mouse immune cells over TLR7 and TLR9 as well as the TLR9-dependent innate immune response in mice [128]. Similarly, CD14 is important for inflammatory cytokine production in macrophages and mice in response to polyinosine-polycytidylic acid (pIpC) exposure over TLR3 [129].

CD14 functions as an imperative element in inflammation and is involved in the pathogenesis of many inflammatory diseases such as sepsis, IRI, atherosclerosis and cancer [130, 131]. An activation or increase in the abundance of CD14 results in exacerbated inflammation though various mechanisms. For example, GM-CSF enhances CD14 expression in microglia, leading to the production of IL-1β, IL-6, TNF-α and nitric oxide (NO) and consequently to inflammation in the central nervous system [132]. Furthermore, CD14 is activated by iNOS during cerebral ischemia, in turn mediating NF-κB activation and TNF-α expression [133]. Beyond that, CD14 plays also an important role in the regulation of immune cells. For instance, the lectin ArtinM induces the polarization of pro-inflammatory M1 macrophages via TLR2 in a CD14-dependent manner [134]. CD14 regulates the synthesis of the pro-apoptotic factor Nur77 through LPS/NFAT activation in order to limit the life of differentiated dendritic cells, an effect particular important to control self-tolerance and autoimmunity [135]. Because of its broad involvement in inflammatory diseases, pharmacological targeting of CD14 became an attractive approach to limit inflammation [136-138].

However, CD14 exerts also anti-inflammatory effects. The absence of CD14 in macrophages lowers the amount of secreted IL-10 in response to *Borrelia burgdorferi* infection, leading to aggravated inflammation [139]. In the same way, CD14 deficiency in mice leads to higher chemokine production, pro-inflammatory cytokine secretion and higher neutrophil recruitment upon *P. aeruginosa* corneal infection [140]. In inflammatory bowel disease (IBD), *Cd14*^{-/-} mice show intestinal barrier dysfunction during inflammation paired with elevated pro-inflammatory cytokine expression [141]. In summary, these data show that the role of CD14 is not reducible to a potentiation of inflammation but rather complex and likely tissue and disease dependent. Further studies are needed to elucidate the exact functions of CD14 in health and disease and could result in a promising target for future therapies.

2.5   ABIN-1

A20 binding inhibitor of NF-κB1 (ABIN-1) or also termed TNIP1 (TNFα-induced protein 3-(TNFAIP3-) interacting protein 1) is an ubiquitously expressed protein located in the cytoplasm and in nuclear compartments [142]. ABIN-1 contains 4 functional domains that it shares with its homologues proteins ABIN-2 and ABIN-3, in turn named ABIN Homology Domains (AHD).

The AHD2 of ABIN-1 is characterized by the presence of an ubiquitin-binding domain of ABIN and NEMO (UBAN), which also shares high sequence homology to the ubiquitin-binding domain (UBD) in optineurin with presumed similar functions [143, 144]. In contrast, the AHD1 of ABIN-1 mediates the binding to A20 [143], a key regulatory enzyme of NF-κB [145]. Additionally, ABIN-1 contains a C-terminal NF-κB essential modulator (NEMO) binding domain (NBD) [146]. Through the capability to bind polyubiquitinated proteins via its UBAN domain and by involvement of the NBD and AHD1 domains, ABIN-1 acts as a key repressor of NF-κB signaling (Fig. 2.2) [144, 146-148].

The UBAN domain of ABIN-1 specifically interacts with polyubiquitin chains of at least 3 ubiquitin moieties [148, 149]. Furthermore, the UBAN domain recognizes ubiquitin in a linkage-dependent manner since only K63-linked as well as linear polyubiquitin chains (M1 linkage) but not K48-linked polyubiquitin chains are shown to bind to the UBAN domain of ABIN-1 [147]. Interestingly, in contrast to K48-chains which are known for proteasomal targeting of proteins, K63-linked polyubiquitin chains are thought to mediate signaling events by providing scaffold for protein complexes or activate kinases by inducing conformational changes in enzymes [150]. In fact, ABIN-1 does not exert enzymatic activity on its own but governs intracellular signaling by binding to the ubiquitin-editing enzyme A20 [151]. The ABIN-1/A20 complex binds and modifies polyubiquitinated proteins such as NEMO in order to impact on NF-κB signaling [146]. Other negatively regulated proteins by ABIN-1 which are dependent on polyubiquitin modification after TLR activation include TANK-binding kinase 1 (TBK1) [152], interleukin-1 receptor-associated kinase 1 (IRAK1) [147] and receptor-interacting serine/threonine kinase 1 (RIPK1) [149, 153]. In the complex, A20 cleaves K63-linked and at the same time constructs K48-linked polyubiquitin chains. Thereby, ABIN-1 represses the activity of NF-κB upstream signaling components by either dissolving K63-chain-mediated complex formation or triggering proteasomal degradation of protein interactors [144]. Binding of ABIN-1 to ubiquitin is nullified by mutation of the UBAN domain at conserved amino acids, in turn abolishing the inhibitory function of ABIN-1 on TNF-induced NF-κB signaling [143, 147]. Early studies showed that protein levels of ABIN-1 positively correlate with the A20-dependent deubiquitination of NEMO and inhibition of NF-κB, while a siRNA-mediated knockdown of ABIN-1 results in decreased A20-dependent removal of ubiquitin from NEMO and elevated NF-κB activity [146, 154].

Besides the importance of A20 for the inhibitory function of ABIN-1 on NF-κB signaling, ABIN-1 is also capable of inhibiting signaling events independently of A20. For instance, ABIN-1 deletion mutants lacking the AHD1 domain still show inhibitory activities on NF-κB [143]. Moreover, tamoxifen-induced deletion of ABIN-1 and or A20 in intestinal epithelial cells (IEC) showed that a double knockout of A20 and ABIN-1 causes IEC cell death and drastic mouse
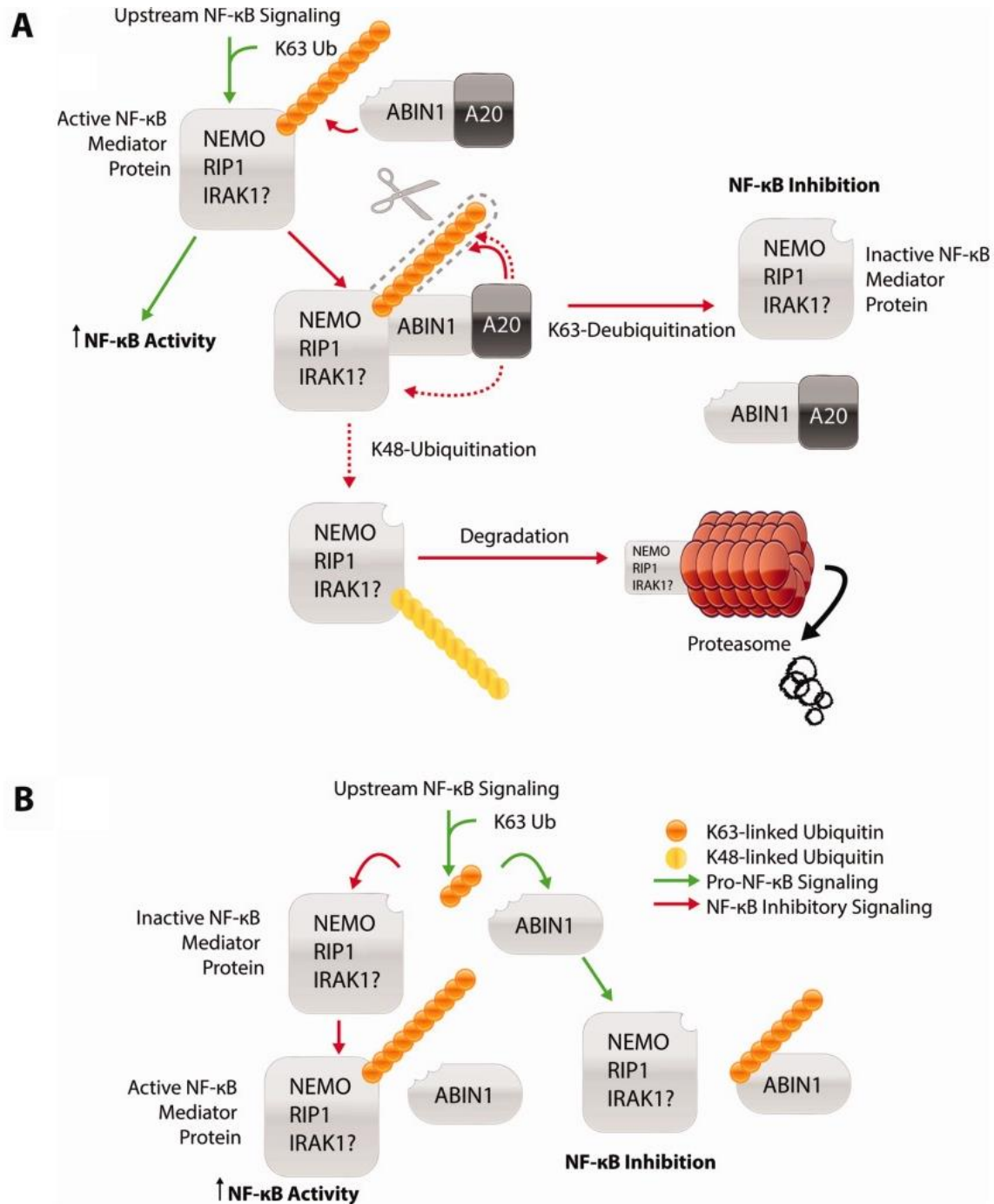
Figure 2.2. Mechanisms of ABIN1-mediated repression of NF-κB. (A) A20-dependent regulation of NF-κB by ABIN-1. ABIN-1 functions as an adaptor protein which tethers A20 to K63-polyubiquitinated active NF-κB mediators like NEMO and RIPK1 (RIP1). The same mechanism is proposed for IRAK1, indicated with a question mark. Accordingly, ABIN-1 promotes A20 recruitment to NF-κB mediators where it modifies ubiquitin by its two ubiquitin-editing domains. Through its enzymatic de-ubiquitinating activity A20 removes K63-linked ubiquitin chains from NF-κB mediators, thereby leading to their inactivation and inhibition of NF-κB signaling. Secondly, after K63-linked ubiquitin chains are cleaved off, A20 functions as an E3 ubiquitin ligase by polyubiquitinating NF-κB mediators with K48-linked ubiquitin chains. Proteins labeled with K48-linked ubiquitin chains are targeted for proteasomal degradation, thereby suppressing NF-κB activity. (B) A20-independent inhibition of NF-κB by ABIN-1 through competition. ABIN-1 competes with NF-κB mediator proteins for K63-linked ubiquitin chains, thus suppressing the activation of NF-κB mediators and subsequent NF-κB signaling. Figure is modified from [144].

mortality [155]. In contrast, either A20 or ABIN-1 alone were capable of compensating IEC cell death and decreasing mouse mortality. Additional experiments with enteroids revealed that A20 and ABIN-1 function synergistically in inhibiting apoptosis and necroptosis by restricting TNF-induced caspase 8 activation and RIPK1 activity [155]. As ABIN-1 compensated A20 loss in a dose-dependent manner to rescue cell survival, ABIN-1 clearly mediates A20-independent functions necessary for cell survival [155]. The ability of ABIN-1 to inhibit signaling events independently of A20 may be attributed to a competition for polyubiquitin binding between ABIN-1 and protein complexes which are dependent on polyubiquitination. Interestingly, this phenomenon is reported for ABIN-2 which competes with TRAF6 for K63-linked ubiquitin chains [154].

Negative regulation of ABIN-1 on TLR downstream molecules extends also on IRAK1 [147], TBK1 [152] and RIPK1 [149, 153]. In LPS-stimulated bone marrow-derived macrophages, interaction of IRAK1 with ABIN-1 is abrogated by mutating the UBAN domain of ABIN-1 [147]. Furthermore, loss of ubiquitin binding function of ABIN-1 abolished the interaction to K63-polyubiquitinated TBK1/IKKi, leading to increased activation of IRF3 and IFN-β production [152]. Similarly, the interaction of ABIN-1 to RIPK1 is lost upon UBAN domain mutation, thereby leading to increased cell death [149]. Later studies showed that ABIN-1 is recruited to the TNFR1-signaling-complex (TNF-RSC) in a M1-ubiquitin-dependent manner to recruit A20 which in turn deubiquitinates RIPK1. As a consequence, loss of ABIN-1 triggers necroptosis by promoting K63-linked polyubiquitination and activation of RIPK1 and RIPK3 [153].

Overreactive NF-κB signaling is associated with the pathogenesis and chronic inflammation in several autoimmune diseases including systemic sclerosis, psoriasis and SLE [156, 157]. Consistent with the findings that ABIN-1 regulates NF-κB signaling, gene targeting studies in mice revealed that alterations in ABIN-1 are associated with autoimmunity. Nanda et al. developed knock-in mice with an ABIN-1 mutant [D485N] defective in the UBAN domain consequently unable to bind polyubiquitin [147]. Even though these mice were born at normal ratios, they develop an age-associated form of severe autoimmunity with a lupus-like inflammatory phenotype characterized by enlarged spleen and lymph nodes, elevated levels of immunoglobulins and autoantibodies in the serum, spontaneous germinal center formation, higher B cell, monocyte and granulocyte numbers, overactivated B and T cells, complement activation and glomerulonephritis [147]. Mechanistically, immune cells in ABIN1[D485N] mice display an increased TLR/MyD88-mediated NF-κB activation which could be rescued by crossing to MyD88 deficient mice, underlining the pivotal role of polyubiquitin binding of ABIN-1 in suppressing autoimmunity [147]. In line with this, ABIN-1 knockout mice show high levels of embryonic lethality, while live born animals perish within 4 months. Live born mice show a cachectic disease marked by various characteristics of SLE [158], highly similar to the phenotype observed by Nanda et al. [147]. Moreover, several other studies closely link ABIN-1

polymorphism to SLE and underline its role in autoimmunity [159-161]. Similarly, loss of ABIN-1 polyubiquitin binding function in human-derived cultured podocytes leads to the expression of NF-κB-dependent cyto- and chemokines in response to TNF-α, resembling human SLE and glomerulonephritis kidney samples [162]. Interestingly, crossing ABIN1[D485N] mice to mice with catalytic inactive mutant forms of the TLR downstream mediators IRAK1 or IRAK4 inhibits autoimmunity and inflammation [163].

Mice, engineered with a dendritic cell-specific ABIN-1 knockout challenged with TLR ligands show an enlargement of the spleen and abnormal lymph nodes, similar to whole ABIN-1 knockout mice, as well as several key signs of psoriasis such as prosaic lesions, Th17 cell differentiation as well as altered neutrophil recruitment and proliferation [164]. Dendritic cells (DCs) lacking ABIN-1 display overreactive NF-κB and MAPK signaling paired with increased IL-23 levels, which could be rescued by DC-specific ablation of MyD88 [164], supporting the mechanistic findings from other mouse models [147]. Additionally, ABIN-1 also plays a role in non-immune cells. By using mice with keratinocyte-specific ABIN-1 deletion, it was shown that ABIN-1 critically contributes to the pathogenesis of psoriasis by regulating IL-17 expression [165].

ABIN-1 polyubiquitin binding also impacts on cell death. By inhibiting TNF-induced FADD-caspase 8 binding though polyubiquitin binding, ABIN-1 protects mice from programed cell death during late embryogenesis [149]. Mice lacking ABIN-1 display high embryonic mortality but are rescued by crossing to a background with TNFR1 deletion [149].

The phenotypes observed in ABIN-1 knockout and knock-in gene targeting studies seem to be restricted to ABIN-1. ABIN-2 knockout mice are phenotypically inconspicuous and display no inflammatory symptoms [166]. Recently, ABIN-2 knock-in mice with mutated UBAN domain were shown to be hypersensitive to DSS-induced colitis [167]. However, ABIN-2 does not contribute to NF-κB inhibition in mice [166] and ABIN-3 misses the UBAN domain required for polyubiquitin binding [168]. Thus, NF-κB suppression is a unique feature of ABIN-1 and seems to be a trigger for autoimmunity and inflammation if absent [144].

2.6   Autophagy

Autophagy defines a process of lysosomal degradation involving cytoplasmatic material from the size of single proteins up to whole organelles such as mitochondria [169]. Autophagy is triggered as a consequence of intra- or extracellular stress conditions including hypoxia, starvation, growth factor depletion or osmotic stress in order to maintain cellular homeostasis. Autophagy can be divided into chaperone-mediated autophagy, microautophagy and macroautophagy. Chaperone-mediated autophagy relies on the delivery of cytoplasmatic soluble proteins directly into lysosome via a KFERQ-like motif [170], while microautophagy

mediates the engulfment of cytoplasmatic material into lysosomes or endosomes in a selective or unselective fashion through membrane invagination [171]. In contrast, macroautophagy (in the following referred to as autophagy) describes the molecular process in which double-membraned vesicles called autophagosomes engulf cytoplasmic components. After lysosomal fusion, the enclosed material is degraded into its constituting amino acids, thereby being recycled for metabolic processes or becoming available as a source of nutrients [172].

Autophagy can be classified into non-selective bulk autophagy and selective autophagy. Bulk autophagy is characterized by the random uptake of cytoplasmic cargo and is induced mainly by nutrient or glucagon deprivation [172-174], in turn contributing to intracellular homeostasis by restoring amino acid availability [172, 175]. On the other hand, selective autophagy specifically targets certain components such as protein aggregates and damaged or excessive organelles into autophagosomes. Up to now the bandwidth of selective autophagy includes the degradation of protein aggregates (aggrephagy) [176], mitochondria (mitophagy) [177, 178], peroxisomes (pexophagy) [179], lysosomes (lysophagy) [180], ribosomes (ribophagy) [181], secretory granules (zymophagy) [182], ER (ER-phagy) [183], nuclear laminas (nuclear lamina autophagy) [184], midbody rings (midbody autophagy) [185], ferritin (ferritinophagy) [186], glycogen (glycophagy) [187] and invading pathogens such as bacteria (xenophagy) [188] or viruses (virophagy) [169, 189]. Considering the broad cellular involvement of autophagy it is of no surprise that dysregulated or impaired autophagy has been implicated in a broad range of biological processes and diseases such as atherosclerosis, diabetes [190], cancer [191], muscular disorders, ischemia, acute and chronic inflammation [192], neurodegeneration [193] and ageing [194].

Mechanistically, induction of autophagy leads to five major steps in autophagosome formation namely i) initiation and nucleation, ii) expansion and cargo sequestration, iii) sealing and maturation, iv) fusion and v) degradation including 15 core autophagy-related proteins (ATGs) (Fig. 2.3) [195]. Initiation of the Unc-51-like kinase 1 (ULK1) complex consisting out of ULK1, ATG13, RB1-inducible coiled- coil protein 1 (FIP200) and ATG101 is commonly triggered by inhibition of the MTOR complex 1 (mTORC1), a potent inhibitor mediating the inactivating phosphorylation of ATG13 and ULK1 [196, 197]. Formation of the ULK1 complex induces the phosphorylation of complex II member ATG9, thereby leading to the elongation of pre-autophagosomal membranes through absorption of lipids originating mainly from the ER [198]. This provides scaffold for the recruitment of the phagophore nucleation complex III consisting out of phosphatidylinositol 3-kinase catalytic subunit type 3 (PI3KC3), vacuolar protein sorting 34 (VPS34), ATG14, Beclin-1, activating molecule in Beclin-1-regulated autophagy protein 1 (AMBRA1) and general vesicular transport factor (p115) which trigger phosphatidylinositol-3-phosphate (PI3P) production at the characteristic ER structure, named the omegasome [171, 195]. Then, PIP3 supports the nucleation of the phagophore by recruiting complex IV)

members WD repeat domain phosphoinositide- interacting (WIPI) proteins and zinc- finger FYVE domain- containing protein 1 (DFCP1) via their PI3P-binding domains [199, 200].
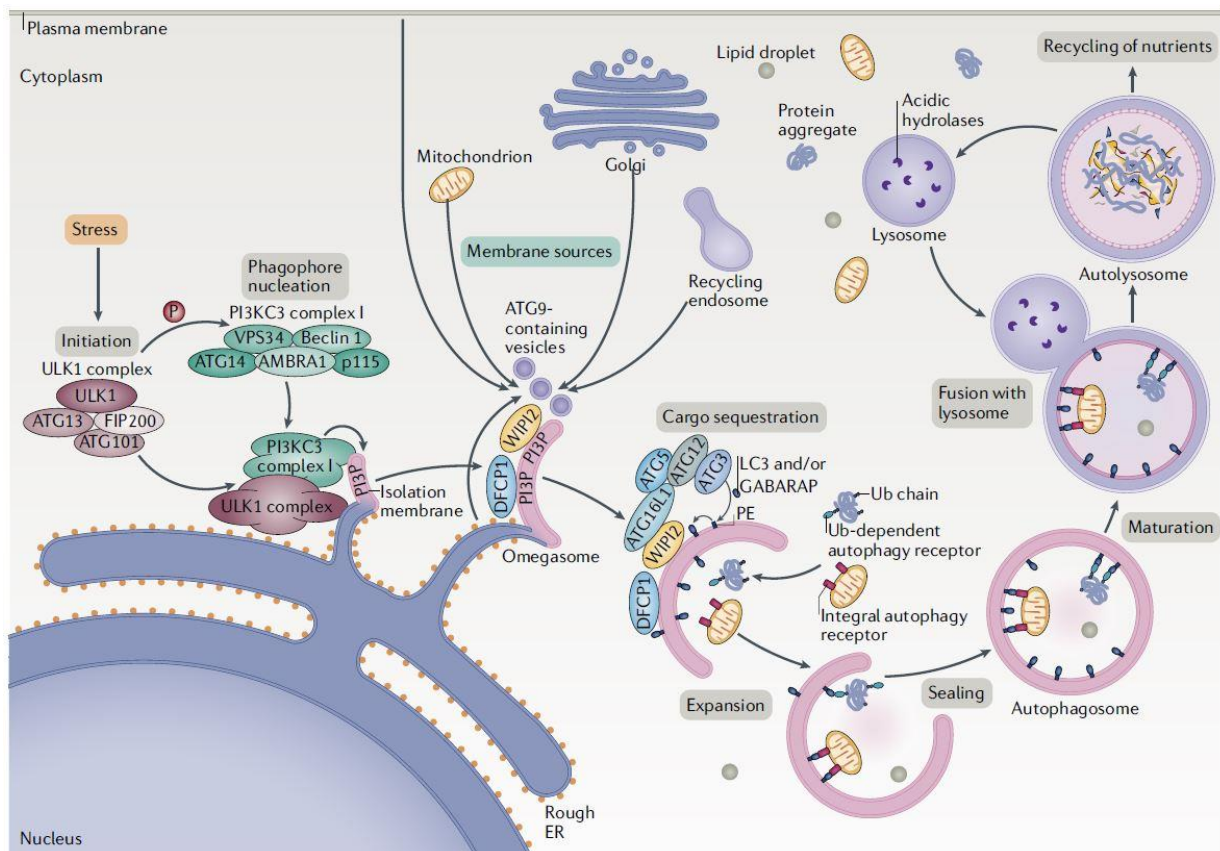
Figure 2.3. Mechanical insights into the molecular autophagy process. Autophagy is initiated by intra- or extracellular stress responses which activate the ULK1 complex consisting out of ULK1, ATG13, FIP200 and ATG101. In turn, the ULK1 complex phosphorylates the PI3KC3 complex including PI3K, VPS34, Beclin-1, ATG14, AMBRA1 and p115. Afterwards, the PI3KC3 and ULK1 complex induce PIP3 production at rough-ER membrane extensions (omegasomes) which serve as a platform for phagophore nucleation. PIP3 recruits WIPI proteins and DFCP1 to the omegasome. WIPI2 binds the AT16L1-ATG5-ATG12 complex, thereby stimulating the ATG3-mediated conjugation of ATG8 family proteins such as LC3 and GABARAP to membrane-bound PE (lipidation). At the same time, membrane material from the plasma membrane, mitochondria, recycling endosomes and Golgi complex is delivered to the phagophore, partially by ATG9-containing vesicles, to help in the elongation process of the autophagosomal membrane. ATG8 proteins not only attract LIR-containing proteins necessary for autophagosome generation but are essential components for the elongation and closure of the phagophore membrane. Additionally, ATG8 proteins are necessary for the recruitment of labeled cargo into the autophagosome via LIR-containing autophagy receptors either in a ubiquitin-dependent or -independent manner. Sealing of the phagophore results in a double-layered vesicle, named the autophagosome. During maturation, PIP3 and ATG8 proteins are removed from the autophagosome by phosphatases and proteases. Upon fusion with the lysosome resulting in an autophagolysosome the containing cargo is degraded by acidic hydrolases and released into the cytoplasm. In this way, the cargo is recycled and used as a source of nutrients for the cell. Figure is adapted from [195].

The major downstream effect of these protein complexes is the covalent attachment of ATG8-family proteins consisting out of microtubule- associated protein light chain 3 (MAP1LC3 or LC3) family proteins LC3A, LC3B and LC3C as well as the γ- aminobutyric acid receptor-associated protein (GABARAP) family GABARAP, GABARAPL1 and GABARAPL2 to the

forming phagophore membrane by lipidation. Once transition from the omegasome structure to phagophore expansion starts, cytosolic ATG8 proteins are processed by ATG4 and then conjugated to membrane-located phosphatidylethanolamine (PE) by two highly regulated conjugation systems by ATG proteins such as ATG3, ATG7, ATG5, ATG10, ATG12 and ATG16L. In this reaction, e.g. LC3-I is lipidated into the PE-conjugated form LC3-II and consequently anchored at the inner or outer membrane of the phagophore [169]. Lipidated LC3 functions as an adaptor and membrane scaffold for the attraction of LC3-interacting region (LIR) containing proteins such as core autophagy proteins ULK1, ATG5 and ATG12 [201, 202]. Secondly, they enable the LIR-dependent recruitment of selective autophagy receptors with or without bound cargo proteins into the phagophore [203]. Importantly, LC3 proteins are required for elongation and closure of the phagophore membrane, leading to the formation of a double layered membrane structure called the autophagosome [169, 171, 195, 204]. As LC3 is present over the complete life cycle of autophagosomes it is regarded as one of the main marker proteins for investigating autophagy. During the maturation of the autophagosome, PIP3 phosphatases in concert with ATG4 proteases mediate the removal of PIP3 and ATG8 family proteins from the surface of the autophagosome [205]. Upon fusion with the lysosome, the life circle of the autophagosome ends as an autophagolysosome in which the containing cargo is degraded [206].

2.6.1   Selective autophagy receptors

Selective autophagy is mediated by specifically tagging cargo (proteins or organelles) and subsequent delivery into the autophagic machinery. The most relevant mechanism for labelling cargo for autophagosomal degradation is by ubiquitination, a feature also shared by the proteasomal pathway [207]. Selectivity is ensured through autophagy receptors which physically link polyubiquitinated cargos with the autophagosomal membrane by binding to ATG8 proteins via an evolutionary conserved LIR domain. Ubiquitin and cargo recognition by autophagy receptors is typically mediated by a ubiquitin binding domain. However, not all autophagy receptors depend on polyubiquitination for cargo recognition but rather bind them directly. As such, sequestosome-1 (p62) binds the autophagic substrate KEAP1 without the need of polyubiquitination [208-210]. Interestingly, autophagy receptors preferentially target proteins decorated with M1- and K63-linked ubiquitin chains for degradation by autophagy [211, 212]. For instance, p62 [213-215] shows higher affinity to M1- and K63-linked polyubiquitinated cargos while optineurin (OPTN) only binds M1- and K63-linked ubiquitin chains [148, 216]. In contrast, proteins labeled by K48-linked chains are delivered to proteasomal degradation. Accordingly, ubiquitination is regarded as a level of regulation and specificity during substrate recognition by selective autophagy receptors [207].

The first mammalian autophagy receptor was identified in 2005 by Bjorkory et al. who demonstrated that p62 protein aggregates are degraded via the lysosome and that ubiquitinated substrates are degraded in a p62-dependent manner [217]. These findings far exceeded the known function of p62 as a scaffold protein of the NF-κB pathway [218] and paved the path for a rapid investigation of selective autophagy receptors. Until now, various autophagy receptors are identified and can be divided into two groups consisting out of either soluble or membrane bound autophagy receptors. Soluble autophagy receptors such as p62, optineurin, neighbor of BRCA1 (NBR1), nuclear dot protein 52 (NDP52) and Tax1-binding protein 1 (TAX1BP1) depend on diverse ubiquitin binding domains to recognize their substrates [206]. In contrast, membrane bound autophagy receptors including NIX (also known as BNIP3L), FUN14 domain-containing protein 1 (FUNDC1) or activating molecule in BECN1-regulated autophagy protein 1 (AMBRA1) are in the majority of cases localized to their specific cargo such as mitochondria [169]. Yet, all autophagy receptors share the LIR domain for ATG8 binding as a common feature in their domain architecture [219].

Regulation of autophagy receptors is mediated by post-translational modifications (PTMs) such as phosphorylation. For instance, phosphorylation of optineurin by TBK1 upstream of its LIR enhances the affinity for LC3 and increases the clearance of *Salmonella* by autophagy [220]. Moreover, phosphorylation by TBK1 increases the affinity of optineurin to ubiquitin, thereby promoting the degradation of damaged mitochondria [221]. In the same way, phosphorylation of p62 at serine 403 by ULK1 or TBK1 enhances the affinity of its UBA domain for ubiquitin chains [222, 223]. Phosphorylation of p62 by ULK1 at serine 409 decreases the stability of p62 dimers [224] which normally inhibit p62-dependent ubiquitin binding [225]. Additionally, ubiquitination of autophagy receptors regulates the activity and binding affinities to their substrates [169, 226, 227].

2.6.2   Mitophagy

Mitochondria, also known as the powerhouse of the cell, are double-membraned organelles with essential roles in energy production by generating ATP through oxidative phosphorylation [228]. Furthermore, mitochondria are hubs for biosynthetic processes such as the tricarboxylic acid (TCA) cycle [229] and are involved in innate immunity, apoptosis [230] and redox signaling [231]. During energy production, mitochondria produce large amounts of ROS which can trigger mitochondrial defects in protein folding and DNA mutations [232]. Accordingly, mitochondria developed several defense mechanisms which take place during physiological and pathological conditions to save the organelle from damage. Mitochondrial integrity is ensured by several quality control mechanisms including mitochondrial biogenesis, mitochondrial dynamics such as fusion, fission and division [233] as well as the degradation of whole mitochondria by autophagy known as mitophagy [234]. Moreover, mitochondrial quality

control (MQC) is essential in order to improve cell survival and enable cell growth and division [235]. Dysregulation in MQC ends in damaged mitochondria with detrimental effects for the cell such as abnormal cellular energetics, inflammasome activation, oxidative stress and apoptosis [230, 236]. Therefore aberrant mitophagy is implicated in various diseases such as cancer, Parkinson's disease (PD), Alzheimer's disease, Huntington's disease and diabetes [237].

Mitophagy is characterized by ubiquitin-dependent or -independent targeting of mitochondria for autophagosomal degradation [234]. Ubiquitin-dependent mitophagy involves the two proteins phosphatase and tensin homologue (PTEN)-induced putative kinase 1 (PINK1) and Parkin who act in concert (Fig. 2.4). When mitochondria are intact, mitochondrial-bound PINK1 is inactivated by intracellular cleavage of the inner membrane-localized protease PARL (presenilins-associated rhomboid-like), releasing PINK1 into the cytosol, followed by K48-linked polyubiquitination and proteasomal degradation [238, 239]. However, if mitochondria are damaged, PINK1 is stabilized at the outer mitochondrial membrane (OMM) and activated through autophosphorylation [240]. Activated PINK1 recruits Parkin to mitochondria and triggers its phosphorylation, a step necessary for activating the E3-ligase activity of Parkin [241-243].
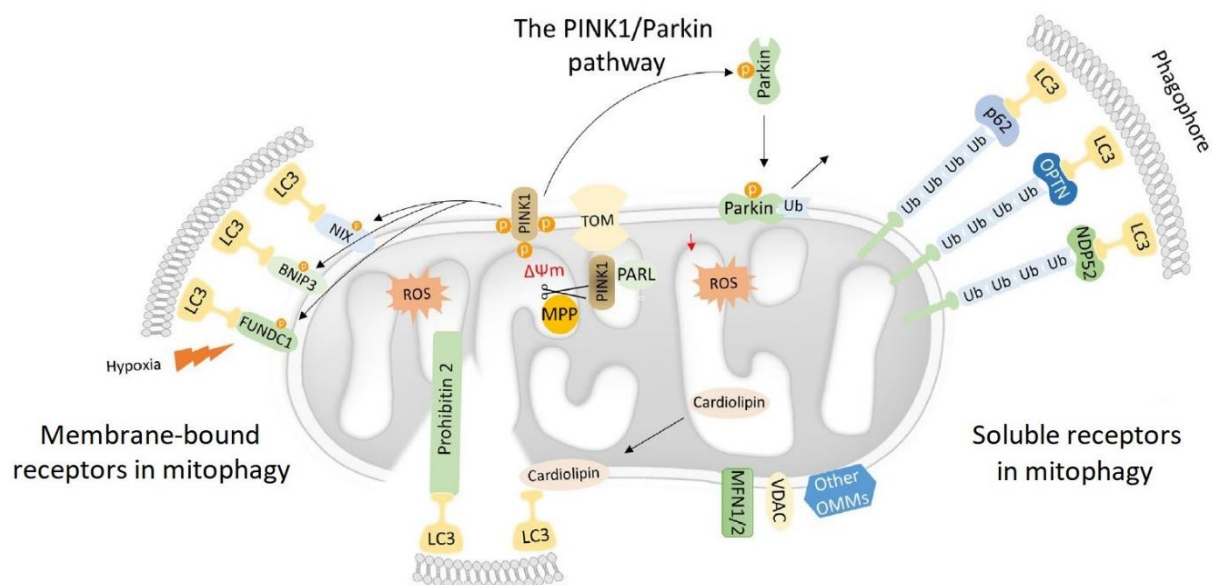
Figure 2.4. Overview of Parkin-dependent and -independent mitophagy. Following mitochondrial dysfunction, PINK1 is recruited to the OMM if its cleavage by mitochondrial processing peptidase (MPP) and PARL proteases is inhibited. In turn, autophosphorylation of PINK1 leads to the recruitment of Parkin to damaged mitochondria by triggering the phosphorylation of ubiquitin and Parkin. Consequently, Parkin induces polyubiquitination of several OMM proteins such as VDAC1 and MFN1/2. Soluble selective autophagy receptors like p62, optineurin or NDP52 recognize polyubiquitinated OMM proteins and tether them simultaneously to LC3-positive phagophores via their LIR domains. In contrast, membrane-bound mitophagy receptors such as BNIP3, NIX and FUNDC1 directly bind to LC3 following mitochondrial damage through hypoxia. Moreover, the IMM proteins PHB2 and cardiolipin are exposed due to mitochondrial damage and subsequently mediate the binding to LC3. Figure is modified from [230].

Interestingly, in a second mechanism PINK1 phosphorylates ubiquitin at serine 65, leading to the recruitment and partial activation of Parkin [244, 245]. Active Parkin assembles polyubiquitin chains on various substrates such as OMM proteins including voltage-dependent anion channel 1 (VDAC1) and mitofusin (MFN) 1 or 2 [246, 247]. Thus, Parkin generates a feed-forward mechanism in mitophagy by synthesizing polyubiquitin chains which serve as substrates for PINK1 [241]. Consequently, polyubiquitinated OMM proteins are recognized by soluble autophagy receptors such as p62, optineurin and NDP52, leading to selective targeting of mitochondria to ATG8/LC3-positive phagophores [248-250].

It would be conceivable that all ubiquitin-dependent soluble autophagy receptors like p62, NDP52, NBR1, optineurin and TAX1BP1 are responsible for the elimination of damaged mitochondria by mitophagy. Surprisingly, only optineurin and NDP52 were shown to be the major receptors in Parkin-dependent mitophagy, nourishing the idea that autophagy receptors fulfill redundant roles [251].

Conversely, NIX, BNIP3 and FUNDC1 are receptors located at the OMM and mediate ubiquitin-independent mitophagy by directly associating with ATG8 proteins via their LIR domains [234, 252-254]. For instance, FUNDC1 mediates elimination of damaged mitochondria during hypoxia [253] and serves as a recruiter of ULK1 to potentially build phagophores around mitochondria [255]. Similarly, also NIX and BNIP3 act as mitophagy receptors during hypoxia [256, 257]. Finally, inner mitochondrial membrane (IMM) proteins such as prohibitin2 (PHB2) and cardiolipin serve as mitophagy receptors by being exposed or transported to the OMM due to mitochondrial damage, consequently binding to LC3B either via a LIR domain [258] or functioning as an elimination signal on their own [259].

Standard methods to detect mitochondrial clearance by mitophagy include electron microscopy or the biochemical analysis of the degradation of mitochondrial proteins [260]. However, all these methods harbor several downsides in sensitivity and quantification potential. The discovery of fluorescence-based reporter probes significantly improved the quantification of mitophagy and resolved several downsides of previous methods [261]. The mito-mKEIMA (mt-mKEIMA) probe is specifically targeted to the mitochondrial matrix by a mitochondrial targeting sequence of COXVIII [261]. Under neutral to alkaline pH, mKEIMA excites a green signal at shorter wavelength (405 nM), whereas under acidic pH the probe excites a red signal at longer wavelength (561 nM). Through its resistance to lysosomal degradation [261], mKEIMA enables a robust quantification of healthy mitochondria (pH 8.0) or those undergoing lysosomal degradation (pH 4.5), consequently representing overall mitophagy levels [260]. Therefore, mKEIMA represents a robust tool in quantifying the whole mitophagic activity of a cell population.

3   Aim of the work

Biglycan-associated inflammation is a key feature of acute inflammatory diseases such as sepsis [31, 64] and IRI [61, 74] and its expression level correlates with kidney damage [262]. Additionally, biglycan is involved in chronic inflammatory diseases like diabetes [54, 62, 68], lupus nephritis (LN) [53, 62], atherosclerosis [71, 72], fibrosis [64, 73] and calcified aortic valve disease (CAVD) [12, 65, 263]. Previous studies brought to light that biglycan selectively utilizes different signaling routes involving a combination of the PRRs TLR2 and TLR4 as well as the TLR adaptor molecules MyD88 and TRIF to drive and regulate the production of inflammatory mediators during sterile inflammation [31, 61, 62, 66, 67, 74]. The selective interaction of biglycan to TLRs and TLR adaptors complicates efficient pharmacological targeting of biglycan-mediated signaling in inflammatory diseases.

The first part of the study was based on previous findings that biglycan is in a complex with MD2 and CD14 [31]. As CD14 functions as a main co-receptor for TLR4 [264] and ligand-dependent for TLR2 [97], we assumed that CD14 plays an important role in biglycan-mediated inflammation. This would be verified by investigating biglycan-induced pro-inflammatory chemo- and cytokine levels, downstream signaling and binding properties of biglycan to CD14 using primary murine macrophages from TLR and CD14 deficient mice. If the involvement of CD14 in biglycan-triggered inflammation was confirmed, the next step would be to test the significance of CD14 in renal IRI, a well-established *in vivo* model of acute inflammation. The ultimate goal was to identify a target protein that allows universal targeting of the TLR2 and TLR4 signaling axis of biglycan-associated inflammation.

In a second project, we focused on novel functions of regulators of sterile inflammation. ABIN-1 is an ubiquitin sensor that has important functions in the regulation of TLR-induced inflammation and cell death by inhibiting NF-κB signaling [151]. Similar to the functional related optineurin which acts as a selective autophagy receptor [220], ABIN-1 binds K63- and M1-linked ubiquitin chains, which preferentially mark cargo for the recognition of the selective autophagy machinery [207]. Therefore, we presumed that ABIN-1 by simultaneously binding to LC3 and polyubiquitinated cargo proteins would serve as an undescribed selective autophagy receptor.

To probe our hypothesis, interactome and proteome studies from murine samples by mass spectrometry would reveal interactions with autophagy-related (ATG) proteins and possible cargo proteins of ABIN-1. Next, sequence alignment analysis would be used to identify possible LC3-interacting regions in ABIN-1 which are known to be essential in mediating the selective transport to ATG8-positive autophagosomes [169]. Afterwards, the association of

ABIN-1 with ATG proteins and other key autophagic markers would be tested in cellular systems in the presence or absence of autophagic stimuli. In parallel, we would verify if protein levels of ABIN-1 are modulated by pharmacological autophagy induction or inhibition. Finally, to assess whether ABIN-1, likewise other soluble autophagy receptors [221, 250, 252], is involved in the selective elimination of mitochondria, we would investigate the recruitment of ABIN-1 to damaged mitochondria and how a genetic ablation of ABIN-1 would affect PINK1/Parkin-dependent mitophagy. As mounting evidence emphasizes a pivotal role of selective autophagy in switching inflammation either into chronification or regeneration [192, 265], the identification of ABIN-1 as a new selective autophagy receptor would provide the basis for new investigations regarding ABIN-1´s inhibitory function in inflammation.

4 Materials and Methods

4.1 Materials

4.1.1 Chemicals

Table 1: List of chemicals

Chemicals	Company
ABC-Chondroitinase	Seikagaku Kogyo, Tokyo, Japan
AccuPrime Pfx DNA polymerase	Thermo Fisher Scientific, Rockford, USA
Acetone	Sigma-Aldrich, Munich
Acrylamide/Bis Solution 30%	Carl Roth, Karlsruhe
Agarose	Carl Roth, Karlsruhe
Ambion Silencer Select Pre-designed siRNAs	Thermo Fisher Scientific, Rockford, USA
ε-Amino-N-Caproic Acid	Sigma-Aldrich, Munich
Ammonium Persulfate (APS)	Carl Roth, Karlsruhe
Ampicillin	Sigma-Aldrich, Munich
Amylose resin	NEB, Frankfurt am Main
Antimycin A	Sigma-Aldrich, Munich
Aprotinin	Merck, Darmstadt
BafilomycinA1 (BafA1)	Cayman Chemical, Ann Arbor, USA
BCA-Protein Assay Kit	Thermo Fisher, Rockford, USA
Bovine Serum Albumine (BSA)	AppliChem, Darmstadt
Brewer Thiglycollate Medium	Sigma-Aldrich, Munich
Buprenorphine	RB Pharmaceuticals Limited, Berkshire, UK
Chloroform	Carl Roth, Karlsruhe
Collagenase A	Roche, Mannheim
DAPI	Vector, Burlingame, USA
Diethylpyrocarbonat (DEPC)	Sigma-Aldrich, Munich
Dimethylsulfoxide (DMSO)	Merck, Darmstadt
Dithiothreitol (DTT)	Invitrogen, Karlsruhe
Doxycycline hyclate	Sigma-Aldrich, Munich
Dulbecco's Modified Eagle Medium (DMEM)	Life Technologies, Darmstadt
Endofree Plasmid Maxi Kit	Qiagen, Hilden
Entellan	Merck, Darmstadt

Ethanol	Sigma-Aldrich, Munich
Ethidium bromide	Invitrogen, Karlsruhe
Ethylendiaminetetraacetic acid (EDTA)	Sigma-Aldrich, Munich
Fetal bovine serum (FBS)	Merck, Darmstadt
FuGENE HD Transfection Reagent	Promega, Mannheim
GENEART Site-Directed Mutagenesis System	Invitrogen, Karlsruhe
Geneticin Disulphate solution (G418)	Carl Roth, Karlsruhe
GFP-Trap®_MA	Chromotek, Martinsried
Glutathione sepharose 4B beads	GE healthcare, Frankfurt am Main
Glycerol/Gelatine	R&D Systems, Minneapolis, USA
Glycine	Carl Roth, Karlsruhe
Heparin 25000	Ratiopharm, Ulm
High-Capacity cDNA Reverse Transcription Kit	Applied Biosystems, Darmstadt
Hydrogen Peroxide	Sigma-Aldrich, Munich
Isopropanol	Sigma-Aldrich, Munich
Isotone NaCl solution (0.9%)	B. Braun Melsungen, Melsungen
Ketamine	Pfizer, Berlin
Lipofectamine RNAiMAX Reagent	Thermo Fisher Scientific, Rockford, USA
LB Broth Base	Invitrogen, Eggstein
Luminaris High Green Low ROX qPCR Mastermix	Thermo Fisher, Rockford, USA
Mayer's Hematoxylin solution	Sigma-Aldrich, Munich
β-Mercaptoethanol	Ferak Laborat GmbH, Berlin
Methanol	Sigma-Aldrich, Munich
Monolith NT Protein Labeling Kit Red	NanoTemper Technologies, Munich
Nitrocellulose membrane	GE healthcare, Frankfurt am Main
Nonidet P-40	Merck, Darmstadt
Oligomycin A	Sigma-Aldrich, Munich
Paraformaldehyde	Sigma-Aldrich, Munich
PCR Master Mix	Bio&Sell, Feucht /Nuremberg
Penicillin-Streptomycin (Pen Strep)	Roche, Mannheim
Pentobarbital	Merial GmbH, Hallbergmoos
Percoll	GE healthcare, Frankfurt am Main
Periodic acid	Carl Roth, Karlsruhe
Phenylmethylsulfonylchloride (PMSF)	Sigma-Aldrich, Munich

Phosphate buffered saline (PBS)	Life Technologies, Darmstadt
Pierce Anti-HA Magnetic Beads	Thermo Fisher Scientific, Rockford, USA
Pierce ECL Western Blotting Substrate	Thermo Fisher Scientific, Rockford, USA
Platinum PCR SuperMix High Fidelity	Life Technologies, Darmstadt
QIAprep Spin Miniprep Kit	Qiagen, Hilden
QIAquick PCR purification Kit	Qiagen, Hilden
Rapamycin	LC Laboratories, Woburn, USA
Roswell Park Memorial Institute 1640 (RPMI)	Life Technologies, Darmstadt
Skimmed milk powder	Sucofin, Zeven
Sodium Deoxycholate	Sigma-Aldrich, Munich
Sodium Dodecyl Sulfate (SDS)	Sigma-Aldrich, Munich
Sodium chloride	Sigma-Aldrich, Munich
Sodium Hydroxide	Sigma-Aldrich, Munich
Sulfuric acid	Merck, Darmstadt
Super Signal West Femto Maximum Sensitivity Substrate	Thermo Fisher, Rockford, USA
TaqMan assay probes	Applied Biosystems, Darmstadt
Tetramethylethyldiamine (TEMED)	Sigma-Aldrich, Munich
TOPO-TA Cloning Kit	Thermo Fisher, Rockford, USA
Torin-1	Bio-Techne GmbH, Wiesbaden
TRI Reagent	Sigma-Aldrich, Munich
Tris	Carl Roth, Karlsruhe
Triton X-100	Sigma-Aldrich, Munich
Trypsin-EDTA 0.5%	Life Technologies, Darmstadt
Tween 20	Sigma-Aldrich, Munich
Xylazine	Bayer, Leverkusen

4.1.2 Consumables

Table 2: List of consumables

Consumables	Company
Amersham Hyperfilm ECL	GE healthcare, Frankfurt am Main
Cell culture plates (6-; 12-; 24; 96-well)	Greiner Bio-One, Solingen
Cell scraper	Sarstedt, Newton, USA
Cell strainer	BD Biosciences, Heidelberg
Costar pipets (5; 10; 25 mL)	Corning Incorporated, Corning, USA
FACS tubes	BD Biosciences, Heidelberg

Falcon tubes (15; 50 mL)	Greiner bio-one, Solingen
MaxiSorp ELISA plates	Nunc, Wiesbaden
MicroAmp Plate sealer	Applied Biosystems, Darmstadt
MicroAmp Reaction plates	Applied Biosystems, Darmstadt
Microscope Cover Glasses	Thermo Fisher, Rockford, USA
Microscope Slides	Thermo Fisher, Rockford, USA
Mixing Rotator	Renner GmbH, Dannstadt
Monolith T.115 Capillaries Standard Treated	NanoTemper Technologies, Munich
Needles	BD Biosciences, Heidelberg
Nitrile glove	B. Braun Melsungen, Melsungen
Pierce centrifuge columns	Thermo Fisher Scientific, Rockford, USA
Pipet tips (10; 100; 1000 µl)	Sarstedt, Newton, USA
Plate sealers	Dynatech, Denkendorf
Safe-lock tubes (0.5 ml; 1 ml; 2 mL)	Eppendorf AG, Hamburg
Scalpels	pfm medical AG, Cologne
Syringes	B. Braun Melsungen AG, Melsungen
Whatman 3MM paper	Hartenstein, Würzburg

4.1.3 Hardware

Table 3: List of hardware

Hardware	Company
Automatic Tissue Processor	Leica, Nussloch
AbiPrism 7500 Fast	Applied Biosystems, Darmstadt
BD LSRFortessa	BD Bioscience, Heidelberg
Mini-PROTEAN Electrophorese	Bio-Rad, Munich
CO_2-Incubator Hereaus BBD 6220	Thermo Fisher, Schwerte
FACSCanto II flow cytometer	BD Bioscience, Heidelberg
Film Developer	Agfa Healthcare, Mortsel, Belgium
Heating block, Thermomixer	Eppendorf, Hamburg
Homogeniser and sonicator	Branson Schallkraft, Heusenstamm
Light Microscope	Olympus, Hamburg
Megacentrifuge Heraeus	Thermo Fisher, Schwerte
Microplate Reader Sunrise	Tecan Trading AG, Mainz
Microtome	Leica, Nussloch
Mini-Trans-Blot System	Bio-Rad, Munich
Monolith NT.115	NanoTemper Technologies GmbH, Munich

Nano-Drop spectrophotometer	PEQLAB Biotechnologie, Munich
Paraffin Embedding Station	Leica, Nussloch
PCR-cycler Primus 96	MWG AG Biotech, Ebersberg
pH meter	Mettler Toledo, Giessen
Precision Balance	Kern & Sohn GmbH, Balingen
Scantainer	Scanbur Technology A/S, Karlslunde, Denmark
Table centrifuge	Thermo Fisher, Schwerte
Water bath	Julabo, Seelbach
LSM780 ELYRA PS.1 Super Resolution confocal microscope	Zeiss, Oberkochen

4.1.4   Software

Table 4: List of software

Software	Company
Adobe Photoshop CS6	Adobe inc., San José, USA
ApE Plasmid Editor	M. Wayne Davis (open source software)
FACS DIVA Software	BD Bioscience, Heidelberg
GraphPad Prism 6	Graphpad Software, Inc.
Quantity One	Bio-Rad, Munich
Zeiss software ZEN2012 SP5	Zeiss, Oberkochen

4.2   Methods

4.2.1   Molecular cloning

4.2.1.1   ABIN-1-HA

Full length human ABIN-1 was amplified by PCR from the template of an open reading frame clone (GeneScript, product ID: OHu13881D) with primers containing an N-terminal BamHI restriction site and a C-terminal human influenza hemagglutinin (HA)-tag together with a XhoI restriction site. A total of 50 ng of template was mixed with Platinum PCR SuperMix High Fidelity, both primers and filled up with ddH$_2$O according to the following protocol (Table 5).

Table 5: PCR conditions for hABIN-1-ORF

Temperature	Time	Number of cycles
94°C	2 min	
94°C	30 sec	
55°C	30 sec	35
68°C	2 min	
4°C	pause	

The PCR product was transferred to a 1% agarose gel and purified using a QIAquick PCR Purification kit. Briefly, the corresponding PCR band of the size of hABIN-1 was cut with a scalpel. A 3-fold volume of buffer QG was added and heated at 55°C for 10 min until the gel piece was dissolved. Then 1 gel volume of isopropanol was added, mixed and the sample was put on a QIAquick column to bind the DNA. The sample was centrifuged at 13.000 rpm for 1 min at RT. Subsequently, the column was washed with 0.5 ml of buffer QG, followed by 0.75 ml of buffer PE. Column was dried from ethanol by another centrifugation step. Afterwards, DNA was eluted with 30 µl of ddH$_2$O and the concentration was determined via Nano-Drop. hABIN-1-HA and the pcDNA3.1(+) vector (Invitrogen, Eggstein) were digested with BamHI and XhoI overnight at 37°C. The next day, samples were purified over a 1% agarose gel and ligated at molar ratios of vector to insert adjusted to 1:3 with T4 DNA ligase overnight at 16°C.

In general, ligations were transformed into One Shot TOP10 Chemically Competent E. coli cells. One Shot TOP10 cells were thawed on ice, then 4 µl of the ligation was added and the reaction was incubated on ice for 30 min. Afterwards, the transformation was heat shocked for 30 sec at 42°C in a water bath and placed on ice for 2 min. An amount of 250 µl SOC Medium were added aseptically and the transformation was shaked horizontally at 37°C for 1 h. The transformation was spread on ampicillin (100 µg/ml) containing LB agar plates and incubated for 16-18 h at 37°C. Single colonies were picked and used for plasmid isolation by inoculation in 4 ml of ampicillin-containing LB medium overnight at 37°C. Plasmid DNA was isolated using the QIAprep Spin Miniprep Kit. Bacterial overnight cultures were harvested by centrifugation at 8000 rpm for 5 min at RT. The bacterial pellet was resuspended in 250 µl Buffer P1 and transferred into a microcentrifuge tube and lysed using 250 µl P2. After 5 min of incubation 350 µl of Buffer N3 were added to stop the bacterial lysis reaction and the samples were centrifuged for 10 min at 13.000 rpm. Supernatant was applied onto QIAprep 2.0 spin columns and centrifuged for 1 min at 13.000 rpm at RT. Bound DNA was washed with 750 µl Buffer PE, followed by a centrifugation step to remove residual wash buffer. Finally, plasmid DNA is eluted with 50 µl ddH$_2$O and measured by Nano-Drop. A small part of purified plasmid DNA was sent for sequencing (Eurofins Genomics, Ebersberg). Sequence verified constructs were then freed from endotoxin by utilization of the Qiagen EndoFree Plasmid Maxi kit. An

amount of 250 ml LB medium were inoculated either from a fresh transformation or from frozen bacterial stocks and incubated overnight at 37°C in a horizontal shaker. The LB culture was harvested by centrifugation at 6000 g for 15 min at 4°C. The pellet was resuspended in 10 ml of ice-cold Buffer P1 and lysed for 5 min at RT by adding 10 ml of Buffer P2. After neutralization with 10 ml Buffer P3, the lysate was poured into the QIAfilfer Cartridge and incubated for 10 min at RT. The filtered lysate was put on ice, mixed with 2.5 ml of Buffer ER and incubated for 30 min. Subsequently, the lysate was poured into a QIAGEN-tip, which was equilibrated with 10 ml of Buffer QBT. The tip was washed 2 times with 30 ml of Buffer QC and eluted in a new falcon by addition of 15 ml Buffer QN. Eluted DNA was precipitated by adding 10.5 ml of isopropanol and centrifugation at 15.000 g for 10 min at 4°C. Supernatant was discarded and the DNA was washed with 5 ml of endotoxin-free 70% ethanol, followed by centrifugation at 13.000 g for 10 min at 4°C. The supernatant was decanted and the remaining plasmid DNA was resuspended in an adequate amount of endotoxin-free H_2O. The concentration was determined by Nano-Drop.

4.2.1.2   Site directed mutagenesis of ABIN-1

The GENEART Site-Directed Mutagenesis System (Invitrogen) was used to generate ABIN-1 mutants with defective LIR domains. For this purpose, 20 ng of pcDNA3.1(+) hABIN-1-HA was mixed with overlapping primer pairs carrying the desired LIR mutations (Table 6) and AccuPrime *Pfx* DNA polymerase. The PCR was performed using the following parameters.

Table 6: PCR conditions for mutagenesis of hABIN-1

Temperature	Time	Number of cycles
37°C	20 min	
94°C	2 min	
94°C	20 sec	
57°C	4 min	18
68°C	2 min	
68°C	5 min	
4°C	pause	

The PCR product was used for the *in vitro* recombination reaction to boost mutagenesis efficiency. 4 μl of PCR sample was mixed with 4 μl of 5x Reaction Buffer, 10 μl of PCR grade water and 2 μl of 10x Enzyme mix. The reaction was incubated for 10 min at RT and stopped by addition of 1 μl of 0.5 M EDTA. Afterwards the reaction mix was put on ice and used for transformation using One Shot MAX Efficiency DH5-T1R competent cells. Purified plasmid DNA was checked by sequencing for correct mutagenesis and used for further experiments.

4.2.1.3 TOPO cloning of mCherry-Parkin and mEGFP-hABIN-1

Primers containing SfiI restriction sites were used to amplify mCherry-Parkin (Table 7) from the mCherry-Parkin donor vector (a gift from Richard Youle; Addgene plasmid # 23956) using the Platinum PCR SuperMix High Fidelity. Platinum PCR SuperMix High Fidelity contains a high fidelity Taq DNA polymerase, which generates 3′ A-overhangs, necessary for subsequent TOPO cloning. The following parameters were used for the PCR.

Table 7: PCR conditions for mCherry-Parkin

Temperature	Time	Number of cycles
94°C	2 min	
94°C	30 sec	
55°C	30 sec	35
68°C	2 min	
4°C	pause	

For the TOPO cloning reaction, 4 µl of fresh PCR product containing 3′ A-overhangs were mixed with 1 µl of Salt Solution, 1 µl of TOPO vector and incubated for 30 min at RT. Then, the reaction was placed on ice and transformed into One Shot TOP10 Chemically Competent cells as described before. Kanamycin (50 µg/ml) containing LB agar plates were used for selection. Plasmid DNA was digested with SfiI restriction enzyme at 50°C overnight to yield the corresponding insert of mCherry-Parkin flanked by two SfiI sites. Subsequently, mCherry-Parkin was cloned into the pSBtet-Pur (Addgene plasmid # 60507) or pSBtet-Neo (Addgene plasmid # 60509) vectors (a gift from Eric Kowarz). Purified plasmid DNA was verified by sequencing before performing endotoxin-free plasmid purification and subsequent experiments.

Similarly, to generate mEGFP-hABIN-1, hABIN-1 was amplified from the ORF clone (GeneScript, product ID: OHu13881D) using primers containing a HindIII and BspE1 restriction site (Table 8). In this case, the same PCR protocol as for HA-tagged ABIN-1 was used. The resulting PCR product and mEGFP-C1 vector (a gift from Michael Davidson; Addgene plasmid # 54759) were both digested using HindIII and BspE1 at 37°C overnight and gel purified on the next day. Insert and vector were ligated at molar ratios of 1:3 with Quick Ligase (NEB). For this purpose, 10 µl of 2x Quick Ligase Reaction Buffer, 50 ng vector, the corresponding amount of insert and 1 µl of Quick Ligase were mixed and incubated at RT for 5 min. The reaction was stopped by placing the mixture on ice and transformed using One Shot TOP10 Chemically Competent cells. After plasmid purification, the correct insertion of hABIN-1 into the mEGFP-C1 vector was verified by sequencing before performing an additional PCR with primers containing SfiI restriction sites (Table 8) and the Platinum PCR SuperMix High Fidelity. TOPO

cloning was performed as described before. Finally, mEGFP-hABIN-1 was cloned into the pSBtet-Pur and pSBtet-Neo vector. Correct insertion was validated by sequencing.

Table 8: Primer table of ABIN-1 and Parkin constructs

Primer	Sequence 5´- 3´
hABIN-1 fwd	CGCGGATCCACCCTCATGGAAGGGAGAGGACCGTACCGGAAAC
hABIN-1-HA rev	CCGCTCGAGTCAAGCGTAATCTGGAACATCGTATGGGTACTGAGGCCCCTCACGGTCATTTTTTG
LIR1 [F83A/L86A] fwd	CCCTCCTTGGGCTCCGCCGACCCCGCGGCTGAGCTCACAGGA
LIR1 [F83A/L86A] rev	TCCTGTGAGCTCAGCCGCGGGGTCGGCGGAGCCCAAGGAGGG
LIR2 [F125A/V128A] fwd	GGCACCTCCTCTGAAGCTGAAGTGGCCACTCCTGAGGAGCAG
LIR2 [F125A/V128A] rev	CTGCTCCTCAGGAGTGGCCACTTCAGCTTCAGAGGAGGTGCC
UBAN [D472N] fwd	GTGAAGATCTTCGAGGAGAACTTCCAGAGGGAGCGCAGT
UBAN [D472N] rev	ACTGCGCTCCCTCTGGAAGTTCTCCTCGAAGATCTTCAC
mCherryParkin fwd	GACGGCCTCTGAGGCCGCCACCATGGTGAGCAAGGGCGAGGAGG
mCherryParkin rev	GACGGCCTGACAGGCCTTACACGTCGAACCAGTGGTCCCCCATG
ABIN-1ORF 3 fwd	GACTCCGGAATCATGGAAGGGAGAGGACCGTACC
ABIN-1ORF 5 rev	GACAAGCTTTCACTGAGGCCCCTCACGGTCA
mEGFP-C1-hABIN-1 fwd	GGCCTCTGAGGCCGCCACCATGGTGAGCAAGGGCGAGGAGC
mEGFP-C1-hABIN-1 rev	GGCCTGACAGGCCTCACTGAGGCCCCTCACGGTCATTTTTTGG

4.2.1.4 Plasmid construction of human biglycan and human CD14

In order to generate the pcDNA3.1(+) human biglycan- (hBGN) expressing vector, full length human biglycan cDNA was reverse transcribed by qRT-PCR from human kidney tissue. From this template hBGN was generated by PCR using primers containing BamHI and XhoI restriction sites. The PCR product and the pcDNA3.1(+) plasmid empty vector were both digested with BamHI and XhoI overnight at 37°C and subsequently gel-purified. PCR product and vector were ligated, transformed and plasmid DNA was purified. For the generation of

human biglycan protein core, site-directed mutagenesis was utilized to generate hBGN [S42AS47A]. In this mutant version of biglycan, both serine GAG attachment sites were mutated into alanine using two overlapping primers including the nucleotide mutations (Table 9). Afterwards, a 6xHis-tag was introduced at the C-terminus of biglycan right before the stop codon.

For the generation of the vector expressing the extracellular domain of human CD14 (Met1-Asn345), cDNA was reverse transcribed from human monocytes as a template. Then, a forward primer containing a BamHI restriction site and a reverse primer including a XbaI restriction site as well as a 6xHis-tag were used to amplify hCD14 by PCR. After digestion of the pcDNA3.1(+) vector as well as hCD14 with BamHI and XbaI, the hCD14 constructs was inserted into the pcDNA3.1(+) vector. All plasmids were checked by sequencing prior to transfection into HEK293 cells. The expression of human biglycan was described before [266].

Table 9: Primers for amplification of hBGN

Primer	Sequence 5´- 3´
hBGN BamHI fwd	TCTGGATCCGCCATGTGGCCCCTGTGGCGC
hBGN XhoI rev	ACTCTCGAGCTACTTTTTGTAGTTGCCAAACTG
hBGN [S42AS47A] fwd	GAACGATGAGGAAGCTGCGGGCGCTGACACCGCAGGCGTCCTGGACC
hBGN [S42AS47A] rev	GGTCCAGGACGCCTGCGGTGTCAGCGCCCGCAGCTTCCTCATCGTTC
hCD14 BamHI fwd	TGCAGGATCCACCATGGAGCGCGCGTCCTGCTTG
hCD14-6xHis XbaI rev	TGCTCTAGATTAGTGGTGATGGTGATGATGCAGCACCAGGGTTCCCGACAC

4.2.2 Purification of recombinant intact human biglycan

Purification of native biglycan with intact glycosaminoglycan chains was achieved by harvesting the conditioned medium of HEK293 cells, stably overexpressing biglycan. In turn, soluble biglycan is released into the cell culture medium (conditioned media). The conditioned media was collected and supplemented with 0.1% Triton X-100, 20 mM Tris-HCl pH 7.4 and proteinase inhibitors. Afterwards the media was passed over a DEAE-Tris acryl-M packed column to specifically bind GAG chains and glycoproteins. For elution, 1 M NaCl in 20 mM Tris-HCl, pH 7.4 was added onto the column. The products were dialyzed for 2 h against 20 mM Tris-HCl, pH 7.4, containing 150 mM NaCl and separated on high performance liquid chromatography on a TSK-GEL-DEAE-5PW column by a discontinuous binary NaCl gradient. Biglycan was then dialyzed against PBS and checked for purity by silver staining on SDS gel electrophoresis.

4.2.3   Purification of His-tagged proteins

His-tagged human biglycan protein core or CD14 were purified using Ni-NTA agarose according to manufacturer's instructions. Briefly, the conditioned media from His-tagged human biglycan protein core- or CD14-expressing HEK293 cells were mixed with Ni-NTA agarose beads at 4°C on a rotary shaker for 2 h. After incubation, samples were transferred onto PierceTM centrifuge columns and washed with 20 mM imidazole (pH 8.0) containing 50 mM NaH_2PO_4 and 300 mM NaCl. Subsequently, His-tagged proteins were competitively eluted by addition of 250 mM imidazole (pH 8.0) containing 50 mM NaH2PO4 and 300 mM NaCl. Finally, proteins were dialyzed against PBS.

4.2.4   Cell culture

Cells were cultured at 37°C with a concentration of 5% CO_2 and 95% relative humidity. HeLa cells (ATCC, USA) were passaged twice a week. For passaging, cells were washed with 5 ml of PBS, followed by 3 ml of 0.5% Trypsin-EDTA for cell detachment. 8 ml of fresh growth medium was added to block trypsinization and cells were centrifuged at 1000 rpm for 5 min at RT. Cells were then resuspended in 1 ml of medium and split into a new cultivation flask. All cells were regularly tested for the presence of mycoplasma contamination.

4.2.4.1   Freezing and thawing of cells

In order to store cells for long-term, cells were diluted in their corresponding medium without antibiotics containing 10% DMSO and 20% FBS and transferred into Cryo tubes. The tubes were put into a Cryo Freezing container that enabled slow freezing overnight at -80°C. The next day, Cryo tubes were transferred into a liquid nitrogen tank for storage. Cells that had to be thawed were defrosted at 37°C in a water bath, then resuspended in 9 ml growth medium and centrifuged at 1000 rpm for 5 min at RT to remove the DMSO. Afterwards, cells were resuspended in their respective medium and cultured as described before.

4.2.4.2   Cell counting, seeding and treatment

Cells were detached using 0.5% Trypsin-EDTA, filled up with 8 ml of medium and centrifuged at 1000 rpm for 5 min. Supernatant was discarded and cells were resuspended in 1 ml of medium. 10 µl of a 1:10 dilution of the cells was counted in a Neubauer chamber. An appropriate number of cells was then diluted in growth medium to achieve the required cell density depending on the experimental setup. The final amount of medium including treatment substances was defined as followed: 100 µl/well in 96-well plates, 1 ml/well in 12-well plates, 2 ml/well in 6-well plates and 10 ml per 100 mm-dish. For analysis of hABIN-1 protein levels upon autophagy induction or inhibition, $0.3x10^6$ HeLa cells were seeded in 6-well plates 24 h

before treatment. The next day, growth medium was replaced including either DMSO as control, Torin-1 (1 µM), rapamycin (100 nM) or Bafilomycin A1 (200 nM or 10 nM for overnight treatment) for the indicated time points.

4.2.4.3 Transfection and generation of stable cell lines

Exemplarily, HeLa cells were seeded 24 h before transfection in a 6-well plate at a density of 0.3×10^6 cells. For transfection, 250 µl of Opti-MEM were mixed with e.g. 1.5 µg of EGFP-LC3 (a gift from Karla Kirkegaard; Addgene plasmid # 11546) vector DNA. Then, FuGENE HD transfection reagent was added at a ratio of 3:1 to the reaction. The transfection mix was incubated for 10 min and then pipetted dropwise onto the cells. Cells were incubated for 24-48 h for protein expression.

The sleeping beauty (SB) expression vector system was utilized [267] to generate stable overexpressing cells. This system is based on transgene integration via transposons. Over inverted terminal repeats (ITRs) present in the pSBtet vectors together with the addition of a transposase-encoding vector the plasmid DNA gets stably integrated into the target genome. To this end, pSBtet-Pur or pSBtet-Neo vectors either containing mCherry-Parkin or mEGFP-hABIN-1 were transfected into HeLa cells using FuGENE HD transfection reagent. Additionally, pCMV(CAT)T7-SB100 (a gift from Zsuzsanna Izsvak; Addgene plasmid # 34879) was co-transfected at a ratio of 1:20 to enable plasmid DNA integration. After 48 h consumed medium was discarded and replaced by medium containing either 3 µg/ml puromycin or 800 µg/ml G418 (selection for neomycin resistance) to select for those cells, which had incorporated the plasmid of interest. Cells were selected in case of puromycin for at least 5 days whereas cells were treated with G418 for a period of 14 days. Medium containing antibiotics was exchanged every 3 days. To guarantee antibiotic selection, parental cells were treated with the same dosage of antibiotics to observe successful cell death. Afterwards, stable cell lines were kept under 1.5 µg/ml puromycin or 400 µg/ml G418 until utilized for further experiments.

4.2.4.4 siRNA-mediated knockdown of ABIN-1

Transient knockdown of ABIN-1 was performed by using Ambion Silencer Select Pre-designed siRNA targeting gene ID (10318). HeLa cells were seeded in 6-well plates in antibiotic-free medium to reach a confluency of roughly 70% at the day of transfection. HeLa cells were transfected with siRNAs using Lipofectamine RNAiMAX. In general, 9 µl Lipofectamine or 4 µl siRNA with a concentration of 5 µM were diluted in 150 µl Opti-MEM. The siRNA-Opti-MEM mixture was transferred to the Lipofectamine-Opti-MEM mixture, mixed carefully by pipetting up and down and incubated for 5 min at RT. Afterwards the lipid complex was added to the

adherent cells topped with a calculated amount of antibiotic-free medium to reach a final siRNA concentration of 5 nM. As a negative control, Silencer Select Negative Control No. 1 siRNA was utilized in parallel in the same concentration. Knockdown efficacy was controlled after 48 h from the same cells used for the experimental setup by Western blot analysis. The following Silencer Select siRNAs were used for gene knockdown of ABIN-1.

Table 10: siRNA primers of ABIN-1

siRNA	Sequence 5´- 3´
Sense ABIN-1	GCAUCCAAGGUGCACAAGAtt
Antisense ABIN-1	UCUUGUGCACCUUGGAUGCca

4.2.4.5 CRISPR/Cas9-mediated knockout of ABIN-1

CRISPR/Cas9-mediated knockout of hABIN-1, 3 single guide RNAs (sgRNAs) targeting PAM motifs of ABIN-1 in exon 3 were designed with the CRISPOR online program by selecting only sgRNAs with the highest scores and low off target effects. The 20-nucleotide long gRNA oligos contain overhangs for ligation into the pair of BbsI sites in the pSpCas9(BB)-2A-Puro vector while a guanine and cytosine (small letters) are added for better U6 transcription of the gRNAs. The pSpCas9(BB)-2A-Puro (PX459) was a gift from Feng Zhang (Addgene plasmid #62988) [268].

Table 10: General structure of sgRNAs

Primer	Sequence 5´- 3´
Sense sgRNA	CACCgNNNNNNNNNNNNNNNNNNNN
Antisense sgRNA	AAACNNNNNNNNNNNNNNNNNNNNc

The following sgRNAs were designed for hABIN-1.

Table 11: sgRNAs for CRISPR/Cas9 of ABIN-1

Primer	Sequence 5´- 3´
Sense sgRNA 1	CACCGGCAAGGGATAAAGATGTTAG
Antisense sgRNA 1	AAACCTAACATCTTTATCCCTTGCC
Sense sgRNA 2	CACCGGAGCCTGGTCGCTTCCATCT
Antisense sgRNA 2	AAACAGATGGAAGCGACCAGGCTCC
Sense sgRNA 3	CACCGAGTCCCAGATGGAAGCGACC
Antisense sgRNA 3	AAACGGTCGCTTCCATCTGGGACTC

sgRNAs were adjusted to a concentration of 100 µm for cloning into the pSpCas9(BB)-2A-Puro vector for co-expression with Cas9. Then 1 µl of each sgRNA pair was mixed with T4 ligation buffer, T4 polynucleotide kinase and filled up to a total volume of 10 µl. Afterwards, sgRNAs were phosphorylated and annealed in a thermocycler at 37°C for 30 min and heat inactivated at 65°C for 20 min. Phosphorylated and annealed oligos were then diluted 1:200, mixed with 100 ng of pSpCas9(BB)-2A-Puro vector, Fast Digest Buffer, 1 µl 10 nM DTT, 1 µl 10 nM ATP, 1 µl Fast digest BbsI, T4 DNA ligase and filled up with ddH$_2$O to a total volume of 20 µl. The ligation mixture is then incubated with the following thermocycler protocol:

Table 12: PCR conditions for Cas9 vector digestion

Temperature	Time	Number of cycles
37°C	5 min	6
21°C	5 min	

Subsequently, the ligation is treated with PlasmidSafe exonuclease to get rid of any residual linearized DNA and incubated at 37°C for 30 min and 70°C for 30 min. The ligation is used for transformation with One Shot TOP-10 bacteria and plated on an ampicillin containing LB plate. Bacterial clones were purified using the Plasmid Miniprep Kit and EndoFree Plasmid Maxi Kit. pSpCas9(BB)-2A-Puro vectors carrying the gRNAs were sequenced before transfection. All 3 gRNAs were transfected at the same ratios at once into HeLa cells. Briefly, 833 ng of each sgRNA were mixed in Opti-MEM with FuGENE HD transfection reagent at a ratio of 3:1. The transfection mix was added dropwise to the cells after 10 min of incubation. After 48 h, cells were selected with puromycin at a concentration of 3 µg/ml. Following 72 h of antibiotic selection, cells were trypsinized, serially diluted to 1 cell/100 µl and plated in a 96-well plate in order to select for single clones. Medium containing puromycin was changed every 3 days. Cells which resulted from one single colony were expanded for 2-3 weeks and screened via Western blot for successful knockout (KO) of ABIN-1. ABIN-1 KO clone 16 and clone 27 showed the highest knockout efficiency, were cultivated at 0.5 µg/ml puromycin and used for further experiments

4.2.4.6   SEAP NF-κB activity assay

A total amount of 1x10^5 HEK-Blue-hTLR2, HEK-Blue-hTLR2/hCD14 and HEK-Blue-hTLR4/hCD14/hMD2 cells containing the secreted embryonic alkaline phosphatase (SEAP) reporter gene for monitoring the activation of the NF-κB pathway were used for the assay. To validate the specificity of the assay, cells were additionally stimulated with the TLR2 ligand peptidoglycan (PGN) and the TLR4 ligand lipopolysaccharide (LPS). Cells were pre-incubated for 1 h with purified NA/LE rat anti-mouse CD14 (10 µg/ml) or purified NA/LE rat IgG2b, κ

isotype control (10 µg/ml) and stimulated with biglycan (4 µg/ml), PGN (2 µg/ml) or LPS (2,5 ng/ml) for 4 h. Activation of TLR2, TLR2/CD14 and TLR4/CD14/MD2 signaling was analyzed by measuring the secreted SEAP according to the manufacturer's instructions. Briefly, 20 µl of the culture medium was mixed with 180 µl of QUANTI-Blue detection medium and incubated for 30 min at 37°C. The presence of SEAP (purple-blue) was measured as absorbance at 655 nm.

4.2.5   Mass spectrometry

4.2.5.1   Label free IP-MS and In-Gel-Digestion

For IP-MS of murine ABIN-1, WT mice were either injected intraperitoneal with 80 µg/g Lipopolysaccharide (LPS) in 0.9% NaCl solution or an equal volume of PBS. Mice were sacrificed after 4 h by intraperitoneal injection of pentobarbital (500 mg/kg). Spleens were harvested, lysed and 2 mg of protein was used for IP with 2 µg sheep anti mouse ABIN-1 antibody (Ubiquigent, 68-0001-100) using Pierce Co-Immunoprecipitation Kit according to manufacturer's instructions. Samples were eluted with 40 µl basic elution buffer (50 mM NaOH) for 5 min at RT and neutralized with 20 µl of 1 M Tris-HCl (pH 8.5). Afterwards samples were run by SDS-Page and stained for 15 min by Coomassie staining using InstantBlue Protein Gel Stain. Protein bands were cut into 1-2 mm^3 pieces and washed 3 times for 10 min with 50 mM ammonium bicarbonate (ABC) containing 40% acetonitrile (ACN) at 37°C and 750 rpm shaking. Samples were dehydrated for 10 min in 100% ACN. Then, ACN was removed and gel pieces were left to dry for 10 min. Afterwards, samples were reduced with 10 mM DTT in 50 mM ABC for 30 min at 56°C and washed for 10 min with 50 mM ABC/40% ACN. Samples were alkylated for 30 min the dark with 40 mM chloroacetamide in 50 mM ABC. Subsequently, samples were washed 2 times with 50 mM ABC/40% ACN, dehydrated in 100% ACN and dried for 10 min. Sample digestion was performed by adding 12.5 ng/µl trypsin in 50 mM ABC and incubation for 30 min at 4°C. Then, 50 mM ABC was added and samples were digested overnight at 37°C. The next day, 60% ACN/1% formic acid (FA) was added and samples were shaken for 30 min at 750 rpm. Supernatants containing the extracted peptides were collected in new microcentrifuge tubes. The extraction step was repeated once and corresponding supernatants were pooled together. Then 100% ACN was added to the gel pieces, samples were shaken for 10 min and the supernatant was transferred to the pooled supernatants. Collected supernatants were put in a SpeedVac at 30°C and reduced to a volume of less than 50 µl. Afterwards, buffer A (0.1 % FA in MS-grade water) was added. In the meantime, stage-tips (consisting out of 3 c18-discs) were assembled and washed with 30 µl methanol. After centrifugation at 2000 rpm for 2 min (stage-tips should not get dry), tips were washed with 30 µl buffer B (80% ACN, 0.1% FA in MS-grade water), centrifuged and washed 2 times with

buffer A. Samples were loaded onto the stage tips and centrifuged at 2000 rpm for 4 min. After the samples passed, 30 µl buffer A was added to the tips, followed by centrifugation at 2000 rpm for 2 min. Elution was performed with 30 µl buffer B. Stage-tips were incubated with buffer B for 15 min at RT, placed into a new microcentrifuge tube and eluted by centrifugation. Eluates were dried by SpeedVac to a volume of 2-3 µl and filled up with 8 µl of buffer A. Finally, samples were analyzed by LC-MS.

4.2.5.2 Proteomic analysis of ABIN-1

For proteome analysis primary murine peritoneal macrophages were isolated from WT and ABIN1[D485N] mice. Macrophages were plated in 100 mm dishes and cultured overnight in RPMI 1640 supplemented with 1% P/S and 2% FBS. The next day, cells were washed 4 times with PBS at RT and subsequently lysed with Proteome lysis buffer (2% SDS, 150 mM NaCl, 50 mM Tris-HCl, pH 8.5, complete protease inhibitor tablet, 10 mM TCEP, 40 mM CAA) heated at 95°C at a concentration of roughly 1.5 mg/ml and transferred into 1.5 ml low binding Eppendorf tubes. Samples were pipetted up and down 20 times to reduce viscosity, boiled for 10 min at 95°C and frozen at -80°C until further processing. For increased cell lysis, samples were sonicated for 1 min (1 sec on 1 sec off, 35% amplitude) and boiled for 5 min at 95°C. For protein precipitation, 4 parts ice cold methanol and 1-part chloroform was added and samples were vigorously vortexed. 3 parts of MS-grade water was added and samples were centrifuged for 5 min at 15.000 g at 4°C. The top layer was removed without disturbing the interphase (contains proteins) and 3 parts ice cold methanol were added. The samples were vortexed and centrifuged for 3 min at 15.000 g at 4°C to pellet the precipitated proteins. Washing with 3 parts ice cold methanol was repeated once more. Afterwards, the supernatant was removed and samples were washed with 1 ml ice cold methanol, vortexed and spinned down for 5 min at 15.000 g at 4°C. Methanol was discarded and the pellet was air-dried for 5-10 min. The protein pellet was dissolved and denatured in 100 µl digestion buffer (8 M urea, 50 mM EPPS, pH 8.2) to reach approximately 1.5 mg/ml protein concentration and incubated for 20 min at 37°C at 750 rpm in a thermomixer. Protein concentration was measured via BCA-assay. 30 µg of protein was filled up with EPPS buffer (50 mM EPPS, pH 8.2) to a volume of 50 µl. Lys-C at a final ratio of 1:100 was added in a volume of 50 µl to the samples to digest the proteins into large fragments. For digestion, samples were incubated for 2 h at 37°C with gentle agitation at 550 rpm. Before trypsin digestion the samples were diluted 1:4 with EPPS buffer. Afterwards, trypsin was added to the samples with a ratio of 1:50 and incubated overnight at 37°C with agitation at 550 rpm. On the next day, the digestion was stopped by adding TFA to a final concentration of 1%. Sep-pak C18 cartridges were washed with 1 ml of methanol followed by 1 ml of 80% ACN and 3x 1 ml 0.1% TFA by applying vacuum until the solution is right above the filter. The sample was loaded with a lower vacuum pressure and washed with 3x 1 ml 0.1%

TFA. Afterwards the samples were eluted into Eppendorf tubes by adding 500 µl 40% ACN followed by 500 µl 60% ACN to the columns and completely dried in a SpeedVac at 45°C for 2 h. The purified dried peptides were resuspended in 20 µl EPPS (200 mM EPPS, pH 8.2, 20% ACN) and measured via peptide assay (Thermo Fisher Scientific, Germany). 10 µg of peptides were labeled by tandem mass tags (TMT) (at a ratio of 2:1; TMT:peptide) for 1 h at RT. Labeling process was stopped by adding 1 µl of 5% hydroxylamine and incubation for at least 15 min at RT. Label incorporation (>98%) and digestion efficiency (>84% without missed cleavage) was confirmed by C18 stage tipping a mixture of 0.5 µl of each sample followed by an analysis via LC-MS/MS. Peptides were fractionated into 8 fractions using the Pierce high-pH reversed phase fractionation kit (Thermo) according to manufacturer`s instructions, dried in a vacuum concentrator and resuspended in 2% ACN, 1% formic acid for LC-MS analysis.

4.2.5.3   Mass spectrometry analyses

Peptides were separated on an easy nLC 1200 (Thermo Fisher) and a 20 cm long, 75µm ID fused-silica column, which has been packed in house with 1.9 µm C18 particles (Reprosil pur, Dr. Maisch) and kept at 45°C using an integrated column oven (Sonation). Peptides were eluted by a non-linear gradient from 4-48% acetonitrile over 25 minutes (IP-samples) or 175 minutes (fractionated proteome samples) and directly sprayed into a QExactive HF mass-spectrometer equipped with a nanoFlex ion source (Thermo Fisher).

For IPs, MS-settings were as follows: Full scan MS spectra (300-1650 m/z) were acquired at a resolution of 60.000 at m/z 200, a maximum injection time of 20 ms and an AGC target value of 3×10^6 charges. Up to 15 most intense peptides per full scan were isolated using a 1.6 Th window and fragmented using higher energy collisional dissociation (normalized collision energy of 27). MS/MS spectra were acquired with a resolution of 30.000 at m/z 200, a maximum injection time of 64 ms and an AGC target value of 1×10^5. Single charged ions, ions with a charge state above 6 and ions with unassigned charge states were not considered for fragmentation and dynamic exclusion was set to 20 s.

For TMT-labelled, fractionated proteome samples, we used MS-settings as follows: Full scan MS spectra (350-1400 m/z for proteomes) were acquired at a resolution of 120.000 at m/z 200, a maximum injection time of 100 ms and an AGC target value of 3×10^6 charges. Up to 10 most intense peptides per full scan were isolated using a 1 Th window and fragmented using higher energy collisional dissociation (collision energy of 35). MS/MS spectra were acquired with a resolution of 60.000 at m/z 200, a maximum injection time of 128 ms and an AGC target value of 1×10^5. Single charged ions, ions with a charge state above 6 and ions with unassigned charge states were not considered for fragmentation and dynamic exclusion was set to 20 s.

4.2.5.4 Mass spectrometry data processing

Data analysis was done with MaxQuant [269] (version 1.6.1.0) adapted for each sample-type, i.e. "type" was set to "standard" with "multiplicity" set to 1 and applying the MaxLFQ algorithm [270] with minimum ratio count set to "1" for label-free IP-samples and "Reporter ion MS2" for the TMT-labelled proteome samples applying the isotope correction factors supplied with the TMT10-kit. Fragment spectra were searched against the Uniprot mouse reference proteome (downloaded September 2017, 60163 sequences), with a false discovery rate of 1% on PSM and protein level and requiring at least one unique peptide for identification. For IP-samples, the "match between runs"-option as well as "second peptides" were activated using default settings, while these features were switched off for the analysis of TMT data. For quantification, only unique peptides were considered, while unmodified versions of oxidized Methionine-containing peptides were also included. All other parameters were set as default. Since MaxQuant provides only non-normalized reporter intensities, values were quantile normalized using the Normalyzer package [271] in R [272].

4.2.6 Animal experiments

C57BL/6 (wild-type) mice were bought from Charles River Laboratories. Breeding pairs for $Cd14^{-/-}$ mice were purchased from Jackson Laboratory and expanded in the animal facility. $Tlr2^{-/-}$ and $Tlr4^{-/-}$ mice were provided by Dr. M. Freudenberg (Max Planck Institute for Immunobiology and Epigenetics, Freiburg, Germany). $Tlr2^{-/-}/Tlr4\text{-}m$ mice ($Tlr2^{-/-}$ mice carrying a functional TLR4 mutation) were provided by Prof. Dr. C.J. Kirschning (Institute of Medical Microbiology, University of Duisburg-Essen, Essen, Germany). ABIN1[D485N] mice [147] were a generously gift by Philip Cohen (Medical Research Council Protein Phosphorylation and Ubiquitylation Unit, University of Dundee, United Kingdom). Mice were housed and paired in a specific pathogen-free (SPF) breeding facility at the Goethe University Frankfurt. All animal work was done in accordance with the German Animal Protection Law and was approved by the Ethics Review Committee for laboratory animals of the District Government of Darmstadt, Germany.

4.2.7 *In vivo* overexpression of soluble biglycan

To transiently overexpress soluble biglycan in mice, human biglycan cDNA (h*BGN*) was inserted into the BamHI/SacII site of the pLIVE™ (Liver In Vivo Expression) vector under control of the albumin promotor [66]. In this way, soluble biglycan is specifically overexpressed in the liver and distributed in its soluble form over the circulation into various organs [66]. For overexpression, 8-10-week-old C57BL/6 and $Cd14^{-/-}$ mice were given a single intravenous injection containing 50 µg of the pLIVE-h*BGN* vector in 300 µl 5% glucose solution together

with ExGen500 TurboFect *In Vivo* Transfection Reagent (Thermo Fisher Scientific, Germany). As a control, empty pLIVE vector was utilized. Mice were transfected with either pLIVE-h*BGN* or pLIVE control for 3 days before animals underwent IRI.

4.2.8 Induction of renal ischemia/reperfusion injury

For induction of renal IRI, mice were anaesthetized by an intraperitoneal injection of ketamine/xylazine (100 mg/kg and 5 mg/kg, respectively). The fur over the left and right kidneys was shaved with a razor and disinfected with 70% ethanol. Only mice which no longer reacted to the toe pinch were used for operation to prevent pain. During operation, mice were put on a heating plate at 37°C. First, a small midline incision was made over the left kidney. The left renal pedicle was tied off with two knots, then distally sectioned and the kidney was removed. After ensuring that no blood is leaking out of the wound, the incisions of the peritoneum and the skin were closed. Afterwards, a second incision over the right kidney was made. The right kidney was taken out of the wound as much as possible without hurting the organ. Then, the right artery of the right kidney was clamped for 25 min with an atraumatic microaneurysm clamp. During the 25 min, the kidney was protected from drying by applying 0.9% NaCl solution. After 25 min the clamp was removed and the restoration of blood flow was observed for 1 min until the kidney returned to its original color and placed back into the peritoneum. Finally, the incision was closed. Mice were kept in the heating plate until they woke up and then transferred into their respective cages. To reduce pain for the animals, buprenorphine (0.1 mg/kg) was given by a subcutaneous injection every 8 h, starting before operation. Sham-operated mice served as controls and received the same surgical procedures except that neither nephrectomy nor application of the microaneurysm clamps was performed. Mice were sacrificed 30 h after reperfusion by an intraperitoneal overdose of pentobarbital. Blood was collected with heparinized syringes. Afterwards, serum was isolated from the blood for ELISA. Kidney tissues were harvested for ELISA, RNA extraction, Western blot analysis and histological analysis. One half of the kidneys were fixed in PBS with 4% paraformaldehyde and 0.1% Tween 20 at 4°C overnight. Kidneys were then washed 3 times with dH_2O and placed into plastic tissue cassettes. Subsequently, samples were put into an automatic tissue processor for further dehydration and processing with 50%, 75%, 90%, 96%, 100% ethanol, isopropanol, xylol, followed by paraffin wax. Ultimately, samples were transferred into a stainless tissue ring filled with melted wax, closed with a plastic block and then chilled on a cold plate until the wax became solid. Hereafter, wax blocks were removed and stored at RT until further analysis.

4.2.9 Immunohistochemical staining and quantification

Tissue structure of kidney sections (4 µm) of paraffin-embedded kidneys from mice was determined by periodic acid-Schiff (PAS) staining. Tissue slides were deparaffinized by treatment with xylol for 20 min. Then, slides were rehydrated by 3 min incubation steps in 100%, 95%, 70% and 50% ethanol and finally dH_2O. Following rehydration, the tissue was oxidized with 0.8% periodic acid for 5 min and rinsed 3 times with dH_2O. Subsequently, Schiff´s reagent was applied for 15 min to the slides. After that, slides were washed under running dH_2O. Counterstaining was performed with Mayer's hematoxylin solution. At last, slides were washed with tap water and covered with Entellan. The degree of severity of renal damage after IRI was graded from 0 to 5 by counting the percentage of tubules, which displayed loss of brush border, cast formation, cell necrosis and tubular dilation: 0, none; 1, < 10%; 2, 11%-25%; 3, 26%-45%; 4, 46%-75%; and 5, > 76% [61]. A minimum of 5 high-power fields with a magnification of x200 were used for quantification of each section/sample by 2 observers blinded to the study.

4.2.10 Serum creatinine assay

Renal failure was analyzed by determination of serum creatinine by using a colorimetric Microplate Assay (Cayman chemical, Germany). In order to measure serum creatinine, serum samples and standard were mixed with creatinine reaction buffer containing sodium borate, sodium hydroxide and surfactant. After adding creatinine color reagent containing 1.2% picric acid the Jaffe reaction starts wherein a yellow/orange color is formed depending on the concentration of creatinine in the serum. For measurement, absorbance was determined at 490 nm after 1 min and again after 7 min. Serum creatinine levels were calculated according to the equation provided in the manufacturers' instruction.

4.2.11 Macrophage isolation and stimulation

Five days after intraperitoneal injection of 2 ml thioglycolate, mice were anesthetized via isoflurane chamber and sacrificed by cervical dislocation. The abdomen was sterilized with 70% ethanol and the peritoneum was freed from excessive skin and fur. Subsequently, peritoneal macrophages were isolated by flushing the peritoneum with PBS. Until stimulation, macrophages were cultured in RPMI 1640 supplemented with 1% P/S and 2% FBS. Macrophages isolated from C57BL/6 and $Cd14^{-/-}$ mice were stimulated with 4 µg/ml (80 nM) intact human biglycan protein in serum-free medium for various time points. To inhibit CD14 function, macrophages were pre-incubated for 1 h with 10 µg/ml of purified NA/LE rat anti-mouse CD14 (4C1, BD Biosciences, Germany) or 10 µg/ml of purified NA/LE rat IgG2b, κ isotype control (A95-1, BD Biosciences, Germany).

4.2.12   Macrophage and tissue lysis

Macrophage or tissues were lysed in buffer containing 150 mM NaCl, 5 mM Tris-HCl (pH 8.0), 0.02% NaN_3, 0.1% SDS, 1 µg/ml aprotinin, 1% NP-40, 0.5% sodium deoxycholate, 100 µg/ml PMSF and 1x protease inhibitors and centrifuged at 10.000 rpm for 10 min at 4°C. Kidney tissues were homogenized in lysis buffer containing 137 mM NaCl, 20 mM Tris-HCl (pH 8.0), 5 mM EDTA, 10% glycerol and 1% Triton X-100. Then samples were centrifuged at 14.000 g for 15 min at 4°C. Supernatants were snap-frozen and stored at -80°C for subsequent analysis. Pierce BCA Protein Assay Kit was used for determination of total protein concentration. BSA standards with a known concentration and samples were diluted in DEPC-treated H_2O in a 96-well plate and mixed with BCA Reagent A and B, prepared according to the manufacturer's protocol. Samples were incubated at 37°C and absorbance was measured at 562 nm. A standard curve derived from the BSA standards was utilized to determine protein concentrations.

4.2.13   RNA Isolation and reverse transcription (RT)

RNA was isolated from kidney tissue or $3x10^6$ murine adherent macrophages using TRI Reagent. 1 ml of TRI reagent was put directly on the smashed tissue or cells on ice. Afterwards, samples were incubated for 2 min at RT. To separate the DNA from the RNA, 200 µl chloroform was added to the samples and the mixture was shaken vigorously for 1 min at RT. After 2 min of incubation, samples were centrifuged at 14.000 rpm for 15 min at 4°C. The upper phase containing the RNA was transferred into a new tube, precipitated using 550 µl isopropanol and vortexed gently. The RNA was left for 10 min at RT and subsequently centrifuged at 14.000 rpm for 15 min at 4°C. The RNA pellet was washed with 1 ml 80% ice cold ethanol and briefly vortexed before centrifugation at 8400 rpm for 5 min at 4°C. Ethanol was discarded and the RNA pellet was dried at RT before being resuspended in DEPC-treated water. The RNA concentration was determined using the Nano-Drop device and quality checked for an A_{260}/A_{280} ratio of 1.8 to 2.0 as well as for a ratio of $A_{260}/A_{230} > 2$. For generation of cDNA, 1 µg of RNA was reverse-transcribed using the High-Capacity cDNA Reverse Transcription Kit (Applied Biosystems, Germany). Samples were added to the reverse transcription mixture consisting out of reverse transcription primers, reverse transcription buffer, dNTP mix and 1 µl MultiScribe® Reverse Transcriptase. The reaction mix was filled up with DEPC-treated water to 30 µl. To start the reaction, the mixture was incubated for 10 min at RT. Finally, the reaction is carried out at 37°C for 2 h and then terminated by incubating at 85°C for 5 min.

4.2.14   Quantitative real-time PCR

For real-time quantitative PCR 1 µl of cDNA was either added to Taqman Fast Advanced Master Mix (Applied Biosystems, Germany) together with TaqMan Gene Expression Assay

primer (Table 13) or Luminaris High Green Low ROX qPCR Mastermix (Thermo Fisher Scientific, Germany) with SyBR Green primer pairs (Table 13).

Table 13: TaqMan and SyBR Green primers for qRT-PCR

Primer	Catalog number/ primer sequence 5´- 3´
mTnfα	Mm00443260_g1
mCcl2	Mm00441242_m1
mCcl5	Mm01302427_m1
mGapdh	Mm 99999915_g1
mGapdh-forward	CATGGCCTTCCGTGTTCCTA
mGapdh-reverse	CCTGCTTCACCACCTTCTTGAT
mHsp70-forward	GCAAGGCCAACAAGATCACCAT
mHsp70-reverse	GGCGCTCTTCATGTTGAAGC

Quantification of changes in gene expression were performed in doublets. Samples were analyzed using the AbiPrism 7500 Sequence Detection System with the PCR conditions shown in table 14 and 15.

Table 14: PCR protocol for Taqman

Temperature	Time	Number of cycles
95°C	20 sec	1
95°C	3 sec	
60°C	30 sec	40x

Table 15: PCR protocol for SyBR Green

Temperature	Time	Number of cycles
95°C	10 min	1
95°C	15 sec	
60°C	60 sec	40x

The dissociation curve of all genes was observed to exclude non-specific amplifications. The Ct value (i.e. significant increase in generated fluorescence compared to the background signal) of each sample was used to determine relative changes in gene expression. mRNA expression of each gene was compared to control, normalized to *Gapdh* and quantified by the $2^{-\Delta\Delta Ct}$ method with the following formulas:

ΔCt = Ct (*gene of interest*) – Ct (*Gapdh*)

ΔΔCt = ΔCt (control) – ΔCt (sample)

Fold change = $2^{-\Delta\Delta Ct}$

4.2.15 Enzyme-linked immunosorbent assay (ELISA)

ELISA kits were used according to the manufacturer's instructions to determine cyto- and chemokine levels in either cell culture supernatants of mouse peritoneal macrophages or in tissue lysates from isolated mouse kidneys. Briefly, capture antibody was diluted in PBS and coated on 96-well plates overnight at RT. The next day, unbound antibody was washed away with wash buffer (PBS with 0.05% Tween-20) and non-specific bindings sites were blocked with 1% BSA for 1 h. Plates were washed again 3 times and samples as well as standards of known concentration were diluted and incubated for 2 h. Afterwards, unbound proteins were removed by washing for 3 times. Biotin-labeled detection antibody was applied for 2 h and subsequently washed 3 times. Thereafter, streptavidin-HRP was coupled to the detection antibody by incubation for 20 min in the dark. Finally, after washing, probes were developed by addition of equal volumes of stabilized hydrogen peroxide and stabilized tetramethylbenzidine until desired intensity. Reaction was stopped by addition of 1 M sulfuric acid. Optical density was analyzed at 450 nm with a reference wavelength of 570 nm. In case of ELISAs from kidney lysates, the measurements were normalized to total protein concentration of the homogenate that was determined by BCA Assay. The following ELISA kits from R&D Systems (Germany) were used: murine TNF-α, (DY410), CCL2 (DY479) and CCL5 (DY478).

4.2.16 SDS-Page and Western blotting

Sodium-dodecyl-sulfate polyacrylamide gel electrophoresis (SDS-PAGE) was used to separate proteins according to their molecular weight. Polyacrylamide concentration was adjusted according to the desired fractionation range of the proteins of interest. Samples were concentrated to one band in a 5% stacking gel (0.125 M Tris-HCl pH 6.8, 0.1% SDS, 5% acrylamide, 0.05% TEMED, 0.01% APS) and separated according to their size on a separation gel (0.375 M Tris-HCl pH 8.8, 0.1% SDS, 0.05% TEMED, 0.01% APS) containing typically 6-15% acrylamide. Protein samples were mixed with 4x loading buffer (125 mM Tris-HCl pH 6.8, 20% glycerol, 6% SDS, 10% mercaptoethanol, 0.02% bromphenolblue) and boiled for 10min at 95°C. Gels were run in SDS-Page running buffer (25 mM Tris-HCl, 192 mM glycine, 0.1% SDS) with a constant voltage between 70 and 100. After SDS-PAGE electrophoresis, the proteins were transferred to a Hybond Amersham nitrocellulose membrane or pre-activated polyvinyl difluoride (PVDF) membrane in transfer buffer (25 mM Tris-HCl, 192 mM glycine, 20% (v/v) isopropanol) at 250 mA for 1 h followed by 350 mA for 30 min. Afterwards, the

membrane was shortly washed in TBST (125 mM Tris-HCl pH 7.4, 150 mM NaCl, 0.05% Tween-20) and blocked in blocking buffer (5% non-dry fat milk in TBST) for 1 h. The membrane was incubated gently shaking with primary antibody (Table 16) diluted in blocking buffer overnight at 4°C. On the following day, the membrane was washed 3x 10 min with TSBT and incubated with secondary HRP antibody. After 3 washing steps á 10 min, the membrane was developed using Pierce ECL Western Blotting Substrate or SuperSignal West Femto maximum sensitivity substrate for 1 min and detected with X-ray films in the dark. The optical density of bands was quantified using the Quantity one software (Bio-Rad, Germany) and normalized to a housekeeping gene.

Table 16: Western blot antibodies

Antibody against	Catalog number	Host	Dilution	Company
Biglycan	TA302434	Goat IgG	1:2000 in ROTI	Acris, Germany
β-actin	A5441	Mouse IgG	1:5000 in 5% milk	Sigma Aldrich, Germany
CD14	ab182032	Mouse IgG1	1:1000 in 5% milk	Abcam, Germany
HSP70	ab181606	Rabbit IgG	1:1000 in 5% milk	Abcam, Germany
P-38	#9211	Rabbit	1:1000 in 5% BSA	Cell Signaling, Germany
p38	#9212	Rabbit	1:1000 in 5% BSA	Cell Signaling, Germany
P-p44/42	#9101	Rabbit	1:1000 in 5% BSA	Cell Signaling, Germany
p-44/42	#9102	Rabbit	1:1000 in 5% BSA	Cell Signaling, Germany
P-NF-κB p65 (Ser536) (93H1)	#3033	Rabbit	1:1000 in 5% BSA	Cell Signaling, Germany
NF-κB p65 (T180/Y182)	sc-109	Rabbit IgG	1:1000 in 5% milk	Santa Cruz, Germany
Rabbit IgG	NA934V	Donkey IgG HRP	1:3500 in buffer of primary AB	GE healthcare, Germany
Mouse IgG	NA931V	Sheep IgG HRP	1:5000 in buffer of primary AB	GE healthcare, Germany
Goat IgG	705-035-147	Donkey IgG HRP	1:3500 in buffer of primary AB	Jackson ImmunoResearch Laboratories, USA
ABIN-1	15104-1-AP	Rabbit IgG	1:1000 in 5% milk	Proteintech, United Kingdom
GFP	sc-9996	Mouse IgG2a	1:500 in 5% milk	Santa Cruz, Germany

LC3B	NB100-2220	Rabbit IgG	1:8000 in 5% milk	Novus Biologicals, Germany
HA	Sc7392	Mouse IgG2a	1:500 in 5% milk	Santa Cruz, Germany
TOM20	sc17764	Mouse IgG2a	1:500 in 5% milk	Santa Cruz, Germany
VDAC1	Ab14734	Mouse IgG2b	1:1000 in 5% milk	Abcam, Germany
MFN2	Ab56889	Mouse IgG2a	1:1000 in 5% milk	Abcam, Germany
COXII	Ab110258	Mouse IgG2a	1:1000 in 5% milk	Abcam, Germany
Parkin	Sc32282	Mouse IgG2b	1:500 in 5% milk	Santa Cruz, Germany

4.2.17   Co-immunoprecipitations

Co-immunoprecipitation (IP) of CD14 and intact biglycan was done using Protein A Agarose affinity chromatography matrix immobilized with anti-biglycan antibody and recombinant biglycan complexes bound via the irreversible cross-linker BS3 according to manufacturer's description. Shortly, 2 mg protein of macrophage lysate derived from WT and $Cd14^{-/-}$ mice was added to the agarose resin coupled with biglycan and eluted via addition of protein loading buffer at 95°C for 8min. Subsequently, eluates were digested with chondroitinase ABC enzyme in presence of 1x protease inhibitor and 50 mM acetate at 37°C for 2 h to remove the GAG chains of biglycan [53, 266] and transferred to SDS-PAGE and Western blotting.

For immunoprecipitation of HA-tagged proteins, hABIN-1-HA was transiently overexpressed in HeLa cells for 24 h. The next day cells were treated with BafA1 for 4 h and lysed. Afterwards, 16 µl of Pierce Anti-HA Magnetic Beads were washed 3 times with PBS containing 0.05% Tween 20 by magnetic separation. A total of 800 µg protein lysate with protease inhibitors was added to the magnetic beads and incubated for 2 h at 4°C on a rotator. Afterwards, beads were washed 3 times with ice cold PBS containing 0.05% Tween 20 and eluted in 2x loading buffer at 95°C for 8 min and analyzed by SDS-PAGE and Western blotting.

4.2.18   GFP-Trap

Immunoprecipitation of GFP-tagged proteins was performed using the GFP-Trap®_MA kit. Briefly, GFP-Trap beads were vortexed and 25 µl were pipetted into 500 µl of ice-cold dilution buffer containing 10 mM Tris-HCl (pH 7.5), 150 mM NaCl and 0.5 mM EDTA. Beads were magnetically separated and washed for a total of 3 times. For protein binding, 800 µg of lysate from cells expressing GFP-fusion proteins was added together with protease inhibitors to the GFP beads, filled up to a total volume of 500 µl and incubated for 1 h at 4°C on a rotator. After incubation, beads were washed 3 times with dilution buffer. Then, beads were resuspended in 40 µl 2x loading buffer and boiled at 95°C for 10 min to dissociate the complexes from the

beads. Afterwards, eluates were transferred to SDS-PAGE and Western blotting or stored at -80°C.

4.2.19 GST protein expression and pulldown

LC3A, LC3B and 4xUbiquitin (4xUb) were cloned into the pGEX-4T-1 (GE healthcare, Frankfurt am Main) vector, while ABIN-1 either as full length, LIR1-, LIR2- or double LIR-mutated (LIR1+2) variant was cloned into the pMAL-c2x (NEB, Frankfurt am Main) vector. GST-tagged proteins or MBP-tagged ABIN-1 were expressed by transformation in *Escherichia coli* BL21 (DE3) cells in LB medium and grown until an OD_{600} of 0.5-0.8 (bacteria in log-phase). Protein expression was induced by adding 0.5 mM Isopropyl-β-D-thiogalactopyranosid (IPTG) overnight at 16°C in a shaking incubator to reduce the likelihood of misfolded or aggregated proteins. The next day, cells were harvested, resuspended in lysis buffer containing 20 mM Tris-HCl (pH 7.5), 10 mM EDTA, 5 mM EGTA and 150 mM NaCl, sonificated and incubated for 50 min at 4°C. Lysates were centrifuged at 8000 rpm for 20 min at 4°C and then applied to washed glutathione sepharose 4B (GST) beads or amylose resin for 2 h at 4°C on a rotator. After 3 times washing with 20 mM Tris-HCl (pH 7.5) and 150 mM NaCl, purified fusion proteins were directly used for GST-pulldown. MBP-tagged ABIN-1 was added to GST-fused protein beads and incubated for 2 h at 4°C on a rotator. Subsequently, beads were centrifuged, washed for 3 times with wash buffer and eluted by boiling in 2x SDS loading buffer at 95°C for 8 min. Finally, purities of GST-fusion proteins were analyzed by Coomassie staining using InstantBlue Protein Gel Stain, while binding of MBP-tagged ABIN-1 to GST-fusion proteins was detected by Western blot.

4.2.20 Mitochondrial degradation assays

To track the degradation of mitochondrial substrates, either $0.8x10^6$ HeLa-mCherry-Parkin or ABIN-1 KO-mCherry-Parkin (clone 16 or 27) cells were seeded 1 day before treatment in growth medium without antibiotics. For mCherry-Parkin protein expression, 0.5 µg/ml doxycycline (DOX) was added to the medium. Cells were stimulated with 10 µM oligomycin/antimycin A (referred to as OA) for 30 min, 2 h or 4 h. For a longer treatment period of 24 h, the concentration of OA was reduced to 1 µM, while 0.5 µg/ml DOX was added simultaneously to OA treatment. The degradation of mitochondrial substrates was observed via Western blot analysis.

4.2.21 Mitochondrial fractionation

For the isolation of a highly enriched mitochondrial fraction, $3.3x10^6$ HeLa-mCherry-Parkin cells were seeded in 100 mm dishes 24 h before stimulation in growth medium containing 0.5 µg/ml DOX to induce mCherry-Parkin protein expression. The next day cells were either

treated with 10 µM OA or 10 µM DMSO as control for 4 h. Then, cells were washed once with ice-cold PBS, carefully scraped and transferred into 15 ml falcons, followed by a washing step with 10 ml ice-cold PBS. Cells were centrifuged at 6000 g for 5 min at 4°C, resuspended in 1 ml Cytosol Extraction Buffer containing DTT and protease inhibitors and incubated for 10 min on ice. Afterwards, cells were homogenized using an ice cold Dounce tissue grinder by 40 passes on ice. The homogenates were transferred into microcentrifuge tubes and centrifuged at 700 g for 10 min at 4°C. The pellet was discarded and the supernatant was centrifuged at 10.000 g for 30 min at 4°C, resulting in a cytosolic supernatant and a pellet containing intact mitochondria. Mitochondrial pellet was lysed with 100 µl of Mitochondrial Extraction Buffer containing DTT and protease inhibitors, vortexed for 10 sec and saved at -80°C. All fractionations were analyzed by Western blot.

4.2.22   Microscale thermophoresis

Binding affinities of intact biglycan and biglycan protein core with recombinant human CD14 were analyzed by microscale thermophoresis (NanoTemper Technologies, Germany). Recombinant intact biglycan and His-tagged biglycan protein core with a starting concentration of 20 µM were labeled with the red fluorescent dye NT-647 (Cy5) by using a Monolith Protein Labeling Kit Red (NanoTemper Technologies, Germany) according to the manufacturer's instructions. A 12-fold titration series of recombinant His-tagged CD14 (2 µM to 0.977 nM) diluted 1:1 with PBST (0.05% Tween-20 in PBS) was performed. The concentration of NT-647–labeled biglycan or NT-647-labeled biglycan protein core-His was kept constant (11 nM). The binding of NT-647-labeled albumin (Thermo Fisher Scientific, Germany) or NT-647-labeled His-tagged albumin (antibodies-online, Germany) to His-tagged CD14 and His-tagged biglycan protein core were used as negative controls in order to exclude protein-His tag or His tag-His tag interactions, respectively. Before measurements, binding partners were incubated for 30 min in the dark to guarantee binding of the proteins. Afterwards, samples were centrifuged for 5 min at 13000 g to remove large aggregates and then aspirated into glass capillaries. The thermophoretic movement of labeled proteins was monitored with a laser On for 30 s and Off for 5 s at a laser power of 100%. The Monolith NT.115 device (NanoTemper Technologies, Germany) was used for measurement. Fluorescence was measured before laser heating ($F_{Initial}$) and after 30 s of laser-on time (F_{Hot}). Binding curves were generated by normalizing the data to fraction bound. In case of the negative controls, the normalized fluorescence $F_{Norm}= F_{Hot}/F_{Initial}$ was plotted directly and multiplied by a factor of 10, generating a relative change in fluorescence per mill (parts per thousand, ‰) specified as F_{Norm} [‰]. F_{Norm} represents the concentration ratio of labeled molecules. Error bars shows standard deviation from three measurements. KD values were calculated by using the NanoTemper analysis

software (NanoTemper Technologies, Germany) and averaged from three independent thermophoresis measurements.

4.2.23 Flow cytometry

4.2.23.1 FACS analysis of infiltrating macrophages

Fresh kidneys from either IRI- or Sham-operated mice were digested in 5 ml 0.5 mg/ml Collagenase A in DMEM with 10% FBS at 37°C for 45 min. After digestion, kidney homogenates were filtered through a 70 µm cell strainer with ice cold PBS. Afterwards, cells were centrifuged for 10 min at 1400 rpm at 4°C. ACK buffer containing 0.15 M NH_4Cl, 10 mM $KHCO_3$ and 0.1 mM Na_2EDTA was used to lyse all red blood cells. Lysis was stopped by addition of 30 ml of ice-cold PBS. Then, cells were centrifuged again at 1400 rpm at 4°C for 10 min and were subsequently washed with FACS buffer (1% FBS, 0.1% NaN_3 in PBS). Washed cells were incubated for 10 min with anti-CD16/32 (FCγ RIII/II) to inhibit unspecific staining during antibody incubation. F4/80-PE and CD11b-APC were used as antibodies to mark infiltrating macrophages together with corresponding isotype controls. After 30 min of incubation in the dark at 4°C, cells were washed once with FACS buffer and then fixed with 1% paraformaldehyde. To exclude dead cells from the analysis, cells were additionally supplemented with -amino-actinomycin D (7-AAD) prior to analysis. All samples were measured at the FACSCanto II flow cytometer and analyzed via the FACS Diva Software.

4.2.23.2 Isolation and analysis of leukocytes from renal tissues

Kidney were collected, minced with a scalpel and incubated with 0.5 mg/ml Collagenase A in DMEM with 10% FBS at 37°C for 45 min. Afterwards, the homogenates were filtered through a 70 µm cell strainer, filled up with ice cold PBS and centrifuged at 1400 rpm at 4°C for 10 min. The supernatant was discarded. Mononuclear cell isolation was done via Percoll density gradient centrifugation (72% and 37%). The remaining cells were resuspended in 25 ml of 37% Percoll. Then, 15 ml of 72% Percoll were layered carefully at the bottom of the 37% Percoll with a syringe and a long needle. Percoll gradient was centrifuged at 1500 rpm for 30 min at RT without break. Mononuclear cells were then transferred from the interface between the 37% and 72% Percoll to a new falcon tube and washed once with ice cold PBS. Cells were resuspended in ice-cold ACK buffer for 5 min and washed with PBS before staining for flow cytometry. Unspecific staining was prevented by treatment with anti-mouse CD16/32 (FCγ RIII/II). Subsequently, cells were washed with FACS buffer and stained with anti-mouse F4/80-PE and anti-mouse CD38-APC for 30 min at 4°C. CD38-APC represents a newly described

exclusive M1-macrophage marker [273] with high specificity. Respective isotype controls were used as a control.

4.2.23.3 Mito-mKEIMA assay

For the mt-mKEIMA assay, HeLa FlpIn TRex cells (clone 33) stably expressing mt-mKEIMA and doxycycline-inducible Parkin (generous gift from Jonas Michaelis, IBCII, Frankfurt am Main) were seeded into 6-well plates one day before siRNA knockdown in growth medium without antibiotics. The next day, siRNA knockdown of hABIN-1 was performed as described before for a period of 48 h with siRNA against hABIN-1 or siRNA Co. After 24 h, 0.25 µg/ml DOX was added to the cell culture medium to for the induction of Parkin expression. After 42 h, cell culture medium was replaced with fresh medium containing 0.25 µg/ml DOX. At the same time, cells were stimulated with DMSO (10 µM), OA (10 µM) or OA (10 µM) together with BafA1 (200 nM) for a period of 6 h. Then, cells were washed with 2 ml PBS, trypsinized and centrifuged at 800 g for 3 min at 4°C. Cells were resuspended in 1 ml of ice-cold PBS and immediately analyzed. 20.000 fluorescent cells per sample were collected and analyzed by FACS for dual-excitation at 405 (pH 8) and 561 (pH 4) nm with 610/20 nm emission filters. By analysis of the 561 nm: 405 nm ratio, the percentage of lysosomal mt-mKEIMA can be calculated. Experiments were performed with BD LSRFortessa equipped with 405, 488, 561 and 640 nm LASER.

4.2.23.4 Analysis of autophagic flux by FACS

In order to determine autophagic flux by flow cytometry, HeLa FlpIn TRex cells (clone 37) stably expressing mKEIMA-hLC3B (generous gift from Jonas Michaelis, IBCII, Frankfurt am Main) were seeded into 6-well plates 24 h before siRNA transfection with siRNA hABIN-1 or siRNA Co. After 44 h growth medium was replaced and cells were treated with either DMSO (1 µM), Torin-1 (1 µM) or Torin-1 with BafA1 (200 nM) for 4 h. Alternatively, cells were starved by medium replacement to EBSS or EBBS in combination with BafA1 (200 nM) for 4 h. Cells were then processed and analyzed in the same way as described for the mt-mKEIMA assay.

4.2.24 Immunofluorescence microscopy

4.2.24.1 Imaging of macrophages via super-resolution microscopy

4×10^5 peritoneal mouse macrophages were seeded 24 h before stimulation on tissue culture-treated 8-well chamber glass slides. For stimulation, either biglycan (4 µg/ml) or DMSO were added to the cell culture medium for 30 min. Afterwards, macrophages were washed once with PBS and fixed with 4% paraformaldehyde at 4°C for 30 min. After 3 times washing with PBS,

cells were permeabilized with 0.2% Triton X-100 for 30 s and blocked in 5% BSA in PBS for 1 h at RT. Primary antibody incubation with either rabbit anti-mouse phospho-p38 MAPK (T180/Y182), phospho-p44/42 MAPK (Thr202/Tyr204) or phospho-NF-κB p65 (S536) was performed by overnight incubation at 4°C (Table 17). The next day, macrophages were washed with 3 times with PBS and incubated with goat anti-rabbit IgG Alexa-Flour488 for 1 h in the dark at RT. Then, macrophages were washed 2 times with PBS, once in H_2O. Nuclei were stained by mounting the slides in VECTASHIELD Antifade Mounting Medium including DAPI. Fluorescence images were taken with a 63x, 1.3 oil-immersion objective, using a Zeiss LSM780 ELYRA PS.1 Super Resolution confocal microscope. Merge images show single optical sections (<0.8 µm), collected with the pinhole set to 1 Airy Unit for the green channel and adjusted to give the same optical slice thickness in the blue channels. All images were obtained in single confocal planes and super-resolved (Structured Illumination Microscopy, SIM) by utilization of the Zeiss software ZEN2012 SP5, with filters set at 488/405 nm for dual-channel imaging and Z-stacks acquired at 0.36 µm intervals. All images were analyzed using Adobe Photoshop CS6.

4.2.24.2 Imaging of HeLa cells by laser scanning microscopy

0.15×10^6 HeLa cells stably expressing mEGFP-hABIN-1 (DOX-inducible) were seeded in 6-well plates on autoclaved round microscope cover glasses in growth medium without antibiotics. To analyze co-localization of hABIN-1 with LC3B, cells were transfected the next day with mCherry-hLC3B-pcDNA3.1 (a gift from David Rubinsztein; Addgene plasmid #40827) using FuGENE HD Transfection Reagent. In case of co-localization studies of hABIN-1 with LAMP-1, cells were left un-transfected. At the same time, growth medium was supplemented with 0.5 µg/ml DOX to induce mEGFP-hABIN-1 protein expression. After 20 h, medium was replaced and cells were either treated with BafA1 (300 nM), Torin-1 (1 µM) or DMSO (1 µM) for 4 h. Afterwards, cells were rinsed with PBS and fixed with methanol for 10 min at -20°C. Cells were washed 3 times with PBS and blocked for 1 h in 5% FBS in PBS at RT. After rinsing with PBS, cells were either stained with anti-LAMP-1 antibody (Table 17) diluted in PBS containing 5% FBS overnight at 4°C. In contrast, mCherry-hLC3B-transfected cells were only blocked in antibody diluent overnight at 4°C. The next day, cells were rinsed 3 times with PBS and if necessary incubated with Goat anti rabbit IgG Alexa-Flour 594 for 1 h in the dark at RT. Then, cells were washed with PBS, once with H_2O and mounted using VECTASHIELD Antifade Mounting Medium including DAPI. Images were acquired using the Leica SP8 laser-scanning microscope and analyzed using Fiji-ImageJ software.

Table 17: Immunofluorescence antibodies

Antibody against	Catalog number	Host	Dilution	Company
phospho-p38 MAPK (T180/Y182)	#9211	Rabbit IgG	1:200 in 5% BSA	Cell Signaling, Germany
phospho-p44/42 MAPK (Thr202/Tyr204)	#9101	Rabbit IgG	1:200 in 5% BSA	Cell Signaling, Germany
phospho-NF-κB p65 (S536)	#3033	Rabbit IgG	1:200 in 5% BSA	Cell Signaling, Germany
LAMP-1	ab24170	Rabbit IgG	1:400 in 5% BSA	Abcam, Germany
Rabbit IgG	#A-11008	Goat IgG Alexa-Flour 488	1:400 in 5% BSA	Life Technologies, Germany
Rabbit IgG	#A-11012	Goat IgG Alexa-Flour 594	1:400 in 5% BSA	Life Technologies, Germany

4.2.25 Statistics

All data are expressed as means ± SD. An unpaired, 2-tailed, Student t test was used to evaluate the differences between 2 groups. For comparisons among more than 2 groups, a one-way ANOVA was used, followed by Bonferroni post hoc test (GraphPad Prism 6, San Diego, CA). Differences were considered significant at P values < 0.05.

5   Results

PART I

The main parts of the results written in 5.1 are described in the publication "Biglycan is a new high-affinity ligand for CD14 in macrophages" in the journal Matrix Biology [274].

5.1   CD14 governs biglycan-mediated pro-inflammatory signaling

So far, research focused on the interaction of biglycan to TLR2 and TLR4. Detailed work revealed that biglycan triggers inflammation by selectively interacting with TLRs and the corresponding TLR adaptor molecules TRIF or MyD88. Accordingly, biglycan engages TLR2/4/MyD88 in order to induce the expression of TNF-α, CCL2 and CCL20, whereas selective interaction of biglycan with TLR4/TRIF triggers CCL5 and CXCL10 expression [61, 62, 66]. The specific interactions of biglycan with various receptors complicate the identification of a druggable target to alleviate biglycan-induced inflammation. Interestingly, in 2005, biglycan was found in a high molecular weight complex together with MD2 and CD14 [31]. As CD14 is known to facilitate the recognition of various TLR ligands [86, 117], we decided to investigate the impact of CD14 in biglycan-triggered TLR2/4 signaling.

5.1.1   Biglycan-mediated TLR2/4 signaling is CD14-dependent

In order to investigate if CD14 is required for biglycan-mediated pro-inflammatory TLR2 and TLR4 signaling we isolated thioglycolate-elicited peritoneal macrophages from wild-type (WT) C57BL/6, *Tlr2^-/-^*, *Tlr4^-/-^*, *Tlr2^-/-^/Tlr4-m* and *Cd14^-/-^* mice and analyzed them after biglycan stimulation via either qRT-PCR or ELISA. Biglycan stimulation led to a high induction of TNF-α and CCL2 on both protein and mRNA levels in WT mice. In agreement with our previous findings [31, 66, 67], genetic ablation of TLR2 or TLR4 led to a significant reduction of TNF-α (Fig. 5.1 A and B) and CCL2 (Fig. 5.1 C and D), proving TLR2/TLR4-dependency in these cases. Interestingly, TLR4 knockout had greater effects on CCL2 protein levels as compared to mRNA, while TLR4 could be validated as the main receptor for TNF-α in both cases. Consistently, with our previous findings [66], biglycan-mediated induction of CCL5 could be determined as TLR4-dependent, since TLR2 ablation did not affect biglycan-induced mRNA or protein levels (Fig. 5.1 E and F). As expected, *Tlr2^-/-^/Tlr4-m* mice did not display any biglycan-mediated induction of TNF-α, CCL2 and CCL5 (Fig. 5.1 A-F). Importantly, *Cd14^-/-^*

mice showed no increase in TNF-α, CCL2 or CCL5 levels upon biglycan-stimulation, mimicking the double-deficient TLR2/4 mice (Fig. 5.1 A-F).
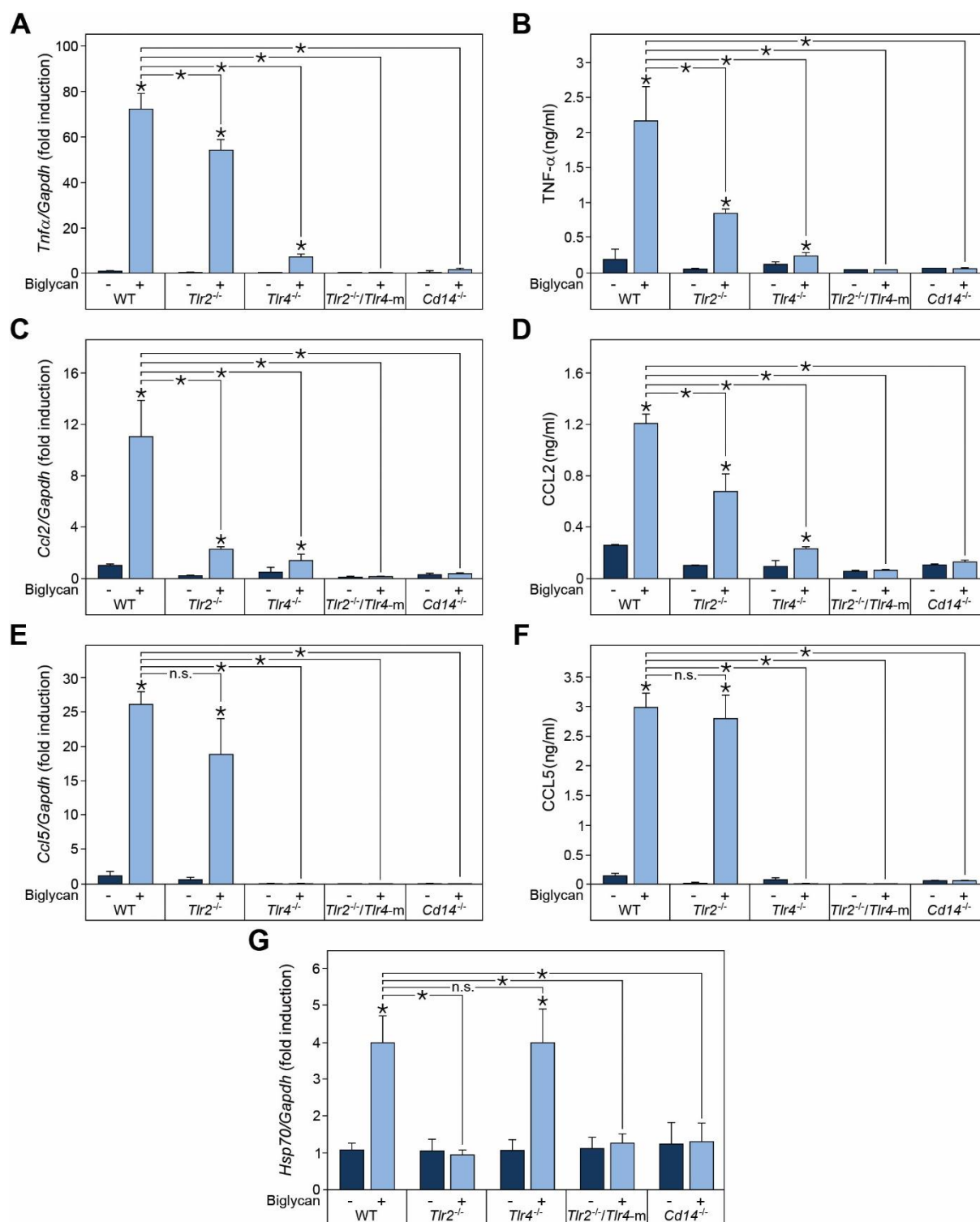

Figure 5.1. Biglycan-induced TNF-α, CCL2, CCL5 and HSP70 production in mouse peritoneal macrophages is CD14-dependent. (A-G) Macrophages isolated from C57BL/6 (WT), *Tlr2⁻/⁻*, *Tlr4⁻/⁻*, *Tlr2⁻/⁻/Tlr4-m* and *Cd14⁻/⁻* mice and treated with biglycan (4 µg/ml). Quantitative qRT-PCR of *Tnfα* (A), *Ccl2* (C), *Ccl5* (E) and *Hsp70* (G) mRNA, normalized to *Gapdh* and given as fold induction to untreated controls. ELISA analysis from the conditional media for protein levels of TNF-α (B), CCL2 (D) and CCL5 (F). Peritoneal macrophages were stimulated with biglycan for either 2 h (A and G) or 12 h (B-F). Data are given as means ± standard deviation (SD); (A-F) n = 3; (G) n = 6; *P < 0.05; n.s. = not significant.

To proof that CD14 is also needed for biglycan-mediated TLR2 signaling we evaluated the expression levels of HSP70, which is induced in macrophages solely in a TLR2-dependent manner [67]. In peritoneal macrophages from the same genetic backgrounds as described above, we confirmed TLR2-dependency of biglycan-mediated HSP70 induction. In agreement with this, a TLR4-deficiency showed no effect on biglycan-induced HSP70 levels after 2 h of stimulation (Fig. 5.1 G). Notably, *Hsp70* mRNA levels were not induced upon biglycan stimulation in *Cd14*^{-/-} mice on a comparable level to *Tlr2*^{-/-} or *Tlr2*^{-/-}/*Tlr4-m* mice (Fig. 5.1 G). This data provides robust evidence that CD14 is critical for pro-inflammatory biglycan signaling over TLR2 and TLR4.

Since, CD14 deficiency provided a strong genetic *in vitro* evidence that TLR2/4-mediated pro-inflammatory signaling of biglycan is CD14-dependent (Fig. 5.1), we investigated if we could corroborate our data by pharmacologically neutralization of CD14. Primary murine peritoneal macrophages isolated from WT mice were pre-incubated with an antibody directed against CD14 or a corresponding IgG isotype control for 1 h before biglycan stimulation (Fig. 5.2 A-C).
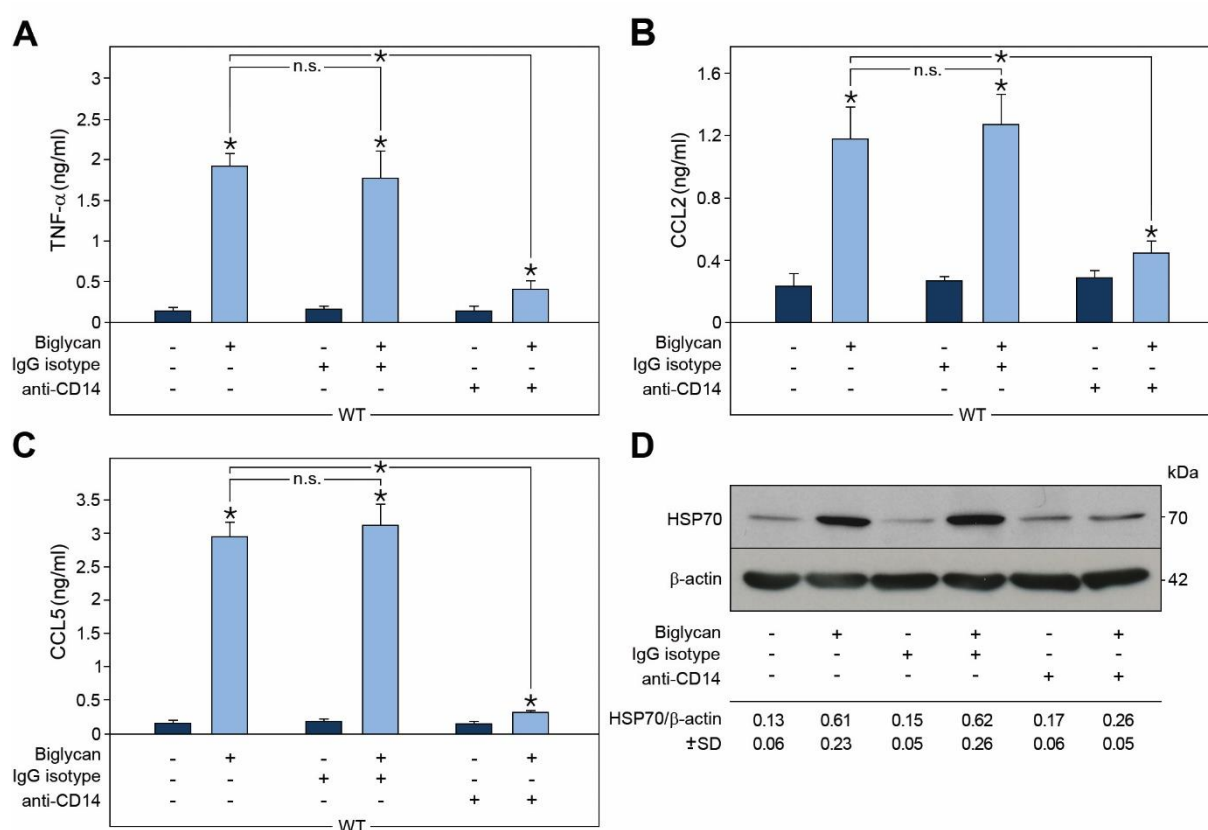

Figure 5.2. Antibody-mediated inhibition of CD14 reduces biglycan-induced TNF-α, CCL2, CCL5 and HSP70 protein levels in mouse peritoneal macrophages. (A-D) Macrophages derived from WT mice were pre-incubated with a specific CD14 antibody (anti-CD14; 10 µg/ml) or respective IgG isotype control (10 µg/ml) for 1 h and then treated with biglycan (4 µg/ml) for 12 h (A-C) or 30 min (D). ELISA (A-C) of TNF-α, CCL2 or CCL5 protein levels measured in the conditional media of macrophages. (D) Western blot analysis of HSP70 protein levels in whole cell lysates. HSP70 protein levels were normalized to β-actin. Data represent means ± SD; n = 3; *P < 0.05; n.s. = not significant.

Protein analysis revealed that biglycan-stimulated macrophages secreted significantly less TNF-α, CCL2 or CCL5 into the conditioned media after pre-incubation with an anti-CD14 antibody (Fig. 5.2 A-C). In the same line, HSP70 protein levels derived from whole macrophage lysates showed that pharmacological inhibition of CD14 halved biglycan-induced HSP70 levels compared to the IgG isotype control or unstimulated situation (Fig. 5.2 D).

To further investigate the role of CD14 as the co-receptor for TLR2 and TLR4 in biglycan-mediated signaling, HEK-Blue cells expressing hTLR2/CD14 (Fig. 5.3 A) as well as hTLR4/CD14/MD2 (Fig. 5.3 B), all carrying a reporter gene, were used. Transcriptional activation of NF-κB was monitored by active secreted alkaline phosphatase (SEAP). Since biglycan as a ligand of TLR2 and TLR4 is known to induce and activate translocation of NF-κB in immune cells [31], the HEK-Blue system was used as a direct readout. Peptidoglycan (PGN) and lipopolysaccharide (LPS) were used as positive controls and ensured that the cell lines only react to the respective TLR ligand. To ascertain whether CD14 is an important co-receptor of biglycan, an anti-CD14 antibody was used to inhibit biglycan-mediated TLR2/4 signaling. Transcriptional NF-κB activation could significantly be reduced by applying an anti-CD14 antibody prior to stimulation with biglycan whereas the respective IgG isotype control showed no effect (Fig. 5.3 A and B). Since CD14 facilitates the binding of LPS to the TLR4-MD2 complex [275] and binding of PGN to TLR2 [276], the blocking potential of the anti-CD14 antibody was tested upon stimulation of the corresponding cell lines by either PGN or LPS. In both cases, inhibition of CD14 led to significant attenuation of SEAP activity (Fig. 5.3 A and B). This shows that CD14 is needed for proper activation of biglycan-induced NF-κB signaling over TLR2/4.
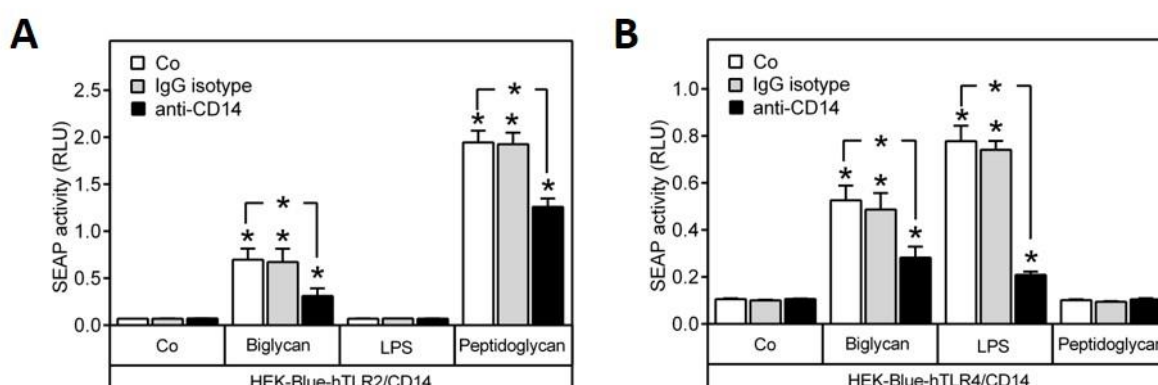

Figure 5.3. Biglycan-induced activation of TLR2/4/NF-κB is CD14-dependent. NF-κB activity represented as activity of secreted alkaline phosphatase (SEAP) in (A) HEK-Blue-hTLR2/CD14 and (B) HEK-Blue-hTLR4/CD14 cells determined using QUANTI-Blue. Cells were pre-treated with anti-CD14 antibody (10 µg/ml) or IgG isotype control (10 µg/ml) for 1 h and stimulated with biglycan (4 µg/ml), peptidoglycan (2 µg/ml) and lipopolysaccharide (LPS, 2.5 ng/ml) for 12 h. Data is shown as relative light units (RLU). Data represent means ± SD; n = 3; *P < 0.05.

5.1.2 CD14 is required for biglycan-mediated downstream signaling

To examine if CD14 affects biglycan-mediated downstream signaling we isolated primary murine peritoneal macrophages from WT and *Cd14-/-* mice and checked for the phosphorylation of p38, p44/42 and NF-κB. As biglycan-stimulation leads to a rapid activation of p38, p44/42 and NF-κB [31], we analyzed the phosphorylation status of p38 (T180/Y182), p44/42 (T202/Y204) and NF-κB (S536) by Western blot analysis after 30 min of biglycan stimulation. As expected, protein levels of P-p38, P-p44/42 and P-NF-κB all increased upon biglycan-stimulation in WT mice. Interestingly, the effect on intracellular signaling proteins by biglycan was completely abrogated in *Cd14-/-* mice (Fig. 5.4).
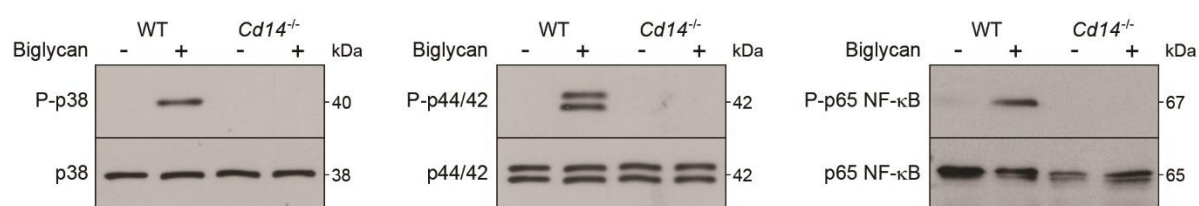

Figure 5.4. Biglycan-induced activation of p38 MAPK, p44/42 and NF-κB is dependent on CD14 in mouse peritoneal macrophages. Macrophages derived from WT or *Cd14-/-* mice were stimulated with biglycan (4 µg/ml) for 30 min and analyzed by immunoblotting for phosphorylated P-p38 (T180/Y182), P-p44/42 (T202/ Y204) and P-p65 NF-κB (S536). n = 3.

One hallmark during the activation process of p38 [277, 278] and p44/42 [279] is their nuclear translocation. This process is also described for NF-κB [280], whereas its intracellular localization highly depends on the phosphorylation of the p65 subunit either at serine 468 or 536 [281]. In order to verify CD14-dependent regulation on biglycan-induced activation and translocation of p38, p44/42 and NF-κB, we isolated peritoneal macrophages from WT and *Cd14-/-* mice and analyzed them by confocal microscopy. For this purpose, macrophages were stimulated with biglycan for 30 min and subsequently stained with antibodies against P-p38, P-p44/42 and P-p65 NF-κB. After biglycan stimulation we observed phosphorylation (T180/Y182) (in green) as well as translocation of cytosolic p38 MAPK protein into the nucleus in WT macrophages (Fig. 5.5, left panel, upper and lower images). In the same way, we could show translocation of p44/42 after its phosphorylation at T202/Y204 (Fig. 5.5, middle panel, upper and lower images) in response to biglycan stimulation. In support to our Western blot data, macrophages derived from *Cd14-/-* mice showed no translocation of p38 and p44/42 upon biglycan stimulation (Fig. 5.5, left and middle panel, upper and lower images). Additionally, biglycan induced the phosphorylation of the p65 NF-κB subunit at S536, in turn triggering its partial translocation into the nucleus in WT macrophages (Fig. 5.5, right panel, upper and lower images). In contrast, phosphorylation of p65 NF-κB was nearly undetectable in *Cd14-/-*

macrophages (Fig. 5.5, right panel, upper and lower images). Thus, CD14 represents a critical upstream element in biglycan-mediated downstream signaling.
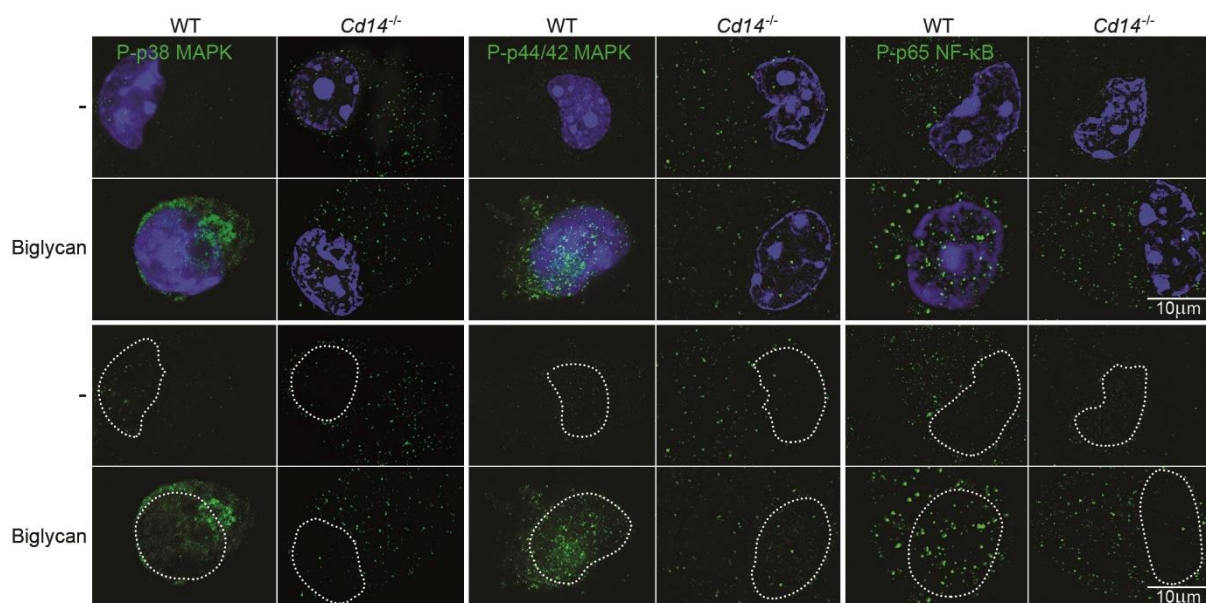

Figure 5.5. CD14 deficiency blocks biglycan-induced phosphorylation and translocation of p38 MAPK, p44/42 and NF-κB. Confocal images from WT- and *Cd14*$^{-/-}$-derived macrophages of phosphorylated P-p38 (T180/ Y182, green, left panel, upper and lower images), P-p44/42 (T202/Y204, green, middle panel, upper and lower images) or P-p65 NF-κB (S536, green, right panel, upper and lower). Nuclei (intimated by dotted lines, lower panel) were stained with DAPI (blue, upper panel). Scale bar indicates 10 µm; n = 3.

5.1.3 Biglycan binds CD14 in macrophages with high affinity

Biglycan binds mainly to TLR2 and TLR4 [61] via the conserved binding motif L-Q-X1-L/V-Y-X2 at LRR2 and LRR10 (Hsieh, unpublished data). As CD14 contains many LRR motifs [115], we analyzed the potential complex formation between biglycan and CD14 in primary peritoneal macrophages from WT and *Cd14*$^{-/-}$ mice by Co-immunoprecipitation utilizing recombinant biglycan. Co-immunoprecipitation with an anti-biglycan antibody revealed that biglycan indeed forms a complex with CD14 in macrophages (Fig. 5.6).
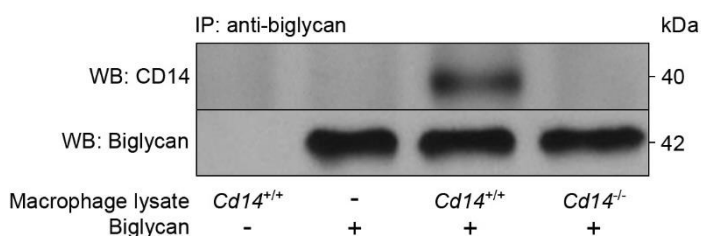

Figure 5.6. Biglycan forms a complex with CD14 in macrophages. Recombinant biglycan was immobilized on Pierce columns by an anti-biglycan antibody and used for Co-immunoprecipitation (Co-IP) with macrophage lysates of WT (*Cd14*$^{+/+}$) and *Cd14*$^{-/-}$ mice. Immunocomplexes were analyzed by Western blot. As negative controls, either anti-biglycan antibody (biglycan -) or lysate (macrophage lysate -) were left out of the Co-IP.

Direct binding between CD14 and biglycan was analyzed by microscale thermophoresis (MST). Binding affinities were quantified by determination of the respective dissociation constants (K_D). To this end, recombinant His-tagged CD14 was serial diluted at a ratio of 1:1 with a starting concentration of 2 µM. A fixed amount of fluorescent-labeled recombinant intact biglycan or His-tagged biglycan protein core were added to initiate direct binding in pure buffer conditions. MST analysis showed direct binding between fluorescent-labeled intact biglycan to CD14-His with a K_D of 67 ± 11 nM (Fig. 5.7 A). Interestingly, this binding affinity exceeds the binding capabilities of biglycan to TLR2 and TLR4 by nearly two-fold [61]. A loss of both GAG chains, using only fluorescent-labeled His-tagged biglycan protein core together with His-tagged CD14 revealed a slight increase in binding affinity with a K_D of 54 ± 18 nM (Fig. 5.7 C). Therefore, GAG chains seem to be irrelevant for binding of biglycan to CD14. As expected, no binding affinities between CD14-His to albumin (Fig. 5.7 B) or His-tagged biglycan protein core to His-tagged albumin (Fig. 5.7 D) could be determined, thereby excluding unspecific binding.
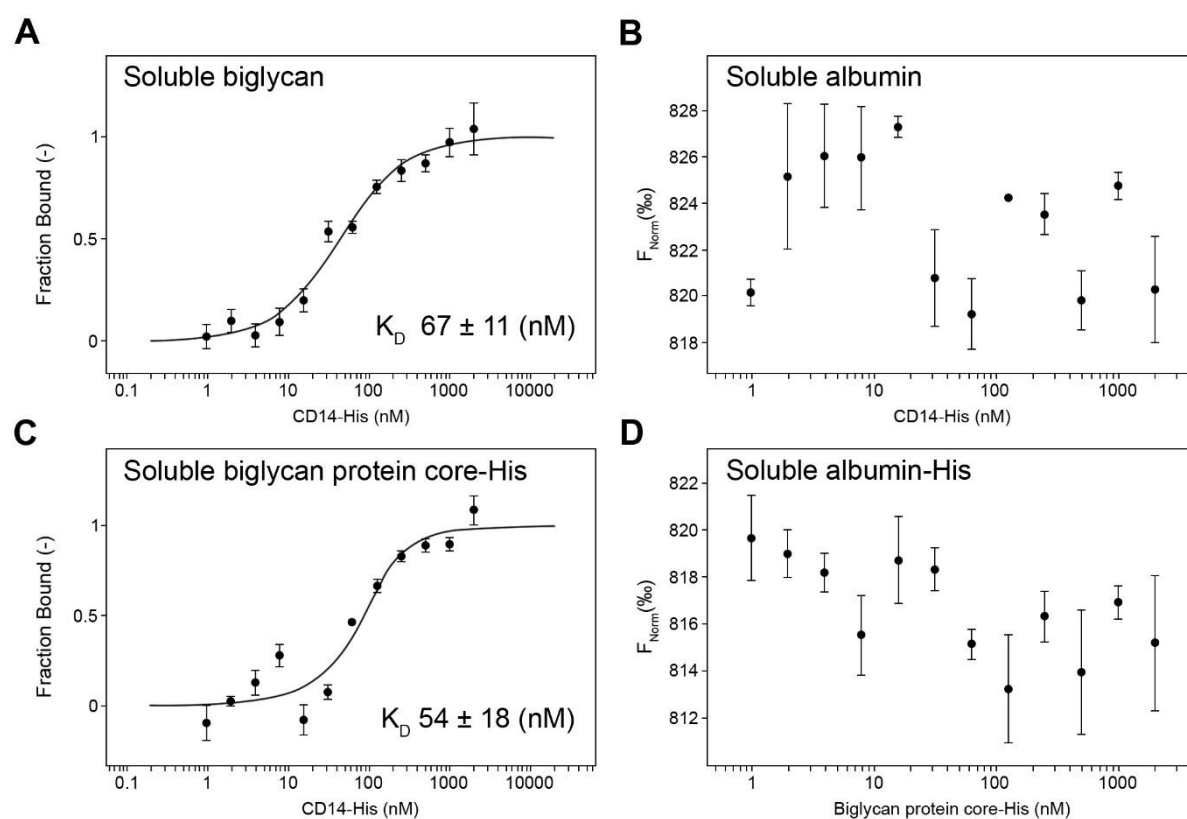

Figure 5.7. Direct interaction of biglycan with CD14. (A-D) Microscale thermophoresis (MS) interaction analysis of recombinant CD14-His and either soluble biglycan (A), soluble biglycan protein core-His (C) or soluble albumin (B) and soluble biglycan protein core-His and soluble albumin-His (D). Dose response curves were either expressed as fraction bound (A and B) or as normalized fluorescence as no binding was observed. K_D values and error bars (indicating SD) were calculated from three independent measurements. F_{Norm} = normalized fluorescence; K_D = dissociation constant.

5.1.4 Biglycan-triggered induction of pro-inflammatory mediators during renal IRI is CD14-dependent

To test, whether our findings might also be applicable for *in vivo* situation we tested biglycan/CD14-dependency in a mouse model of renal ischemia/reperfusion injury (IRI). Previous studies showed that soluble biglycan aggravates the outcome of renal IRI in a TLR2/4-dependent manner [61]. In renal IRI, overexpression of biglycan increases protein levels of TNF-α, CCL2 and CCL5 in plasma and reperfused kidneys, leading to the recruitment of several types of immune cells into the inflamed kidney [61]. Additionally, in macrophages, the anti-inflammatory effect of biglycan on the maturation of IL-1β through synthesis and activation of NOX2 is counteracted by biglycan/TLR2-induced expression of HSP70 [74]. To reveal potential beneficial effects of CD14-depeletion for biglycan-mediated exacerbation of renal IRI, we evaluated the effects of CD14 deficiency on biglycan-triggered renal expression of TNF-α, CCL2, CCL5 and HSP70 under both physiological and pathological conditions. For this purpose, soluble biglycan was transiently overexpressed 3 days before IRI in WT and *Cd14*$^{-/-}$ mice using the pLIVE-vector system by a single intravenously injection [61, 66, 75]. Using this approach, biglycan is specifically overexpressed in hepatocytes over the albumin promotor and released in its soluble form into the blood stream, reaching various organs [53, 66]. Empty pLIVE vector-injected animals were utilized as corresponding controls. IRI was performed for a total duration of 30 h, while sham operated animals served as additional controls. Overexpression of soluble biglycan in sham-operated WT mice by pLIVE-h*BGN* resulted in a significant increase in *Tnfα*, *Ccl2*, *Hsp70* and *Ccl5* mRNA (Fig. 5.8 A, C, E and G) and protein levels (Fig. 5.8 B, D, F and H) compared to pLIVE-injected WT mice. TNF-α and CCL5 levels from reperfused kidneys of pLIVE-h*BGN*-injected mice showed comparable levels to pLIVE-injected WT mice undergoing IRI. Furthermore, we found that during IRI, h*BGN*-overexpression substantially increased mRNA (Fig. 5.8 A, C, E and G) and protein levels (Fig. 5.8 B, D, F and H) of *Tnfα*, *Ccl2*, *Hsp70* and *Ccl5* compared to pLIVE-injected WT. To proof that CD14 deficiency shows beneficial effects via impairment of biglycan signaling, *Cd14*$^{-/-}$ mice underwent same procedure as WT mice. Interestingly, CD14 deficiency abolished the biglycan-induced expression of *Tnfα*, *Ccl2*, *Hsp70* and *Ccl5* on both, mRNA and protein level in sham-operated as well as in IRI-subjected mice (Fig. 5.8). Notably, *Tnfα*, *Ccl2*, *Ccl5* and *Hsp70* mRNA and protein levels were overall lower in pLIVE-injected *Cd14*$^{-/-}$ mice compared to pLIVE-injected WT mice, indicating a renoprotective effect by CD14 deficiency. Altogether, CD14-depletion rescued and, in some cases, even improved the pro-inflammatory phenotype of mice which underwent IRI or h*BGN*-overexpression. Therefore, CD14 seems to represent a crucial element in biglycan-induced expression of TNF-α, CCL2, CCL5 and HSP70 in renal IRI.
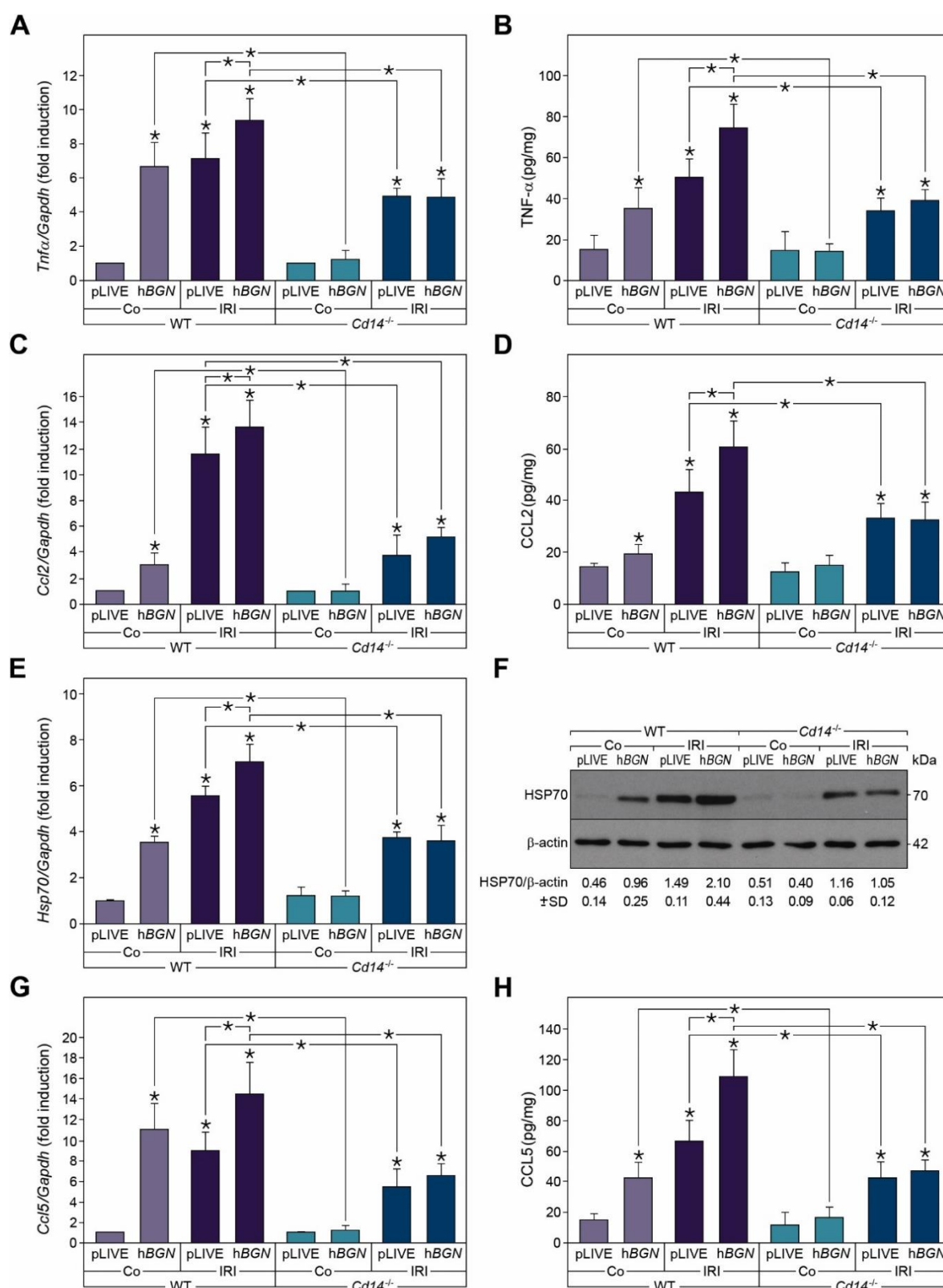
Figure 5.8. Transient overexpression of soluble biglycan in murine renal ischemia/reperfusion injury triggers the expression of TNF-α, CCL2, HSP70 and CCL5 via CD14. Quantitative qRT-PCR of mRNA expression of *Tnfα* (A), *Ccl2* (C), *Hsp70* (E) and *Ccl5* (G) in kidneys from pLIVE-h*BGN*- or pLIVE-injected WT or *Cd14⁻/⁻* mice either sham operated or subjected to renal IRI (30 h). mRNA expression was normalized to *Gapdh* and shown as fold induction compared to WT. ELISA (B, D and H) of TNF-α (B), CCL2 (D) and CCL5 (H) or Western blot analysis of HSP70 (F) in kidney homogenates. HSP70 protein levels were normalized to β-actin. Data represent means ± SD; n = 6 per group; *P < 0.05.

5.1.5   CD14 is pivotal for biglycan-induced renal macrophage recruitment during IRI

IRI is characterized through a vast release of DAMPs which lead to the activation of the innate immune system by engaging PRRs, triggering both cell death and chemo- and cytokine release [282]. The acute inflammation caused by ischemia and reperfusion is accompanied by infiltrating immune cells like neutrophils, monocytes, dendritic cells and macrophages, which are detrimental modulators of disease outcome [283-285]. We have previously shown that overexpression of biglycan triggers macrophage recruitment into the kidney [66]. Furthermore we were able to show that biglycan-induced renal macrophage recruitment is dependent on the expression of the macrophage chemoattractants CCL2 and CCL5 [31, 61, 66, 67]. As CD14-depletion affected the mRNA and protein levels of CCL2 and CCL5 we asked ourselves, whether CD14 deficiency affects biglycan-induced macrophage recruitment. To this end, we determined the number of CD11b- and F4/80-positive cells by FACS in total kidney homogenates from pLIVE- or pLIVE-h*BGN*-injected WT or *Cd14*$^{-/-}$ mice after 30 h of IRI.
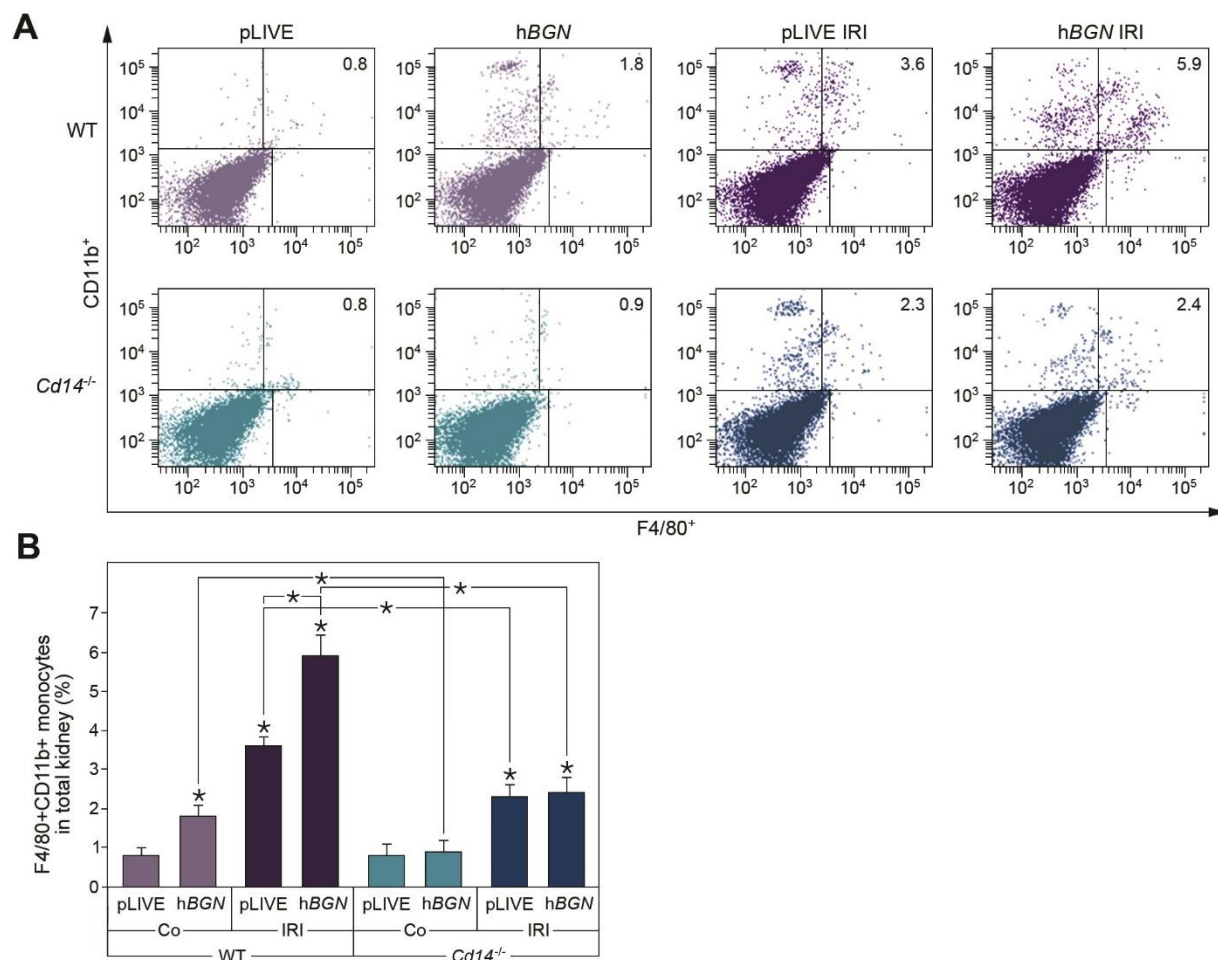
Figure 5.9. Biglycan-dependent increase of renal macrophage infiltration in renal ischemia/reperfusion injury is lowered by CD14 deficiency. (A and B) FACS analysis of pLIVE-h*BGN*- or pLIVE-injected WT and *Cd14*$^{-/-}$ mice subjected to renal IRI (30 h) or sham-operation. pLIVE-h*BGN* or pLIVE empty vector were injected 3 days before renal IRI or sham-operation. (A and B) Quantification of F4/80$^+$CD11b$^+$ cells in kidney homogenates. Data are given as means ± SD; n = 6 per group; *P < 0.05.

In vivo overexpression of h*BGN* under physiological conditions already increased the number of F4/80+CD11b+ cells in the kidneys of sham-operated WT mice (Fig. 5.9 A and B). As expected, pLIVE-injected WT mice which were subjected to IRI showed a strong renal infiltration of F4/80+CD11b+ cells, which was further increased in pLIVE-h*BGN*-injected WT mice (Fig. 5.9 A and B). In contrast, the number of F4/80+CD11b+ cells in the kidneys of IRI-subjected *Cd14-/-* mice were reduced compared to WT mice (Fig. 5.9 A and B). Moreover, the number of F4/80+CD11b+ cells did not increase upon h*BGN*-overexpression in *Cd14-/-* mice during sham-operation or IRI. In conclusion, this data suggest that biglycan-triggered renal macrophage recruitment is completely dependent on the presence of the CD14 co-receptor. Previous research could show that the majority of renal infiltrating macrophages during the early phase of IRI is polarized as a M1 phenotype, who classically induce cytotoxicity and tissue injury, thereby impacting on the outcome of renal IRI [286, 287]. CD14 has a critical role in M1 polarization of macrophages [134].

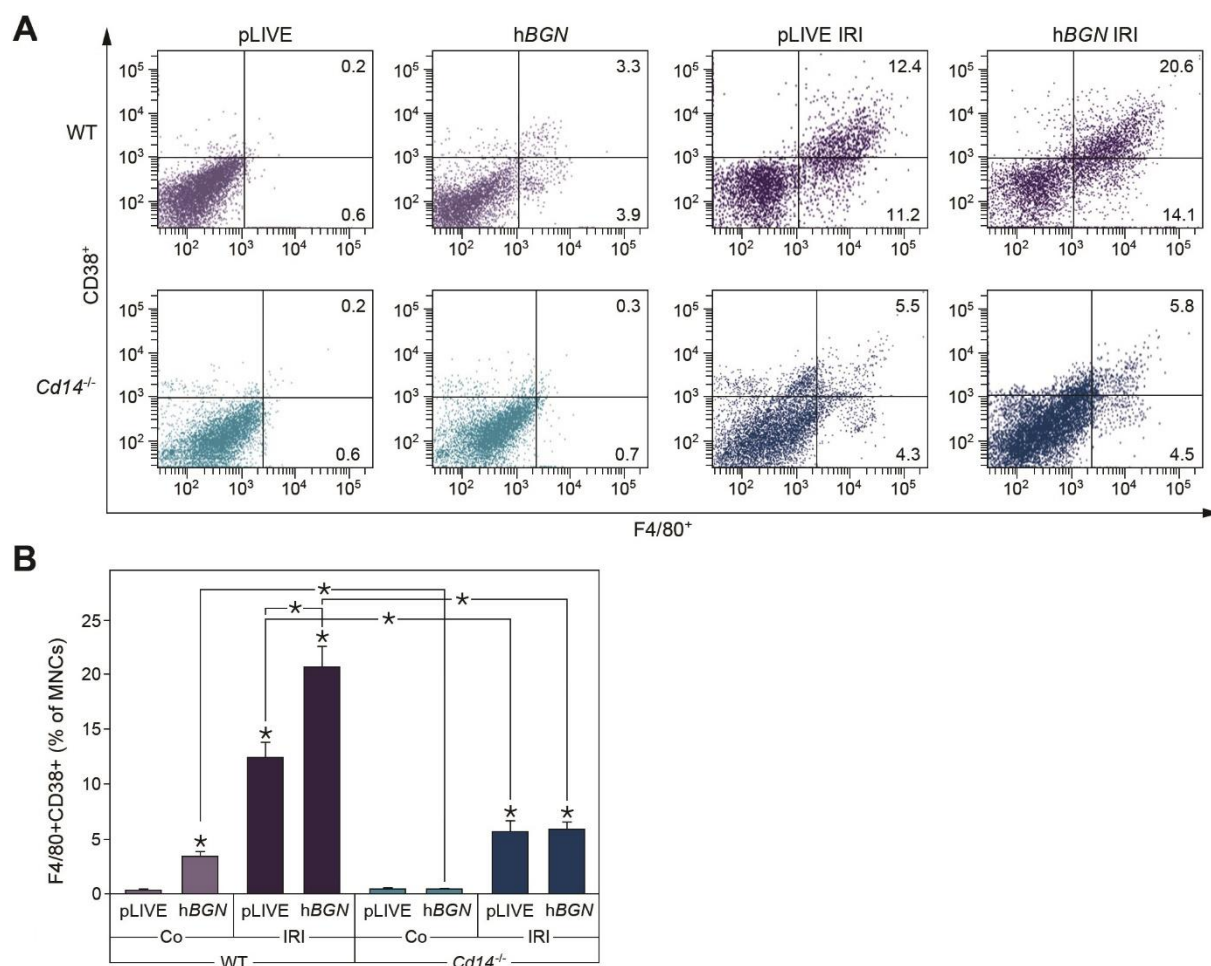**Figure 5.10. Biglycan triggers M1 macrophage polarization in renal IRI in a CD14-dependent manner.** (A and B) WT and *Cd14-/-* mice were injected with pLIVE-h*BGN* or pLIVE empty vector 3 days prior of being subjected to renal IRI (30 h) or sham-operation. (A and B) Quantification of F4/80+CD38+ M1 macrophages in kidney-derived MNCs by FACS. Data are given as means ± SD; n = 6 per group; *P < 0.05. MNCs = mononuclear cells.

To corroborate our findings regarding F4/80+CD11b+ cells, we asked ourselves whether biglycan and CD14 could also be involved in M1 macrophage recruitment during renal IRI. For this purpose we extracted mononuclear cells by gradient centrifugation from pLIVE- or pLIVE-h*BGN*-injected WT or *Cd14*-/- mice and analyzed the subset of M1 macrophages by FACS through staining with antibodies against F4/80 and CD38, a newly described highly specific marker for M1 macrophages [273]. Interestingly, FACS analysis revealed that overexpression of human biglycan in WT mice resulted in increased numbers of renal M1 macrophages compared to pLIVE-injected control mice (Fig. 5.10 A and B). Moreover, WT mice which underwent 30 h of IRI showed a huge increase in the number of M1 macrophages compared to sham-operated mice, while an overexpression of soluble biglycan further amplified this effect (Fig. 5.10 A and B). In contrast, CD14 ablation abolished the biglycan-mediated increase of renal M1 macrophages in sham-operated animals. In line with previous data, M1 macrophage numbers in ischemic *Cd14*-/- mice were significantly reduced compared to WT mice (Fig. 5.10 A and B). Consistently, renal M1 macrophage numbers were not elevated in response to soluble biglycan overexpression in *Cd14*-/- mice during IRI (Fig. 5.10 A and B). Hence, these results show that soluble biglycan is able to trigger M1 macrophage recruitment into the kidney in a CD14-dependent manner.

5.1.6 Biglycan aggravates the outcome of renal IRI in a CD14-dependent manner

To unmask, if CD14 deficiency has beneficial effects on the biglycan-induced renal tubular damage during IRI, we analyzed PAS-stained kidney sections from sham-operated or IRI-subjected pLIVE- or pLIVE-h*BGN*-injected WT and *Cd14*-/- mice. PAS-stained kidney sections were analyzed by two observers blinded to the study. Severe tubular damage during IRI was designated by widespread tubular dilatation, loss of brush border, cast formation and tubular necrosis. Overexpression of soluble biglycan did not induce tubular damage in WT and *Cd14*-/- mice in sham-operated mice (Fig. 5.11 A and B). However, a considerable amount of tubular damage could be observed in IRI-subjected WT and *Cd14*-/- mice. In this case, pLIVE-h*BGN*-injection in WT mice worsened tubular damage, when compared to pLIVE-injected WT littermates. On the contrary, biglycan-induced aggravation of tubular damage during IRI was completely absent in *Cd14*-/- mice (Fig. 5.11 A and B). At the same time, we could observe less IRI-induced tubular damage in *Cd14*-/- mice compared to WT mice (Fig. 5.11 A and B). As another parameter for assessing tubular damage, we measured serum creatinine levels. Creatinine is normally removed from the blood by glomerular filtration in the kidney. Due to kidney damage, the glomerular filtration rate is decreased, creatinine levels rise in serum and can be used to estimate renal function [288]. Each genotype subjected to IRI showed enhanced serum creatinine levels, while *Cd14*-/- mice exhibited significant lower levels (Fig. 5.11 C). Moreover, serum creatinine levels were increased in IRI-subjected pLIVE-h*BGN*-

injected WT mice compared to pLIVE-injected littermates (Fig. 5.11 C). Importantly, tubular damage and serum creatinine levels reflecting renal function positively correlated in both experiments (Fig. 5.11 A-C). As a result, we draw the conclusion that a lack of CD14 alleviates biglycan-induced renal damage during physiological and IRI conditions. As CD14 is essential for both biglycan-induced TLR2 and TLR4 signaling, CD14 could represent a promising therapeutic target for inflammatory diseases with high biglycan levels.
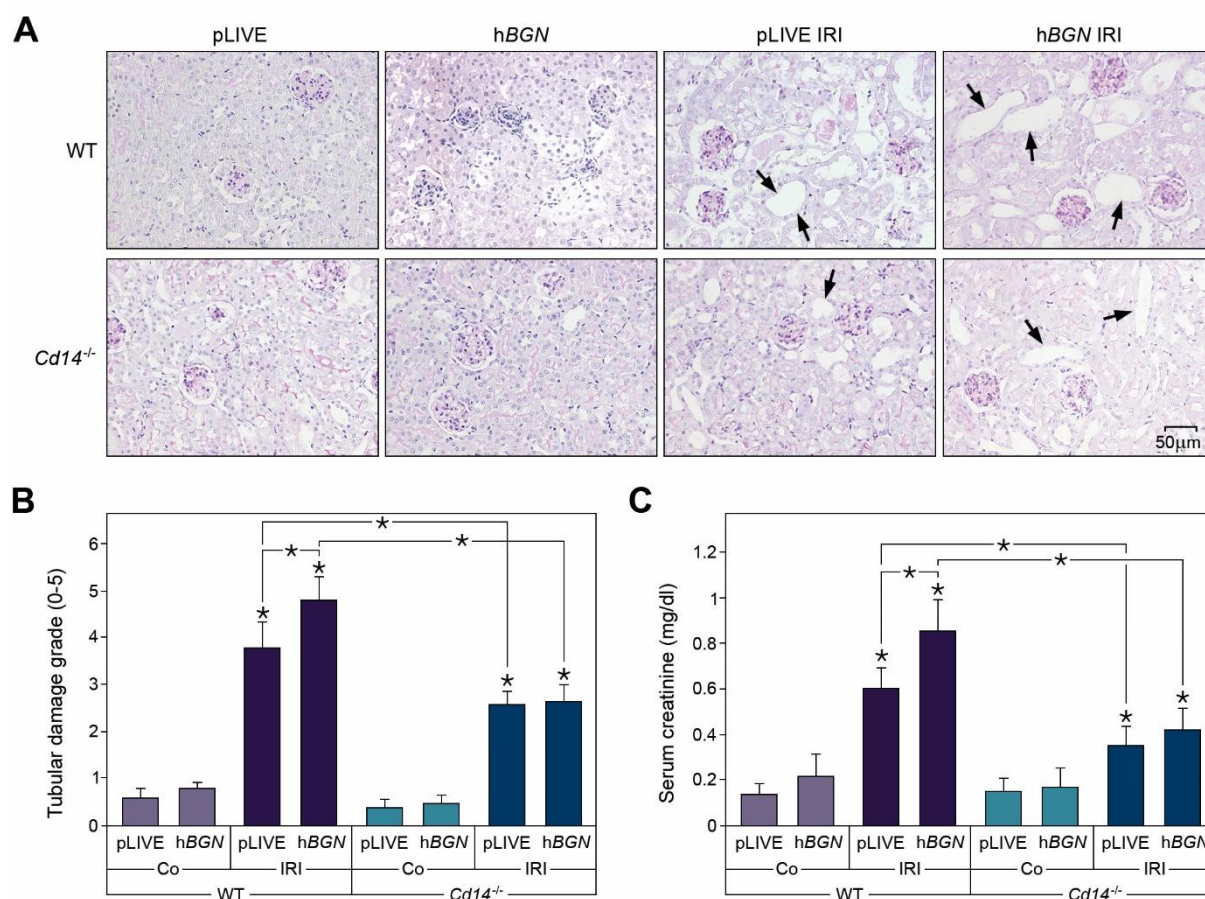
Figure 5.11. Biglycan-dependent renal damage is alleviated by CD14 deficiency in renal ischemia/reperfusion injury. (A) PAS stained kidney sections sham-operated control or 30 h reperfused IRI kidneys of WT and *Cd14⁻/⁻* mice either injected with pLIVE-hBGN or pLIVE empty vector. Scale bar = 50 μm. (B) Semiquantitative scoring of tubular damage. (C) Serum creatinine levels of pLIVE-h*BGN*- or pLIVE-injected WT and *Cd14⁻/⁻* mice after 30 h of IRI or sham-operation. Data represent means ± SD; n = 6 per group; *P < 0.05.

PART II

GST-pulldown experiments were performed in collaboration by Dr. Jaime López-Mosqueda from Prof. Ivan Dikic´s group at the Institute of Biochemistry II, Frankfurt am Main. Mass spectrometry experiments were done in collaboration with Dr. Georg Tascher from the lab of Dr. Christian Münch within the SFB1177 Autophagy. Molecular cloning was done in collaboration with Eric Kowarz from the lab of Prof. Dr. Rolf Marschalek of the Institute of Pharmaceutical Biology, Frankfurt am Main.

5.2 ABIN-1 is a potential autophagy receptor for damaged mitochondria

ABIN-1 is an important intracellular player in sterile inflammation which potently suppresses inflammatory signaling downstream of TLRs [151]. Moreover, ABIN-1 specifically binds to K63- or M1-linked and not to K48-linked ubiquitin chains via its UBAN domain [147]. Through its polyubiquitin binding function, ABIN-1 inhibits NF-κB and MAPK activation [143, 289] as well as TNF-induced apoptosis by inhibiting FADD-caspase-8 association [149]. Notably, the UBAN domain of ABIN-1 shares sequence homology with optineurin, which exhibit similar inhibitory roles in TNF-induced NF-κB activation but impacts also on cell division, vesicular trafficking and functions as a selective autophagy receptor [290]. Moreover, ABIN-1 binds K63- and M1-linked ubiquitin chains, thought to preferentially mark cargo for the recognition of the selective autophagy machinery [207]. Therefore, we aimed to examine if ABIN-1 functions as a new selective autophagy receptor.

5.2.1 Interactome and proteome analysis of ABIN-1 by mass spectrometry

To identify new interaction partners of ABIN-1 during pathogen-induced inflammation, we performed immunoprecipitation of ABIN-1 followed by mass spectrometry (IP-MS) in WT spleen homogenates from mice subjected to sepsis by LPS-induced endotoxemia. Immunoprecipitated proteins were extracted after SDS-Page, in-gel digested and identified by label-free liquid chromatography tandem mass spectroscopy (LC-MS/MS). Only proteins found in both groups consisting out of 3 replicates were regarded as possible hits. Moreover, proteins which were identified by only one peptide hit were considered false positive and therefore excluded from the whole analysis. Proteins with a -log 10 p-value > 2.0 and a log2 ratio of ± 0.5 were regarded as significantly changed between both groups. Full interactome analysis revealed 86 significantly enriched or decreased proteins upon LPS-stimulation. As expected, ABIN-1 (TNIP1) was highly enriched in IP-MS. Moreover, several known binding proteins of ABIN-1 such as TNFAIP3 (A20) [291], TRAF1 [147] and Nuclear factor NF-κB p105 [292] could be validated. Besides the identified proteins enriched or decreased upon LPS-induced sepsis,

we focused our attention on the high amount of proteins connected to autophagy. Intrudingly, IP-MS of ABIN-1 showed several bona fide candidates connected to auto- and mitophagy including MAP1LC3B, ATG5, ATG7, Beclin-1, TOM20, VDAC1 and LAMP1 (Fig. 5.12 A). Proteins were filtered by Gene Ontology (GO) terms linked to cellular processes associated with autophagy or mitophagy and analyzed by STRING: functional protein association networks. STRING analysis of all autophagy-related proteins showed two cluster of proteins resembling various core proteins of the basic autophagy machinery as well as distinct mitochondrial outer membrane proteins connected to mitophagy (Fig. 5.12 C), further supporting ABIN-1 involvement in these processes.

ABIN1[D485N] mice have a disrupted K63 and linear ubiquitin binding, resulting in enhanced MAPK and NF-κB-mediated gene transcription and signaling. Accordingly, ABIN1[D485N] mice develop a severe type of autoimmune disease with systemic lupus erythematosus (SLE) like characteristics [147]. In order to determine new signaling pathways regulated through the ability of ABIN-1 to bind and regulate ubiquitinated proteins, we performed proteome analysis from primary murine peritoneal macrophages derived from WT and ABIN1[D485N] mice. For this purpose, unstimulated macrophages were in-solution digested, labeled via TMT and analyzed by LC-MS/MS in 4 replicates for each group. Proteins with a -log 10 p-value of greater than 2.0 and a log2 ratio of ± 0.5 were regarded as significantly changed between both groups. Analysis showed 6294 unique proteins identified by MS, while 261 proteins were significantly up or downregulated in ABIN1[D485N] mice compared to WT mice. As expected, several proteins involved in innate immunity and cytokine regulation such as PYCARD (6.46-fold increase), Nuclear factor NF-κB p100 (7.13-fold increase), HMGB1 (6.15-fold increase) and ICAM1 (14.18-fold increase) were significantly enriched in ABIN1[D485N] mice with dysregulated immune system (Fig. 5.12 B). Interestingly, defective ubiquitin binding of ABIN-1 resulted in the accumulation of two protein connected to mitophagy, mitofusin 2 (MFN2) (5.23-fold increase) and TBC1 domain family member 17(TBC1D17) (5.29-fold increase) (Fig. 5.12 B). MFN2, as part of the outer mitochondrial membrane (OMM) is ubiquitinated during mitophagy and subsequently recognized by selective autophagy receptors for autophagosomal degradation [232]. Moreover, cells with depleted MFN2 are unable to recruit Parkin to mitochondria, resulting in the accumulation of damaged mitochondria [293, 294]. In contrast, TBC1D17 regulates the autophagic engulfment of mitochondria by impacting on Rab7 activity [295]. Additionally, WDR45b a protein connected to autophagy was decreased in ABIN1[D485N] mice by 17.5-fold. WDR45, homologous to yeast Atg18, provides a scaffold for the autophagy signal control and is involved in autophagosome formation [296] (Fig. 5.12 B). Hence, ABIN-1 may be involved in auto- and mitophagy by regulating the target-oriented degradation of autophagy substrates, likely through its ability to recognize ubiquitinated cargo.
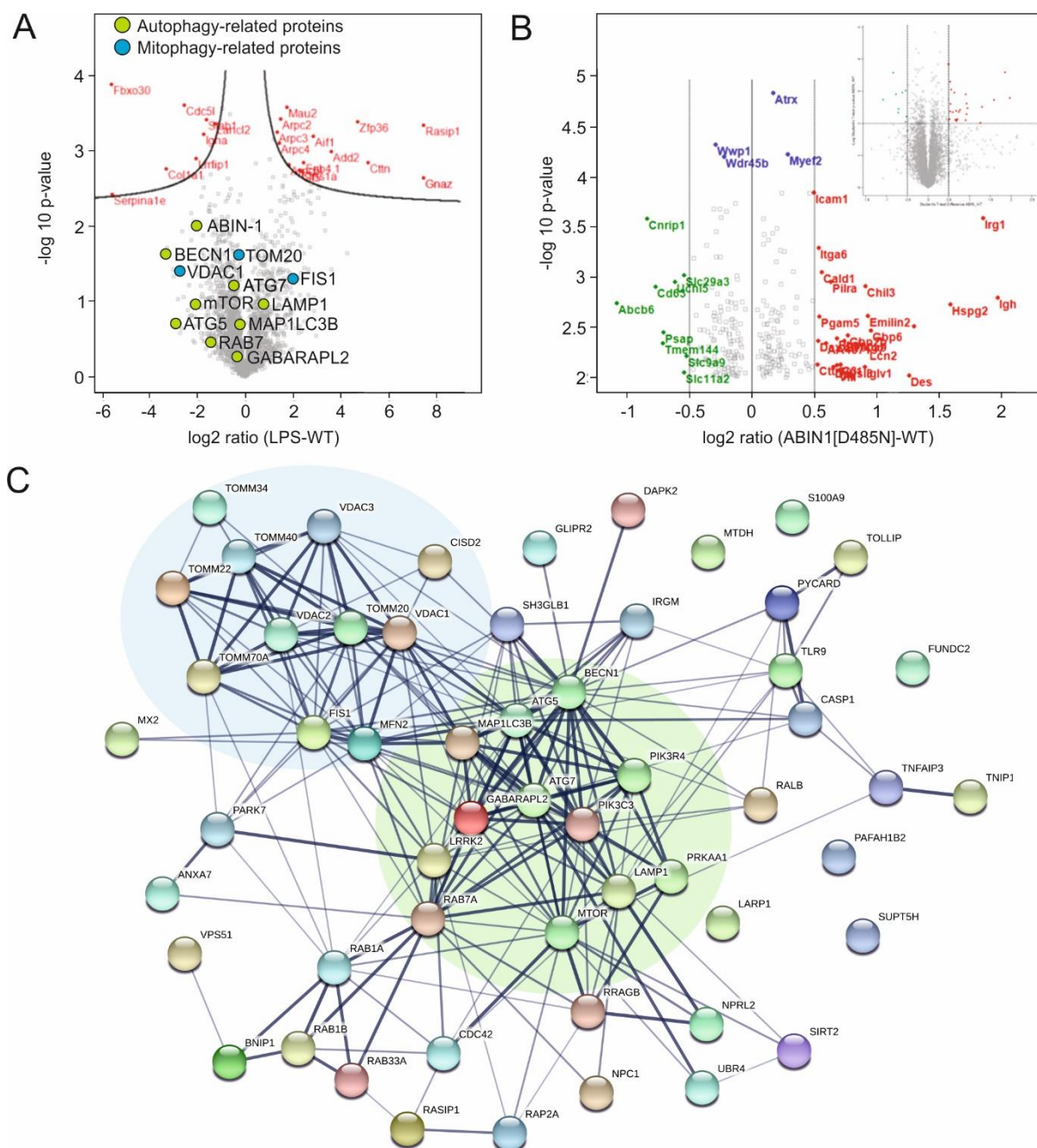
Figure 5.12. Interactome and proteome analysis associates ABIN-1 with autophagy. (A) Volcano-plot of ABIN-1 immunoprecipitation in combination with mass spectrometry (IP-MS). WT macrophages were stimulated with or without lipopolysaccharide (LPS) for 4 h and immunoprecipitated with anti-ABIN-1 antibody. The logarithmic ratios of protein intensities are plotted against negative logarithmic p-values of the t-test. The hyperbolic curve separates specifically interacting proteins marked in red under LPS condition. Autophagy-related proteins from the whole interactome are marked with green circles, whereas mitophagy-related proteins are labeled with blue circles. (B) Volcano-plot of full proteome analysis of macrophages derived from ABIN1[D485N] mice compared with WT mice. Peptides with a log2 ratio (ABIN1[D485N]-WT) ± 0.5 and -log 10 p value > 2.0 are displayed as significantly decreased (green) or significantly enriched (red). (C) STRING-network analysis of all autophagy- and mitophagy-related interaction partners of ABIN-1 from (A). Cluster of mitophagy-related proteins is highlighted in blue while the cluster containing core autophagy proteins is highlighted in green. (A) n = 3; (B) n = 4.

5.2.2   ABIN-1 forms a complex with LC3B

Selective autophagy requires target-oriented delivery of cargo into LC3-containing autophagosomes by selective autophagy receptors. Most of the autophagy receptors rely on cargo recognition though a ubiquitin-binding domain (UBD). Bound cargo is then delivered to LC3-coated phagophores via a conserved LC3-interacting region (LIR) motif [219]. Since, IP-MS of ABIN-1 revealed various proteins connected to autophagy, including LC3B (Fig. 5.12 A and B) and ABIN-1 is known to bind linear and K63-linked ubiquitin chains [147], we asked ourselves if ABIN-1 represents an undescribed autophagy receptor. One prerequisite of ABIN-1 to be structurally related to autophagy receptors represents the ability to specifically bind LC3 via a LIR domain. The canonical LIR sequence consists out of the motif $[W/F/Y]_0$-X_1-X_2-$[L/V/I]_3$ in which the position X_0 and X_3 are conserved through all known LIRs and Phe (F) and Trp (W) are most represented at position X_0 [169]. Moreover, the N- and C-terminal region is often flanked by acidic residues such as Asp (D), Glu (E), Ser (S) or Thr (T) which constitute potential phosphorylation sites as part of an extended LIR [169]. Motif mapping of human ABIN-1 revealed two undescribed LIR motifs at the amino acids 83 to 86 (FDPL) and 125 to 128 (FEVV) (Fig. 5.13 A).
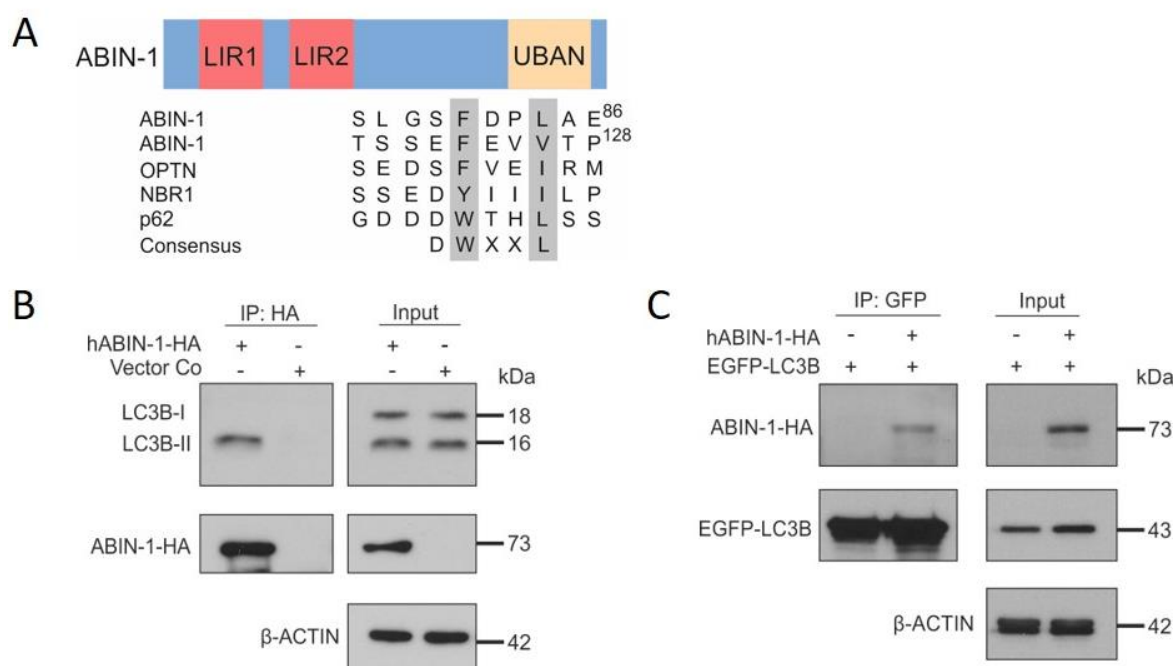

Figure 5.13. ABIN-1 is in complex with LC3B. (A) Schematic representation of the domain architecture of ABIN-1. The alignment of LIR motifs of known autophagy receptors is illustrated underneath. LIR sequences are emphasized in bold. (B) HeLa cells were transiently transfected with hABIN-1-HA or empty vector control (Vector Co). 24 h after transfection, cells were incubated with BafA1 (200 nM) for 4 h, immunoprecipitated using anti-HA-beads and analyzed by immunoblotting. (C) Reciprocal IP of (B) using HeLa cells transfected with EGFP-LC3B and hABIN-1-HA for 24 h. Cells were incubated with BafA1 (200 nM) for 4 h, immunoprecipitated using anti-GFP-beads and analyzed by Western blot. β-ACTIN served as loading control for the input whereas immunoprecipitated ABIN-1-HA or EGFP-LC3B were used as loading controls for the respective immunoprecipitations. LIR = LC3-interacting region, UBAN = ubiquitin-binding domain in ABIN and NEMO. (B) n = 3; (C) n = 2.

This motif is conserved in the murine variant of ABIN-1 at the amino acids 84 to 87 (FDDL) and 137 to 140 (FEVV). To determine if ABIN-1 binds LC3B *in vitro*, HeLa cells were transfected with HA-tagged hABIN-1 or empty plasmid control and incubated with the autophagosome-lysosome fusion inhibitor Bafilomycin A1 (BafA1) for 4 h to enrich for autophagosomal complexes. Subsequently, cells were lysed and subjected to Co-immunoprecipitation (Co-IP) via HA antibody. Co-IP studies showed that ABIN-1-HA binds predominantly the lipidated form of endogenous LC3B (LC3B-II) (Fig. 5.13 B). Binding specificity was validated by reciprocal IP of hABIN-1-HA by enhanced green fluorescent protein (EGFP)-tagged LC3B (Fig. 5.13 C). In summary, ABIN-1 interacts with LC3B likely through its two newly described LIR motifs. Considering the ability of ABIN-1 to bind ubiquitinated proteins, we postulate that ABIN-1 may serve as an autophagy receptor during selective autophagy.

5.2.3   LIR motifs of ABIN-1 mediate binding to LC3 proteins

To determine if both LIR motifs are required for the binding of ABIN-1 to LC3B we utilized site directed mutagenesis to insert single point mutations at either ABIN-1 $Phe^{83} \rightarrow Ala^{83}$ and $Leu^{86} \rightarrow Ala^{86}$ (F83A/L86A, referred to as LIR1) or $Phe^{125} \rightarrow Ala^{125}$ and $Val^{128} \rightarrow Ala^{128}$ (F125A/V128A, referred to as LIR2). Concurrently, site directed mutagenesis was used to inactivate the UBAN domain of ABIN-1 by mutating $Asp^{472} \rightarrow Asn^{472}$ (D472N, referred to as UBAN), disabling its ability to bind linear and K63-linked ubiquitin chains [147]. To this end, HA-tagged hABIN-1 was overexpressed either as a full length (FL), LIR1-, LIR2-, double LIR (LIR1+2)-mutated or ubiquitin-binding defective variant (UBAN) in HeLa cells. Subsequently, ABIN-1-HA-transfected HeLa cells were treated with BafA1 for 4 h and Co-immunoprecipitated with HA antibody. Co-IP analysis revealed that ABIN-1 is in complex with LC3B and has a high affinity to LC3B-II (Fig. 5.14 A). Mutation of LIR1 reduced the binding affinity to LC3B-II, whereas a mutation of LIR2 led to a stronger reduction in the binding capabilities of ABIN-1 to LC3B (Fig. 5.14 A). As expected, mutation of both LIR domains (LIR1+2) abrogated the interaction of ABIN-1 with LC3B, while the ubiquitin-binding defective variant of ABIN-1 bound equally good to LC3B as compared to ABIN-1-HA FL (Fig. 5.14 A). Glutathione-S-transferase (GST) pull-down experiments, employing ABIN-1 full-length protein and ABIN-1 LIR mutant proteins were performed to verify the observations made by Co-IP and to test direct interaction between ABIN-1 and LC3 proteins. GST alone or fused to either 4xUbiquitin (4xUb), LC3A or LC3B were expressed in *E. coli*, immobilized on GST-agarose beads and incubated with recombinant maltose binding protein (MBP)-tagged ABIN-1. Consistent with the results obtained from Co-IP studies, single point mutations in both LIR domains abrogated the interaction of ABIN-1 to LC3B (Fig. 5.14 B). Interestingly, GST-pulldown verified that the LIR2 domain of ABIN-1 is more essential for binding to LC3B compared to LIR1. In contrast, both

LIR domains mediate the interaction to LC3A, since only double LIR-mutated ABIN-1 showed no binding to LC3A. All mutants were still able to bind linear ubiquitin chains fused to GST (GST-4xUb). Therefore, the LIR domains mediate the binding of ABIN-1 to LC3 proteins, whereas the LIR2 domain encompassing amino acids 125 to 128 shows stronger binding affinities to LC3B than the LIR1 domain.
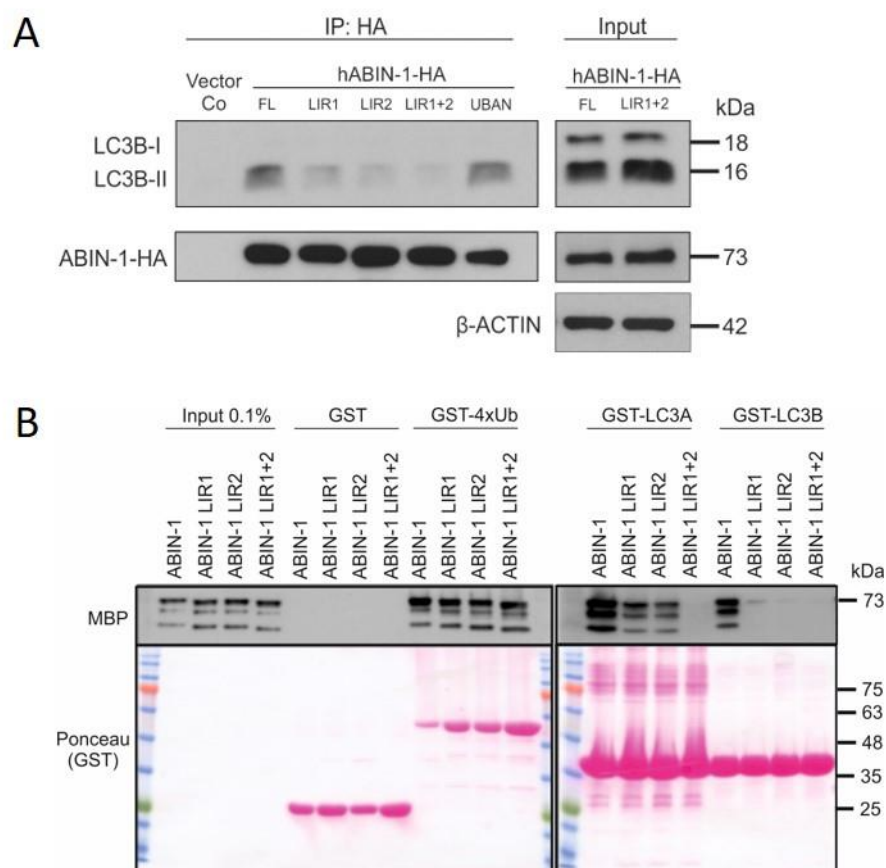

Figure 5.14. ABIN-1 binds to LC3B in a LIR-dependent manner. (A) HeLa cells were either transfected with empty vector control (Vector Co), plasmids encoding hABIN-1-HA full length (FL), or mutants defective in the LIR1-, LIR2-, LIR1+2- or UBAN-domain for 24 h. Transfected cells were treated with BafA1 (200 nM) for 4 h, subjected to immunoprecipitation with anti-HA antibody and analyzed for LC3B by Western blotting. β-ACTIN served as loading control for the input while immunoprecipitated ABIN-1-HA served as loading control for the immunoprecipitation. (B) GST-pulldown assay of ABIN-1 or the indicated mutants. Purified GST, GST4x-Ubiquitin (Ub), GST-LC3A or GST-LC3B purified from *E. coli* was immobilized on GST beads and incubated with bacterial purified MBP-tagged ABIN-1 protein. ABIN-1 fused to MBP was detected by Western blotting. Ponceau S staining was used to visualize GST-fusion proteins. (A) n = 2; (B) n = 3.

5.2.4   ABIN-1 co-localizes with autophagic markers

In an effort to validate ABIN-1 involvement in autophagy we analyzed the co-localization of ABIN-1 with the autophagic markers LC3B and LAMP-1 by laser-scanning microscopy. For this purpose, HeLa cells stably expressing DOX-inducible monomeric enhanced green fluorescent protein (mEGFP)-hABIN-1 were either co-transfected with mCherry-LC3B or

stained for endogenous LAMP-1. The expression pattern of mEGFP-hABIN-1 showed even distribution in the cytosol under basal conditions and did not cluster into cytoplasmatic mCherry-LC3B or endogenous LAMP-1 containing structures (Fig. 5.15 A and C). Upon induction of autophagy with the mTOR inhibitor Torin-1 and blockage of lysosomal fusion with BafA1 for 4 h, mEGFP-hABIN-1 highly localized to LC3B-positive vesicles.
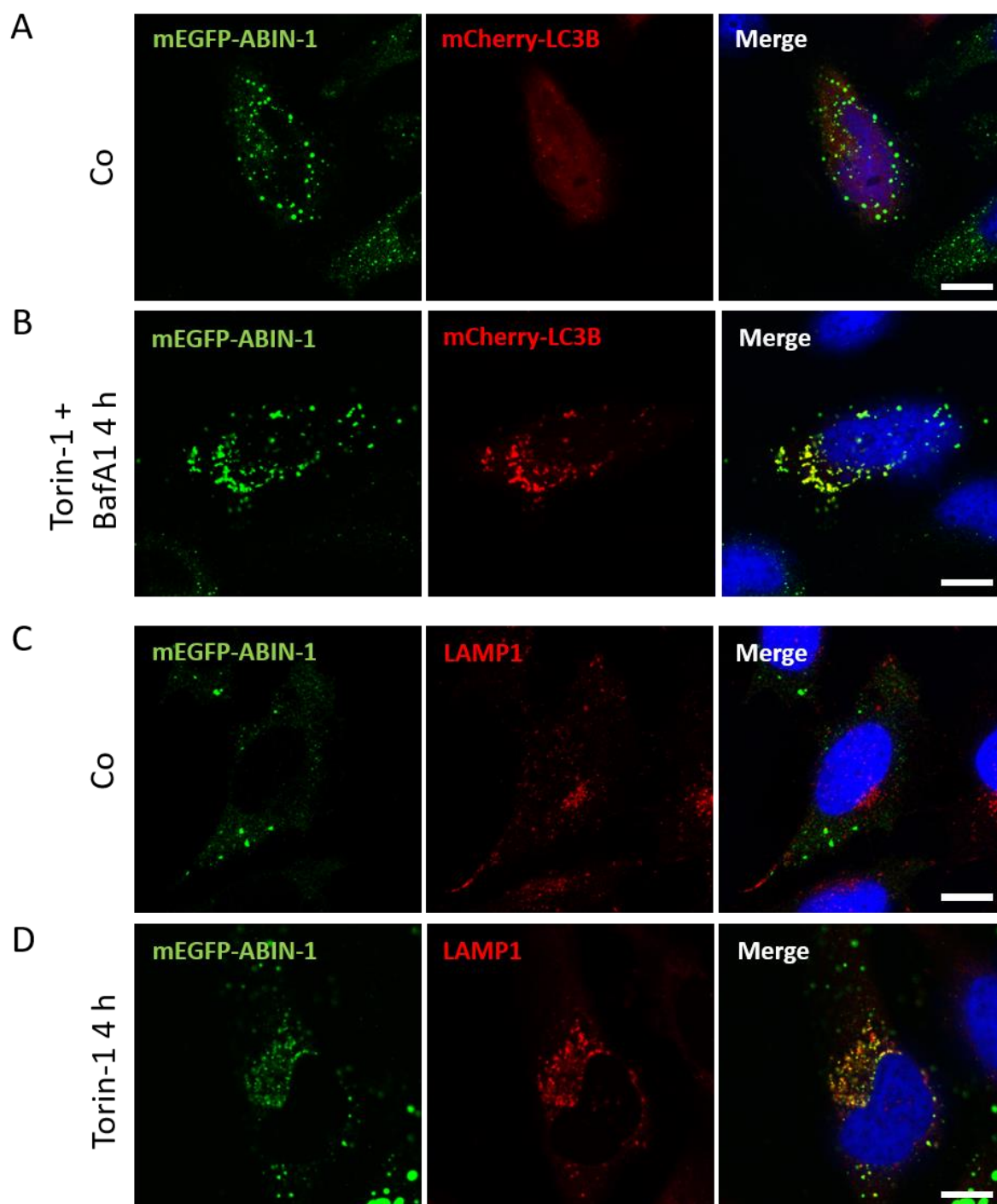
Figure 5.15. ABIN-1 co-localizes with autophagic markers. (A-D) Representative confocal images of HeLa cells overexpressing mEGFP-ABIN-1 (green). (A and B) Cells were co-transfected with mCherry-LC3B (red) for 24 h and treated with Torin-1 (1 µM) and BafA1 (300 nM) for 4 h. (C and D) HeLa cells were stimulated with Torin-1 (1 µM) for 4 h. Endogenous LAMP-1 was immunostained with anti-LAMP-1 antibody (red). Nuclei were stained with DAPI. Scale bars = 10 µm. n = 3.

Moreover, by single treatment with Torin-1 for 4 h, mEGFP-hABIN-1 clustered into LAMP-1 containing lysosomes (Fig. 5.15 D). In summary, ABIN-1 binds and localizes to LC3B- and LAMP1-positive vesicles upon autophagy induction, supporting the concept that ABIN-1 represents a potential autophagy receptor.

5.2.5   ABIN-1 is processed via the autophagic pathway

Next, we tried to evaluate if ABIN-1 protein levels are influenced by the autophagic machinery. To this end, HeLa cells were by incubated with the mTOR-inhibitor rapamycin or in combination with BafA1 for various time points and analyzed by immunoblotting. ABIN-1 protein levels significantly increased after 4 h and 24 h of rapamycin/BafA1 treatment, while rapamycin-treatment alone elevated ABIN-1 protein levels only after 4 h (Fig. 5.16 A and B). Similarly, co-treatment of rapamycin and BafA1 led to an accumulation of the known autophagy receptor p62 at all time points, whereas rapamycin failed to induce p62 accumulation after 24 h (Fig. 5.16 A and C). Accumulation of ABIN-1 can be attributed to an increase in the formation of autophagosomes or just an impaired autophagosome-lysosome fusion. Therefore, BafA1 was used to inhibit autolysosome content degradation to differentiate between both cases [297]. ABIN-1 and p62 protein levels were significantly increased at 4 h by combinational treatment of rapamycin and BafA1 compared to rapamycin treatment alone (Fig. 5.16 A-C), showing autophagic flux of both proteins. Hence, we decided to use 4 h of autophagy induction as our starting point for further experiments. To verify autophagy induction and inhibition of autophagosome-lysosome fusion we monitored LC3B protein levels of the same cell lysates. As expected, rapamycin treatment increased the lipidation of LC3B-I to LC3B-II, while rapamycin and BafA1 incubation induced a massive accumulation of LC3B-II (Fig. 5.16 A). Intriguingly, we expected that p62 and ABIN-1 proteins would be degraded after prolonged autophagy stimulation, yet both protein levels remained increased. It is conceivable that the steady-state levels of p62 and ABIN-1 were not affected due to a compensation through *de novo* synthesis of both proteins [298]. To corroborate our findings, we asked ourselves whether ABIN-1 protein levels would increase by co-treatment of rapamycin and BafA1 compared to the corresponding single treatment. HeLa cells were stimulated with rapamycin and BafA1 for 4 h and analyzed by Western blot for ABIN-1 and p62 protein levels. Interestingly, ABIN-1 protein levels significantly increased upon treatment with rapamycin and BafA1 compared to either rapamycin or BafA1 alone (Fig. 5.16 D and E). Moreover, p62 showed a similar expression pattern in response to rapamycin and BafA1, however p62 protein levels upon BafA1 treatment remained nearly similar to rapamycin/BafA1 co-treatment (Fig. 5.16 D and F). Therefore, we conclude that ABIN-1 in the same way as p62 is targeted by autophagy into autophagolysosomes for lysosomal degradation.
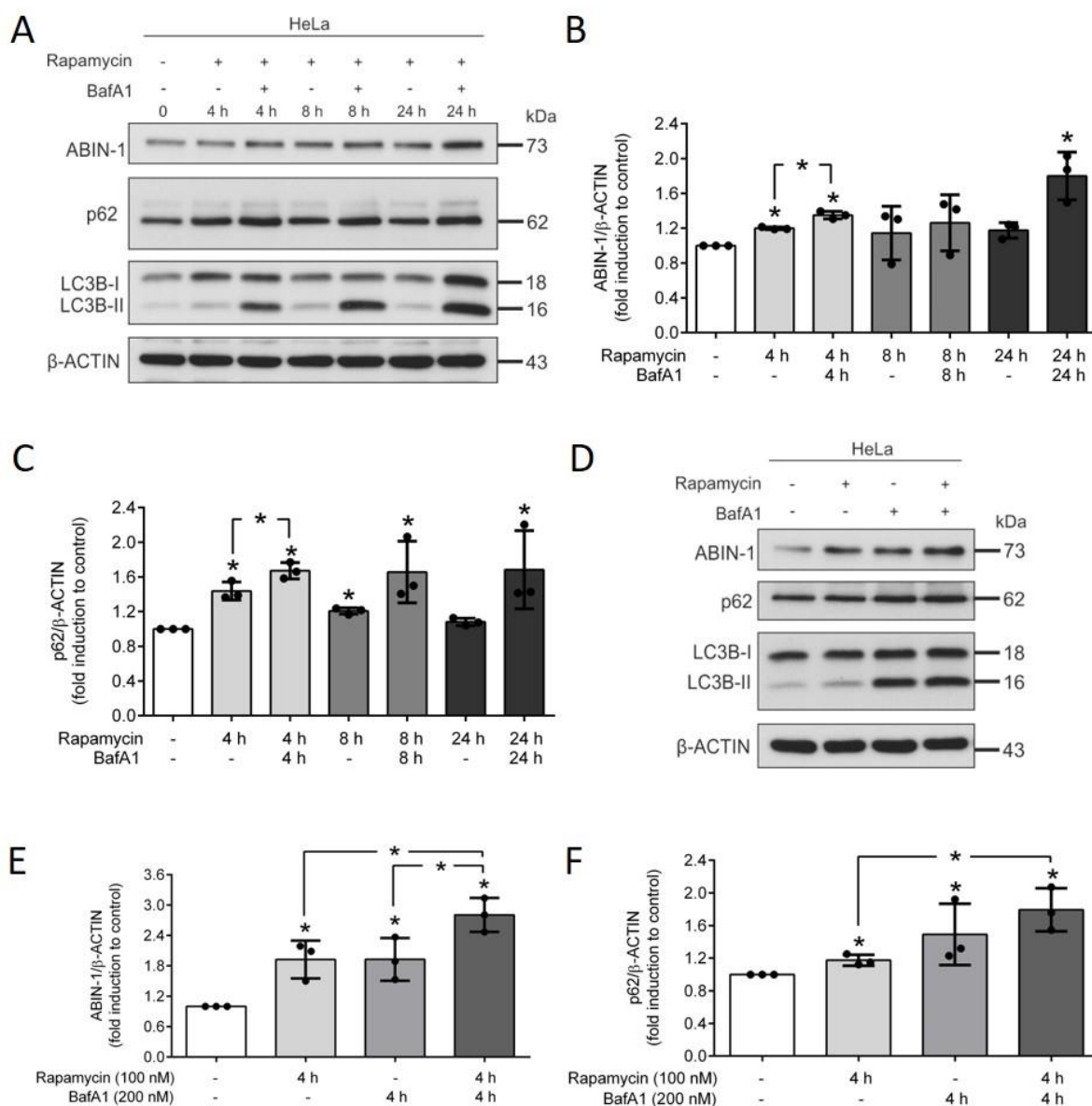
Figure 5.16. ABIN-1 protein levels increase upon autophagy induction or blockage. (A) Western blot analysis of ABIN-1, p62 and LC3B expression in HeLa cells incubated with rapamycin (100 nM) and BafA1 (4 h and 8 h, 200 nM; 24 h, 10 nM) for the indicated time points. Quantification of (A) of ABIN-1 (B) and p62 (C) protein levels normalized to β-ACTIN. (D) HeLa cells were treated with rapamycin (100 nM) and BafA1 (200 nM) for 4 h. ABIN-1, p62 and LC3B protein levels were detected by Western blotting. Quantification of (D) of ABIN-1 (E) and p62 (F) normalized to β-ACTIN. Data represent means ± SD; n = 3; *P < 0.05.

5.2.6   ABIN-1 is recruited to damaged mitochondria

Our IP-MS data of ABIN-1 showed several candidates involved not only in macroautophagy but also candidates which are part of the selective degradation of damaged or excessive mitochondria by autophagy, called mitophagy (Fig. 5.12). During mitophagy, PINK1 recruits the E3 ubiquitin ligase Parkin to damaged mitochondria [299-301]. Subsequently, Parkin ubiquitinates various mitochondrial membrane (OMM) proteins such as mitofusin 2 (MFN2), translocase of outer mitochondrial membrane 20 (TOM20), voltage-dependent anion channel

1 (VDAC1) or mitochondrial fission 1 protein (Fis1). Ubiquitinated OMM proteins are then recognized by selective autophagy receptors like optineurin, NDP52 or p62 and targeted to the phagophore membrane for autophagosomal degradation [302]. To clarify, if ABIN-1 is involved in Parkin-dependent mitophagy we generated HeLa cells stably expressing DOX-inducible Parkin, because HeLa cells lack endogenous Parkin [303]. HeLa-Parkin-expressing cells were treated with DOX for 24 h to induce Parkin expression. Mitophagy was activated by the addition of oligomycin/antimycin A (OA), which in contrast to the respiratory chain uncoupler carbonyl cyanide *m*-chlorophenyl hydrazone (CCCP) is generally considered more specific, less toxic and therefore represents a more physiological approach in inducing mitochondrial damage [304]. After 4 h of OA treatment, HeLa-Parkin cells were fractionated by centrifugation into a cytosolic and mitochondrial fraction and compared to whole cell lysates. Effective fractionation was controlled by analyzing the mitochondrial protein levels of TOM20 and COXII, which were absent in the cytosolic fraction (Fig. 5.17). Successful induction of mitophagy was ensured by observing the reduction in TOM20 and COXII protein levels after OA treatment in whole cell lysates. As expected, PARKIN, p62 and ABIN-1 were found in all fractions. Interestingly, ABIN-1 protein levels were enriched in the mitochondrial fraction in response to mitophagy induction, indicating a translocation of ABIN-1 to mitochondria (Fig. 5.17). Similarly, PARKIN and p62 were increased in the mitochondrial fraction upon OA treatment (Fig. 5.17). Taken together, our data show that ABIN-1 is recruited to mitochondria upon mitochondrial damage.
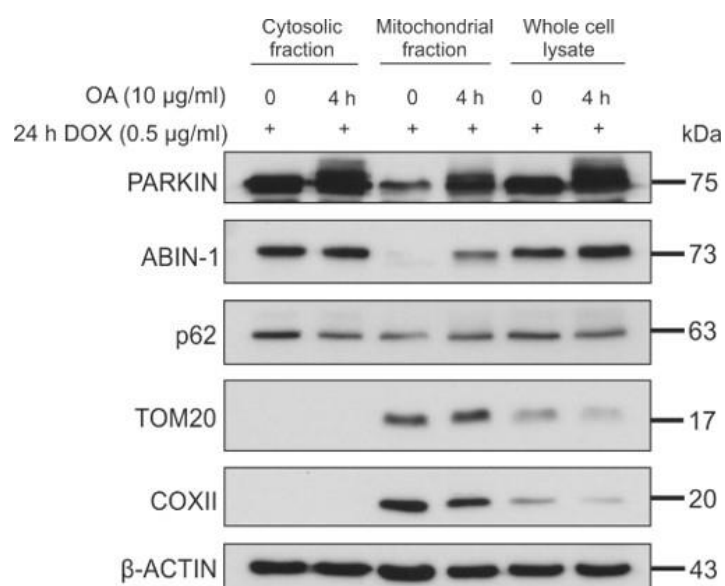

Figure 5.17. ABIN-1 translocates to damaged mitochondria. mCherry-Parkin expressing HeLa cells were treated with oligomycin/antimycin A (OA) (10 µg/ml) for 4 h. Mitochondrial and cytosolic fractions as well as whole cell lysates were assessed by immunoblotting. TOM20 and COXII served as mitochondrial marker, whereas β-ACTIN was used as a loading control. n = 3.

5.2.7 The degradation of mitophagy substrates is dependent on ABIN-1

ABIN-1 was highly enriched in the mitochondrial fractionation upon mitophagy induction (Fig. 5.17). Thus, we were interested in understanding if ABIN-1 protein levels effect mitochondrial clearance by mitophagy. For this purpose, CRISPR/Cas9-mediated genome editing was used to knock out ABIN-1 in HeLa cells stably expressing Parkin. We analyzed mitophagy by quantifying the degradation of MFN2, VDAC1, TOM20 and COXII in HeLa-Parkin or ABIN-1 KO-Parkin cells, following mitochondrial damage by OA treatment for various time points. Mitophagy-induction triggered a rapid degradation of MFN2 and a gradually decrease in VDAC1 protein levels in a time-dependent manner in HeLa-Parkin and ABIN-1 KO-Parkin cells (Fig. 5.18 A-C).

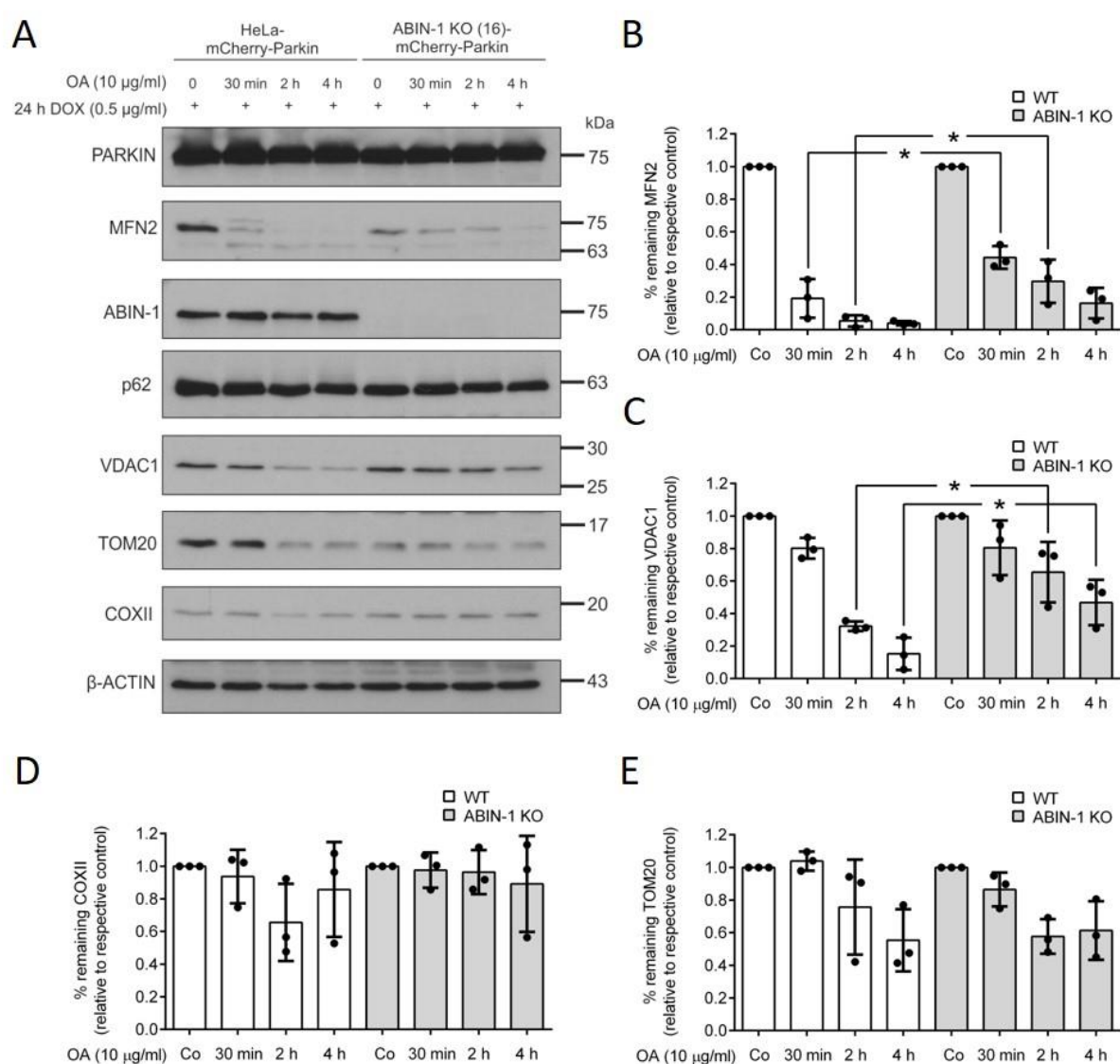**Figure 5.18. CRISPR/Cas9-mediated knockout of ABIN-1 delays degradation of mitophagy substrates.** (A) Western blot analysis of mCherry-Parkin-overexpressing HeLa or ABIN-1 knockout (KO) cells exposed to OA (10 µg/ml) for the indicated time points. Quantification of remaining MFN2 (B), VDAC1 (C), COXII (D) or TOM20 (E) protein levels normalized to β-ACTIN. Data represent means ± SD; n = 3; *$P < 0.05$.

Interestingly, MFN2 and VDAC1 protein levels were significantly slower degraded in cells lacking ABIN-1 (Fig. 5.18 A-C), whereas TOM20 and COXII levels were not affected even after 4 h of OA treatment (Fig. 5.18 A, D and E). To validate the knockout phenotype of ABIN-1 (clone 16), another CRISPR/Cas9-mediated knockout clone of ABIN-1 was used for the same experiment. ABIN-1 KO-Parkin (clone 27) cells responded in the same way as cells-derived from clone 16, therefore proving ABIN-1-specific effects (Suppl. Fig. 8.1 A). Of note, HeLa-Parkin cells, treated with siRNA against ABIN-1 did not slow the degradation of mitochondrial proteins in response to OA treatment (Suppl. Fig. 8.1 B).

To further demonstrate that ABIN-1 affects the degradation of mitochondrial proteins upon mitophagy, we exposed HeLa-Parkin and ABIN-1 KO-Parkin cells to prolonged OA treatment for a period of 24 h.
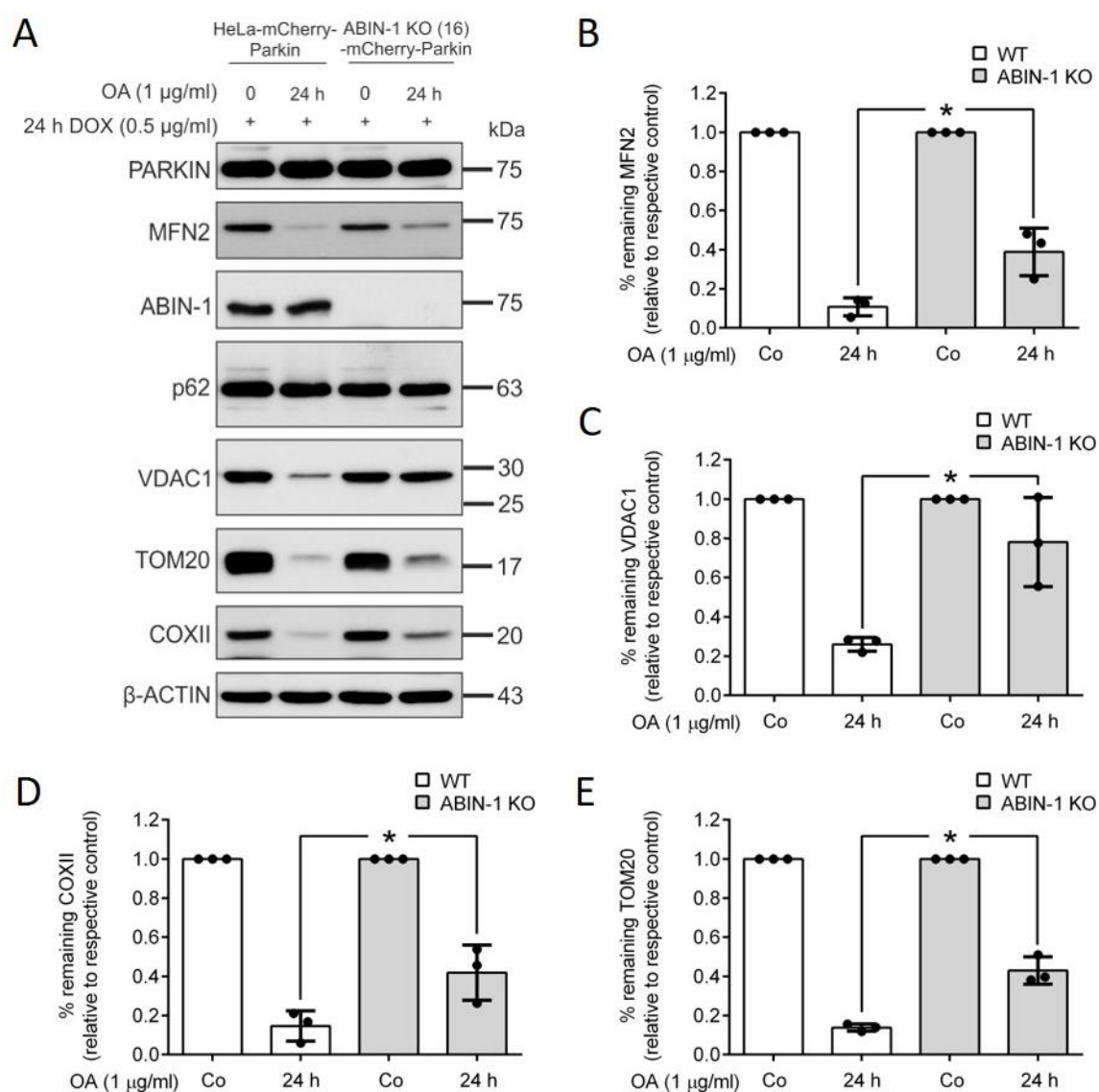

Figure 5.19. Absence of ABIN-1 slows degradation of mitophagy substrates. (A) mCherry-Parkin-overexpressing HeLa or ABIN-1 knockout (KO) cells were stimulated with OA (1 µg/ml) for 24 h and analyzed by Western blotting. Quantification of MFN2 (B), VDAC1 (C), COXII (D) or TOM20 (E) protein levels normalized to β-ACTIN. Data represent means ± SD; n = 3; *$P < 0.05$.

Strikingly, we found that the degradation of MFN2, VDAC1, TOM20 and COXII induced by OA could be significantly prevented in ABIN-1 KO-Parkin cells compared to HeLa-Parkin cells, indicating a partial block in mitophagy (Fig. 5.19 A-E). As the degradation of all mitochondrial proteins were highly reduced in ABIN-1 KO-Parkin cells, we conclude that ABIN-1 could target ubiquitinated mitochondrial proteins for autophagosomal degradation. Therefore, lack of ABIN-1 negatively impacts on mitophagy.

5.2.8 Knockdown of ABIN-1 reduces overall mitophagy levels

To corroborate our findings, we tested the influence of ABIN-1 on mitophagy via the FACS-based sensitive mt-mKEIMA assay. Mt-mKEIMA is a fluorescence-based reporter which is specifically targeted to mitochondria via a mitochondria-targeting signal peptide sequence and changes its excitation spectrum from 405 nm in a neutral pH environment to 561 nm in an acidic environment. By analyzing the spectral shift from 405 to 561 nm, the percentage of lysosomal engulfed mt-mKEIMA representing mitochondria undergoing mitophagy can be quantified. Since, this marker is resistant to degradation within lysosomes it represents a robust way to quantify the overall mitophagy activity of a cell population [261]. In an effort to determine, if ABIN-1 is involved in Parkin-dependent mitophagy we overexpressed Parkin in mt-mKEIMA-cells and depleted ABIN-1 via siRNA-mediated knockdown (Fig. 5.20 A and B). Mitochondrial damage was induced by 6 h of OA treatment to effectively push all mitochondria into mitophagy, while autophagosome-lysosome fusion was blocked by addition of BafA1 for 6 h. Mt-mKEIMA-Parkin-expressing cells treated with siRNA control showed only minor mitophagy levels at basal conditions (Fig. 5.20 A and C). However, when treated with OA, mt-mKEIMA-Parkin cells showed a drastically increase in mitophagy up to 89% (Fig. 5.20 A and C). Interestingly, a siRNA-mediated knockdown of ABIN-1 significantly decreased mitophagy levels under OA treatment by 8% compared to cells treated with siRNA control and OA. Similarly, in both cases the addition of BafA1 efficiently blocked mitophagy, apparent through a drastically lowered amount of mt-mKEIMA delivered into lysosomes (Fig. 5.20 A and C). Hence, this data supports that ABIN-1 is either a mitophagy receptor (ligand-receptor interaction) or an adaptor protein in mitophagy which is recruited to mitochondria in order to mediate their autophagosomal degradation.
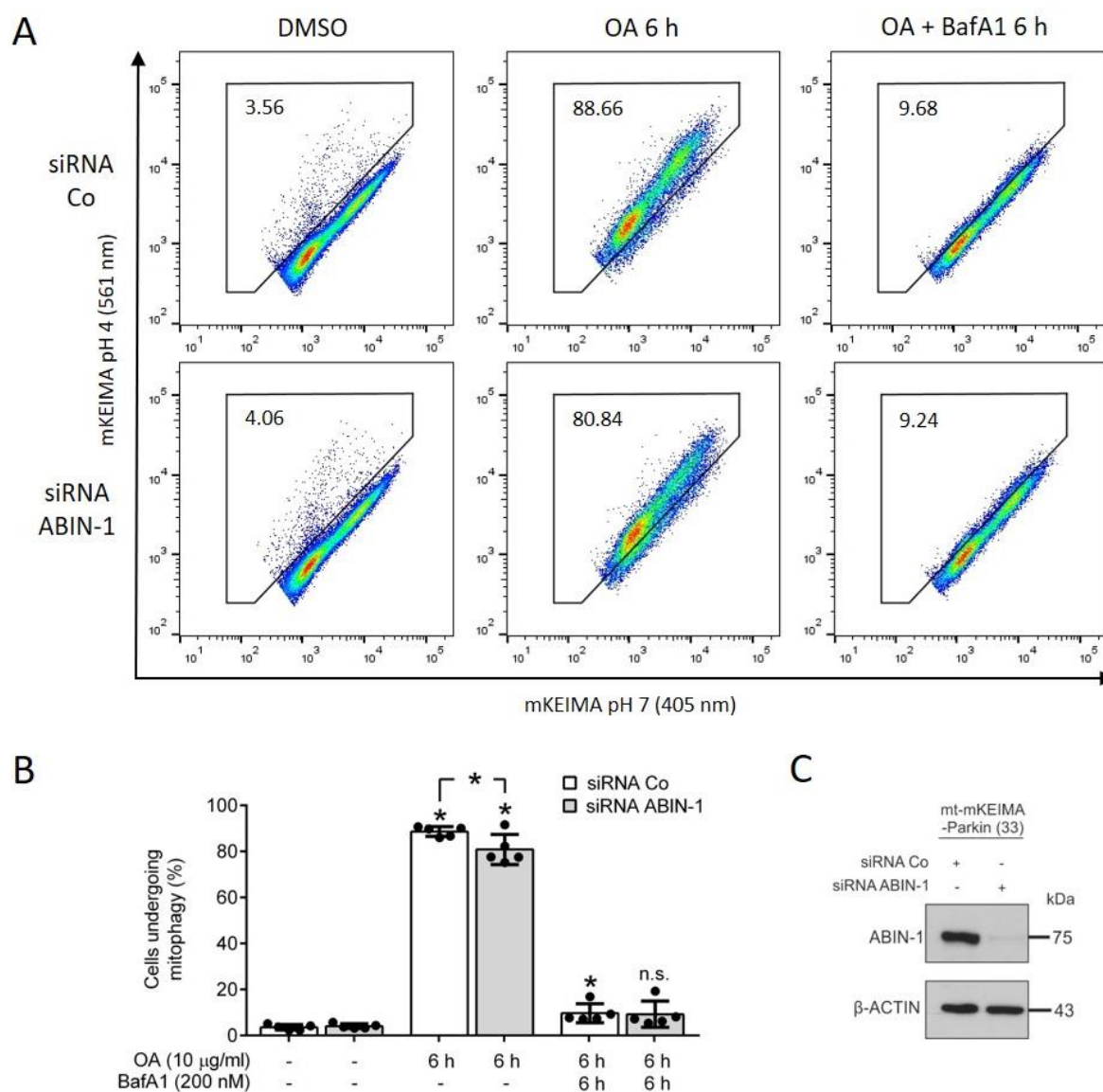
Figure 5.20. ABIN-1 is involved in Parkin-dependent mitophagy. (A) Representative data for mt-mKEIMA-Parkin-expressing HeLa FlpIn TRex cells transfected with siRNA control of siRNA against ABIN-1 for 48 h. Cells were treated with OA (10 µg/ml) and BafA1 (200 nM) for 6 h and analyzed by FACS for lysosomal positive mt-mKEIMA, representing cells undergoing mitophagy. (B) Quantification of (A). (C) Western bot analysis of mt-mKEIMA-Parkin-expressing HeLa FlpIn TRex cells treated with siRNA control or siRNA against ABIN-1 after 48 h. β-ACTIN served as a loading control. Data represent means ± SD; n = 5; *P < 0.05; n.s. = not significant.

5.2.9 ABIN-1-depletion does not affect macroautophagy

We then addressed, if ABIN-1 is required for overall autophagic activity by using the FACS-based reporter mKEIMA-hLC3B. HeLa FlpIn TRex cells stably expressing mKEIMA-hLC3B were either treated with siRNA control or siRNA against ABIN-1 (Fig. 5.21 A and B). To assess autophagic flux, cells were incubated either with Torin-1 or EBBS starvation medium alone or in the presence of BafA1 for 4 h. Overexpression of mKEIMA-hLC3B already induced high levels of autophagy in cells treated with siRNA control or siRNA against ABIN-1 (Fig. 5.21 A

and C). ABIN-1 knockdown did not affect autophagy levels triggered by EBBS starvation or Torin-1 treatment. Autophagic flux was determined by the addition of BafA1, resulting in a complete block of autophagy under both conditions (Fig. 5.21 A and C). High autophagy levels under basal conditions complicated the exact determination of the impact of ABIN-1 on overall autophagy. Since autophagy inducers elevated autophagy levels only between 12-20% compared to control situation, the effect of a knockdown of ABIN-1 as observed for mitophagy could be out of the detection limit of the assay. As autophagy levels did not significantly dropped upon ABIN-1-depletion, ABIN-1 may only has complementary or supportive roles in overall autophagy.
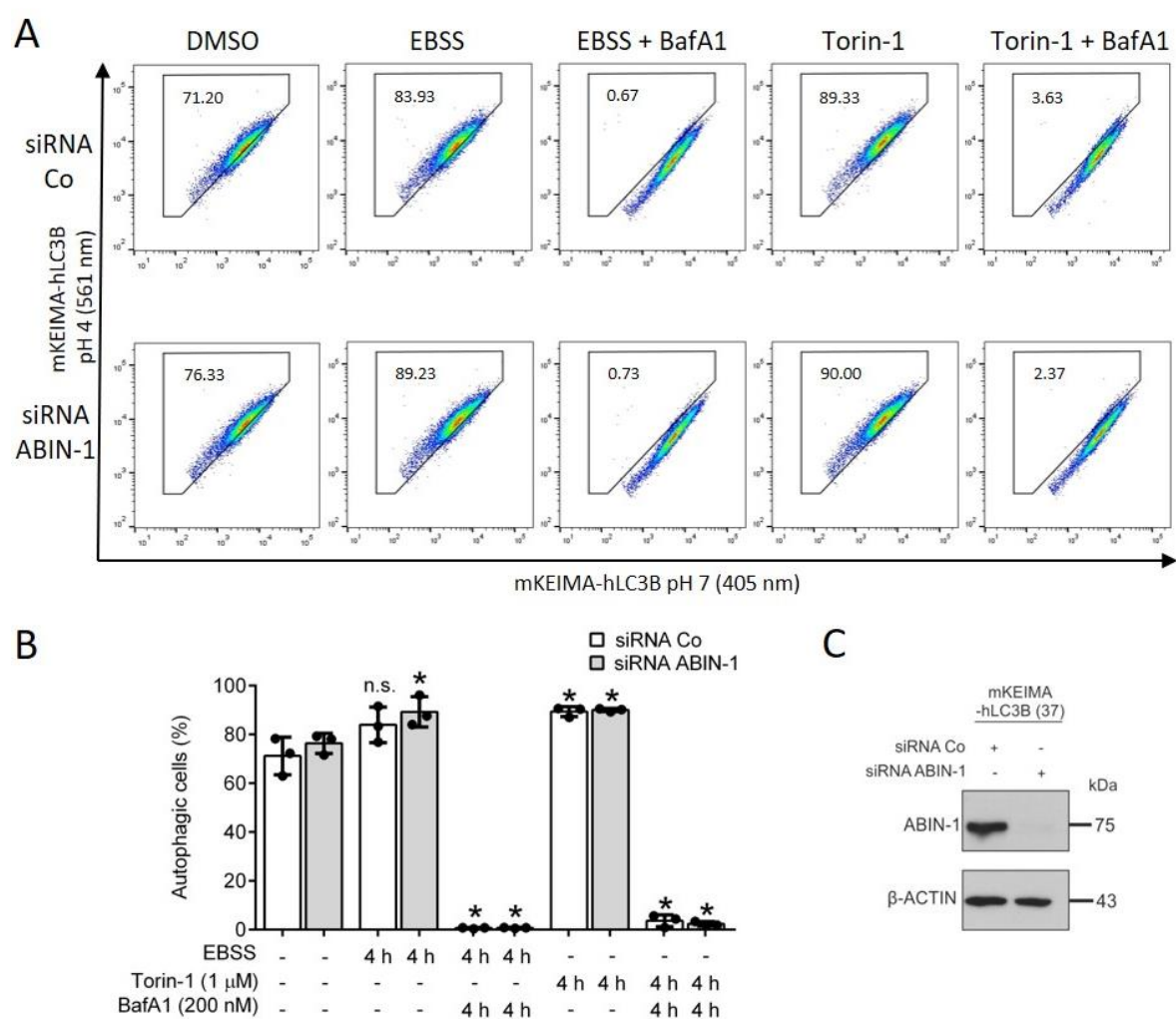
Figure 5.21. siRNA-mediated knockdown of ABIN-1 does not affect overall autophagy levels. (A) Representative data for HeLa FlpIn TRex cells stably expressing mKEIMA-hLC3B transfected with siRNA control or siRNA against ABIN-1 for 48 h. Transfected cells were stimulated with Torin-1 (1 µM) or serum-starved with EBSS with or without BafA1 (200 nM) for 4 h. (B) Quantification of (A). (C) Representative Western bot analysis of mKEIMA-hLC3B cells transfected with siRNA control or siRNA against ABIN-1 after 48 h. β-ACTIN served as a loading control. Data represent means ± SD; n = 3; *P < 0.05; n.s. = not significant.

6 Discussion

6.1 PART I: Biglycan-induced pro-inflammatory signaling in macrophages is CD14-dependent

In the first part of this study, we investigated the impact of the cell-surface co-receptor CD14 for biglycan-mediated TLR2/4 signaling in inflammation. Here, we report that in mouse peritoneal macrophages, soluble biglycan interacts directly with CD14 via a high affinity interaction. The specific interaction of biglycan with CD14 regulates the production of pro-inflammatory mediators over TLR2 and TLR4 as well as biglycan-induced downstream signaling. Importantly, we confirm our findings in an *in vivo* mouse model of renal IRI in WT and *Cd14*^{-/-} mice by transiently overexpressing soluble biglycan. In renal IRI, CD14 ablation mitigates biglycan-induced production of pro-inflammatory mediators, macrophage infiltration and M1 polarization as well as improves overall kidney function.

6.1.1 CD14 is an essential co-receptor for biglycan-mediated TLR2/4 signaling in macrophages

Biglycan regulates the production of pro-inflammatory mediators by selectively engaging TLR2/4 and the TLR adaptor proteins MyD88 and TRIF [12]. Previous work showed that biglycan triggers the synthesis of TNF-α, CCL2 and CCL20 over TLR2/4 by involving MyD88, while inducing CCL5 and CXCL10 production over TLR4/TRIF [61, 62, 66], however, the involvement of co-receptors had not been defined. Based on the findings that biglycan was found in a high molecular complex with MD2 and CD14 [31] we aimed to elucidate if CD14 is needed for biglycan signaling in sterile inflammation. As CD14 functions as a co-receptor for both, TLR4 [121, 123] and TLR2 [86] as well as for TLR3, TLR7, TLR8 and TLR9 [117], it was conceivable that biglycan would also be recognized by CD14. In line with previous work we found that biglycan triggers TNF-α and CCL2 production over TLR2/4 [31, 53, 66], while CCL5 expression was exclusively regulated over TLR4 in macrophages [66]. Furthermore, *Hsp70* expression in macrophages was confirmed as TLR2-dependent [74]. Importantly, CD14 ablation abolished the production of TNF-α, CCL2, CCL5 and HSP70, mimicking the response of TLR2/4-double deficient mice upon biglycan exposure. Accordingly, these data agree with our hypothesis that CD14 represents an imperative element in biglycan-mediated TLR4 and TLR2 signaling. The fact, that CD14 is also needed for proper TLR2 activation via biglycan is of great importance since, in contrast to TLR4 signaling which highly depends on CD14 for ligand recognition [264], TLR2 signaling requires CD14 only in a ligand-dependent manner [87, 88, 94, 96, 305]. Therefore, it is tempting to speculate that CD14 represents a common co-

receptor in all biglycan-mediated pro-inflammatory responses. So far, it is not yet clear how biglycan engages CD14 and TLR2/4. It is imaginable that, similar to LPS [121], soluble CD14 binds biglycan and transfers it to TLR2 or the TLR4/MD2 complex, thereby greatly lowering the threshold for biglycan recognition. As a consequence, CD14 represents a very attractive target to interfere with biglycan-induced inflammation. Importantly, pharmacological inhibition of either TLR2 or TLR4 alone would not completely block all biglycan-triggered inflammatory responses and may evoke compensatory effects. It is highly likely that pharmacological inhibition of CD14 could circumvent the downsides of single targeting of TLRs. This is supported by the line of evidence that numerous TLR2 and TLR4 inhibitors and antagonists were tested in clinical trials, but yet most of them failed to show the desired effects and none have been approved for clinical use [306, 307]. For instance, the use of the potent TLR4-MD2-complex inhibitor eritoran was used to counteract the high mortality in sepsis, however failed to improve patient survival in phase III clinical trials [308]. Generally, it is presumed that the inhibitory effect on only one PRR is overwritten by the compensatory effects of other PRR receptors [309], thereby accounting for the limited effects of single TLR targeting approaches. In contrast, CD14 inhibition, either alone or by concomitant targeting the complement system not only efficiently lowers pro-inflammatory cytokines during TLR-mediated sepsis [136, 310-313] but is also regarded as a promising candidate in clinical trials due to its broad effect on several TLRs [314-316].

In agreement with cumulative reports, the present study provides evidence that pharmacological targeting of CD14 limits inflammation. Pre-incubation of biglycan-treated WT macrophages with an anti-CD14 antibody lowered the synthesis and secretion of TNF-α, CCL2, CCL5 and HSP70 protein levels, thereby supporting the notion that CD14 is essential in biglycan-triggered inflammation. Similarly, by using HEK-Blue cells expressing hTLR2/CD14 or hTLR4/CD14/MD2 we were able to demonstrate that pre-treatment with a specific anti-CD14 antibody lowered biglycan-induced NF-κB activation comparable to the reduction in response to the TLR4 ligand LPS [275] as well as the TLR2 ligand PGN [276]. This finding implies that the same mechanism of CD14-dependent regulation of biglycan signaling applies not only to macrophages but also to non-immune cells.

Following TLR2/4 interaction, biglycan induces the activation of p38 MAPK, p44/42 (Erk1/2) and NF-κB in a predominantly MyD88-dependent manner in order to trigger the synthesis of pro-inflammatory cytokines [31, 67]. Activation of p38 MAPK, p44/42 (Erk1/2) and NF-κB requires their phosphorylation [317-319]. Interestingly, by using primary murine peritoneal macrophages from WT and $Cd14^{-/-}$ mice stimulated with soluble biglycan we were able to show that biglycan-induced phosphorylation of the intracellular signaling proteins p38 MAPK, p44/42 (Erk1/2) and NF-κB highly depends on CD14, further supporting the known role of CD14 in mediating MyD88-dependent gene induction [320]. This is consistent with previous studies in

which NF-κB and MAPK activation by the TLR4 ligand LPS was blunted in *Cd14-/-* macrophages at 30 min [321]. An important step in the activation of p38, p44/42 and NF-κB is their nuclear translocation [277, 279, 280]. Along this line, we evaluated whether biglycan-mediated translocation is affected by CD14 deficiency. Importantly, biglycan triggered a CD14-dependent increase and translocation of phosphorylated p38, p44/42 and NF-κB from the cytosol to nuclear compartments. However, phosphorylation of the p65 NF-κB subunit at S536 by biglycan only resulted in partial translocation into the nucleus. The unexpected localization is likely due to antibody specificity as the employed antibody only recognizes phosphorylated NF-κB at serine 536. Indeed, S536 phosphorylated p65 is known to predominantly localize in the cytosol, whereas S468 phosphorylated p65 is localized in nuclear speckles [281]. Collectively, these data emphasize the important role of CD14 in the activation and subsequent translocation of biglycan/TLR-induced downstream mediators. In accordance with our data, physical interaction of CD14 with TLR4 precedes nuclear translocation of NF-κB [322]. Furthermore, MyD88 represents the main driver for p38 and NF-κB phosphorylation and translocation to the nucleus upon TLR4-ligand stimulation such as LPS or HMGB1 [323, 324]. As biglycan-induced activation of downstream mediators by TLR2/4 is mainly MyD88-dependent [31] and CD14 is needed for biglycan-evoked TLR2/4 activation, it is very likely that ablation of CD14 blocks subsequent MyD88-dependent activation of p38, p44/42 and NF-κB by biglycan.

6.1.2 CD14 binds biglycan directly with high affinity

Next, the binding properties of biglycan to CD14 were investigated. We have previously shown that biglycan appeared in a high molecular weight complex consisting out of TLR2, TLR4, CD14 and MD2 [31]. Moreover, by microscale thermophoresis analysis we were able to determine the high affinity binding capacities of TLR2 ($K_D \sim 31$ nM) and TLR4 ($K_D \sim 23$ nM) to biglycan [61]. In accordance, we were able to show with Co-immunoprecipitation in primary macrophages that biglycan is in complex with CD14. Additionally, by utilizing microscale thermophoresis analysis we determined the direct binding affinity of CD14 to soluble intact biglycan ($K_D \sim 67$ nM). CD14 interacts with various TLR ligands in order to increase or enable their ability to evoke TLR signaling [95]. Remarkably, the binding affinity of biglycan to CD14 is similar to the one of soluble CD14 to LPS ($K_D \sim 41$ nM) without the LPS-binding protein (LBP) and a bit weaker than the TLR2 ligand peptidoglycan to LPS ($K_D \sim 25$ nM) [325], suggesting similar mechanisms in ligand recognition by CD14. If binding of biglycan to CD14 is enhanced by the presence of accessory molecules such as LBP for LPS [325] or if the TLR-mediate response and binding affinity is not changed by additional complex members as such for the case of peptidoglycan [325, 326], remains an open question to be addressed. Structural studies of CD14 revealed that leucine rich repeats (LRRs) in CD14 enable binding of LPS to

CD14 [115]. It is conceivable that biglycan binding to CD14 and TLR2/4 is mediated by LRR domains in biglycan and the corresponding receptors. In support of this, recent work identified a common binding motif of biglycan consisting out of LRR2 and LRR10 which mediates the binding to CD14, TLR2 and TLR4 (Hsieh, unpublished data). Apart from biglycan, several other DAMPS/proteoglycans are known to interact with CD14 to trigger inflammatory responses. For instance, versican binds to TLR2, TLR6 and CD14 to activate macrophages and induce pro-inflammatory cytokine production [126]. Furthermore, versican promotes the expression of growth factor human cationic antimicrobial protein (hCAP)18/LL-37 (promoter of ovarian cancer) in macrophages by engaging TLR2, TLR6 and CD114 [327]. Lumican promotes the innate immune activity by binding to CD14 and TLR4 [328]. Moreover, lumican regulates the CD14-regulated phagocytosis on the surface of peritoneal macrophages, thereby protecting against Gram-negative bacterial infection [329]. In contrast, hyaluronan triggers inflammation independently of CD14 by utilizing TLR4, MD2 and CD44 [103].

Surprisingly, the GAG side chains of soluble biglycan were superfluous in binding CD14 as the protein core of biglycan bound CD14 even with a higher binding affinity ($K_D \sim 54$ nM). Similarly, GAG chain removal of biglycan or decorin increases the binding affinity to TGF-β [33, 330]. In the same vein, binding of biglycan to TLR2/4 is also mediated via the protein core biglycan [31]. While binding of biglycan to CD14 and TLR2/4 clearly seems to be mediated by the protein core, only fully glycanated biglycan is able to trigger inflammatory signaling in macrophages [31]. In the same manner, decorin and biglycan suppress the proliferation of preadipocytes by triggering apoptosis depending on the presence of their GAG side chains [331]. Therefore, GAG side chains seem be dispensable for mediating binding to innate immune receptors, but still represent a necessary element in evoking signaling responses. It is likely that GAG side chain modifications mediate the recruitment of additional molecules to the complex consisting out of biglycan/TLR/CD14 in order to regulate signaling outcomes. As CD14 seems to represent a common co-receptor for biglycan/TLR-mediated inflammatory signaling the question rises why biglycan selectively engages one TLR and a corresponding TLR adaptor molecule. It is plausible that additional factors are implicated in the complex formation of biglycan/CD14/TLRs and the TLR adaptors.

6.1.3   Biglycan aggravates renal IRI in a CD14-dependent fashion

Ischemia reperfusion injury (IRI) results from a temporary obstructed blood flow of the associated organ followed by the restoration of perfusion. Renal IRI is a major factor of acute kidney injury (AKI) and chronic kidney diseases (CKD [332]) and is characterized by hypoxic injury together with high amounts of ROS production [282]. Subsequently, oxidative stress triggers apoptosis, necrosis and a strong sterile inflammatory immune response which is mainly mediated by the transcriptional activity of NF-κB [285]. Furthermore, ischemia evokes

a vast release DAMPs from damaged cells such as hyaluronic acid, HMGB1, HSPs and biglycan which activate TLRs to augment the inflammatory response by inducing the production of pro-inflammatory cytokines and death signaling pathways [333]. Since, previous studies found out that biglycan exacerbates the outcome of renal IRI in a TLR2- and TLR4-dependent manner [61, 74], the present study aimed to elucidate the importance of CD14 in this mechanism. In line with previous observations, biglycan aggravated the pathophysiology of acute kidney inflammation during renal IRI (30 h) by increasing the production of TNF-α, CCL2, CCL5 and HSP70 on protein and gene level. Importantly, chemo- and cytokine production was not increased in $Cd14^{-/-}$ mice, providing proof-of-principle for our $in\ vitro$ data that CD14 is necessary for biglycan-induced inflammation. Mounting evidence suggests that NF-κB mediates ROS, chemo- and cytokines expression as well as apoptosis [334, 335]. Since CD14 ablation abolished biglycan-induced NF-κB activation in macrophages, it is quite likely that chemo- and cytokine production by biglycan during renal IRI is abrogated by loss of NF-κB activity. Accordingly, inhibition of NF-κB gene modification impedes kidney damage after ischemia [336, 337].

Moreover, transient overexpression of biglycan promoted the number of infiltrating macrophages into the kidney in a CD14-dependent manner. Further analysis revealed that the majority of these recruited macrophages were polarized as a pro-inflammatory M1 phenotype. Macrophages are polarized in response to TNF-α, exogenous and endogenous ligands or IFN-γ into an M1 phenotype [338]. M1 macrophages secrete high amounts of inflammatory chemo- and cytokines such as TNF-α, IL-6, IL-1β and iNOS, leading to cytotoxicity [339, 340]. Especially in first 48 h of renal IRI, most of the recruited macrophages are polarized as a M1 phenotype [341] and critically determine the outcome of IRI [342], whereas at later time points, regenerative M2 macrophages predominate the site of injury [341, 343]. Therefore, biglycan seems to aggravate renal IRI not only by increasing the number of recruited macrophages but also polarizes macrophages into a pro-inflammatory M1 phenotype. CD14 ablation improved the clinical outcome in biglycan-exacerbated renal IRI, visible through reduced serum creatinine levels and decreased tubular damage. In accordance, several studies showed that M1 macrophage depletion prevents the immunopathology in injured kidneys. For instance, macrophage depletion by pre-injection of clodronate in mice before unilateral or bilateral IRI significantly improved renal function at early stages of IRI, visible through reduced tubular necrosis, decreased tubular apoptosis diminished inflammation and less oxidative stress [284, 341, 344-348]. A recent study shows that the lectin ArtinM, is required for M1 macrophage polarization by binding to CD14 and TLR2 [134]. In a similar way, LPS, one of the most prominent triggers of M1 macrophage polarization, also highly depends on CD14 [340]. Hence, it is conceivable that other PAMPs and DAMPs which depend on CD14 require this co-receptor in order to induce M1 macrophage polarization.

Until now, specific deletion of TLR adaptor molecules or co-receptors of TLR2 and TLR4 in mice have been well studied in IRI. Yet, there exists controversial data regarding the outcome. Many studies identify MyD88 as the main target in the TLR2/4-mediated activation of the immune system in IRI [262, 349-352]. However, these results partly contrast with the findings of other studies that show no beneficial effect of MyD88 or TRIF deficiency in IRI [350, 353]. In the same line, even though CD14 expression is increased during IRI [354, 355], the role of CD14 in IRI is not fully clarified. Controversially, during hepatic IRI, CD14 deficient mice either are protected from IRI [356] or do not show any alteration in the disease outcome [357]. In contrast, during cardiac IRI, CD14 along MyD88, TRIF and HMGB1 clearly contribute to the inflammatory cascade [358]. Accordingly, our findings display a protective effect of CD14 deficiency during renal IRI even in the absence of transient biglycan overexpression. Therefore, our data establish CD14 as a crucial player in the inflammatory response in renal IRI and also highlight its function as a co-receptor for the inflammatory signaling of an extracellular ligand of TLR2 and TLR4.

The collective results are presented in our working model (Fig. 6.1). The present study identified CD14 as a novel co-receptor for biglycan-induced pro-inflammatory signaling over
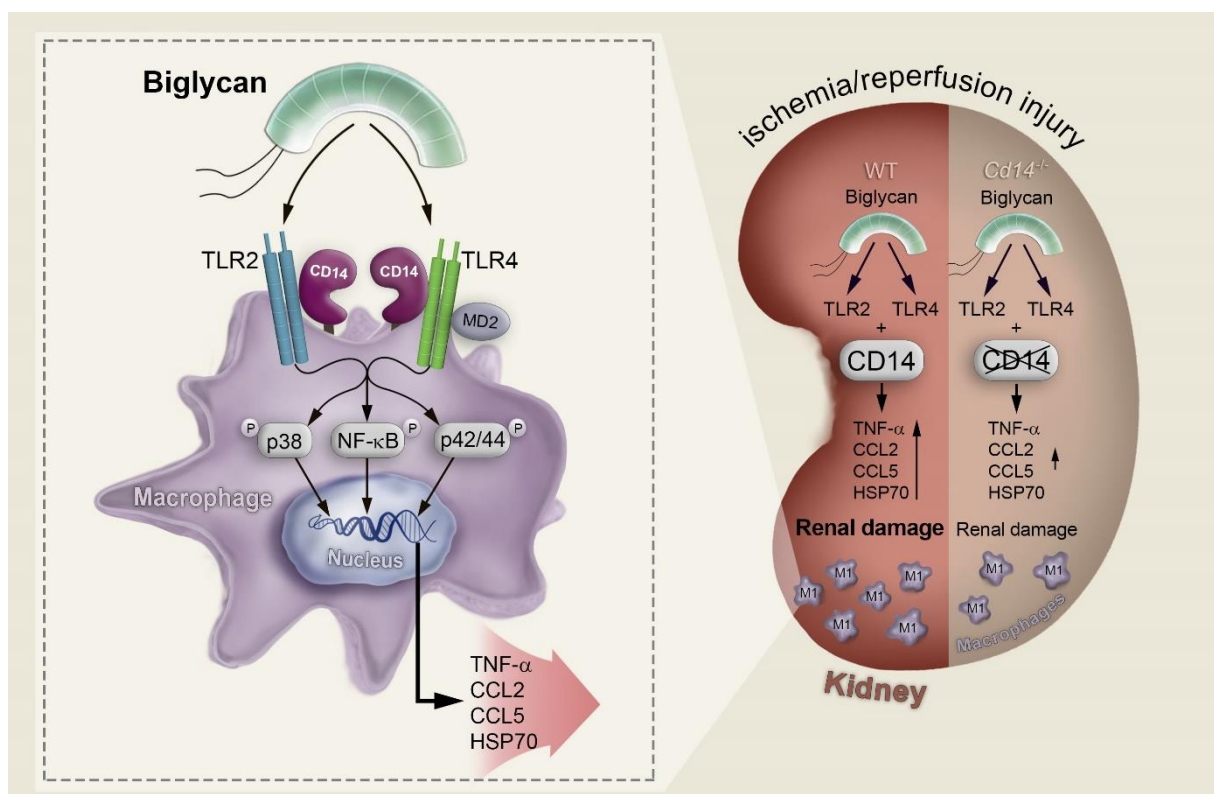
Figure 6.1. Schematic drawing of CD14-dependent biglycan signaling in macrophages and renal IRI. Soluble biglycan interacts with TLR2/4 to induce the phosphorylation of downstream mediators such as p38, p42/44 and NF-κB by utilizing the co-receptor CD14. Consequently, this leads to the production and release of TNF-α, CCL2, CCL5 and HSP70. During renal IRI, transient overexpression of biglycan triggers the expression of TNF-α, CCL2, CCL5 and HSP70 as well as increases macrophage infiltration, the number of M1 macrophages and renal damage. CD14 deficiency blunts biglycan-mediated pro-inflammatory signaling during renal IRI. Figure is reproduced from [274].

TLR2 and TLR4 in primary peritoneal macrophages. In detail, biglycan triggers the production of TNF-α, CCL2, CCL5 and HSP70 by selectively interacting with TLR2 and TLR4 in macrophages. The biglycan-induced production of chemo- and cytokines as well as HSP70 could be abolished by applying either genetic ablation of *Cd14* or treating macrophages with a specific anti-CD14 antibody. Mechanistically, biglycan binds directly to CD14 with high affinity and regulates the activation and translocation of p38, p42/44 and NF-κB via engaging CD14. At last, this study confirms the concept in an *in vivo* model of renal IRI in WT and *Cd14⁻/⁻* mice. In a CD14-dependent manner, biglycan exacerbates the expression of the pro-inflammatory mediators TNF-α, CCL2, CCL5 and HSP70 and leads to increased macrophage infiltration, M1 macrophage polarization, tubular damage and serum creatinine levels during renal IRI [274]. Therefore, pharmacological targeting of CD14 represents a new attractive approach in inhibiting biglycan-mediated inflammation.

6.2   PART II: ABIN-1 is a selective autophagy receptor for damaged mitochondria

In the second part of the study, we analyzed the role of ABIN-1 as a new selective autophagy receptor. We report several bona fide interaction partners of ABIN-1 by mass spectrometry analysis which are highly connected to autophagy. We show that ABIN-1 harbors two undescribed LC3-interacting domains and confirm the binding of ABIN-1 to several ATG8 proteins. Moreover, we show that ABIN-1 protein levels are regulated by pharmacological interference with the autophagy machinery. Additionally, we validate ABIN-1 co-localization with autophagic marker proteins in response to autophagic stimuli. Finally, we show that ABIN-1 translocates to damaged mitochondria and is involved in their selective degradation by mitophagy.

6.2.1   ABIN-1 associates with various protein of the autophagic machinery

ABIN-1 is well known as a major suppressor of inflammation downstream of TLRs by limiting NF-κB signaling [144, 151]. Inhibition of NF-κB is mediated either by ABIN-1 alone or in concert with A20 via the ability of ABIN-1 to bind polyubiquitinated proteins [147]. So far, ABIN-1 is implicated only in inflammation, apoptosis and necroptosis [149, 151, 153, 359]. Our interactome analysis of ABIN-1 by IP-MS in septic spleens confirmed the interaction of ABIN-1 to known mediators of inflammation such as A20 [289], TRAF1 [147] and NF-κB [290]. Surprisingly, IP-MS of ABIN-1 revealed a huge number of bona fide interactions to proteins which are involved in autophagy. For instance, we found that ABIN-1 binds to ATG5 and ATG7. ATG5 and ATG7 are members of the PE conjugation system, mediating the lipidation of ATG8 proteins [360] which represents a necessary step in autophagosome formation [195]. Indeed,

other autophagy receptors such as p62, NDP52 and optineurin also interact with ATG5 in order to stimulate ATG8 conjugation around cargo proteins [361]. It is likely that ABIN-1 drives phagophore expansion around cargo proteins in a similar fashion by stabilizing the ATG5-containing ATG8 conjugation complex. In support of this notion, ABIN-1 interacts with the ATG8 proteins GABARAPL2 and MAP1LC3B (LC3B) who can serve as membrane scaffolds for the attraction for LC3-interacting region-containing (LIR) proteins, thereby mediating the selective transport of autophagy receptors together with their cargo into the phagophore [362]. After maturation, autophagosomes fuse with lysosomes to initiate the degradation of the engulfed cargo [363]. Notably, ABIN-1 also showed binding to the lysosomal marker LAMP-1 [364], implying autophagolysosomal degradation of ABIN-1. Since, ATG8 proteins were identified as binding partners in this screen and ABIN-1 binds to polyubiquitinated proteins via its UBAN domain, it is conceivable that ABIN-1 functions as a selective autophagy receptor. In line with this, the UBAN domain of ABIN-1 shows sequence similarities with those of optineurin, an autophagy receptor which regulates NF-κB signaling by its ubiquitin binding domain [290, 365]. Moreover, ABIN-1 binds only K63- and M1-linked polyubiquitin chains, which primarily label cargo proteins for autophagic clearance by autophagy receptors [207]. Besides multiple interactions of ABIN-1 to proteins involved in core autophagic processes such as Beclin-1 and PIK3C3 [366, 367], a cohort of mitochondrial proteins which are localized to the OMM and participate in mitochondrial quality control [368] were identified as putative binding partners. As OMM proteins are decorated with polyubiquitin chains during mitophagy for their recognition by selective autophagy receptors [369], these interactions favor a role of ABIN-1 in mitochondrial clearance via mitophagy by its ability to simultaneously bind LC3-positive phagophores and polyubiquitinated cargo. As with any screening approach, these bona fide interactors need to be validated by further experiments in cellular systems. Nevertheless, various putative functional links could be proposed by this analysis, linking ABIN-1 with the process of autophagy.

Next, we employed TMT-based proteomics to identify putative cargo proteins of ABIN-1 by utilizing primary murine macrophages from WT or ABIN1[D485N] mice. ABIN1[D485N] mice harbor a mutation in the UBAN domain of ABIN-1, rendering its ability to bind polyubiquitinated proteins [147]. Accordingly, these mice display an age dependent form of autoimmunity [147, 159]. In confirmation of ABIN-1´s inhibitory role on NF-κB and inflammation, protein levels of several inflammatory mediators were increased in ABIN1[D485N] mice such as NF-κB p100, PYCARD (also known as ASC) and ICAM1. Interestingly, M1- or K63-linked ubiquitination of ASC, activates the inflammasome [370, 371]. Moreover, K63-linked ubiquitination of ASC can lead to its autophagic degradation by the selective autophagy receptor p62 [372]. Due to the role of ABIN-1 in binding M1- or K63-linked ubiquitin chains and the high increase of ASC levels in ABIN1[D485N] mice it is possible that ABIN-1 mediates the selective degradation of

K63-decorated ASC. However, if i) increased ASC levels result from defective autophagic clearance by ABIN-1, ii) are a consequence from indirect effects due to the autoimmune phenotype from ABIN1[D485N] mice or iii) if ABIN-1 regulates the activation or proteasomal degradation of ASC in a similar fashion as NF-κB remains an open question to be addressed. Consistently with our interactome analysis, the abundance of proteins connected to autophagy and mitophagy were modulated in the proteome analysis of ABIN-1. Mutation of the UBAN domain of ABIN-1 resulted in the accumulation of the mitophagy-associated proteins MFN2 [232] and TBC1D17 [295] in macrophages derived from ABIN1[D485N] mice. Upon mitophagy induction, several OMM proteins such as MFN2 get ubiquitinated in a PINK1/Parkin-dependent manner, leading to their autophagic degradation [195, 373]. Thus, decreased MFN2 levels in ABIN1[D485N] macrophages could indicate reduced mitochondrial clearance in an ABIN-1-dependent manner. However, protein levels of other OMM proteins like VDAC1, COXII were nearly unchanged (data not shown). Notably, macrophages were analyzed under basal conditions without the presence of autophagy inhibitors or inducers. As autophagy receptors play redundant roles [169], direct effects of mutating the polyubiquitin binding domain of ABIN-1 under basal conditions may be negligible. Additional experiments utilizing autophagy/mitophagy inducers and methods such as proximity labeling combined with quantitative proteomics of autophagosomes [374] could shed more light on cargo proteins which are selectively degraded by ABIN-1. Interestingly, the protein expression of WDR45b (WIPI3) was decreased in ABIN1[D485N] mice. While the function of WIPI3 in autophagy remained relatively unknown [375], recent data indicate that WIPI3 is required for the formation of functional autophagosomes [296]. Accordingly, decreased WIPI3 levels could indicate lower autophagy levels due to incomplete autophagosome formation. While p62 is known to co-localize with WIPI3 at autophagosomes [296], the direct influence of p62 and as well ABIN-1 on WIPI3 is still unresolved.

6.2.2   ABIN-1 binds LC3 proteins via two conserved LIR motifs

In selective autophagy, ATG8 proteins recruit cargo proteins to the inner site of the phagophore membrane by interacting with autophagy receptors and adaptors [376]. Autophagy receptors harbor a LC3-interacting region (LIR) which mediates the binding to ATG8 proteins [169, 362]. The canonical LIR sequence consists out of the motif $[W/F/Y]_0\text{-}X_1\text{-}X_2\text{-}[L/V/I]_3$ in which positions 0 and 3 are absolutely conserved [169]. Analysis of the amino acid sequence of human ABIN-1 revealed two undescribed LIR motifs FDPL and FEVV which were conserved in mice with small alterations (FDDL and FEVV). N-terminal to the core LIR at position X_{-1} to X_{-3} the acidic residues Asp (D), Glu (E), Ser (S) or Thr (T) are often found as potential phosphorylation sites, greatly enhancing the binding to ATG8 proteins or activating the receptor itself. For example, phosphorylation of optineurin at S177 at its LIR motif by TBK1 is essential in order to function

in xenophagy [220] or mitophagy [221]. Similarly, phosphorylation of LIR motifs of the membrane bound receptors NIX, BNIP3 and FUNDC1 enhances their binding to LC3 [377, 378]. The LIR motifs of ABIN-1 both contain N-terminal phosphorylation sites, implying the same mechanism of activation. The presence of two LIR motifs in ABIN-1 can result from the need of multivalency in binding ATG8 proteins to exclude other components from being engulfed by the phagophore membrane. In line with this, NDP52, TAX1BP1 and NBR1 all harbor multiple LIR motifs which may be involved in multivalent ATG8 protein interaction. Autophagy receptors with only one LIR domain typically form polymers to bind multiple ATG8 proteins at once [169, 215]. By using a cellular expression system, we validated the result from our ABIN-1 interactome analysis that ABIN-1 binds to LC3B by Co-IP. Furthermore, we show that binding of ABIN-1 to LC3B is indeed dependent on its LIR domains, since single point mutations in the LIR motifs abrogated complex formation of ABIN-1 to LC3B. Moreover, by utilizing bacterial purified proteins we were able to show direct binding of ABIN-1 to the ATG8 proteins LC3A and LC3B in a LIR-dependent manner, whereas these mutants were still able to bind to linear ubiquitin chains as expected. Autophagy receptors need to bind lipidated ATG8 proteins at the inner phagophore membrane in order to specifically transfer their cargo into growing autophagosomes [379]. Interestingly, ABIN-1 shows preferential binding to the lipidated membrane-bound form of LC3 (LC3-II) and less binding to cytoplasmatic LC3-I. Accordingly, we show that under basal conditions, ABIN-1 is localized to the cytoplasm, whereas under autophagy induction and concurrent blockage of lysosomal fusion, ABIN-1 clusters with LC3B-positive autophagosomes. At the same time, upon triggering autophagy, ABIN-1 co-localizes with LAMP-1-positive lysosomes. These data support the concept that ABIN-1 may mediate specific targeting of cargo during selective autophagy by directly interacting with LC3-positive autophagosomes and LAMP-1-positive autophagolysosomes.

6.2.3 ABIN-1 protein levels are modulated by autophagic stimuli

Selective autophagy receptors are getting degraded through the autophagic pathway [169]. For instance, under basal conditions p62 protein levels remain constant. In contrast, autophagy induction increases the degradation of p62, whereas decreased autophagy or autophagy blockage leads to an increase in p62 levels [364, 380]. Optineurin is a particular case. Under basal conditions, optineurin is degraded mainly by the proteasome, while after phosphorylation and activation at its LIR motif, optineurin is degraded by autophagy [220]. All other selective autophagy receptors are degraded independently of cargo-binding even under basal conditions [169]. Consistently, our data shows that ABIN-1, similarly to p62, accumulates upon blockage of autophagy and that ABIN-1 and p62 protein levels undergo true autophagic flux. Surprisingly, p62 and as well ABIN-1 levels did not decrease upon autophagy induction. It is conceivable that ABIN-1 and p62 levels did not decrease due to transcriptional regulation. In

line with this, p62 levels are reported to increase in some cell lines because of *de novo* synthesis, even though autophagy is induced [381]. Therefore, newly synthesized ABIN-1 and p62 exceeds the amount which is degraded by autophagy. Recent data indicates that all selective autophagy receptors except optineurin are quickly degraded by an endosomal microautophagy pathway in reaction to starvation [382]. Importantly, the authors show that ABIN-1 is degraded upon EBSS-mediated starvation in A549 adenocarcinomic epithelial cells and BJ fibroblasts [382]. Therefore, it is conceivable that ABIN-1 degradation may be cell type dependent. Furthermore, from our data it cannot be excluded that ABIN-1 represents an autophagy adaptor protein. Autophagy adaptors are LIR-containing proteins which are not degraded by autophagy. For instance, BRUCE [383], PLEKHM1 [384] or FYCO1 [385] provide scaffold functions and regulate autophagosomal transport or lysosomal fusion. Therefore, specific autophagosomal cargos of ABIN-1 need to be identified in order to verify ABIN-1 as a selective autophagy receptor.

6.2.4 ABIN-1 is involved in the selective elimination of damaged mitochondria by mitophagy

Elimination of damaged mitochondria by mitophagy can either take place in a ubiquitin-dependent or -independent mechanism [369, 386]. In the ubiquitin-dependent pathway, PINK1 recruits Parkin to damaged mitochondria to amplify the conjugation ubiquitin chains onto OMM proteins such as VDAC1, TOM20, COXII or MFN2 [368]. Coating of mitochondria with polyubiquitin chains triggers the recruitment of selective autophagy receptors, thereby enabling clearance through the autophagy machinery [387]. Accordingly, we show that ABIN-1, similar to p62 and Parkin is recruited to depolarized mitochondria in response to OA treatment. Next, by using CRISPR/Cas9-mediated deletion of ABIN-1 we show that the degradation of OMM proteins is decreased in ABIN-1 deficient cells at various time points. Similarly, by employing the fluorescence-based mitophagy reporter mt-mKEIMA, we demonstrate that knockdown of ABIN-1 significantly lowers overall mitophagy levels after OA treatment. However, knockdown of ABIN-1 only slightly decreased mitophagic activity. At the same time, knockdown of ABIN-1 did not decrease the number of autophagolysosomes in response to autophagy induction by starvation or Torin-1 treatment. These data imply that other receptors compensate for the loss of ABIN-1. Indeed, efficient binding of cargo material to the forming phagophore membrane is thought to depend on multiple receptor and ATG8 interactions [215, 388]. Selective autophagy receptors rely on ubiquitin in binding their respective cargo. For instance, optineurin and NDP52 bind damaged mitochondria via their ubiquitin binding domains to mediate their degradation by mitophagy [220, 221, 251]. Because all soluble selective autophagy receptors bind ubiquitin, they are likely to be recruited to the same cargo, thereby fulfilling either unique or redundant roles [169]. In accordance, even though the selective autophagy receptors p62,

NBR1, optineurin, NDP52, TAX1BP1 and TOLLIP are recruited to damaged mitochondria, only optineurin and NDP52 are the main receptors for Parkin-mediated mitophagy [251]. Especially p62 and NBR1 seem to be dispensable for mitochondrial clearance by mitophagy [251]. Surprisingly, NDP52 or optineurin deletion alone did not cause a defect in mitophagy, while NDP52/optineurin double KO cells and even more prominently NDP52/optineurin/TAX1BP1 triple KO cells highly decreased mitophagy [251]. Up to now, it is unknown if and how selective autophagy receptors act in concert to regulate mitophagy. To efficiently determine the role of ABIN-1 in mitophagy, experiments utilizing NDP52/optineurin double KO cells with WT or LIR/UBAN-defective ABIN-1 need to be performed to exclude compensatory effects by the main mitophagy receptors optineurin and NDP52. Interestingly, a recent study identifies the matrix proteins 4-Nitrophenylphosphatase domain and non-neuronal SNAP25-like protein homolog 1 (NIPSNAP1) and NIPSNAP2 proteins as signaling hubs and recruiters of ubiquitin-dependent selective autophagy receptors (p62, NBR1, NDP52 and TAX1BP1) and ATG8 proteins on damaged mitochondria during Parkin-dependent mitophagy [389]. This could explain the redundancy of autophagy receptors in being recruited to damaged mitochondria [206]. Nevertheless, the discovery that ABIN-1 is involved in selective autophagy opens new point of views on established functions of ABIN-1 in immunity. For instance, as ABIN-1 is involved in regulating M1 macrophages polarization [390] and mounting evidence implicates selective autophagy in macrophage polarization [391-393], it is possible that ABIN-1 regulates macrophage polarization by mediating the selective degradation of macrophage polarization factors. While most of the experiments were performed under artificial conditions utilizing immortal HeLa cells with stable overexpression of Parkin, these data favor a role of ABIN-1 as a selective autophagy receptor but cannot exclude that ABIN-1 only serves as an adaptor protein during selective autophagy. Future studies using primary cells such as macrophages or LIR-defective ABIN-1 mice could be useful tools to clarify the role of ABIN-1 in selective autophagy.

In conclusion, the second part of this study identified various new interactions partners of ABIN-1 by mass spectrometry which implicate ABIN-1 in the process of selective autophagy. We discovered two undescribed LIR motifs of ABIN-1 and showed that ABIN-1 binds LC3B and LC3A directly in a LIR-dependent manner. Moreover, ABIN-1 co-localizes with LC3B-positive autophagosomes and LAMP-1-containing autophagolysosomes in response to autophagy induction. Consistently, ABIN-1 protein levels are increased in response to pharmacological inhibition of autophagy. Secondly, this work shows that ABIN-1 translocates to damaged mitochondria during Parkin-dependent mitophagy. Importantly, ablation of ABIN-1 decreases the degradation of the mitochondrial outer membrane proteins MFN2, TOM20, VDAC1 and COXII. At last this study shows that a lack of ABIN-1 slows the selective degradation of mitochondria by mitophagy.

7 References

[1] R.V. Iozzo, L. Schaefer, Proteoglycan form and function: A comprehensive nomenclature of proteoglycans, Matrix Biol 42 (2015) 11-55.

[2] V.H. Pomin, B. Mulloy, Glycosaminoglycans and Proteoglycans, Pharmaceuticals (Basel) 11(1) (2018).

[3] E. Listik, J. Azevedo Marques Gaschler, M. Matias, M.F. Neuppmann Feres, L. Toma, A.C. Raphaelli Nahas-Scocate, Proteoglycans and dental biology: the first review, Carbohydr Polym 225 (2019) 115199.

[4] S.O. Kolset, G. Pejler, Serglycin: a structural and functional chameleon with wide impact on immune cells, Journal of immunology 187(10) (2011) 4927-33.

[5] J. Douaiher, J. Succar, L. Lancerotto, M.F. Gurish, D.P. Orgill, M.J. Hamilton, S.A. Krilis, R.L. Stevens, Development of mast cells and importance of their tryptase and chymase serine proteases in inflammation and wound healing, Adv Immunol 122 (2014) 211-52.

[6] L. Schaefer, R.M. Schaefer, Proteoglycans: from structural compounds to signaling molecules, Cell Tissue Res 339(1) (2010) 237-46.

[7] M.A. Gubbiotti, T. Neill, R.V. Iozzo, A current view of perlecan in physiology and pathology: A mosaic of functions, Matrix Biol 57-58 (2017) 285-298.

[8] S. Kalamajski, A. Oldberg, The role of small leucine-rich proteoglycans in collagen fibrillogenesis, Matrix Biol 29(4) (2010) 248-53.

[9] L. Ameye, M.F. Young, Mice deficient in small leucine-rich proteoglycans: novel in vivo models for osteoporosis, osteoarthritis, Ehlers-Danlos syndrome, muscular dystrophy, and corneal diseases, Glycobiology 12(9) (2002) 107R-16R.

[10] A.D. Theocharis, S.S. Skandalis, C. Gialeli, N.K. Karamanos, Extracellular matrix structure, Adv Drug Deliv Rev 97 (2016) 4-27.

[11] M.V. Nastase, A. Janicova, H. Roedig, L.T. Hsieh, M. Wygrecka, L. Schaefer, Small Leucine-Rich Proteoglycans in Renal Inflammation: Two Sides of the Coin, The journal of histochemistry and cytochemistry : official journal of the Histochemistry Society 66(4) (2018) 261-272.

[12] H. Roedig, M.V. Nastase, M. Wygrecka, L. Schaefer, Breaking down chronic inflammatory diseases: the role of biglycan in promoting a switch between inflammation and autophagy, FEBS J (2019).

[13] R. Merline, R.M. Schaefer, L. Schaefer, The matricellular functions of small leucine-rich proteoglycans (SLRPs), J Cell Commun Signal 3(3-4) (2009) 323-35.

[14] H. Roedig, R. Damiescu, J. Zeng-Brouwers, I. Kutija, J. Trebicka, M. Wygrecka, L. Schaefer, Danger matrix molecules orchestrate CD14/CD44 signaling in cancer development, Semin Cancer Biol (2019).

[15] I. Matsuo, C. Kimura-Yoshida, Extracellular distribution of diffusible growth factors controlled by heparan sulfate proteoglycans during mammalian embryogenesis, Philos Trans R Soc Lond B Biol Sci 369(1657) (2014).

[16] H. Frey, N. Schroeder, T. Manon-Jensen, R.V. Iozzo, L. Schaefer, Biological interplay between proteoglycans and their innate immune receptors in inflammation, FEBS J 280(10) (2013) 2165-79.

[17] M.V. Nastase, M.F. Young, L. Schaefer, Biglycan: a multivalent proteoglycan providing structure and signals, The journal of histochemistry and cytochemistry : official journal of the Histochemistry Society 60(12) (2012) 963-75.

[18] K. Moreth, R.V. Iozzo, L. Schaefer, Small leucine-rich proteoglycans orchestrate receptor crosstalk during inflammation, Cell cycle 11(11) (2012) 2084-91.

[19] P.J. Roughley, R.J. White, Dermatan sulphate proteoglycans of human articular cartilage. The properties of dermatan sulphate proteoglycans I and II, The Biochemical journal 262(3) (1989) 823-7.

[20] H.U. Choi, T.L. Johnson, S. Pal, L.H. Tang, L. Rosenberg, P.J. Neame, Characterization of the dermatan sulfate proteoglycans, DS-PGI and DS-PGII, from bovine articular cartilage and skin isolated by octyl-sepharose chromatography, J Biol Chem 264(5) (1989) 2876-84.

[21] L. Schaefer, R.V. Iozzo, Biological functions of the small leucine-rich proteoglycans: from genetics to signal transduction, J Biol Chem 283(31) (2008) 21305-9.

[22] E. Schonherr, P. Witsch-Prehm, B. Harrach, H. Robenek, J. Rauterberg, H. Kresse, Interaction of biglycan with type I collagen, J Biol Chem 270(6) (1995) 2776-83.

[23] C. Wiberg, E. Hedbom, A. Khairullina, S.R. Lamande, A. Oldberg, R. Timpl, M. Morgelin, D. Heinegard, Biglycan and decorin bind close to the n-terminal region of the collagen VI triple helix, J Biol Chem 276(22) (2001) 18947-52.

[24] C. Wiberg, D. Heinegard, C. Wenglen, R. Timpl, M. Morgelin, Biglycan organizes collagen VI into hexagonal-like networks resembling tissue structures, J Biol Chem 277(51) (2002) 49120-6.

[25] C. Wiberg, A.R. Klatt, R. Wagener, M. Paulsson, J.F. Bateman, D. Heinegard, M. Morgelin, Complexes of matrilin-1 and biglycan or decorin connect collagen VI microfibrils to both collagen II and aggrecan, J Biol Chem 278(39) (2003) 37698-704.

[26] T. Douglas, S. Heinemann, S. Bierbaum, D. Scharnweber, H. Worch, Fibrillogenesis of collagen types I, II, and III with small leucine-rich proteoglycans decorin and biglycan, Biomacromolecules 7(8) (2006) 2388-93.

[27] B. Reinboth, E. Hanssen, E.G. Cleary, M.A. Gibson, Molecular interactions of biglycan and decorin with elastic fiber components: biglycan forms a ternary complex with tropoelastin and microfibril-associated glycoprotein 1, J Biol Chem 277(6) (2002) 3950-7.

[28] T. Xu, P. Bianco, L.W. Fisher, G. Longenecker, E. Smith, S. Goldstein, J. Bonadio, A. Boskey, A.M. Heegaard, B. Sommer, K. Satomura, P. Dominguez, C. Zhao, A.B. Kulkarni, P.G. Robey, M.F. Young, Targeted disruption of the biglycan gene leads to an osteoporosis-like phenotype in mice, Nat Genet 20(1) (1998) 78-82.

[29] A. Corsi, T. Xu, X.D. Chen, A. Boyde, J. Liang, M. Mankani, B. Sommer, R.V. Iozzo, I. Eichstetter, P.G. Robey, P. Bianco, M.F. Young, Phenotypic effects of biglycan deficiency are linked to collagen fibril abnormalities, are synergized by decorin deficiency, and mimic Ehlers-Danlos-like changes in bone and other connective tissues, J Bone Miner Res 17(7) (2002) 1180-9.

[30] P. Bianco, L.W. Fisher, M.F. Young, J.D. Termine, P.G. Robey, Expression and localization of the two small proteoglycans biglycan and decorin in developing human skeletal and non-skeletal tissues, The journal of histochemistry and cytochemistry : official journal of the Histochemistry Society 38(11) (1990) 1549-63.

[31] L. Schaefer, A. Babelova, E. Kiss, H.J. Hausser, M. Baliova, M. Krzyzankova, G. Marsche, M.F. Young, D. Mihalik, M. Gotte, E. Malle, R.M. Schaefer, H.J. Grone, The matrix component biglycan is proinflammatory and signals through Toll-like receptors 4 and 2 in macrophages, The Journal of clinical investigation 115(8) (2005) 2223-33.

[32] T. Hara, E. Yoshida, Y. Shinkai, C. Yamamoto, Y. Fujiwara, Y. Kumagai, T. Kaji, Biglycan Intensifies ALK5-Smad2/3 Signaling by TGF-beta1 and Downregulates Syndecan-4 in Cultured Vascular Endothelial Cells, J Cell Biochem 118(5) (2017) 1087-1096.

[33] A. Hildebrand, M. Romaris, L.M. Rasmussen, D. Heinegard, D.R. Twardzik, W.A. Border, E. Ruoslahti, Interaction of the small interstitial proteoglycans biglycan, decorin and fibromodulin with transforming growth factor beta, The Biochemical journal 302 (Pt 2) (1994) 527-34.

[34] A.D. Berendsen, E.L. Pinnow, A. Maeda, A.C. Brown, N. McCartney-Francis, V. Kram, R.T. Owens, P.G. Robey, K. Holmbeck, L.F. de Castro, T.M. Kilts, M.F. Young, Biglycan modulates angiogenesis and bone formation during fracture healing, Matrix Biol 35 (2014) 223-31.

[35] X.D. Chen, L.W. Fisher, P.G. Robey, M.F. Young, The small leucine-rich proteoglycan biglycan modulates BMP-4-induced osteoblast differentiation, FASEB journal : official publication of the Federation of American Societies for Experimental Biology 18(9) (2004) 948-58.

[36] Y. Mochida, D. Parisuthiman, M. Yamauchi, Biglycan is a positive modulator of BMP-2 induced osteoblast differentiation, Adv Exp Med Biol 585 (2006) 101-13.

[37] M. Moreno, R. Munoz, F. Aroca, M. Labarca, E. Brandan, J. Larrain, Biglycan is a new extracellular component of the Chordin-BMP4 signaling pathway, EMBO J 24(7) (2005) 1397-405.

[38] P. Jongwattanapisan, M. Terajima, P.A. Miguez, W. Querido, H. Nagaoka, N. Sumida, E.G. Gurysh, K.M. Ainslie, N. Pleshko, L. Perera, M. Yamauchi, Identification of the effector domain of biglycan that facilitates BMP-2 osteogenic function, Scientific reports 8(1) (2018) 7022.

[39] L. Desnoyers, D. Arnott, D. Pennica, WISP-1 binds to decorin and biglycan, J Biol Chem 276(50) (2001) 47599-607.

[40] A.D. Berendsen, L.W. Fisher, T.M. Kilts, R.T. Owens, P.G. Robey, J.S. Gutkind, M.F. Young, Modulation of canonical Wnt signaling by the extracellular matrix component biglycan, Proceedings of the National Academy of Sciences of the United States of America 108(41) (2011) 17022-7.

[41] J. Santiago-Garcia, T. Kodama, R.E. Pitas, The class A scavenger receptor binds to proteoglycans and mediates adhesion of macrophages to the extracellular matrix, J Biol Chem 278(9) (2003) 6942-6.

[42] Y. Bi, C.H. Stuelten, T. Kilts, S. Wadhwa, R.V. Iozzo, P.G. Robey, X.D. Chen, M.F. Young, Extracellular matrix proteoglycans control the fate of bone marrow stromal cells, J Biol Chem 280(34) (2005) 30481-9.

[43] R. Fadic, V. Mezzano, K. Alvarez, D. Cabrera, J. Holmgren, E. Brandan, Increase in decorin and biglycan in Duchenne Muscular Dystrophy: role of fibroblasts as cell source of these proteoglycans in the disease, J Cell Mol Med 10(3) (2006) 758-69.

[44] J.R. Fallon, E.M. McNally, Non-Glycanated Biglycan and LTBP4: Leveraging the extracellular matrix for Duchenne Muscular Dystrophy therapeutics, Matrix Biol 68-69 (2018) 616-627.

[45] A.R. Amenta, H.E. Creely, M.L. Mercado, H. Hagiwara, B.A. McKechnie, B.E. Lechner, S.G. Rossi, Q. Wang, R.T. Owens, E. Marrero, L. Mei, W. Hoch, M.F. Young, D.J. McQuillan, R.L. Rotundo, J.R. Fallon, Biglycan is an extracellular MuSK binding protein important for synapse stability, J Neurosci 32(7) (2012) 2324-34.

[46] M. Myren, D.J. Kirby, M.L. Noonan, A. Maeda, R.T. Owens, S. Ricard-Blum, V. Kram, T.M. Kilts, M.F. Young, Biglycan potentially regulates angiogenesis during fracture repair by altering expression and function of endostatin, Matrix Biol 52-54 (2016) 141-150.

[47] X. Xing, X. Gu, T. Ma, H. Ye, Biglycan up-regulated vascular endothelial growth factor (VEGF) expression and promoted angiogenesis in colon cancer, Tumour Biol 36(3) (2015) 1773-80.

[48] J. Aggelidakis, A. Berdiaki, D. Nikitovic, A. Papoutsidakis, D.J. Papachristou, A.M. Tsatsakis, G.N. Tzanakakis, Biglycan Regulates MG63 Osteosarcoma Cell Growth Through a LPR6/beta-Catenin/IGFR-IR Signaling Axis, Front Oncol 8 (2018) 470.

[49] C.K. Weber, G. Sommer, P. Michl, H. Fensterer, M. Weimer, F. Gansauge, G. Leder, G. Adler, T.M. Gress, Biglycan is overexpressed in pancreatic cancer and induces G1-arrest in pancreatic cancer cell lines, Gastroenterology 121(3) (2001) 657-67.

[50] L. Schaefer, C. Tredup, M.A. Gubbiotti, R.V. Iozzo, Proteoglycan neofunctions: regulation of inflammation and autophagy in cancer biology, FEBS J 284(1) (2017) 10-26.

[51] C. Poluzzi, M.V. Nastase, J. Zeng-Brouwers, H. Roedig, L.T. Hsieh, J.B. Michaelis, E.M. Buhl, F. Rezende, Y. Manavski, A. Bleich, P. Boor, R.P. Brandes, J. Pfeilschifter, E.H.K. Stelzer, C. Munch, I. Dikic, C. Brandts, R.V. Iozzo, M. Wygrecka, L. Schaefer, Biglycan evokes autophagy in macrophages via a novel CD44/Toll-like receptor 4 signaling axis in ischemia/reperfusion injury, Kidney Int 95(3) (2019) 540-562.

[52] L.T. Hsieh, M.V. Nastase, J. Zeng-Brouwers, R.V. Iozzo, L. Schaefer, Soluble biglycan as a biomarker of inflammatory renal diseases, The international journal of biochemistry & cell biology 54 (2014) 223-35.

[53] K. Moreth, R. Brodbeck, A. Babelova, N. Gretz, T. Spieker, J. Zeng-Brouwers, J. Pfeilschifter, M.F. Young, R.M. Schaefer, L. Schaefer, The proteoglycan biglycan regulates expression of the B cell chemoattractant CXCL13 and aggravates murine lupus nephritis, The Journal of clinical investigation 120(12) (2010) 4251-72.

[54] L. Schaefer, I. Raslik, H.J. Grone, E. Schonherr, K. Macakova, J. Ugorcakova, S. Budny, R.M. Schaefer, H. Kresse, Small proteoglycans in human diabetic nephropathy: discrepancy between glomerular expression and protein accumulation of decorin, biglycan, lumican, and fibromodulin, FASEB journal : official publication of the Federation of American Societies for Experimental Biology 15(3) (2001) 559-61.

[55] R. Ciftciler, S. Ozenirler, A.A. Yucel, M. Cengiz, G. Erkan, E. Buyukdemirci, C. Sonmez, G.Y. Esendagli, The importance of serum biglycan levels as a fibrosis marker in patients with chronic hepatitis B, J Clin Lab Anal 31(5) (2017) e22109.

[56] G. Barreto, A. Soininen, P. Ylinen, J. Sandelin, Y.T. Konttinen, D.C. Nordstrom, K.K. Eklund, Soluble biglycan: a potential mediator of cartilage degradation in osteoarthritis, Arthritis research & therapy 17 (2015) 379.

[57] S.Y. Ritter, J. Collins, B. Krastins, D. Sarracino, M. Lopez, E. Losina, A.O. Aliprantis, Mass spectrometry assays of plasma biomarkers to predict radiographic progression of knee osteoarthritis, Arthritis research & therapy 16(5) (2014) 456.

[58] T. Ueland, P. Aukrust, S.H. Nymo, J. Kjekshus, J.J. McMurray, J. Wikstrand, D. Block, C. Zaugg, L. Gullestad, Novel extracellular matrix biomarkers as predictors of adverse outcome in chronic heart failure: association between biglycan and response to statin therapy in the CORONA trial, Journal of cardiac failure 21(2) (2015) 153-9.

[59] C.R. Flannery, Usurped SLRPs: novel arthritis biomarkers exposed by catabolism of small leucine-rich proteoglycans?, Arthritis research & therapy 8(2) (2006) 106.

[60] J.H. Mortensen, T. Manon-Jensen, M.D. Jensen, P. Hagglund, L.G. Klinge, J. Kjeldsen, A. Krag, M.A. Karsdal, A.C. Bay-Jensen, Ulcerative colitis, Crohn's disease, and irritable bowel syndrome have different profiles of extracellular matrix turnover, which also reflects disease activity in Crohn's disease, PLoS One 12(10) (2017) e0185855.

[61] K. Moreth, H. Frey, M. Hubo, J. Zeng-Brouwers, M.V. Nastase, L.T. Hsieh, R. Haceni, J. Pfeilschifter, R.V. Iozzo, L. Schaefer, Biglycan-triggered TLR-2- and TLR-4-signaling exacerbates the pathophysiology of ischemic acute kidney injury, Matrix Biol 35 (2014) 143-51.

[62] M.V. Nastase, J. Zeng-Brouwers, J. Beckmann, C. Tredup, U. Christen, H.H. Radeke, M. Wygrecka, L. Schaefer, Biglycan, a novel trigger of Th1 and Th17 cell recruitment into the kidney, Matrix Biol 68-69 (2018) 293-317.

[63] A. Avenoso, A. D'Ascola, M. Scuruchi, G. Mandraffino, A. Calatroni, A. Saitta, S. Campo, G.M. Campo, The proteoglycan biglycan mediates inflammatory response by activating TLR-4 in human chondrocytes: Inhibition by specific siRNA and high polymerized Hyaluronan, Arch Biochem Biophys 640 (2018) 75-82.

[64] A. Babelova, K. Moreth, W. Tsalastra-Greul, J. Zeng-Brouwers, O. Eickelberg, M.F. Young, P. Bruckner, J. Pfeilschifter, R.M. Schaefer, H.J. Grone, L. Schaefer, Biglycan, a danger signal that activates the NLRP3 inflammasome via toll-like and P2X receptors, J Biol Chem 284(36) (2009) 24035-48.

[65] R. Song, Q. Zeng, L. Ao, J.A. Yu, J.C. Cleveland, K.S. Zhao, D.A. Fullerton, X. Meng, Biglycan induces the expression of osteogenic factors in human aortic valve interstitial cells via Toll-like receptor-2, Arterioscler Thromb Vasc Biol 32(11) (2012) 2711-20.

[66] J. Zeng-Brouwers, J. Beckmann, M.V. Nastase, R.V. Iozzo, L. Schaefer, De novo expression of circulating biglycan evokes an innate inflammatory tissue response via MyD88/TRIF pathways, Matrix Biol 35 (2014) 132-42.

[67] L.T. Hsieh, M.V. Nastase, H. Roedig, J. Zeng-Brouwers, C. Poluzzi, S. Schwalm, C. Fork, C. Tredup, R.P. Brandes, M. Wygrecka, A. Huwiler, J. Pfeilschifter, L. Schaefer, Biglycan- and Sphingosine Kinase-1 Signaling Crosstalk Regulates the Synthesis of Macrophage Chemoattractants, Int J Mol Sci 18(3) (2017).

[68] R. Merline, S. Lazaroski, A. Babelova, W. Tsalastra-Greul, J. Pfeilschifter, K.D. Schluter, A. Gunther, R.V. Iozzo, R.M. Schaefer, L. Schaefer, Decorin deficiency in diabetic mice: aggravation of nephropathy due to overexpression of profibrotic factors, enhanced apoptosis and mononuclear cell infiltration, Journal of physiology and pharmacology : an official journal of the Polish Physiological Society 60 Suppl 4 (2009) 5-13.

[69] Z.V. Popovic, S. Wang, M. Papatriantafyllou, Z. Kaya, S. Porubsky, M. Meisner, M. Bonrouhi, S. Burgdorf, M.F. Young, L. Schaefer, H.J. Grone, The proteoglycan biglycan

enhances antigen-specific T cell activation potentially via MyD88 and TRIF pathways and triggers autoimmune perimyocarditis, Journal of immunology 187(12) (2011) 6217-26.

[70] C. Garcia-Rodriguez, I. Parra-Izquierdo, I. Castanos-Mollor, J. Lopez, J.A. San Roman, M. Sanchez Crespo, Toll-Like Receptors, Inflammation, and Calcific Aortic Valve Disease, Frontiers in physiology 9 (2018) 201.

[71] M. Grandoch, C. Kohlmorgen, A. Melchior-Becker, K. Feldmann, S. Homann, J. Muller, L.S. Kiene, J. Zeng-Brouwers, F. Schmitz, N. Nagy, A. Polzin, N.S. Gowert, M. Elvers, P. Skroblin, X. Yin, M. Mayr, L. Schaefer, L.R. Tannock, J.W. Fischer, Loss of Biglycan Enhances Thrombin Generation in Apolipoprotein E-Deficient Mice: Implications for Inflammation and Atherosclerosis, Arterioscler Thromb Vasc Biol 36(5) (2016) e41-50.

[72] A. Marzoll, A. Melchior-Becker, F. Cipollone, J.W. Fischer, Small leucine-rich proteoglycans in atherosclerotic lesions: novel targets of chronic statin treatment?, J Cell Mol Med 15(2) (2011) 232-43.

[73] J.C. Leemans, L.M. Butter, W.P. Pulskens, G.J. Teske, N. Claessen, T. van der Poll, S. Florquin, The role of Toll-like receptor 2 in inflammation and fibrosis during progressive renal injury, PLoS One 4(5) (2009) e5704.

[74] L.T. Hsieh, H. Frey, M.V. Nastase, C. Tredup, A. Hoffmann, C. Poluzzi, J. Zeng-Brouwers, T. Manon-Jensen, K. Schroder, R.P. Brandes, R.V. Iozzo, L. Schaefer, Bimodal role of NADPH oxidases in the regulation of biglycan-triggered IL-1beta synthesis, Matrix Biol 49 (2016) 61-81.

[75] H. Frey, K. Moreth, L.T. Hsieh, J. Zeng-Brouwers, B. Rathkolb, H. Fuchs, V. Gailus-Durner, R.V. Iozzo, M.H. de Angelis, L. Schaefer, A novel biological function of soluble biglycan: Induction of erythropoietin production and polycythemia, Glycoconj J 34(3) (2017) 393-404.

[76] C. Hashimoto, K.L. Hudson, K.V. Anderson, The Toll gene of Drosophila, required for dorsal-ventral embryonic polarity, appears to encode a transmembrane protein, Cell 52(2) (1988) 269-79.

[77] K. Vijay, Toll-like receptors in immunity and inflammatory diseases: Past, present, and future, Int Immunopharmacol 59 (2018) 391-412.

[78] M.K. Vidya, V.G. Kumar, V. Sejian, M. Bagath, G. Krishnan, R. Bhatta, Toll-like receptors: Significance, ligands, signaling pathways, and functions in mammals, Int Rev Immunol 37(1) (2018) 20-36.

[79] S.A. Wasserman, Toll signaling: the enigma variations, Curr Opin Genet Dev 10(5) (2000) 497-502.

[80] N.J. Gay, M.F. Symmons, M. Gangloff, C.E. Bryant, Assembly and localization of Toll-like receptor signalling complexes, Nat Rev Immunol 14(8) (2014) 546-58.

[81] T. Areschoug, S. Gordon, Pattern recognition receptors and their role in innate immunity: focus on microbial protein ligands, Contrib Microbiol 15 (2008) 45-60.

[82] I. Vasileiou, G. Kostopanagiotou, A. Katsargyris, C. Klonaris, D. Perrea, S. Theocharis, Toll-like receptors: a novel target for therapeutic intervention in intestinal and hepatic ischemia-reperfusion injury?, Expert Opin Ther Targets 14(8) (2010) 839-53.

[83] L. Oliveira-Nascimento, P. Massari, L.M. Wetzler, The Role of TLR2 in Infection and Immunity, Frontiers in immunology 3 (2012) 79.

[84] Y. Guan, D.R. Ranoa, S. Jiang, S.K. Mutha, X. Li, J. Baudry, R.I. Tapping, Human TLRs 10 and 1 share common mechanisms of innate immune sensing but not signaling, Journal of immunology 184(9) (2010) 5094-103.

[85] T. Kawai, S. Akira, The role of pattern-recognition receptors in innate immunity: update on Toll-like receptors, Nat Immunol 11(5) (2010) 373-84.

[86] J. van Bergenhenegouwen, T.S. Plantinga, L.A. Joosten, M.G. Netea, G. Folkerts, A.D. Kraneveld, J. Garssen, A.P. Vos, TLR2 & Co: a critical analysis of the complex interactions between TLR2 and coreceptors, J Leukoc Biol 94(5) (2013) 885-902.

[87] A. Asea, M. Rehli, E. Kabingu, J.A. Boch, O. Bare, P.E. Auron, M.A. Stevenson, S.K. Calderwood, Novel signal transduction pathway utilized by extracellular HSP70: role of toll-like receptor (TLR) 2 and TLR4, J Biol Chem 277(17) (2002) 15028-34.

[88] W. Wang, G.L. Xu, W.D. Jia, J.L. Ma, J.S. Li, Y.S. Ge, W.H. Ren, J.H. Yu, W.B. Liu, Ligation of TLR2 by versican: a link between inflammation and metastasis, Arch Med Res 40(4) (2009) 321-3.

[89] R. Merline, K. Moreth, J. Beckmann, M.V. Nastase, J. Zeng-Brouwers, J.G. Tralhao, P. Lemarchand, J. Pfeilschifter, R.M. Schaefer, R.V. Iozzo, L. Schaefer, Signaling by the matrix proteoglycan decorin controls inflammation and cancer through PDCD4 and MicroRNA-21, Sci Signal 4(199) (2011) ra75.

[90] G. Schmitz, E. Orso, CD14 signalling in lipid rafts: new ligands and co-receptors, Curr Opin Lipidol 13(5) (2002) 513-521.

[91] M. Triantafilou, F.G.J. Gamper, R.M. Haston, M.A. Mouratis, S. Morath, T. Hartung, K. Triantafilou, Membrane sorting of toll-like receptor (TLR)-2/6 and TLR2/1 heterodimers at the cell surface determines heterotypic associations with CD36 and intracellular targeting, Journal of Biological Chemistry 281(41) (2006) 31002-31011.

[92] B.N. Gantner, R.M. Simmons, S.J. Canavera, S. Akira, D.M. Underhill, Collaborative induction of inflammatory responses by dectin-1 and toll-like receptor 2, Journal of Experimental Medicine 197(9) (2003) 1107-1117.

[93] G. Gerold, K. Abu Ajaj, M. Bienert, H.J. Laws, A. Zychlinsky, J.L. de Diego, A Toll-like receptor 2-integrin beta(3) complex senses bacterial lipopeptides via vitronectin, Nature Immunology 9(7) (2008) 761-768.

[94] T. Nakata, M. Yasuda, M. Fujita, H. Kataoka, K. Kiura, H. Sano, K. Shibata, CD14 directly binds to triacylated lipopeptides and facilitates recognition of the lipopeptides by the receptor complex of Toll-like receptors 2 and 1 without binding to the complex, Cell Microbiol 8(12) (2006) 1899-909.

[95] C.C. Lee, A.M. Avalos, H.L. Ploegh, Accessory molecules for Toll-like receptors and their function, Nature Reviews Immunology 12(3) (2012) 168-179.

[96] M.E. Ariza, R. Glaser, P.T. Kaumaya, C. Jones, M.V. Williams, The EBV-encoded dUTPase activates NF-kappa B through the TLR2 and MyD88-dependent signaling pathway, Journal of immunology 182(2) (2009) 851-9.

[97] F. Debierre-Grockiego, S. Niehus, B. Coddeville, E. Elass, F. Poirier, R. Weingart, R.R. Schmidt, J. Mazurier, Y. Guerardel, R.T. Schwarz, Binding of Toxoplasma gondii glycosylphosphatidylinositols to galectin-3 is required for their recognition by macrophages, J Biol Chem 285(43) (2010) 32744-50.

[98] S.T. Qureshi, L. Lariviere, G. Leveque, S. Clermont, K.J. Moore, P. Gros, D. Malo, Endotoxin-tolerant mice have mutations in toll-like receptor 4 (Tlr4), Journal of Experimental Medicine 189(4) (1999) 615-625.

[99] C. Termeer, F. Benedix, J. Sleeman, C. Fieber, U. Voith, T. Ahrens, K. Miyake, M. Freudenberg, C. Galanos, J.C. Simon, Oligosaccharides of Hyaluronan activate dendritic cells via toll-like receptor 4, The Journal of experimental medicine 195(1) (2002) 99-111.

[100] S.P. Gondokaryono, H. Ushio, F. Niyonsaba, M. Hara, H. Takenaka, S.T.M. Jayawardana, S. Ikeda, K. Okumura, H. Ogawa, The extra domain A of fibronectin stimulates murine mast cells via Toll-like receptor 4, J Leukocyte Biol 82(3) (2007) 657-665.

[101] M.T. Lotze, K.J. Tracey, High-mobility group box 1 protein (HMGB): Nuclear weapon in the immune arsenal, Nature Reviews Immunology 5(4) (2005) 331-342.

[102] L.A. O'Neill, A.G. Bowie, The family of five: TIR-domain-containing adaptors in Toll-like receptor signalling, Nat Rev Immunol 7(5) (2007) 353-64.

[103] K.R. Taylor, K. Yamasaki, K.A. Radek, A. Di Nardo, H. Goodarzi, D. Golenbock, B. Beutler, R.L. Gallo, Recognition of hyaluronan released in sterile injury involves a unique receptor complex dependent on Toll-like receptor 4, CD44, and MD-2, J Biol Chem 282(25) (2007) 18265-75.

[104] S. Uematsu, S. Akira, Toll-like receptors and innate immunity, Journal of molecular medicine 84(9) (2006) 712-25.

[105] S. Manicassamy, B. Pulendran, Modulation of adaptive immunity with Toll-like receptors, Semin Immunol 21(4) (2009) 185-93.

[106] L. Chovanova, M. Vlcek, K. Krskova, A. Penesova, Z. Radikova, J. Rovensky, D. Cholujova, J. Sedlak, R. Imrich, Increased production of IL-6 and IL-17 in lipopolysaccharide-

stimulated peripheral mononuclears from patients with rheumatoid arthritis, Gen Physiol Biophys 32(3) (2013) 395-404.

[107] J.T. Tsao, S.C. Hsieh, B.L. Chiang, C.L. Yu, S.C. Lin, Altered IL-10 and TNF-alpha production in peripheral blood mononuclear cells of systemic lupus erythematosus patients after Toll-like receptor 2, 4, or 9 activation, Clin Exp Med 12(3) (2012) 153-8.

[108] M. Li, L. Song, X. Gao, W. Chang, X. Qin, Toll-like receptor 4 on islet beta cells senses expression changes in high-mobility group box 1 and contributes to the initiation of type 1 diabetes, Exp Mol Med 44(4) (2012) 260-7.

[109] J.A. Sloane, C. Batt, Y. Ma, Z.M. Harris, B. Trapp, T. Vartanian, Hyaluronan blocks oligodendrocyte progenitor maturation and remyelination through TLR2, Proceedings of the National Academy of Sciences of the United States of America 107(25) (2010) 11555-60.

[110] Y. Liu, H. Yin, M. Zhao, Q. Lu, TLR2 and TLR4 in autoimmune diseases: a comprehensive review, Clin Rev Allergy Immunol 47(2) (2014) 136-47.

[111] A. Gluba, M. Banach, S. Hannam, D.P. Mikhailidis, A. Sakowicz, J. Rysz, The role of Toll-like receptors in renal diseases, Nature reviews. Nephrology 6(4) (2010) 224-35.

[112] C.L. Lakshmikanth, S.P. Jacob, V.H. Chaithra, H.C. de Castro-Faria-Neto, G.K. Marathe, Sepsis: in search of cure, Inflammation research : official journal of the European Histamine Research Society ... [et al.] 65(8) (2016) 587-602.

[113] A.M. Philp, E.T. Davis, S.W. Jones, Developing anti-inflammatory therapeutics for patients with osteoarthritis, Rheumatology 56(6) (2017) 869-881.

[114] H. Zhao, J.S. Perez, K. Lu, A.J. George, D. Ma, Role of Toll-like receptor-4 in renal graft ischemia-reperfusion injury, Am J Physiol Renal Physiol 306(8) (2014) F801-11.

[115] S.L. Kelley, T. Lukk, S.K. Nair, R.I. Tapping, The crystal structure of human soluble CD14 reveals a bent solenoid with a hydrophobic amino-terminal pocket, Journal of immunology 190(3) (2013) 1304-11.

[116] J.M. Ruysschaert, C. Lonez, Role of lipid microdomains in TLR-mediated signalling, Biochimica et biophysica acta 1848(9) (2015) 1860-7.

[117] M. Di Gioia, I. Zanoni, Toll-like receptor co-receptors as master regulators of the immune response, Mol Immunol 63(2) (2015) 143-152.

[118] F.I. Schmidt, E. Latz, CD14-New Tricks of an Old Acquaintance, Immunity 47(4) (2017) 606-608.

[119] R.R. Schumann, S.R. Leong, G.W. Flaggs, P.W. Gray, S.D. Wright, J.C. Mathison, P.S. Tobias, R.J. Ulevitch, Structure and function of lipopolysaccharide binding protein, Science 249(4975) (1990) 1429-31.

[120] S.D. Wright, R.A. Ramos, P.S. Tobias, R.J. Ulevitch, J.C. Mathison, CD14, a receptor for complexes of lipopolysaccharide (LPS) and LPS binding protein, Science 249(4975) (1990) 1431-3.

[121] Y. Nagai, S. Akashi, M. Nagafuku, M. Ogata, Y. Iwakura, S. Akira, T. Kitamura, A. Kosugi, M. Kimoto, K. Miyake, Essential role of MD-2 in LPS responsiveness and TLR4 distribution, Nat Immunol 3(7) (2002) 667-72.

[122] J. da Silva Correia, K. Soldau, U. Christen, P.S. Tobias, R.J. Ulevitch, Lipopolysaccharide is in close proximity to each of the proteins in its membrane receptor complex. transfer from CD14 to TLR4 and MD-2, J Biol Chem 276(24) (2001) 21129-35.

[123] I. Zanoni, R. Ostuni, L.R. Marek, S. Barresi, R. Barbalat, G.M. Barton, F. Granucci, J.C. Kagan, CD14 controls the LPS-induced endocytosis of Toll-like receptor 4, Cell 147(4) (2011) 868-80.

[124] J.C. Kagan, T. Su, T. Horng, A. Chow, S. Akira, R. Medzhitov, TRAM couples endocytosis of Toll-like receptor 4 to the induction of interferon-beta, Nat Immunol 9(4) (2008) 361-8.

[125] A. Haziot, E. Ferrero, F. Kontgen, N. Hijiya, S. Yamamoto, J. Silver, C.L. Stewart, S.M. Goyert, Resistance to endotoxin shock and reduced dissemination of gram-negative bacteria in CD14-deficient mice, Immunity 4(4) (1996) 407-14.

[126] S. Kim, H. Takahashi, W.W. Lin, P. Descargues, S. Grivennikov, Y. Kim, J.L. Luo, M. Karin, Carcinoma-produced factors activate myeloid cells through TLR2 to stimulate metastasis, Nature 457(7225) (2009) 102-6.

[127] S.R. Liu, Y. Liu, W.L. Hao, L. Wolf, A.J. Kiliaan, B. Penke, C.E. Rube, J. Walter, M.T. Heneka, T. Hartmann, M.D. Menger, K. Fassbender, TLR2 Is a Primary Receptor for Alzheimer's Amyloid beta Peptide To Trigger Neuroinflammatory Activation, Journal of immunology 188(3) (2012) 1098-1107.

[128] C.L. Baumann, I.M. Aspalter, O. Sharif, A. Pichlmair, S. Bluml, F. Grebien, M. Bruckner, P. Pasierbek, K. Aumayr, M. Planyavsky, K.L. Bennett, J. Colinge, S. Knapp, G. Superti-Furga, CD14 is a coreceptor of Toll-like receptors 7 and 9, The Journal of experimental medicine 207(12) (2010) 2689-701.

[129] H.K. Lee, S. Dunzendorfer, K. Soldau, P.S. Tobias, Double-stranded RNA-mediated TLR3 activation is enhanced by CD14, Immunity 24(2) (2006) 153-63.

[130] Z. Wu, Z. Zhang, Z. Lei, P. Lei, CD14: Biology and role in the pathogenesis of disease, Cytokine Growth Factor Rev 48 (2019) 24-31.

[131] I. Zanoni, F. Granucci, Role of CD14 in host protection against infections and in metabolism regulation, Front Cell Infect Microbiol 3 (2013) 32.

[132] B. Parajuli, Y. Sonobe, J. Kawanokuchi, Y. Doi, M. Noda, H. Takeuchi, T. Mizuno, A. Suzumura, GM-CSF increases LPS-induced production of proinflammatory mediators via upregulation of TLR4 and CD14 in murine microglia, J Neuroinflammation 9 (2012) 268.

[133] M. Zhou, C.M. Wang, W.L. Yang, P. Wang, Microglial CD14 activated by iNOS contributes to neuroinflammation in cerebral ischemia, Brain Res 1506 (2013) 105-14.

[134] T.A. da Silva, A.L.V. Zorzetto-Fernandes, N.T. Cecilio, A. Sardinha-Silva, F.F. Fernandes, M.C. Roque-Barreira, CD14 is critical for TLR2-mediated M1 macrophage activation triggered by N-glycan recognition, Scientific reports 7(1) (2017) 7083.

[135] I. Zanoni, R. Ostuni, G. Capuano, M. Collini, M. Caccia, A.E. Ronchi, M. Rocchetti, F. Mingozzi, M. Foti, G. Chirico, B. Costa, A. Zaza, P. Ricciardi-Castagnoli, F. Granucci, CD14 regulates the dendritic cell life cycle after LPS exposure through NFAT activation, Nature 460(7252) (2009) 264-8.

[136] E.B. Thorgersen, S.E. Pischke, A. Barratt-Due, H. Fure, J.K. Lindstad, A. Pharo, B.C. Hellerud, T.E. Mollnes, Systemic CD14 inhibition attenuates organ inflammation in porcine Escherichia coli sepsis, Infect Immun 81(9) (2013) 3173-81.

[137] K.A. Shirey, W. Lai, A.J. Scott, M. Lipsky, P. Mistry, L.M. Pletneva, C.L. Karp, J. McAlees, T.L. Gioannini, J. Weiss, W.H. Chen, R.K. Ernst, D.P. Rossignol, F. Gusovsky, J.C. Blanco, S.N. Vogel, The TLR4 antagonist Eritoran protects mice from lethal influenza infection, Nature 497(7450) (2013) 498-502.

[138] A.C. Raby, B. Holst, E. Le Bouder, C. Diaz, E. Ferran, L. Conraux, J.C. Guillemot, B. Coles, A. Kift-Morgan, C.S. Colmont, T. Szakmany, P. Ferrara, J.E. Hall, N. Topley, M.O. Labeta, Targeting the TLR co-receptor CD14 with TLR2-derived peptides modulates immune responses to pathogens, Sci Transl Med 5(185) (2013) 185ra64.

[139] B. Sahay, K. Bashant, N.L.J. Nelson, R.L. Patsey, S.K. Gadila, R. Boohaker, A. Verma, K. Strle, T.J. Sellati, Induction of Interleukin 10 by Borrelia burgdorferi Is Regulated by the Action of CD14-Dependent p38 Mitogen-Activated Protein Kinase and cAMP-Mediated Chromatin Remodeling, Infect Immun 86(4) (2018).

[140] S. Roy, M. Karmakar, E. Pearlman, CD14 mediates Toll-like receptor 4 (TLR4) endocytosis and spleen tyrosine kinase (Syk) and interferon regulatory transcription factor 3 (IRF3) activation in epithelial cells and impairs neutrophil infiltration and Pseudomonas aeruginosa killing in vivo, J Biol Chem 289(2) (2014) 1174-82.

[141] S. Buchheister, M. Buettner, M. Basic, A. Noack, G. Breves, B. Buchen, L.M. Keubler, C. Becker, A. Bleich, CD14 Plays a Protective Role in Experimental Inflammatory Bowel Disease by Enhancing Intestinal Barrier Function, Am J Pathol 187(5) (2017) 1106-1120.

[142] I. Gurevich, C. Zhang, N. Francis, B.J. Aneskievich, TNIP1, a retinoic acid receptor corepressor and A20-binding inhibitor of NF-kappaB, distributes to both nuclear and cytoplasmic locations, The journal of histochemistry and cytochemistry : official journal of the Histochemistry Society 59(12) (2011) 1101-12.

[143] K. Heyninck, M.M. Kreike, R. Beyaert, Structure-function analysis of the A20-binding inhibitor of NF-kappa B activation, ABIN-1, FEBS Lett 536(1-3) (2003) 135-40.

[144] R.T. G'Sell, P.M. Gaffney, D.W. Powell, A20-Binding Inhibitor of NF-kappaB Activation 1 is a Physiologic Inhibitor of NF-kappaB: A Molecular Switch for Inflammation and Autoimmunity, Arthritis Rheumatol 67(9) (2015) 2292-302.

[145] T. Das, Z. Chen, R.W. Hendriks, M. Kool, A20/Tumor Necrosis Factor alpha-Induced Protein 3 in Immune Cells Controls Development of Autoinflammation and Autoimmunity: Lessons from Mouse Models, Frontiers in immunology 9 (2018) 104.

[146] C. Mauro, F. Pacifico, A. Lavorgna, S. Mellone, A. Iannetti, R. Acquaviva, S. Formisano, P. Vito, A. Leonardi, ABIN-1 binds to NEMO/IKKgamma and co-operates with A20 in inhibiting NF-kappaB, J Biol Chem 281(27) (2006) 18482-8.

[147] S.K. Nanda, R.K. Venigalla, A. Ordureau, J.C. Patterson-Kane, D.W. Powell, R. Toth, J.S. Arthur, P. Cohen, Polyubiquitin binding to ABIN1 is required to prevent autoimmunity, The Journal of experimental medicine 208(6) (2011) 1215-28.

[148] S. Wagner, I. Carpentier, V. Rogov, M. Kreike, F. Ikeda, F. Lohr, C.J. Wu, J.D. Ashwell, V. Dotsch, I. Dikic, R. Beyaert, Ubiquitin binding mediates the NF-kappaB inhibitory potential of ABIN proteins, Oncogene 27(26) (2008) 3739-45.

[149] S. Oshima, E.E. Turer, J.A. Callahan, S. Chai, R. Advincula, J. Barrera, N. Shifrin, B. Lee, T.S. Benedict Yen, T. Woo, B.A. Malynn, A. Ma, ABIN-1 is a ubiquitin sensor that restricts cell death and sustains embryonic development, Nature 457(7231) (2009) 906-9.

[150] R. Yau, M. Rape, The increasing complexity of the ubiquitin code, Nature cell biology 18(6) (2016) 579-86.

[151] R. Shamilov, B.J. Aneskievich, TNIP1 in Autoimmune Diseases: Regulation of Toll-like Receptor Signaling, J Immunol Res 2018 (2018) 3491269.

[152] L. Gao, H. Coope, S. Grant, A. Ma, S.C. Ley, E.W. Harhaj, ABIN1 protein cooperates with TAX1BP1 and A20 proteins to inhibit antiviral signaling, J Biol Chem 286(42) (2011) 36592-602.

[153] S.A. Dziedzic, Z. Su, V. Jean Barrett, A. Najafov, A.K. Mookhtiar, P. Amin, H. Pan, L. Sun, H. Zhu, A. Ma, D.W. Abbott, J. Yuan, ABIN-1 regulates RIPK1 activation by linking Met1 ubiquitylation with Lys63 deubiquitylation in TNF-RSC, Nature cell biology 20(1) (2018) 58-68.

[154] S. Yuan, X. Dong, X. Tao, L. Xu, J. Ruan, J. Peng, A. Xu, Emergence of the A20/ABIN-mediated inhibition of NF-kappaB signaling via modifying the ubiquitinated proteins in a basal chordate, Proceedings of the National Academy of Sciences of the United States of America 111(18) (2014) 6720-5.

[155] M.G. Kattah, L. Shao, Y.Y. Rosli, H. Shimizu, M.I. Whang, R. Advincula, P. Achacoso, S. Shah, B.H. Duong, M. Onizawa, P. Tanbun, B.A. Malynn, A. Ma, A20 and ABIN-1 synergistically preserve intestinal epithelial cell survival, The Journal of experimental medicine 215(7) (2018) 1839-1852.

[156] S.C. Sun, J.H. Chang, J. Jin, Regulation of nuclear factor-kappaB in autoimmunity, Trends Immunol 34(6) (2013) 282-9.

[157] B. Miraghazadeh, M.C. Cook, Nuclear Factor-kappaB in Autoimmunity: Man and Mouse, Frontiers in immunology 9 (2018) 613.

[158] J. Zhou, R. Wu, A.A. High, C.A. Slaughter, D. Finkelstein, J.E. Rehg, V. Redecke, H. Hacker, A20-binding inhibitor of NF-kappaB (ABIN1) controls Toll-like receptor-mediated CCAAT/enhancer-binding protein beta activation and protects from inflammatory disease, Proceedings of the National Academy of Sciences of the United States of America 108(44) (2011) E998-1006.

[159] D.J. Caster, E.A. Korte, S.K. Nanda, K.R. McLeish, R.K. Oliver, T. G'Sell R, R.M. Sheehan, D.W. Freeman, S.C. Coventry, J.A. Kelly, J.M. Guthridge, J.A. James, K.L. Sivils, M.E. Alarcon-Riquelme, R.H. Scofield, I. Adrianto, P.M. Gaffney, A.M. Stevens, B.I. Freedman, C.D. Langefeld, B.P. Tsao, B.A. Pons-Estel, C.O. Jacob, D.L. Kamen, G.S. Gilkeson, E.E. Brown, G.S. Alarcon, J.C. Edberg, R.P. Kimberly, J. Martin, J.T. Merrill, J.B. Harley, K.M. Kaufman, J.D. Reveille, J.M. Anaya, L.A. Criswell, L.M. Vila, M. Petri, R. Ramsey-Goldman, S.C. Bae, S.A. Boackle, T.J. Vyse, T.B. Niewold, P. Cohen, D.W. Powell, ABIN1 dysfunction as a genetic basis for lupus nephritis, J Am Soc Nephrol 24(11) (2013) 1743-54.

[160] H. Zhong, X.L. Li, M. Li, L.X. Hao, R.W. Chen, K. Xiang, X.B. Qi, R.Z. Ma, B. Su, Replicated associations of TNFAIP3, TNIP1 and ETS1 with systemic lupus erythematosus in a southwestern Chinese population, Arthritis research & therapy 13(6) (2011) R186.

[161] A. Kawasaki, S. Ito, H. Furukawa, T. Hayashi, D. Goto, I. Matsumoto, M. Kusaoi, J. Ohashi, R.R. Graham, K. Matsuta, T.W. Behrens, S. Tohma, Y. Takasaki, H. Hashimoto, T. Sumida, N. Tsuchiya, Association of TNFAIP3 interacting protein 1, TNIP1 with systemic lupus erythematosus in a Japanese population: a case-control association study, Arthritis research & therapy 12(5) (2010) R174.

[162] E.A. Korte, D.J. Caster, M.T. Barati, M. Tan, S. Zheng, C.C. Berthier, F.C. Brosius, 3rd, M.B. Vieyra, R.M. Sheehan, M. Kosiewicz, M. Wysoczynski, P.M. Gaffney, D.J. Salant, K.R. McLeish, D.W. Powell, ABIN1 Determines Severity of Glomerulonephritis via Activation of Intrinsic Glomerular Inflammation, Am J Pathol 187(12) (2017) 2799-2810.

[163] S.K. Nanda, M. Lopez-Pelaez, J.S. Arthur, F. Marchesi, P. Cohen, Suppression of IRAK1 or IRAK4 Catalytic Activity, but Not Type 1 IFN Signaling, Prevents Lupus Nephritis in Mice Expressing a Ubiquitin Binding-Defective Mutant of ABIN1, Journal of immunology 197(11) (2016) 4266-4273.

[164] J.A. Callahan, G.E. Hammer, A. Agelides, B.H. Duong, S. Oshima, J. North, R. Advincula, N. Shifrin, H.A. Truong, J. Paw, J. Barrera, A. DeFranco, M.D. Rosenblum, B.A. Malynn, A. Ma, Cutting edge: ABIN-1 protects against psoriasis by restricting MyD88 signals in dendritic cells, Journal of immunology 191(2) (2013) 535-9.

[165] S.K. Ippagunta, R. Gangwar, D. Finkelstein, P. Vogel, S. Pelletier, S. Gingras, V. Redecke, H. Hacker, Keratinocytes contribute intrinsically to psoriasis upon loss of Tnip1 function, Proceedings of the National Academy of Sciences of the United States of America 113(41) (2016) E6162-E6171.

[166] S. Papoutsopoulou, A. Symons, T. Tharmalingham, M.P. Belich, F. Kaiser, D. Kioussis, A. O'Garra, V. Tybulewicz, S.C. Ley, ABIN-2 is required for optimal activation of Erk MAP kinase in innate immune responses, Nat Immunol 7(6) (2006) 606-15.

[167] S.K. Nanda, T. Nagamori, M. Windheim, S. Amu, G. Aviello, J. Patterson-Kane, J.S.C. Arthur, S.C. Ley, P. Fallon, P. Cohen, ABIN2 Function Is Required To Suppress DSS-Induced Colitis by a Tpl2-Independent Mechanism, Journal of immunology 201(11) (2018) 3373-3382.

[168] B.K. Weaver, E. Bohn, B.A. Judd, M.P. Gil, R.D. Schreiber, ABIN-3: a molecular basis for species divergence in interleukin-10-induced anti-inflammatory actions, Mol Cell Biol 27(13) (2007) 4603-16.

[169] T. Johansen, T. Lamark, Selective Autophagy: ATG8 Family Proteins, LIR Motifs and Cargo Receptors, J Mol Biol (2019).

[170] J.F. Dice, Peptide sequences that target cytosolic proteins for lysosomal proteolysis, Trends Biochem Sci 15(8) (1990) 305-9.

[171] L. Galluzzi, E.H. Baehrecke, A. Ballabio, P. Boya, J.M. Bravo-San Pedro, F. Cecconi, A.M. Choi, C.T. Chu, P. Codogno, M.I. Colombo, A.M. Cuervo, J. Debnath, V. Deretic, I. Dikic, E.L. Eskelinen, G.M. Fimia, S. Fulda, D.A. Gewirtz, D.R. Green, M. Hansen, J.W. Harper, M. Jaattela, T. Johansen, G. Juhasz, A.C. Kimmelman, C. Kraft, N.T. Ktistakis, S. Kumar, B. Levine, C. Lopez-Otin, F. Madeo, S. Martens, J. Martinez, A. Melendez, N. Mizushima, C. Munz, L.O. Murphy, J.M. Penninger, M. Piacentini, F. Reggiori, D.C. Rubinsztein, K.M. Ryan, L. Santambrogio, L. Scorrano, A.K. Simon, H.U. Simon, A. Simonsen, N. Tavernarakis, S.A. Tooze, T. Yoshimori, J. Yuan, Z. Yue, Q. Zhong, G. Kroemer, Molecular definitions of autophagy and related processes, EMBO J 36(13) (2017) 1811-1836.

[172] C. Munch, I. Dikic, Publisher Correction: Hitchhiking on selective autophagy, Nature cell biology 20(8) (2018) 990.

[173] G.E. Mortimore, C.M. Schworer, Induction of autophagy by amino-acid deprivation in perfused rat liver, Nature 270(5633) (1977) 174-6.

[174] K. Takeshige, M. Baba, S. Tsuboi, T. Noda, Y. Ohsumi, Autophagy in yeast demonstrated with proteinase-deficient mutants and conditions for its induction, The Journal of cell biology 119(2) (1992) 301-11.

[175] G. Zaffagnini, S. Martens, Mechanisms of Selective Autophagy, J Mol Biol 428(9 Pt A) (2016) 1714-24.

[176] S. Pankiv, T.H. Clausen, T. Lamark, A. Brech, J.A. Bruun, H. Outzen, A. Overvatn, G. Bjorkoy, T. Johansen, p62/SQSTM1 binds directly to Atg8/LC3 to facilitate degradation of ubiquitinated protein aggregates by autophagy, J Biol Chem 282(33) (2007) 24131-45.

[177] C. Van Humbeeck, T. Cornelissen, H. Hofkens, W. Mandemakers, K. Gevaert, B. De Strooper, W. Vandenberghe, Parkin interacts with Ambra1 to induce mitophagy, J Neurosci 31(28) (2011) 10249-61.

[178] J.M. Heo, A. Ordureau, J.A. Paulo, J. Rinehart, J.W. Harper, The PINK1-PARKIN Mitochondrial Ubiquitylation Pathway Drives a Program of OPTN/NDP52 Recruitment and TBK1 Activation to Promote Mitophagy, Mol Cell 60(1) (2015) 7-20.

[179] T. Nishimura, T. Kaizuka, K. Cadwell, M.H. Sahani, T. Saitoh, S. Akira, H.W. Virgin, N. Mizushima, FIP200 regulates targeting of Atg16L1 to the isolation membrane, EMBO Rep 14(3) (2013) 284-91.

[180] I. Maejima, A. Takahashi, H. Omori, T. Kimura, Y. Takabatake, T. Saitoh, A. Yamamoto, M. Hamasaki, T. Noda, Y. Isaka, T. Yoshimori, Autophagy sequesters damaged lysosomes to control lysosomal biogenesis and kidney injury, EMBO J 32(17) (2013) 2336-47.

[181] G.A. Wyant, M. Abu-Remaileh, E.M. Frenkel, N.N. Laqtom, V. Dharamdasani, C.A. Lewis, S.H. Chan, I. Heinze, A. Ori, D.M. Sabatini, NUFIP1 is a ribosome receptor for starvation-induced ribophagy, Science 360(6390) (2018) 751-758.

[182] D. Grasso, A. Ropolo, A. Lo Re, V. Boggio, M.I. Molejon, J.L. Iovanna, C.D. Gonzalez, R. Urrutia, M.I. Vaccaro, Zymophagy, a novel selective autophagy pathway mediated by VMP1-USP9x-p62, prevents pancreatic cell death, J Biol Chem 286(10) (2011) 8308-24.

[183] S. Bernales, S. Schuck, P. Walter, ER-phagy: selective autophagy of the endoplasmic reticulum, Autophagy 3(3) (2007) 285-7.

[184] Z. Dou, C. Xu, G. Donahue, T. Shimi, J.A. Pan, J. Zhu, A. Ivanov, B.C. Capell, A.M. Drake, P.P. Shah, J.M. Catanzaro, M.D. Ricketts, T. Lamark, S.A. Adam, R. Marmorstein, W.X. Zong, T. Johansen, R.D. Goldman, P.D. Adams, S.L. Berger, Autophagy mediates degradation of nuclear lamina, Nature 527(7576) (2015) 105-9.

[185] P. Isakson, A.H. Lystad, K. Breen, G. Koster, H. Stenmark, A. Simonsen, TRAF6 mediates ubiquitination of KIF23/MKLP1 and is required for midbody ring degradation by selective autophagy, Autophagy 9(12) (2013) 1955-64.

[186] J.D. Mancias, X. Wang, S.P. Gygi, J.W. Harper, A.C. Kimmelman, Quantitative proteomics identifies NCOA4 as the cargo receptor mediating ferritinophagy, Nature 509(7498) (2014) 105-9.

[187] S. Jiang, B. Heller, V.S. Tagliabracci, L. Zhai, J.M. Irimia, A.A. DePaoli-Roach, C.D. Wells, A.V. Skurat, P.J. Roach, Starch binding domain-containing protein 1/genethonin 1 is a novel participant in glycogen metabolism, J Biol Chem 285(45) (2010) 34960-71.

[188] I. Nakagawa, A. Amano, N. Mizushima, A. Yamamoto, H. Yamaguchi, T. Kamimoto, A. Nara, J. Funao, M. Nakata, K. Tsuda, S. Hamada, T. Yoshimori, Autophagy defends cells against invading group A Streptococcus, Science 306(5698) (2004) 1037-40.

[189] M.A. Mandell, T. Kimura, A. Jain, T. Johansen, V. Deretic, TRIM proteins regulate autophagy: TRIM5 is a selective autophagy receptor mediating HIV-1 restriction, Autophagy 10(12) (2014) 2387-8.

[190] M. Moulis, C. Vindis, Autophagy in Metabolic Age-Related Human Diseases, Cells 7(10) (2018).

[191] C.W. Yun, S.H. Lee, The Roles of Autophagy in Cancer, International Journal of Molecular Sciences 19(11) (2018).

[192] M. Qian, X. Fang, X. Wang, Autophagy and inflammation, Clin Transl Med 6(1) (2017) 24.

[193] T. Bar-Yosef, O. Damri, G. Agam, Dual Role of Autophagy in Diseases of the Central Nervous System, Front Cell Neurosci 13 (2019) 196.

[194] M.C. Barbosa, R.A. Grosso, C.M. Fader, Hallmarks of Aging: An Autophagic Perspective, Front Endocrinol (Lausanne) 9 (2018) 790.

[195] I. Dikic, Z. Elazar, Mechanism and medical implications of mammalian autophagy, Nat Rev Mol Cell Biol 19(6) (2018) 349-364.

[196] C.H. Jung, C.B. Jun, S.H. Ro, Y.M. Kim, N.M. Otto, J. Cao, M. Kundu, D.H. Kim, ULK-Atg13-FIP200 complexes mediate mTOR signaling to the autophagy machinery, Mol Biol Cell 20(7) (2009) 1992-2003.

[197] F. Nazio, F. Strappazzon, M. Antonioli, P. Bielli, V. Cianfanelli, M. Bordi, C. Gretzmeier, J. Dengjel, M. Piacentini, G.M. Fimia, F. Cecconi, mTOR inhibits autophagy by controlling

ULK1 ubiquitylation, self-association and function through AMBRA1 and TRAF6, Nature cell biology 15(4) (2013) 406-16.

[198] C.A. Lamb, T. Yoshimori, S.A. Tooze, The autophagosome: origins unknown, biogenesis complex, Nat Rev Mol Cell Biol 14(12) (2013) 759-74.

[199] S. Baskaran, M.J. Ragusa, E. Boura, J.H. Hurley, Two-site recognition of phosphatidylinositol 3-phosphate by PROPPINs in autophagy, Mol Cell 47(3) (2012) 339-48.

[200] A.C. Nascimbeni, P. Codogno, E. Morel, Phosphatidylinositol-3-phosphate in the regulation of autophagy membrane dynamics, FEBS J 284(9) (2017) 1267-1278.

[201] E.A. Alemu, T. Lamark, K.M. Torgersen, A.B. Birgisdottir, K.B. Larsen, A. Jain, H. Olsvik, A. Overvatn, V. Kirkin, T. Johansen, ATG8 family proteins act as scaffolds for assembly of the ULK complex: sequence requirements for LC3-interacting region (LIR) motifs, J Biol Chem 287(47) (2012) 39275-90.

[202] A.B. Birgisdottir, S. Mouilleron, Z. Bhujabal, M. Wirth, E. Sjottem, G. Evjen, W. Zhang, R. Lee, N. O'Reilly, S.A. Tooze, T. Lamark, T. Johansen, Members of the autophagy class III phosphatidylinositol 3-kinase complex I interact with GABARAP and GABARAPL1 via LIR motifs, Autophagy 15(8) (2019) 1333-1355.

[203] V. Rogov, V. Dotsch, T. Johansen, V. Kirkin, Interactions between autophagy receptors and ubiquitin-like proteins form the molecular basis for selective autophagy, Mol Cell 53(2) (2014) 167-78.

[204] H. Nakatogawa, K. Suzuki, Y. Kamada, Y. Ohsumi, Dynamics and diversity in autophagy mechanisms: lessons from yeast, Nat Rev Mol Cell Biol 10(7) (2009) 458-67.

[205] F. Reggiori, C. Ungermann, Autophagosome Maturation and Fusion, J Mol Biol 429(4) (2017) 486-496.

[206] V. Kirkin, History of the Selective Autophagy Research: How Did It Begin and Where Does It Stand Today?, J Mol Biol (2019).

[207] P. Grumati, I. Dikic, Ubiquitin signaling and autophagy, J Biol Chem 293(15) (2018) 5404-5413.

[208] A. Khaminets, C. Behl, I. Dikic, Ubiquitin-Dependent And Independent Signals In Selective Autophagy, Trends Cell Biol 26(1) (2016) 6-16.

[209] M. Komatsu, H. Kurokawa, S. Waguri, K. Taguchi, A. Kobayashi, Y. Ichimura, Y.S. Sou, I. Ueno, A. Sakamoto, K.I. Tong, M. Kim, Y. Nishito, S. Iemura, T. Natsume, T. Ueno, E. Kominami, H. Motohashi, K. Tanaka, M. Yamamoto, The selective autophagy substrate p62 activates the stress responsive transcription factor Nrf2 through inactivation of Keap1, Nature cell biology 12(3) (2010) 213-23.

[210] A. Jain, T. Lamark, E. Sjottem, K.B. Larsen, J.A. Awuh, A. Overvatn, M. McMahon, J.D. Hayes, T. Johansen, p62/SQSTM1 is a target gene for transcription factor NRF2 and creates a positive feedback loop by inducing antioxidant response element-driven gene transcription, J Biol Chem 285(29) (2010) 22576-91.

[211] J.A. Olzmann, L. Li, M.V. Chudaev, J. Chen, F.A. Perez, R.D. Palmiter, L.S. Chin, Parkin-mediated K63-linked polyubiquitination targets misfolded DJ-1 to aggresomes via binding to HDAC6, The Journal of cell biology 178(6) (2007) 1025-38.

[212] J.F. Linares, A. Duran, T. Yajima, M. Pasparakis, J. Moscat, M.T. Diaz-Meco, K63 polyubiquitination and activation of mTOR by the p62-TRAF6 complex in nutrient-activated cells, Mol Cell 51(3) (2013) 283-96.

[213] J. Long, T.R. Gallagher, J.R. Cavey, P.W. Sheppard, S.H. Ralston, R. Layfield, M.S. Searle, Ubiquitin recognition by the ubiquitin-associated domain of p62 involves a novel conformational switch, J Biol Chem 283(9) (2008) 5427-40.

[214] M.L. Seibenhener, J.R. Babu, T. Geetha, H.C. Wong, N.R. Krishna, M.W. Wooten, Sequestosome 1/p62 is a polyubiquitin chain binding protein involved in ubiquitin proteasome degradation, Mol Cell Biol 24(18) (2004) 8055-68.

[215] B. Wurzer, G. Zaffagnini, D. Fracchiolla, E. Turco, C. Abert, J. Romanov, S. Martens, Oligomerization of p62 allows for selection of ubiquitinated cargo and isolation membrane during selective autophagy, Elife 4 (2015) e08941.

[216] G. Zhu, C.J. Wu, Y. Zhao, J.D. Ashwell, Optineurin negatively regulates TNFalpha-induced NF-kappaB activation by competing with NEMO for ubiquitinated RIP, Curr Biol 17(16) (2007) 1438-43.

[217] G. Bjorkoy, T. Lamark, A. Brech, H. Outzen, M. Perander, A. Overvatn, H. Stenmark, T. Johansen, p62/SQSTM1 forms protein aggregates degraded by autophagy and has a protective effect on huntingtin-induced cell death, The Journal of cell biology 171(4) (2005) 603-14.

[218] J. Moscat, M.T. Diaz-Meco, M.W. Wooten, Signal integration and diversification through the p62 scaffold protein, Trends Biochem Sci 32(2) (2007) 95-100.

[219] B.W. Kim, D.H. Kwon, H.K. Song, Structure biology of selective autophagy receptors, BMB Rep 49(2) (2016) 73-80.

[220] P. Wild, H. Farhan, D.G. McEwan, S. Wagner, V.V. Rogov, N.R. Brady, B. Richter, J. Korac, O. Waidmann, C. Choudhary, V. Dotsch, D. Bumann, I. Dikic, Phosphorylation of the autophagy receptor optineurin restricts Salmonella growth, Science 333(6039) (2011) 228-33.

[221] B. Richter, D.A. Sliter, L. Herhaus, A. Stolz, C. Wang, P. Beli, G. Zaffagnini, P. Wild, S. Martens, S.A. Wagner, R.J. Youle, I. Dikic, Phosphorylation of OPTN by TBK1 enhances its binding to Ub chains and promotes selective autophagy of damaged mitochondria, Proceedings of the National Academy of Sciences of the United States of America 113(15) (2016) 4039-44.

[222] G. Matsumoto, K. Wada, M. Okuno, M. Kurosawa, N. Nukina, Serine 403 phosphorylation of p62/SQSTM1 regulates selective autophagic clearance of ubiquitinated proteins, Mol Cell 44(2) (2011) 279-89.

[223] M. Pilli, J. Arko-Mensah, M. Ponpuak, E. Roberts, S. Master, M.A. Mandell, N. Dupont, W. Ornatowski, S. Jiang, S.B. Bradfute, J.A. Bruun, T.E. Hansen, T. Johansen, V. Deretic, TBK-1 promotes autophagy-mediated antimicrobial defense by controlling autophagosome maturation, Immunity 37(2) (2012) 223-34.

[224] J. Lim, M.L. Lachenmayer, S. Wu, W. Liu, M. Kundu, R. Wang, M. Komatsu, Y.J. Oh, Y. Zhao, Z. Yue, Proteotoxic stress induces phosphorylation of p62/SQSTM1 by ULK1 to regulate selective autophagic clearance of protein aggregates, PLoS Genet 11(2) (2015) e1004987.

[225] J. Long, T.P. Garner, M.J. Pandya, C.J. Craven, P. Chen, B. Shaw, M.P. Williamson, R. Layfield, M.S. Searle, Dimerisation of the UBA domain of p62 inhibits ubiquitin binding and regulates NF-kappaB signalling, J Mol Biol 396(1) (2010) 178-94.

[226] J.A. Pan, Y. Sun, Y.P. Jiang, A.J. Bott, N. Jaber, Z. Dou, B. Yang, J.S. Chen, J.M. Catanzaro, C. Du, W.X. Ding, M.T. Diaz-Meco, J. Moscat, K. Ozato, R.Z. Lin, W.X. Zong, TRIM21 Ubiquitylates SQSTM1/p62 and Suppresses Protein Sequestration to Regulate Redox Homeostasis, Mol Cell 62(1) (2016) 149-51.

[227] Y. Lee, T.F. Chou, S.K. Pittman, A.L. Keith, B. Razani, C.C. Weihl, Keap1/Cullin3 Modulates p62/SQSTM1 Activity via UBA Domain Ubiquitination, Cell Rep 20(8) (2017) 1994.

[228] J.B. Spinelli, M.C. Haigis, The multifaceted contributions of mitochondria to cellular metabolism, Nature cell biology 20(7) (2018) 745-754.

[229] I. Martinez-Reyes, N.S. Chandel, Mitochondrial TCA cycle metabolites control physiology and disease, Nature communications 11(1) (2020) 102.

[230] I. Gkikas, K. Palikaras, N. Tavernarakis, The Role of Mitophagy in Innate Immunity, Frontiers in immunology 9 (2018) 1283.

[231] E. Schulz, P. Wenzel, T. Munzel, A. Daiber, Mitochondrial redox signaling: Interaction of mitochondrial reactive oxygen species with other sources of oxidative stress, Antioxid Redox Signal 20(2) (2014) 308-24.

[232] S. Pickles, P. Vigie, R.J. Youle, Mitophagy and Quality Control Mechanisms in Mitochondrial Maintenance, Curr Biol 28(4) (2018) R170-R185.

[233] X. Jiang, T. Jin, H. Zhang, J. Miao, X. Zhao, Y. Su, Y. Zhang, Current Progress of Mitochondrial Quality Control Pathways Underlying the Pathogenesis of Parkinson's Disease, Oxid Med Cell Longev 2019 (2019) 4578462.

[234] K. Palikaras, E. Lionaki, N. Tavernarakis, Mechanisms of mitophagy in cellular homeostasis, physiology and pathology, Nature cell biology 20(9) (2018) 1013-1022.

[235] L. Sedlackova, V.I. Korolchuk, Mitochondrial quality control as a key determinant of cell survival, Biochim Biophys Acta Mol Cell Res 1866(4) (2019) 575-587.

[236] H. Ichimura, K. Parthasarathi, S. Quadri, A.C. Issekutz, J. Bhattacharya, Mechano-oxidative coupling by mitochondria induces proinflammatory responses in lung venular capillaries, The Journal of clinical investigation 111(5) (2003) 691-9.

[237] J.H. Um, J. Yun, Emerging role of mitophagy in human diseases and physiology, BMB Rep 50(6) (2017) 299-307.

[238] K. Yamano, R.J. Youle, PINK1 is degraded through the N-end rule pathway, Autophagy 9(11) (2013) 1758-69.

[239] A.W. Greene, K. Grenier, M.A. Aguileta, S. Muise, R. Farazifard, M.E. Haque, H.M. McBride, D.S. Park, E.A. Fon, Mitochondrial processing peptidase regulates PINK1 processing, import and Parkin recruitment, EMBO Rep 13(4) (2012) 378-85.

[240] S. Sekine, R.J. Youle, PINK1 import regulation; a fine system to convey mitochondrial stress to the cytosol, BMC Biol 16(1) (2018) 2.

[241] A. Ordureau, S.A. Sarraf, D.M. Duda, J.M. Heo, M.P. Jedrychowski, V.O. Sviderskiy, J.L. Olszewski, J.T. Koerber, T. Xie, S.A. Beausoleil, J.A. Wells, S.P. Gygi, B.A. Schulman, J.W. Harper, Quantitative proteomics reveal a feedforward mechanism for mitochondrial PARKIN translocation and ubiquitin chain synthesis, Mol Cell 56(3) (2014) 360-75.

[242] C. Kondapalli, A. Kazlauskaite, N. Zhang, H.I. Woodroof, D.G. Campbell, R. Gourlay, L. Burchell, H. Walden, T.J. Macartney, M. Deak, A. Knebel, D.R. Alessi, M.M. Muqit, PINK1 is activated by mitochondrial membrane potential depolarization and stimulates Parkin E3 ligase activity by phosphorylating Serine 65, Open Biol 2(5) (2012) 120080.

[243] K. Shiba-Fukushima, Y. Imai, S. Yoshida, Y. Ishihama, T. Kanao, S. Sato, N. Hattori, PINK1-mediated phosphorylation of the Parkin ubiquitin-like domain primes mitochondrial translocation of Parkin and regulates mitophagy, Scientific reports 2 (2012) 1002.

[244] K. Shiba-Fukushima, T. Arano, G. Matsumoto, T. Inoshita, S. Yoshida, Y. Ishihama, K.Y. Ryu, N. Nukina, N. Hattori, Y. Imai, Phosphorylation of mitochondrial polyubiquitin by PINK1 promotes Parkin mitochondrial tethering, PLoS Genet 10(12) (2014) e1004861.

[245] K. Okatsu, F. Koyano, M. Kimura, H. Kosako, Y. Saeki, K. Tanaka, N. Matsuda, Phosphorylated ubiquitin chain is the genuine Parkin receptor, The Journal of cell biology 209(1) (2015) 111-28.

[246] N.C. Chan, A.M. Salazar, A.H. Pham, M.J. Sweredoski, N.J. Kolawa, R.L. Graham, S. Hess, D.C. Chan, Broad activation of the ubiquitin-proteasome system by Parkin is critical for mitophagy, Hum Mol Genet 20(9) (2011) 1726-37.

[247] A. Tanaka, M.M. Cleland, S. Xu, D.P. Narendra, D.F. Suen, M. Karbowski, R.J. Youle, Proteasome and p97 mediate mitophagy and degradation of mitofusins induced by Parkin, The Journal of cell biology 191(7) (2010) 1367-80.

[248] T. Johansen, T. Lamark, Selective autophagy mediated by autophagic adapter proteins, Autophagy 7(3) (2011) 279-96.

[249] Y.C. Wong, E.L. Holzbaur, Optineurin is an autophagy receptor for damaged mitochondria in parkin-mediated mitophagy that is disrupted by an ALS-linked mutation, Proceedings of the National Academy of Sciences of the United States of America 111(42) (2014) E4439-48.

[250] S. Geisler, K.M. Holmstrom, D. Skujat, F.C. Fiesel, O.C. Rothfuss, P.J. Kahle, W. Springer, PINK1/Parkin-mediated mitophagy is dependent on VDAC1 and p62/SQSTM1, Nature cell biology 12(2) (2010) 119-31.

[251] M. Lazarou, D.A. Sliter, L.A. Kane, S.A. Sarraf, C. Wang, J.L. Burman, D.P. Sideris, A.I. Fogel, R.J. Youle, The ubiquitin kinase PINK1 recruits autophagy receptors to induce mitophagy, Nature 524(7565) (2015) 309-314.

[252] M.N. Quinsay, R.L. Thomas, Y. Lee, A.B. Gustafsson, Bnip3-mediated mitochondrial autophagy is independent of the mitochondrial permeability transition pore, Autophagy 6(7) (2010) 855-62.

[253] L. Liu, D. Feng, G. Chen, M. Chen, Q. Zheng, P. Song, Q. Ma, C. Zhu, R. Wang, W. Qi, L. Huang, P. Xue, B. Li, X. Wang, H. Jin, J. Wang, F. Yang, P. Liu, Y. Zhu, S. Sui, Q. Chen, Mitochondrial outer-membrane protein FUNDC1 mediates hypoxia-induced mitophagy in mammalian cells, Nature cell biology 14(2) (2012) 177-85.

[254] W.X. Ding, H.M. Ni, M. Li, Y. Liao, X. Chen, D.B. Stolz, G.W. Dorn, 2nd, X.M. Yin, Nix is critical to two distinct phases of mitophagy, reactive oxygen species-mediated autophagy induction and Parkin-ubiquitin-p62-mediated mitochondrial priming, J Biol Chem 285(36) (2010) 27879-90.

[255] W. Wu, W. Tian, Z. Hu, G. Chen, L. Huang, W. Li, X. Zhang, P. Xue, C. Zhou, L. Liu, Y. Zhu, X. Zhang, L. Li, L. Zhang, S. Sui, B. Zhao, D. Feng, ULK1 translocates to mitochondria and phosphorylates FUNDC1 to regulate mitophagy, EMBO Rep 15(5) (2014) 566-75.

[256] I. Novak, V. Kirkin, D.G. McEwan, J. Zhang, P. Wild, A. Rozenknop, V. Rogov, F. Lohr, D. Popovic, A. Occhipinti, A.S. Reichert, J. Terzic, V. Dotsch, P.A. Ney, I. Dikic, Nix is a selective autophagy receptor for mitochondrial clearance, EMBO Rep 11(1) (2010) 45-51.

[257] A. Schiavi, S. Maglioni, K. Palikaras, A. Shaik, F. Strappazzon, V. Brinkmann, A. Torgovnick, N. Castelein, S. De Henau, B.P. Braeckman, F. Cecconi, N. Tavernarakis, N. Ventura, Iron-Starvation-Induced Mitophagy Mediates Lifespan Extension upon Mitochondrial Stress in C. elegans, Curr Biol 25(14) (2015) 1810-22.

[258] Y. Wei, W.C. Chiang, R. Sumpter, Jr., P. Mishra, B. Levine, Prohibitin 2 Is an Inner Mitochondrial Membrane Mitophagy Receptor, Cell 168(1-2) (2017) 224-238 e10.

[259] C.T. Chu, J. Ji, R.K. Dagda, J.F. Jiang, Y.Y. Tyurina, A.A. Kapralov, V.A. Tyurin, N. Yanamala, I.H. Shrivastava, D. Mohammadyani, K.Z.Q. Wang, J. Zhu, J. Klein-Seetharaman, K. Balasubramanian, A.A. Amoscato, G. Borisenko, Z. Huang, A.M. Gusdon, A. Cheikhi, E.K. Steer, R. Wang, C. Baty, S. Watkins, I. Bahar, H. Bayir, V.E. Kagan, Cardiolipin externalization to the outer mitochondrial membrane acts as an elimination signal for mitophagy in neuronal cells, Nature cell biology 15(10) (2013) 1197-1205.

[260] N. Sun, D. Malide, J. Liu, Rovira, II, C.A. Combs, T. Finkel, A fluorescence-based imaging method to measure in vitro and in vivo mitophagy using mt-Keima, Nat Protoc 12(8) (2017) 1576-1587.

[261] H. Katayama, T. Kogure, N. Mizushima, T. Yoshimori, A. Miyawaki, A sensitive and quantitative technique for detecting autophagic events based on lysosomal delivery, Chem Biol 18(8) (2011) 1042-52.

[262] H. Wu, G. Chen, K.R. Wyburn, J. Yin, P. Bertolino, J.M. Eris, S.I. Alexander, A.F. Sharland, S.J. Chadban, TLR4 activation mediates kidney ischemia/reperfusion injury, The Journal of clinical investigation 117(10) (2007) 2847-59.

[263] M. Barth, J.I. Selig, S. Klose, A. Schomakers, L.S. Kiene, S. Raschke, U. Boeken, P. Akhyari, J.W. Fischer, A. Lichtenberg, Degenerative aortic valve disease and diabetes: Implications for a link between proteoglycans and diabetic disorders in the aortic valve, Diab Vasc Dis Res (2018) doi.org/10.1177/1479164118817922.

[264] A.M. Piccinini, K.S. Midwood, DAMPening inflammation by modulating TLR signalling, Mediators Inflamm 2010 (2010).

[265] R.T. Netea-Maier, T.S. Plantinga, F.L. van de Veerdonk, J.W. Smit, M.G. Netea, Modulation of inflammation by autophagy: Consequences for human disease, Autophagy 12(2) (2016) 245-60.

[266] H. Kresse, D.G. Seidler, M. Muller, E. Breuer, H. Hausser, P.J. Roughley, E. Schonherr, Different usage of the glycosaminoglycan attachment sites of biglycan, J Biol Chem 276(16) (2001) 13411-6.

[267] E. Kowarz, D. Loscher, R. Marschalek, Optimized Sleeping Beauty transposons rapidly generate stable transgenic cell lines, Biotechnol J 10(4) (2015) 647-53.

[268] F.A. Ran, P.D. Hsu, J. Wright, V. Agarwala, D.A. Scott, F. Zhang, Genome engineering using the CRISPR-Cas9 system, Nat Protoc 8(11) (2013) 2281-2308.

[269] S. Tyanova, T. Temu, J. Cox, The MaxQuant computational platform for mass spectrometry-based shotgun proteomics, Nat Protoc 11(12) (2016) 2301-2319.

[270] J. Cox, M.Y. Hein, C.A. Luber, I. Paron, N. Nagaraj, M. Mann, Accurate proteome-wide label-free quantification by delayed normalization and maximal peptide ratio extraction, termed MaxLFQ, Mol Cell Proteomics 13(9) (2014) 2513-26.

[271] A. Chawade, E. Alexandersson, F. Levander, Normalyzer: a tool for rapid evaluation of normalization methods for omics data sets, Journal of proteome research 13(6) (2014) 3114-20.

[272] R.B. Dessau, C.B. Pipper, ["R"--project for statistical computing], Ugeskr Laeger 170(5) (2008) 328-30.

[273] K.A. Jablonski, S.A. Amici, L.M. Webb, D. Ruiz-Rosado Jde, P.G. Popovich, S. Partida-Sanchez, M. Guerau-de-Arellano, Novel Markers to Delineate Murine M1 and M2 Macrophages, PLoS One 10(12) (2015) e0145342.

[274] H. Roedig, M.V. Nastase, H. Frey, K. Moreth, J. Zeng-Brouwers, C. Poluzzi, L.T. Hsieh, C. Brandts, S. Fulda, M. Wygrecka, L. Schaefer, Biglycan is a new high-affinity ligand for CD14 in macrophages, Matrix Biol 77 (2019) 4-22.

[275] B.S. Park, D.H. Song, H.M. Kim, B.S. Choi, H. Lee, J.O. Lee, The structural basis of lipopolysaccharide recognition by the TLR4-MD-2 complex, Nature 458(7242) (2009) 1191-5.

[276] R. Dziarski, D. Gupta, Role of MD-2 in TLR2- and TLR4-mediated recognition of Gram-negative and Gram-positive bacteria and activation of chemokine genes, J Endotoxin Res 6(5) (2000) 401-5.

[277] C.D. Wood, T.M. Thornton, G. Sabio, R.A. Davis, M. Rincon, Nuclear localization of p38 MAPK in response to DNA damage, International journal of biological sciences 5(5) (2009) 428-37.

[278] P. Brand, S. Plochmann, E. Valk, S. Zahn, J. Saloga, J. Knop, D. Becker, Activation and translocation of p38 mitogen-activated protein kinase after stimulation of monocytes with contact sensitizers, J Invest Dermatol 119(1) (2002) 99-106.

[279] E. Wainstein, R. Seger, The dynamic subcellular localization of ERK: mechanisms of translocation and role in various organelles, Curr Opin Cell Biol 39 (2016) 15-20.

[280] K. Flores, S.S. Yadav, A.A. Katz, R. Seger, The Nuclear Translocation of Mitogen-Activated Protein Kinases: Molecular Mechanisms and Use as Novel Therapeutic Target, Neuroendocrinology 108(2) (2019) 121-131.

[281] R. Moreno, J.M. Sobotzik, C. Schultz, M.L. Schmitz, Specification of the NF-kappaB transcriptional response by p65 phosphorylation and TNF-induced nuclear translocation of IKK epsilon, Nucleic Acids Res 38(18) (2010) 6029-44.

[282] M.Y. Wu, G.T. Yiang, W.T. Liao, A.P. Tsai, Y.L. Cheng, P.W. Cheng, C.Y. Li, C.J. Li, Current Mechanistic Concepts in Ischemia and Reperfusion Injury, Cell Physiol Biochem 46(4) (2018) 1650-1667.

[283] S.R. Satpute, J.M. Park, H.R. Jang, P. Agreda, M. Liu, M.T. Gandolfo, L. Racusen, H. Rabb, The role for T cell repertoire/antigen-specific interactions in experimental kidney ischemia reperfusion injury, Journal of immunology 183(2) (2009) 984-92.

[284] S.K. Jo, S.A. Sung, W.Y. Cho, K.J. Go, H.K. Kim, Macrophages contribute to the initiation of ischaemic acute renal failure in rats, Nephrol Dial Transplant 21(5) (2006) 1231-9.

[285] A. Kezic, N. Stajic, F. Thaiss, Innate Immune Response in Kidney Ischemia/Reperfusion Injury: Potential Target for Therapy, J Immunol Res 2017 (2017) 6305439.

[286] S. Tian, S.Y. Chen, Macrophage polarization in kidney diseases, Macrophage (Houst) 2(1) (2015).

[287] T. Inoue, M1 macrophage triggered by Mincle leads to a deterioration of acute kidney injury, Kidney Int 91(3) (2017) 526-529.

[288] M. Peake, M. Whiting, Measurement of serum creatinine--current status and future goals, Clin Biochem Rev 27(4) (2006) 173-84.

[289] L. Verstrepen, I. Carpentier, R. Beyaert, The biology of A20-binding inhibitors of NF-kappaB activation (ABINs), Adv Exp Med Biol 809 (2014) 13-31.

[290] K. Slowicka, L. Vereecke, G. van Loo, Cellular Functions of Optineurin in Health and Disease, Trends Immunol 37(9) (2016) 621-633.

[291] K. Heyninck, D. De Valck, W. Vanden Berghe, W. Van Criekinge, R. Contreras, W. Fiers, G. Haegeman, R. Beyaert, The zinc finger protein A20 inhibits TNF-induced NF-kappaB-dependent gene expression by interfering with an RIP- or TRAF2-mediated transactivation signal and directly binds to a novel NF-kappaB-inhibiting protein ABIN, The Journal of cell biology 145(7) (1999) 1471-82.

[292] S. Cohen, A. Ciechanover, Y. Kravtsova-Ivantsiv, D. Lapid, S. Lahav-Baratz, ABIN-1 negatively regulates NF-kappaB by inhibiting processing of the p105 precursor, Biochemical and biophysical research communications 389(2) (2009) 205-10.

[293] Y. Chen, G.W. Dorn, 2nd, PINK1-phosphorylated mitofusin 2 is a Parkin receptor for culling damaged mitochondria, Science 340(6131) (2013) 471-5.

[294] R. Filadi, D. Pendin, P. Pizzo, Mitofusin 2: from functions to disease, Cell death & disease 9(3) (2018) 330.

[295] K. Yamano, A.I. Fogel, C. Wang, A.M. van der Bliek, R.J. Youle, Mitochondrial Rab GAPs govern autophagosome biogenesis during mitophagy, Elife 3 (2014) e01612.

[296] D. Bakula, A.J. Muller, T. Zuleger, Z. Takacs, M. Franz-Wachtel, A.K. Thost, D. Brigger, M.P. Tschan, T. Frickey, H. Robenek, B. Macek, T. Proikas-Cezanne, WIPI3 and WIPI4 beta-propellers are scaffolds for LKB1-AMPK-TSC signalling circuits in the control of autophagy, Nature communications 8 (2017) 15637.

[297] D. Kliosnky, Guidelines for the Use and Interpretation of Assays for Monitoring Autophagy (3rd edition) (vol 12, pg 1, 2015), Autophagy 12(2) (2016) 443-443.

[298] Y. Xie, R. Kang, D. Tang, Assessment of Posttranslational Modifications of ATG proteins, Methods Enzymol 587 (2017) 171-188.

[299] D. Narendra, A. Tanaka, D.F. Suen, R.J. Youle, Parkin is recruited selectively to impaired mitochondria and promotes their autophagy, Journal of Cell Biology 183(5) (2008) 795-803.

[300] D.P. Narendra, S.M. Jin, A. Tanaka, D.F. Suen, C.A. Gautier, J. Shen, M.R. Cookson, R.J. Youle, PINK1 Is Selectively Stabilized on Impaired Mitochondria to Activate Parkin, Plos Biol 8(1) (2010).

[301] C. Vives-Bauza, C. Zhou, Y. Huang, M. Cui, R.L.A. de Vries, J. Kim, J. May, M.A. Tocilescu, W.C. Liu, H.S. Ko, J. Magrane, D.J. Moore, V.L. Dawson, R. Grailhe, T.M. Dawson, C.J. Li, K. Tieu, S. Przedborski, PINK1-dependent recruitment of Parkin to mitochondria in mitophagy, Proceedings of the National Academy of Sciences of the United States of America 107(1) (2010) 378-383.

[302] S. Von Stockum, A. Nardin, E. Schrepfer, E. Ziviani, Mitochondrial dynamics and mitophagy in Parkinson's disease: A fly point of view, Neurobiol Dis 90 (2016) 58-67.

[303] S.R. Denison, F. Wang, N.A. Becker, B. Schule, N. Kock, L.A. Phillips, C. Klein, D.I. Smith, Alterations in the common fragile site gene Parkin in ovarian and other cancers, Oncogene 22(51) (2003) 8370-8378.

[304] G. Ashrafi, T.L. Schwarz, The pathways of mitophagy for quality control and clearance of mitochondria, Cell death and differentiation 20(1) (2013) 31-42.

[305] A. Asea, S.K. Kraeft, E.A. Kurt-Jones, M.A. Stevenson, L.B. Chen, R.W. Finberg, G.C. Koo, S.K. Calderwood, HSP70 stimulates cytokine production through a CD14-dependant pathway, demonstrating its dual role as a chaperone and cytokine, Nat Med 6(4) (2000) 435-42.

[306] W. Gao, Y. Xiong, Q. Li, H. Yang, Inhibition of Toll-Like Receptor Signaling as a Promising Therapy for Inflammatory Diseases: A Journey from Molecular to Nano Therapeutics, Frontiers in physiology 8 (2017) 508.

[307] M.C. Patel, K.A. Shirey, L.M. Pletneva, M.S. Boukhvalova, A. Garzino-Demo, S.N. Vogel, J.C. Blanco, Novel drugs targeting Toll-like receptors for antiviral therapy, Future Virol 9(9) (2014) 811-829.

[308] S.M. Opal, P.F. Laterre, B. Francois, S.P. LaRosa, D.C. Angus, J.P. Mira, X. Wittebole, T. Dugernier, D. Perrotin, M. Tidswell, L. Jauregui, K. Krell, J. Pachl, T. Takahashi, C. Peckelsen, E. Cordasco, C.S. Chang, S. Oeyen, N. Aikawa, T. Maruyama, R. Schein, A.C. Kalil, M. Van Nuffelen, M. Lynn, D.P. Rossignol, J. Gogate, M.B. Roberts, J.L. Wheeler, J.L. Vincent, A.S. Group, Effect of eritoran, an antagonist of MD2-TLR4, on mortality in patients with severe sepsis: the ACCESS randomized trial, JAMA 309(11) (2013) 1154-62.

[309] A. Savva, T. Roger, Targeting toll-like receptors: promising therapeutic strategies for the management of sepsis-associated pathology and infectious diseases, Frontiers in immunology 4 (2013) 387.

[310] E.B. Thorgersen, B.C. Hellerud, E.W. Nielsen, A. Barratt-Due, H. Fure, J.K. Lindstad, A. Pharo, E. Fosse, T.I. Tonnessen, H.T. Johansen, A. Castellheim, T.E. Mollnes, CD14 inhibition efficiently attenuates early inflammatory and hemostatic responses in Escherichia coli sepsis in pigs, FASEB journal : official publication of the Federation of American Societies for Experimental Biology 24(3) (2010) 712-22.

[311] M. Huber-Lang, A. Barratt-Due, S.E. Pischke, O. Sandanger, P.H. Nilsson, M.A. Nunn, S. Denk, W. Gaus, T. Espevik, T.E. Mollnes, Double blockade of CD14 and complement C5 abolishes the cytokine storm and improves morbidity and survival in polymicrobial sepsis in mice, Journal of immunology 192(11) (2014) 5324-31.

[312] E.W. Skjeflo, C. Sagatun, K. Dybwik, S. Aam, S.H. Urving, M.A. Nunn, H. Fure, C. Lau, O.L. Brekke, M. Huber-Lang, T. Espevik, A. Barratt-Due, E.W. Nielsen, T.E. Mollnes,

Combined inhibition of complement and CD14 improved outcome in porcine polymicrobial sepsis, Crit Care 19 (2015) 415.

[313] A. Barratt-Due, E.B. Thorgersen, K. Egge, S. Pischke, A. Sokolov, B.C. Hellerud, J.K. Lindstad, A. Pharo, A.K. Bongoni, R. Rieben, M. Nunn, H. Scott, T.E. Mollnes, Combined inhibition of complement C5 and CD14 markedly attenuates inflammation, thrombogenicity, and hemodynamic changes in porcine sepsis, Journal of immunology 191(2) (2013) 819-27.

[314] K. Reinhart, T. Gluck, J. Ligtenberg, K. Tschaikowsky, A. Bruining, J. Bakker, S. Opal, L.L. Moldawer, T. Axtelle, T. Turner, S. Souza, J. Pribble, CD14 receptor occupancy in severe sepsis: results of a phase I clinical trial with a recombinant chimeric CD14 monoclonal antibody (IC14), Crit Care Med 32(5) (2004) 1100-8.

[315] C.A. Spek, A. Verbon, H. Aberson, J.P. Pribble, C.J. McElgunn, T. Turner, T. Axtelle, J. Schouten, T. Van Der Poll, P.H. Reitsma, Treatment with an anti-CD14 monoclonal antibody delays and inhibits lipopolysaccharide-induced gene expression in humans in vivo, J Clin Immunol 23(2) (2003) 132-40.

[316] D.P. Olszyna, A. Verbon, J.P. Pribble, T. Turner, T. Axtelle, S.J. van Deventer, T. van der Poll, Effect of IC14, an anti-CD14 antibody, on plasma and cell-associated chemokines during human endotoxemia, European cytokine network 14(3) (2003) 158-62.

[317] R. Roskoski, Jr., ERK1/2 MAP kinases: structure, function, and regulation, Pharmacol Res 66(2) (2012) 105-43.

[318] M. Cargnello, P.P. Roux, Activation and function of the MAPKs and their substrates, the MAPK-activated protein kinases, Microbiol Mol Biol Rev 75(1) (2011) 50-83.

[319] F. Christian, E.L. Smith, R.J. Carmody, The Regulation of NF-kappaB Subunits by Phosphorylation, Cells 5(1) (2016).

[320] P.Y. Perera, S.N. Vogel, G.R. Detore, A. Haziot, S.M. Goyert, CD14-dependent and CD14-independent signaling pathways in murine macrophages from normal and CD14 knockout mice stimulated with lipopolysaccharide or taxol, Journal of immunology 158(9) (1997) 4422-9.

[321] R. Rajaiah, D.J. Perkins, D.D. Ireland, S.N. Vogel, CD14 dependence of TLR4 endocytosis and TRIF signaling displays ligand specificity and is dissociable in endotoxin tolerance, Proceedings of the National Academy of Sciences of the United States of America 112(27) (2015) 8391-6.

[322] Q. Jiang, S. Akashi, K. Miyake, H.R. Petty, Lipopolysaccharide induces physical proximity between CD14 and toll-like receptor 4 (TLR4) prior to nuclear translocation of NF-kappa B, Journal of immunology 165(7) (2000) 3541-4.

[323] J. Sakai, E. Cammarota, J.A. Wright, P. Cicuta, R.A. Gottschalk, N. Li, I.D.C. Fraser, C.E. Bryant, Lipopolysaccharide-induced NF-kappaB nuclear translocation is primarily dependent on MyD88, but TNFalpha expression requires TRIF and MyD88, Scientific reports 7(1) (2017) 1428.

[324] Y. Cheng, D. Wang, B. Wang, H. Li, J. Xiong, S. Xu, Q. Chen, K. Tao, X. Yang, Y. Zhu, S. He, HMGB1 translocation and release mediate cigarette smoke-induced pulmonary inflammation in mice through a TLR4/MyD88-dependent signaling pathway, Mol Biol Cell 28(1) (2017) 201-209.

[325] R. Dziarski, R.I. Tapping, P.S. Tobias, Binding of bacterial peptidoglycan to CD14, J Biol Chem 273(15) (1998) 8680-90.

[326] B. Weidemann, H. Brade, E.T. Rietschel, R. Dziarski, V. Bazil, S. Kusumoto, H.D. Flad, A.J. Ulmer, Soluble peptidoglycan-induced monokine production can be blocked by anti-CD14 monoclonal antibodies and by lipid A partial structures, Infect Immun 62(11) (1994) 4709-15.

[327] F. Hu, O. Dzaye, A. Hahn, Y. Yu, R.J. Scavetta, G. Dittmar, A.K. Kaczmarek, K.R. Dunning, C. Ricciardelli, J.L. Rinnenthal, F.L. Heppner, S. Lehnardt, M. Synowitz, S.A. Wolf, H. Kettenmann, Glioma-derived versican promotes tumor expansion via glioma-associated microglial/macrophages Toll-like receptor 2 signaling, Neuro Oncol 17(2) (2015) 200-10.

[328] F. Wu, N. Vij, L. Roberts, S. Lopez-Briones, S. Joyce, S. Chakravarti, A novel role of the lumican core protein in bacterial lipopolysaccharide-induced innate immune response, J Biol Chem 282(36) (2007) 26409-17.

[329] H. Shao, S. Lee, S. Gae-Scott, C. Nakata, S. Chen, A.R. Hamad, S. Chakravarti, Extracellular matrix lumican promotes bacterial phagocytosis, and Lum-/- mice show increased Pseudomonas aeruginosa lung infection severity, J Biol Chem 287(43) (2012) 35860-72.

[330] Y. Yamaguchi, D.M. Mann, E. Ruoslahti, Negative regulation of transforming growth factor-beta by the proteoglycan decorin, Nature 346(6281) (1990) 281-4.

[331] M. Ward, K.M. Ajuwon, Regulation of pre-adipocyte proliferation and apoptosis by the small leucine-rich proteoglycans, biglycan and decorin, Cell proliferation 44(4) (2011) 343-51.

[332] A. Kaddourah, R.K. Basu, S.M. Bagshaw, S.L. Goldstein, A. Investigators, Epidemiology of Acute Kidney Injury in Critically Ill Children and Young Adults, N Engl J Med 376(1) (2017) 11-20.

[333] A.O. Aliprantis, R.B. Yang, D.S. Weiss, P. Godowski, A. Zychlinsky, The apoptotic signaling pathway activated by Toll-like receptor-2, EMBO J 19(13) (2000) 3325-36.

[334] C.A. Latanich, L.H. Toledo-Pereyra, Searching for NF-kappaB-based treatments of ischemia reperfusion injury, J Invest Surg 22(4) (2009) 301-15.

[335] F.L. Sung, T.Y. Zhu, K.K. Au-Yeung, Y.L. Siow, K. O, Enhanced MCP-1 expression during ischemia/reperfusion injury is mediated by oxidative stress and NF-kappaB, Kidney Int 62(4) (2002) 1160-70.

[336] X. Wan, J. Yang, L. Xing, L. Fan, B. Hu, X. Chen, C. Cao, Inhibition of IkappaB Kinase beta attenuates hypoxia-induced inflammatory mediators in rat renal tubular cells, Transplant Proc 43(5) (2011) 1503-10.

[337] X. Wan, L. Fan, B. Hu, J. Yang, X. Li, X. Chen, C. Cao, Small interfering RNA targeting IKKbeta prevents renal ischemia-reperfusion injury in rats, Am J Physiol Renal Physiol 300(4) (2011) F857-63.

[338] N. Wang, H. Liang, K. Zen, Molecular mechanisms that influence the macrophage m1-m2 polarization balance, Frontiers in immunology 5 (2014) 614.

[339] E. Dhana, I. Ludwig-Portugall, C. Kurts, Role of immune cells in crystal-induced kidney fibrosis, Matrix Biol 68-69 (2018) 280-292.

[340] A. Shapouri-Moghaddam, S. Mohammadian, H. Vazini, M. Taghadosi, S.A. Esmaeili, F. Mardani, B. Seifi, A. Mohammadi, J.T. Afshari, A. Sahebkar, Macrophage plasticity, polarization, and function in health and disease, J Cell Physiol 233(9) (2018) 6425-6440.

[341] S. Lee, S. Huen, H. Nishio, S. Nishio, H.K. Lee, B.S. Choi, C. Ruhrberg, L.G. Cantley, Distinct macrophage phenotypes contribute to kidney injury and repair, J Am Soc Nephrol 22(2) (2011) 317-26.

[342] X.M. Meng, P.M. Tang, J. Li, H.Y. Lan, Macrophage Phenotype in Kidney Injury and Repair, Kidney Dis (Basel) 1(2) (2015) 138-46.

[343] J.M. Lever, T.D. Hull, R. Boddu, M.E. Pepin, L.M. Black, O.O. Adedoyin, Z. Yang, A.M. Traylor, Y. Jiang, Z. Li, J.E. Peabody, H.E. Eckenrode, D.K. Crossman, M.R. Crowley, S. Bolisetty, K.A. Zimmerman, A.R. Wende, M. Mrug, B.K. Yoder, A. Agarwal, J.F. George, Resident macrophages reprogram toward a developmental state after acute kidney injury, JCI Insight 4(2) (2019).

[344] Y.J. Day, L. Huang, H. Ye, J. Linden, M.D. Okusa, Renal ischemia-reperfusion injury and adenosine 2A receptor-mediated tissue protection: role of macrophages, Am J Physiol Renal Physiol 288(4) (2005) F722-31.

[345] E. Vinuesa, G. Hotter, M. Jung, I. Herrero-Fresneda, J. Torras, A. Sola, Macrophage involvement in the kidney repair phase after ischaemia/reperfusion injury, The Journal of pathology 214(1) (2008) 104-13.

[346] D.A. Ferenbach, T.A. Sheldrake, K. Dhaliwal, T.M. Kipari, L.P. Marson, D.C. Kluth, J. Hughes, Macrophage/monocyte depletion by clodronate, but not diphtheria toxin, improves renal ischemia/reperfusion injury in mice, Kidney Int 82(8) (2012) 928-33.

[347] L.H. Lu, D.J. Oh, B. Dursun, Z. He, T.S. Hoke, S. Faubel, C.L. Edelstein, Increased macrophage infiltration and fractalkine expression in cisplatin-induced acute renal failure in mice, The Journal of pharmacology and experimental therapeutics 324(1) (2008) 111-7.

[348] J.H. Baek, The Impact of Versatile Macrophage Functions on Acute Kidney Injury and Its Outcomes, Frontiers in physiology 10 (2019) 1016.

[349] A.A. Shigeoka, T.D. Holscher, A.J. King, F.W. Hall, W.B. Kiosses, P.S. Tobias, N. Mackman, D.B. McKay, TLR2 is constitutively expressed within the kidney and participates in

ischemic renal injury through both MyD88-dependent and -independent pathways, Journal of immunology 178(10) (2007) 6252-8.

[350] F. Braza, S. Brouard, S. Chadban, D.R. Goldstein, Role of TLRs and DAMPs in allograft inflammation and transplant outcomes, Nature reviews. Nephrology 12(5) (2016) 281-90.

[351] L.M. Zhang, J.H. Liu, C.B. Xue, M.Q. Li, S. Xing, X. Zhang, W.T. He, F.C. Jiang, X. Lu, P. Zhou, Pharmacological inhibition of MyD88 homodimerization counteracts renal ischemia reperfusion-induced progressive renal injury in vivo and in vitro, Scientific reports 6 (2016) 26954.

[352] J.H. Liu, L. He, Z.M. Zou, Z.C. Ding, X. Zhang, H. Wang, P. Zhou, L. Xie, S. Xing, C.Z. Yi, A Novel Inhibitor of Homodimerization Targeting MyD88 Ameliorates Renal Interstitial Fibrosis by Counteracting TGF-beta1-Induced EMT in Vivo and in Vitro, Kidney Blood Press Res 43(5) (2018) 1677-1687.

[353] W.P. Pulskens, G.J. Teske, L.M. Butter, J.J. Roelofs, T. van der Poll, S. Florquin, J.C. Leemans, Toll-like receptor-4 coordinates the innate immune response of the kidney to renal ischemia/reperfusion injury, PLoS One 3(10) (2008) e3596.

[354] J. Morrissey, G. Guo, R. McCracken, T. Tolley, S. Klahr, Induction of CD14 in tubular epithelial cells during kidney disease, J Am Soc Nephrol 11(9) (2000) 1681-90.

[355] D.N. Grigoryev, M. Liu, H.T. Hassoun, C. Cheadle, K.C. Barnes, H. Rabb, The local and systemic inflammatory transcriptome after acute kidney injury, J Am Soc Nephrol 19(3) (2008) 547-58.

[356] C. Cai, X. Shi, S. Korff, J. Zhang, P.A. Loughran, X. Ruan, Y. Zhang, L. Liu, T.R. Billiar, CD14 contributes to warm hepatic ischemia-reperfusion injury in mice, Shock 40(2) (2013) 115-21.

[357] A. Tsung, R. Sahai, H. Tanaka, A. Nakao, M.P. Fink, M.T. Lotze, H. Yang, J. Li, K.J. Tracey, D.A. Geller, T.R. Billiar, The nuclear factor HMGB1 mediates hepatic injury after murine liver ischemia-reperfusion, The Journal of experimental medicine 201(7) (2005) 1135-43.

[358] D.J. Kaczorowski, A. Nakao, R. Vallabhaneni, K.P. Mollen, R. Sugimoto, J. Kohmoto, B.S. Zuckerbraun, K.R. McCurry, T.R. Billiar, Mechanisms of Toll-like receptor 4 (TLR4)-mediated inflammation after cold ischemia/reperfusion in the heart, Transplantation 87(10) (2009) 1455-63.

[359] N. Mirza, A.S. Sowa, K. Lautz, T.A. Kufer, NLRP10 Affects the Stability of Abin-1 To Control Inflammatory Responses, Journal of immunology 202(1) (2019) 218-227.

[360] H. Nakatogawa, Two ubiquitin-like conjugation systems that mediate membrane formation during autophagy, Essays Biochem 55 (2013) 39-50.

[361] D. Fracchiolla, J. Sawa-Makarska, B. Zens, A. Ruiter, G. Zaffagnini, A. Brezovich, J. Romanov, K. Runggatscher, C. Kraft, B. Zagrovic, S. Martens, Mechanism of cargo-directed Atg8 conjugation during selective autophagy, Elife 5 (2016).

[362] A.B. Birgisdottir, T. Lamark, T. Johansen, The LIR motif - crucial for selective autophagy, J Cell Sci 126(Pt 15) (2013) 3237-47.

[363] V. Lahiri, W.D. Hawkins, D.J. Klionsky, Watch What You (Self-) Eat: Autophagic Mechanisms that Modulate Metabolism, Cell Metab 29(4) (2019) 803-826.

[364] S.R. Yoshii, N. Mizushima, Monitoring and Measuring Autophagy, Int J Mol Sci 18(9) (2017).

[365] T.A. Ryan, D.A. Tumbarello, Optineurin: A Coordinator of Membrane-Associated Cargo Trafficking and Autophagy, Frontiers in immunology 9 (2018) 1024.

[366] L. Yu, Y. Chen, S.A. Tooze, Autophagy pathway: Cellular and molecular mechanisms, Autophagy (2017) 1-9.

[367] N.C. McKnight, Y. Zhenyu, Beclin 1, an Essential Component and Master Regulator of PI3K-III in Health and Disease, Current pathobiology reports 1(4) (2013) 231-238.

[368] S.M. Yoo, Y.K. Jung, A Molecular Approach to Mitophagy and Mitochondrial Dynamics, Mol Cells 41(1) (2018) 18-26.

[369] J.W. Harper, A. Ordureau, J.M. Heo, Building and decoding ubiquitin chains for mitophagy, Nat Rev Mol Cell Biol 19(2) (2018) 93-108.

[370] K. Guan, C. Wei, Z. Zheng, T. Song, F. Wu, Y. Zhang, Y. Cao, S. Ma, W. Chen, Q. Xu, W. Xia, J. Gu, X. He, H. Zhong, MAVS Promotes Inflammasome Activation by Targeting ASC

for K63-Linked Ubiquitination via the E3 Ligase TRAF3, Journal of immunology 194(10) (2015) 4880-90.

[371] J.S. Bednash, R.K. Mallampalli, Regulation of inflammasomes by ubiquitination, Cell Mol Immunol 13(6) (2016) 722-728.

[372] C.S. Shi, K. Shenderov, N.N. Huang, J. Kabat, M. Abu-Asab, K.A. Fitzgerald, A. Sher, J.H. Kehrl, Activation of autophagy by inflammatory signals limits IL-1beta production by targeting ubiquitinated inflammasomes for destruction, Nat Immunol 13(3) (2012) 255-63.

[373] M. Escobar-Henriques, M. Joaquim, Mitofusins: Disease Gatekeepers and Hubs in Mitochondrial Quality Control by E3 Ligases, Frontiers in physiology 10 (2019) 517.

[374] F. Le Guerroue, F. Eck, J. Jung, T. Starzetz, M. Mittelbronn, M. Kaulich, C. Behrends, Autophagosomal Content Profiling Reveals an LC3C-Dependent Piecemeal Mitophagy Pathway, Mol Cell 68(4) (2017) 786-796 e6.

[375] T. Proikas-Cezanne, Z. Takacs, P. Donnes, O. Kohlbacher, WIPI proteins: essential PtdIns3P effectors at the nascent autophagosome, J Cell Sci 128(2) (2015) 207-17.

[376] M. Wirth, W. Zhang, M. Razi, L. Nyoni, D. Joshi, N. O'Reilly, T. Johansen, S.A. Tooze, S. Mouilleron, Molecular determinants regulating selective binding of autophagy adapters and receptors to ATG8 proteins, Nature communications 10(1) (2019) 2055.

[377] V.V. Rogov, H. Suzuki, M. Marinkovic, V. Lang, R. Kato, M. Kawasaki, M. Buljubasic, M. Sprung, N. Rogova, S. Wakatsuki, A. Hamacher-Brady, V. Dotsch, I. Dikic, N.R. Brady, I. Novak, Phosphorylation of the mitochondrial autophagy receptor Nix enhances its interaction with LC3 proteins, Scientific reports 7(1) (2017) 1131.

[378] M. Tagaya, K. Arasaki, Regulation of Mitochondrial Dynamics and Autophagy by the Mitochondria-Associated Membrane, Adv Exp Med Biol 997 (2017) 33-47.

[379] T. Lamark, S. Svenning, T. Johansen, Regulation of selective autophagy: the p62/SQSTM1 paradigm, Essays Biochem 61(6) (2017) 609-624.

[380] G. Bjorkoy, T. Lamark, S. Pankiv, A. Overvatn, A. Brech, T. Johansen, Monitoring autophagic degradation of p62/SQSTM1, Methods Enzymol 452 (2009) 181-97.

[381] M.H. Sahani, E. Itakura, N. Mizushima, Expression of the autophagy substrate SQSTM1/p62 is restored during prolonged starvation depending on transcriptional upregulation and autophagy-derived amino acids, Autophagy 10(3) (2014) 431-41.

[382] J. Mejlvang, H. Olsvik, S. Svenning, J.A. Bruun, Y.P. Abudu, K.B. Larsen, A. Brech, T.E. Hansen, H. Brenne, T. Hansen, H. Stenmark, T. Johansen, Starvation induces rapid degradation of selective autophagy receptors by endosomal microautophagy, The Journal of cell biology 217(10) (2018) 3640-3655.

[383] P. Ebner, I. Poetsch, L. Deszcz, T. Hoffmann, J. Zuber, F. Ikeda, The IAP family member BRUCE regulates autophagosome-lysosome fusion, Nature communications 9(1) (2018) 599.

[384] D.G. McEwan, D. Popovic, A. Gubas, S. Terawaki, H. Suzuki, D. Stadel, F.P. Coxon, D. Miranda de Stegmann, S. Bhogaraju, K. Maddi, A. Kirchof, E. Gatti, M.H. Helfrich, S. Wakatsuki, C. Behrends, P. Pierre, I. Dikic, PLEKHM1 regulates autophagosome-lysosome fusion through HOPS complex and LC3/GABARAP proteins, Mol Cell 57(1) (2015) 39-54.

[385] S. Pankiv, E.A. Alemu, A. Brech, J.A. Bruun, T. Lamark, A. Overvatn, G. Bjorkoy, T. Johansen, FYCO1 is a Rab7 effector that binds to LC3 and PI3P to mediate microtubule plus end-directed vesicle transport, The Journal of cell biology 188(2) (2010) 253-69.

[386] B.S. Padman, T.N. Nguyen, L. Uoselis, M. Skulsuppaisarn, L.K. Nguyen, M. Lazarou, LC3/GABARAPs drive ubiquitin-independent recruitment of Optineurin and NDP52 to amplify mitophagy, Nature communications 10(1) (2019) 408.

[387] B. Bingol, M. Sheng, Mechanisms of mitophagy: PINK1, Parkin, USP30 and beyond, Free Radic Biol Med 100 (2016) 210-222.

[388] J. Sawa-Makarska, C. Abert, J. Romanov, B. Zens, I. Ibiricu, S. Martens, Cargo binding to Atg19 unmasks additional Atg8 binding sites to mediate membrane-cargo apposition during selective autophagy, Nature cell biology 16(5) (2014) 425-433.

[389] Y. Princely Abudu, S. Pankiv, B.J. Mathai, A. Hakon Lystad, C. Bindesboll, H.B. Brenne, M. Yoke Wui Ng, B. Thiede, A. Yamamoto, T. Mutugi Nthiga, T. Lamark, C.V. Esguerra, T. Johansen, A. Simonsen, NIPSNAP1 and NIPSNAP2 Act as "Eat Me" Signals for Mitophagy, Developmental cell 49(4) (2019) 509-525 e12.

[390] C. Fan, Y. Zhang, Y. Zhou, B. Li, Y. He, Y. Guo, Z. Jia, Up-regulation of A20/ABIN1 contributes to inefficient M1 macrophage polarization during Hepatitis C virus infection, Virol J 12 (2015) 147.

[391] M. Yang, J. Liu, J. Shao, Y. Qin, Q. Ji, X. Zhang, J. Du, Cathepsin S-mediated autophagic flux in tumor-associated macrophages accelerate tumor development by promoting M2 polarization, Mol Cancer 13 (2014) 43.

[392] K. Liu, E. Zhao, G. Ilyas, G. Lalazar, Y. Lin, M. Haseeb, K.E. Tanaka, M.J. Czaja, Impaired macrophage autophagy increases the immune response in obese mice by promoting proinflammatory macrophage polarization, Autophagy 11(2) (2015) 271-84.

[393] C.P. Chang, Y.C. Su, C.W. Hu, H.Y. Lei, TLR2-dependent selective autophagy regulates NF-kappaB lysosomal degradation in hepatoma-derived M2 macrophage differentiation, Cell death and differentiation 20(3) (2013) 515-23.

8 Supplementary Data
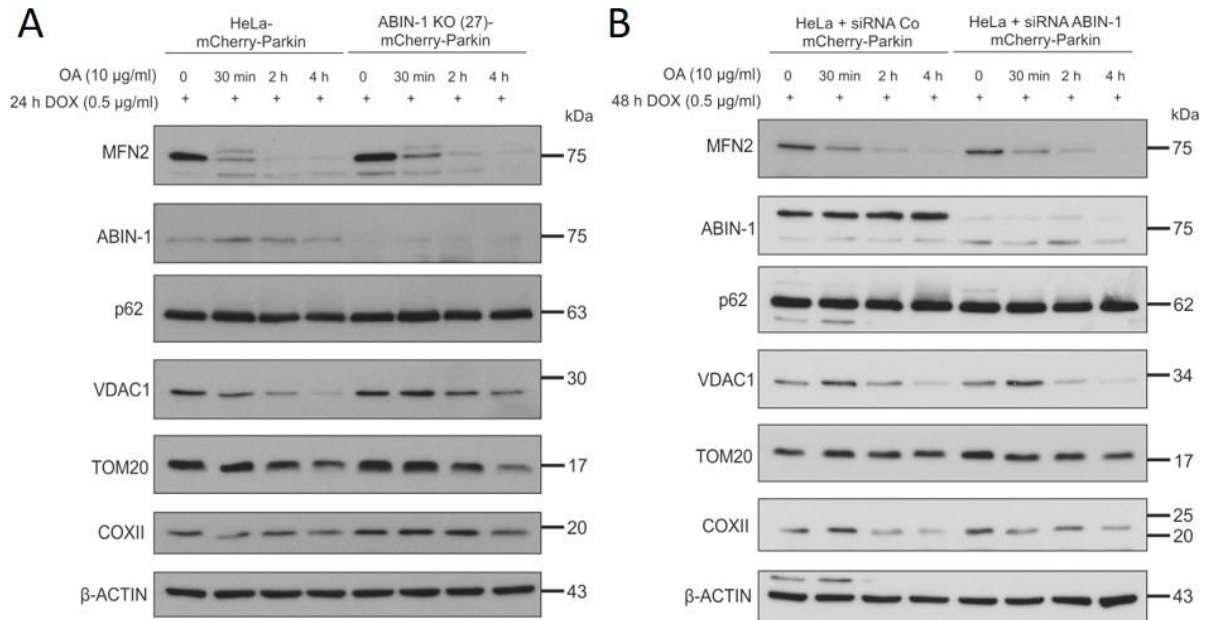
Figure 8.1. Effects of ABIN-1 gene suppression on the degradation of mitophagy substrates. (A) mCherry-Parkin-overexpressing HeLa or ABIN-1 knockout (KO) cells from clone 27 were treated with OA (10 µg/ml) for the indicated time points and analyzed by Western blot. (B) mCherry-Parkin-overexpressing HeLa cells either transfected with siRNA against ABIN-1 or siRNA control for 48 h. Cells were treated with OA (10 µg/ml) for the indicated time points and protein levels were assessed by immunoblotting. β-ACTIN served as a loading control. n = 3.

9 Eidesstattliche Erklärung

Ich, Heiko Rödig, erkläre hiermit, dass ich die vorgelegte Dissertation *„Regulation of inflammation and autophagy: Role of CD14 in biglycan-mediated sterile inflammation and impact of ABIN-1 on selective autophagy"* eigenständig angefertigt und mich anderer Hilfsmittel als der in ihr angegebenen nicht bedient habe, insbesondere, dass alle Entlehnungen aus anderen Schriften mit Angabe der entsprechenden Schrift gekennzeichnet sind.

Ich versichere, die Grundsätze der guten wissenschaftlichen Praxis beachtet und nicht die Hilfe einer kommerziellen Promotionsvermittlung in Anspruch genommen zu haben.

Frankfurt am Main, den 25. Februar 2020

Heiko Rödig

10 Acknowledgements

11   Curriculum vitae

Heiko Rödig

Date of birth: 17.12.1989
Nationality: German
Address: Holzstraße 26, 55116 Mainz
Email: heiko.roedig@live.de

STUDIES

Jul. 2016 - Dec. 2019
PhD studies, Institute for General Pharmacology and Toxicology, Goethe University Frankfurt, Germany, primary supervisor Prof. Dr. Rolf Marschalek

Feb. 2016
Master degree (MSc) in "Biology", Institute of Zoology, Department 1 Cell & Matrix Biology, Johannes Gutenberg University Mainz, Germany, supervisor Prof. Dr. Uwe Wolfrum
Thesis title: "Analysis of VLGR1 and associated protein-complexes in primary cilia". **Grade: 1.0**

2013 - 2016
Master studies (MSc) in "Biology", Faculty of Biology, Johannes Gutenberg University Mainz, Germany

Apr. 2013
Bachelor degree (BSc) in "Biology", Institute of Molecular Genetics, Genetic Engineering Research and Consulting, Johannes Gutenberg University Mainz, Germany, supervisor Prof. Dr. Erwin Schmidt
Thesis title: "Mapping of polytene chromosomes of chironomids across species by FISH". **Grade: 2.4**

2010 - 2013
Bachelor studies (BSc) in "Biology", Faculty of Biology, Johannes Gutenberg University Mainz, Germany

2000 -2009
Highschool "Max-Planck secondary school", Rüsselsheim, Germany. **National final exam grade: 1.6**

PUBLICATIONS

1) **Roedig H.**, Damiescu R., Zeng-Brouwers J., Kutija I., Trebicka J., Wygrecka M., Schaefer L. **2019**. Danger matrix molecules orchestrate CD14/CD44 signaling in cancer development. *Semin Cancer Biol.* https://doi.org/10.1016 /j.semcancer.2019.07.026
2) **Roedig H.**, Nastase M.V., Wygrecka M., Schaefer L., **2019**. Breaking down chronic inflammatory diseases: the role of biglycan in promoting a switch between inflammation and autophagy. *FEBS J.*, 286(15), 2965-2979.
3) Poluzzi C., Nastase M.V., Zeng-Brouwers J., **Roedig H.**, Hsieh L.T., Michaelis J.B., Buhl E.M., Rezende F., Manavski Y., Bleich A., Boor P., Brandes R.P., Pfeilschifter J., Stelzer E.H.K., Münch C., Dikic I., Brandts C., Iozzo R.V., Wygrecka M., Schaefer L., **2019**. Biglycan evokes autophagy in macrophages via a novel CD44/Toll-like receptor 4 signaling axis in ischemia/reperfusion injury. *Kidn. Int.*, 95(3), 540-562.
4) **Roedig H.**, Nastase M.V., Frey H., Moreth K., Zeng-Brouwers J., Poluzzi C., Hsieh L.T., Brandts C., Fulda S., Wygrecka M., Schaefer L., **2019**. Biglycan is a new high-affinity ligand for CD14 in macrophages. *Matrix Biol.*, 77, 4-22.
5) Nastase M.V., Janicova A., **Roedig H.**, Hsieh L.T., Wygrecka M., Schaefer L., **2018**. Small leucine-rich proteoglycans in renal inflammation: two sides of the coin. *J. Histochem. Cytochem.*, 66, 261-272. 22155417738752.
6) Hsieh L.T., Nastase M.V., **Roedig H.**, Zeng-Brouwers J., Poluzzi C., Schwalm S., Fork C., Tredup C., Brandes R.P., Wygrecka M., Huwiler A., Pfeilschifter J., Schaefer L., **2017**. Biglycan- and Sphingosine Kinase-1 Signaling Crosstalk Regulates the Synthesis of Macrophage Chemoattractants. *Int J Mol Sci.,* 18, 1-18.

CERTIFICATIONS
Aug. 2019: **Project Management Training Course** Certificate, FernUniversität in Hagen, Germany
Nov. 2018: **International European Business Competence* License (EBC*L)** Certificate, FernUniversität in Hagen, Germany
Nov. 2016: **FELASA Category B** Certificate CM Prognostic, Advanced training for working with lab animals, Frankfurt am Main, Germany

FINANCING
2016 - 2019: **PhD position**, offered by SFB1177 - Molecular and Functional Characterization of Selective Autophagy, Frankfurt am Main, Germany
2015 - 2016: **Master position**, given by DFG-FOR 2149 - Elucidation of Adhesion-GPCR signaling, Mainz, Germany

SCIENTIFIC CONFERENCES
Oct. 2019, IRTG-Retreat SFB1177, Zell an der Mosel, Germany **[selected talk]**
Jun. 2019, Cardio Pulmonary Institute (CPI) Annual Retreat, Bad Nauheim, Germany **[poster]**
Mar. 2019, Annual Meeting of the German Society for Matrix Biology, Regensburg, Germany **[selected talk and poster]**
Mar. 2018, IRTG-Retreat SFB1177, Bad Kreuznach, Germany **[selected talk]**
Feb. 2017, IRTG-Retreat SFB1177, Kirchberg, Germany **[selected talk]**
Feb. 2016, Young Scientist Retreat FOR 2149, Eisenach, Germany **[poster]**

PARTICIPATIONS AT INTERNATIONAL CONFERENCES AND MEETINGS
Mar. 2018, Joint Meeting of the German and Swiss Societies for Matrix Biology, Stuttgart, Germany
Jul. 2016, Frankfurt Conference on Ubiquitin and Autophagy, Frankfurt, Germany
Apr. 2015, First Meeting of the Research Unit FOR 2149, Kleinlüder, Germany

LANGUAGES
German - native speaker
English - fluent
French - basic